Development of Mass Spectrometry Techniques for Real-Time Reaction Monitoring

by

Eric Janusson
B.Sc., University of Victoria, Canada, 2012

A Dissertation Submitted in Partial Fulfillment
of the Requirements for the Degree of

DOCTOR OF PHILOSOPHY

in the Department of Chemistry

Supervisory Committee

Development of Mass Spectrometry Techniques for Real-Time Reaction Monitoring

by

Eric Janusson
B.Sc., University of Victoria, 2012

Supervisory Committee

Dr. J. Scott McIndoe, Department of Chemistry
Supervisor

Dr. Natia Frank, Department of Chemistry
Department of Chemistry

Dr. Dennis Hore, Department of Chemistry
Department of Chemistry

Dr. Christoph Borchers, Outside Member
Department of Microbiology and Biochemistry

Abstract

Supervisory Committee

Dr. J. Scott McIndoe, Department of Chemistry
Supervisor

Dr. Natia Frank, Department of Chemistry
Department of Chemistry

Dr. Dennis Hore, Department of Chemistry
Department of Chemistry

Dr. Christoph Borchers, Outside Member
Department of Microbiology and Biochemistry

Electrospray ionization (ESI) facilitates the transfer of ions in solution into the gas-phase for analysis by mass spectrometry. The ionization process is intricate and required further investigation, especially because of the lack of in-depth literature on the subject. Furthermore, investigations into the ESI process will serve to assist development of real-time reaction monitoring. To do this, a cationic ionic liquid, butyl methylimidazolium, $[BMIM]^+$, was paired with several counterions and mixed in various solvents. This was analyzed by ESI mass spectrometry to determine the relative response ratio between two observable aggregates. The findings assisted in the elucidation of differential surface activity of chemically distinct ions in ESI, with respect to changes in solvent. Furthermore, the results obtained suggested acetonitrile is an optimal solvent for the analysis of ions of this type due to a reduction in differential effects, whereas other common ESI solvents prove to enhance the surface activity of specific aggregate ions.

Further investigations into ESI-MS involved effects of spray head geometry relative to the inlet to the mass spectrometer. The position of the spray-head, the solvent, and additional instrumental parameters were independently adjusted during the analysis of an equimolar mixture of two different ions. It was found that these parameters have dramatic effects on the distribution of signal intensity from one ion to another, and therefore the resulting usefulness of acquired spectra. The sharp contrast in ion intensity, and even differential ion activity, with relatively minor instrument changes (such as temperature programming, gas flow rates and solvent choice) demonstrated the importance of finding the optimal spot for the ESI spray head, especially when signal intensity and a quality analysis is key.

Additional ESI-MS work involved working with an industry partner to develop selective charge-tagging reagents for the characterization of petroleum fractions by ESI-MS. A simple chemical derivatization technique was developed in which thiols and disulfides may be selectively analyzed in a complex matrix and easily characterized. These reagents enhanced detection of thiols and disulfides solely due to the nature of the charged tag derivatization agent. The charged disulfides readily and exclusively react with thiols in a complex matrix in a short amount of time. The synthesis of these reagents was simple and resulted in a pure and stable reagent. The efficacy of the reaction was demonstrated using on-line monitoring, while the scope and usefulness of the reaction was demonstrated in petroleum fractions.

A combination of UV-Vis spectroscopy and electrospray ionization mass spectrometry was used for real-time monitoring of $Pd_2(dba)_3$ activation with sulfonated versions of PPh_3 and a Buchwald-type ligand. This provides insight into the effect of ligand and preparation conditions on activation and allows for establishment of rational activation protocols. It is expected that this reaction monitoring technique will be enhanced through the use of tandem mass spectrometry.

Finally, an experimental method of visualizing atomic orbitals was developed as a demonstration intended for first year chemistry students. This demonstration involved the examination of nodal and anti-nodal regions of Chladni figures which students could then connect to the concept of quantum mechanical parameters and their relationship to atomic orbital shape.

Table of Contents

List of Tables

List of Figures

List of Schemes

List of Equations

Acknowledgments

Firstly, I would like to thank Scott who I have been lucky to call my supervisor for five years. His infectious curiosity and uncanny ability to spark my interest have motivated me greatly. More importantly, Scott has taught me to teach myself, take initiative, and become an effective manager of my own time. I have developed as a scientist and as a person under Scott's mentorship and I know in my heart that I chose the right supervisor to conduct my PhD research with.

Ori Granot possesses an incredible amount of technical and analytical knowledge. He is a repository of information and he has taught me more about mass spectrometry and analytical techniques than anyone in my academic career. His time and patience helped make me scientist I am today. He also gave me a passion for electronics which launched new hobbies in electronics. He is a mentor, but also a great friend of mine. I will deeply miss my conversations with Ori and greatly value all he has taught me.

This dissertation is for my mother and father. I am very lucky to have two wonderful parents who love and support me. They are truly incredible people and raised me well. I love them very much and I hope I have made them proud.

Dedication

For Mom and Dad.

“In ardua tendit”.

Chapter 1. Literature Review

1.1 Overview

This work contains several projects primarily associated with the development of electrospray ionization mass spectrometry (ESI-MS) as an analytical instrument to study chemical reactions. ESI-MS is a common analytical technique; however, it is underwhelmingly used in the study of organometallic reactions. The McIndoe group has developed much mass spectrometric methodology for the real-time monitoring of these types of reactions, and have repeatedly demonstrated that the speed, accuracy, and sensitivity of ESI-MS for reaction monitoring is outstanding.[1–5]

The goal of the work featured in the first few chapters of this dissertation was to develop ESI-MS methodologies by investigating the electrospray process in more detail. The benefits and shortcomings of ESI-MS were examined in detail. These projects ensured that later projects, such as investigation of catalyst activation, were approached with an eye for detail and appreciation for the power of mass spectrometry.

1.2 History of Mass Spectrometry

Mass spectrometry (MS) is an analytical technique in which ions are generated, sorted and detected based on their mass-to-charge ratio, thus yielding qualitative and quantitative information about the analytes. The technique is powerful because both compositional and

structural information may be obtained with the right experiments. Mass spectrometry was the brainchild of J. J. Thomson who developed the first mass spectrometers based on a fascinating discovery.[6] His 1913 work demonstrated that individual isotopes of ionized neon could be manipulated with electric and magnetic fields. These early "mass spectrographs" laid out the foundation for the development of the first working mass spectrometer by a student of Thomson's, Francis William Aston, in 1919. For this work, Aston was awarded the Nobel Prize in chemistry in 1921. Just prior to this, in 1918, Arthur Jeffrey Dempster had developed the theory and design of a mass spectrometer which laid out the road to modern mass spectrometers. Importantly, Dempster had also developed electron ionization (EI), a generally useful ionization source, as a part of his work.

1.3 Ionization Sources

There are three parts found in any mass spectrometer: the ionization source, the mass selector, and the detector. In many ways, the ionization source is the most critical component to consider for a given experiment. A so-called "hard ionization technique", EI produces electrons from a heated filament which collide with molecules in the gas phase with sufficient energy to ionize them. The high energy of this process generally results in fragmentation of the molecule (hence "hard" ionization) in a characteristic way. Because of this, electron ionization is one of the most used ionization sources and has massive libraries of mass spectra generated by this source which can be used to "fingerprint" an analyte.

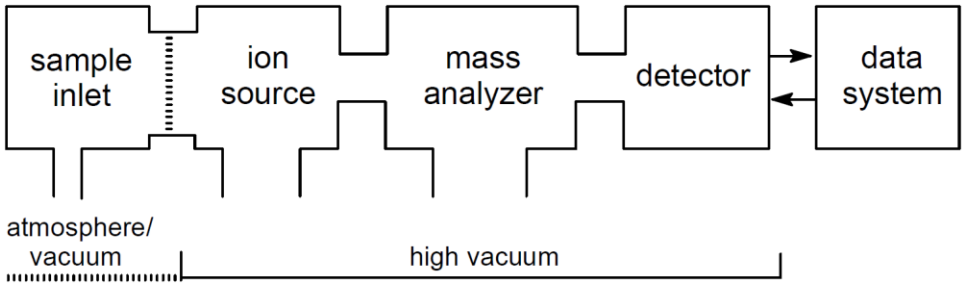

Figure 1. General outline of a Mass Spectrometer[7]

Of course, hard ionization isn't necessarily desirable. EI spectra of a single molecule can be somewhat complex due to fragmentation and the analysis of mixtures can create complicated overlap of signals. Therefore, "soft" ionization techniques were developed to minimize molecular fragmentation. A soft ionization technique is one which imparts very little energy on the analytes themselves. The first of these was chemical ionization (CI) which yielded little or no fragmentation, which greatly simplified a spectrum. CI produces ions indirectly by first ionizing a gas (such as methane), which collides with another molecule to produce a protonated molecule (e.g. CH_5^+) that on collision with an analyte molecule (M) will produce a characteristic protonated pseudomolecular ion peak $[M+H]^+$. Transfer of sample to the gas phase is a crucial step, since the analyte ions must be in the gas phase to be selected and detected. There are several ways of accomplishing this when analytes are in a condensed phase. One of the most popular soft ionization methods for large molecules is matrix-assisted laser desorption ionization (MALDI). As the name implies, the sample is held within some matrix (several are available depending on the analysis), which absorbs the energy from a pulsed laser that ablates the analyte/matrix mixture. Ionization occurs in the resulting energetic plume. There are also several spray techniques such as electrospray ionization (ESI), desorption-ESI, and thermospray which

are excellent for the analysis of liquid samples.[8–10] These are now very popular for sample introduction and ionization.

1.4 Electrospray Ionization

ESI was first reported as an ionization technique for mass spectrometry by Malcolm Dole in 1968.[11] His efforts were focused on developing a mass spectrometric method to determine molecular weights of polymers. Since these dissolved polymers required a method to transfer liquids into the gas phase for analysis, he considered utilizing an electrospray system to facilitate this. The development of ESI-MS, however, is primarily attributed to John Bennett Fenn whose work in the late 1980s ended up with him being awarded the 2002 Nobel Prize in Chemistry. His initial work involved using ESI with a quadrupole mass analyzer in the negative ion mode to characterize solutions of relatively small ions such as sodium iodide in water and acetone.[12] Later work developed ESI as an interface for liquid chromatography and showed that ESI-MS was very useful for large molecules.[13] This work enabled the science of proteomics since large biological molecules such as proteins and peptides were now analyzable via ESI-MS due to multiple charging of these larger analytes.

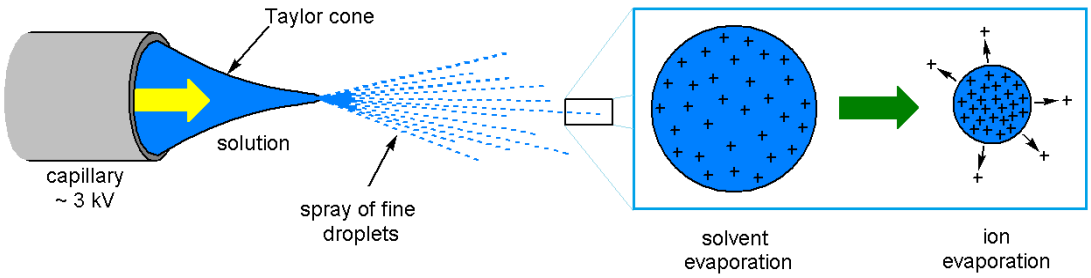

Figure 2. Simple diagram of the electrospray process

Electrospray ionization mass spectrometry (ESI-MS) functions by transferring ions from solution into the gas phase through the evaporation of a spray of charged droplets.[14] As a "soft" ionization technique, ESI does not expose the analytes to a great deal of energy and, therefore, does not inherently excel at producing charged species (as compared to "hard" ionization techniques such as electron ionization). Because of this, some form of derivatization is commonly employed with ESI-MS analyses in order to promote the appearance of target analytes. In order to do this, a compound must readily acquire a charge through adventitious protonation, deprotonation, aggregation with a cation (most commonly with alkali metals), or are charged.[15] Several examples of producing charged compounds for observation by mass spectrometry, notably from the Chen group, are present in the literature.[16–20]

1.5 Mass Analyzers

Following ionization, the next crucial consideration for any MS experiment is the method by which the ions are sorted prior to detection. At this stage in the mass spectrometer (partly depending on the configuration of the sample introduction and ionization source), a high (10^{-3}-10^{-7} mBar) to ultra-high (10^{-7}-10^{-12} mBar) vacuum is necessary to ensure ions reach

the detector without collision. This “ion sorting” stage is referred to as the mass analyzer of the instrument.

The idea behind mass separation in a given mass analyzer is largely based on how ions behave when exposed to an external field. Magnetic sector (B) instruments are extensions of the very first mass spectrometers which made use of a strong magnetic field. The Lorentz force describes the force exerted on ions in a magnetic field (equation X describes this force including the electric field, E, and magnetic field components, B).

$$F = qE + qv \times B$$

Equation 1. Lorentz force on an ion in a magnetic field

They are very large instruments capable of accurately deflecting ions travelling through them. These instruments served as the go-to high resolution mass spectrometer until FTICR, Orbitrap and Time-of-Flight (TOF) instruments eventually rendered them largely obsolete.[6] The quadrupole (Q) mass analyzer is a much smaller alternative to sector instruments. Quadrupole mass analyzers and quadrupole ion traps apply alternating sweeps of RF and DC current which stabilizes and collimates a beam of ions of particular mass-to-charge ratio (*m/z*) while destabilizing the majority. The sweeping potential, therefore, facilitates mass separation due to the instability of ion trajectories based on their mass to charge as described by the Mathieu equation. While reasonably small and reliable, quadrupoles are also less accurate and of lower resolution than most other instruments. That being said, the triple-quadrupole mass spectrometer, a linear combination of three

separate mass analyzers, is the industry standard today in quantitative analytical applications.

TOF instruments were developed in the late 1940s to the mid-1950s by William C. Wiley and I. H. McLaren.[6] Originally possessing relatively poor resolution, TOF instruments are very capable instruments today. A TOF instrument gauges the mass-to-charge ratio of ions by determining the ion flight time. All ions introduced into the spectrometer are accelerated by an electric field (the extraction voltage) into a field-free drift tube and allowed to travel for a short distance before being detected. On being exposed to the electric field, all ions are given the same kinetic energy and travel with a velocity related to the energy applied and inversely to their mass (equation 2). The flight time can be measured by the instrument (relative to external calibration standards) and registered with the appropriate *m/z* once they arrive at the detector. This rapid detection, combined with resolving powers of over 60,000 in reflectron mode has made TOF instruments a very attractive choice.

$$a = \frac{Eq}{m}$$

Equation 2. Acceleration of an ion in an electric field

The unmatched champion of modern high-resolution mass spectrometry is the Fourier transform ion cyclotron resonance (FT-ICR) mass analyzer which was developed in 1974 at the University of British Columbia by Melvin B. Comisarow and Alan G. Marshall.[6] These instruments determine molecular weight by measuring the cyclotron frequency of ions in a magnetic field. FT-ICR mass spectrometers are capable of incredible resolutions

(with resolving powers of over 2 million) and are ideal for extremely accurate and precise measurements; however, they are also very expensive and fairly slow in terms of spectra acquisition. Practically, the consideration of which mass analyzer to use for an experiment mostly depends on the desired resolution and sensitivity.

Mass spectrometers continue to be developed into powerful analytical tools. Mass spectrometry has revolutionized proteomics and helped to map out the human genome, enabled detailed analysis of contamination in water bodies, and will be sent to Europa to determine whether that moon could be suitable for life. Many other applications have been and continue to be discovered, and my focus has been on developing methodologies for unravelling reaction mechanisms.

1.6 Palladium Catalysis

The field of catalysis has a massive impact on our daily lives. The most obvious example is the chemical industry, which employs various catalysts for the production of enormous quantities of commodity materials such as polyethylene to relatively small amounts of important and complex pharmaceuticals and vitamins.[21,22] Some of the most important reactions in organometallic and synthetic organic chemistry are the family of palladium-catalyzed cross-couplings. This class of reaction is generally associated with the formation of carbon-carbon bonds due to the popularity of reactions such as the Sonogashira, Suzuki and Heck couplings, which have extensive applications in the production of pharmaceuticals, natural products, and polymers.[23–25]

Organometallic chemists continue to develop new applications for catalysts in synthetic chemistry and industrial processes. Unfortunately, catalysis is occasionally viewed (especially in industry) as a black-box process in which empirically useful catalysts serve to improve the production of a target molecule. As chemists, we are more interested in the intricacies of these reactions and this kind of in-depth analysis can be extremely advantageous to other fields which employ catalysts. Mechanistic and kinetic studies of catalytic reactions allow organometallic chemists to rationally develop new and enhanced catalysts. Some catalytic systems have been well-studied whereas others lack detail. New analytical techniques are continuously developed in order to better approach the challenges in studying catalytic systems. Catalytic reactions are so commonly studied that a specific branch of analytical chemistry known as *in operando* spectroscopy is devoted to the *in situ* spectroscopic investigation of catalytic mechanisms in order to enhance our understanding of such systems.[26–28] The *in operando* methodology is primarily used in combination with more traditional techniques for studying reactions especially IR and UV-Vis in order to characterize products of a reaction or monitor their individual rates of formation. Additional techniques such as X-ray crystallography and cyclic voltammetry are frequently used for the characterization of isolable catalytic species. Each of these techniques have their own benefits and pitfalls and despite the best efforts of these techniques (and many more) there is still much to learn and discover in many of the most frequently used catalytic reactions.

1.7 Electrospray Ionization applied to the study of organometallic catalytic reactions

Since the early 90's, ESI-MS has seen use for the analysis of organometallic complexes. The first analysis of organometallic complexes was from Berman in 1991 in which ESI-MS was used to detect ionic organoarsenic complexes as part of an ion-exchange and ion-paring chromatographic separation system.[29] Other examples include MSMS detection of palladium and platinum species,[30] and cationic chromium, rhenium, and iron organometallic complexes.[31] Following these early successes, ESI-MS has been deployed in the investigation of a myriad of catalytic reactions.

The McIndoe group has employed ESI-MS to examine several organometallic and catalytic reactions.[1–4,32–40] We employ a variety of methods to monitor catalytic reaction progress, including pressurized sample infusion (PSI) to directly sample a reaction mixture,[41,42] in addition to the use of charged substrates to highlight low-level intermediate complexes.[39,43–45] ESI-MS is a provably valuable tool in the study of catalytic reactions since it provides a rapid and simple analysis of air-sensitive and/or complex species. Electrospray is an ideal technique for on-line reaction monitoring since it facilitates the transfer of ions in solution into the gas-phase with minimum fragmentation. This is done by forcing a solution through a highly charged capillary (held at 2-5 kV) which produces a fine spray of droplets. The droplets are desolvated thermally using cartridge heaters and pneumatically by a counter-flow of nitrogen gas. Through a combination of ion evaporation and microdroplet fissioning events, condensed-phase ions are transferred into the gas-phase and focused into the mass spectrometer for analysis.

Figure 3. An electrospray ionization source

Importantly, the electrospray ionization source is uniquely well-suited to study homogeneous catalytic systems because the source features an extremely low degree of fragmentation which helps with interpretation while maintaining the delicate structure of certain organometallic species.[39,46] However, because it transfers ions from the solution phase to the gas phase the generation of ions should not be left to the electrospray process since many neutral compounds are undetectable using ESI-MS if they do not contain sites that strongly associate with ions in solution. ESI-MS can be used to monitor catalytic reactions both directly and in real time to yield kinetic and mechanistic data that are not accessible through other means allowing one to, for example, observe transient catalytic intermediates of a reaction as they appear.[39]

Furthermore, due to the soft mechanism of ESI the potentially fragile metal-coordinated intermediate species remain intact for direct observation. It is certainly possible to induce fragmentation with ESI alone; however, it is commonly not used for this purpose and analytes are instead adventitiously charged via acquisition (or loss) of a proton or adduct

formation with alkali metals. In contrast to MALDI, ESI features a clean baseline which facilitates superior signal-to-noise ratios. Recently, the McIndoe group has demonstrated the importance of "softer" ionization conditions and that even weakly bound organometallic complexes will survive the ionization process, but only if tuned properly.[47] As a final note, many examples exist in the literature of ESI-MS applied to the identification of organometallic intermediate species in catalytic hydrogenations,[40,48–50] cycloaddition,[4] epoxidation,[51] hydrodehalogenation,[1] and other diverse reactions many of which involve C-C coupling.[52–57]

Another notable example of the effectiveness of ESI-MS applied to the mechanistic study of organometallic catalytic reactions comes from a recent paper from our own group. Ahmadi, et. al.[58] studied the copper-free Sonogashira coupling reaction. In doing so, the authors were able to probe the proposed catalytic cycle through tracking of reaction intermediates, reagents, products, and by-products. This was facilitated by applying a charge-tag species (a phosphonium substrate) which is easily detected by the mass spectrometer due to the intrinsic charge. More importantly, the charge-tag species allowed the authors to observe key palladium intermediates of the catalytic reaction which would normally (by ESI-MS) be undetectable. It was found that while the rate of the reaction was initially quite fast the reaction is soon slowed to a zero-order process. This tied in with the disappearance of an intermediate species, suggesting the transmetalation step of the proposed cycle was rate-determining after this stage. Their conclusion was further tested with the addition of stronger base in order to drive the more desirable first-order process for a greater duration. This change effectively shut down by-product formation leading to

the faster synthesis of a cleaner product. Changes in the catalytic reaction scheme based on rational mechanistic evaluation are, as shown, paramount and ESI-MS is an effective tool for studying such systems. There also exist several notable examples of the effectiveness of ESI-MS when applied to the mechanistic study of organometallic catalytic reactions in the literature within and outside of the McIndoe group.[2,39,46,59]

1.8 Adventitiously-charged Analytes

An adventitiously-charged analyte is one which is neutral but picks up a positive or negative charge from another species. In ESI-MS, common mechanisms of charging include protonation of a relatively basic site, association with alkali metals (sodiation, potassiation), loss of a poorly coordinating anionic ligand (hexafluorophosphate, BArF-type anions), or deprotonation of an acidic site. In terms of organometallics, some of the original examples involve loss of an anionic ligand to facilitate detection. For example, in 1993, the Raney nickel-catalyzed coupling reaction involved detection of the dimer $[(dmbp)Ni(\mu\text{-}Br)_2Ni(dmbp)Br]^+$ through loss of bromide.[60] Another example in the 1990s of this involved the ESI-MS detection of reactive titanium intermediates in a titanium sulfoxidation catalytic reaction through ligand protonation.[61]

Due to the popularity of palladium-catalyzed cross coupling reactions, several examples of adventitiously charged intermediates detected with ESI-MS appear in the literature. An investigation of arylboronic acid coupling was facilitated with the loss of an anionic boron ligand, as well as during quenching of the reaction with trifluoroacetic acid.[62] Chelating ligands were used in the Heck coupling and intermediates were detected via halide loss.[63]

1.9 Charged-tagged Compounds

An issue with monitoring adventitiously-charged species in ESI-MS is that the ionization process depends on ionization efficiency. Often, a reaction may involve intermediates or by-products that are incapable of being charged such as the lack of a basic site which prevents protonation. The McIndoe group frequently circumvents ionization efficiency issue through the use of charged tags which do not affect the course of the reaction.

An early example of this is the work of Canary, *et.al.* who, in 1994, employed a substrate with the goal of protonating the substrate's basic site to facilitate detection. A common technique used today, the pyridyl bromide ligand contains an easily protonated nitrogen atom. Several examples of similar derivatization tactics (with a focus on chemoselectivity) are nicely summarized in a series of articles by Quirke *et.al*.[64]

Chargeable tags do suffer some ionization efficiency issues and in order to get around this the McIndoe group employs a large amount of tags with a fixed, permanent charge. This methodology, referred to as charge-tagging, has been frequently employed in our group's work with ESI-MS to achieve excellent limits-of-detection (LOD).[1,2,65,66] The application of the charge-tagging methodology paired with ESI-MS to detect catalytic species was conceived by Adlhart and Chen who used quaternary phosphonium and ammonium tags to examine a ring-opening metathesis polymerization (ROMP) reaction in 2000.[43] In 2010, Schade, *et.al*. employed quaternary ammonium charge tags in palladium catalyzed cross-coupling reactions to monitor the abundance of chemical species using

ESI-MS.[67] The McIndoe group has developed this further by crafting charged phosphonium substrates and charged analogues of normally neutral ligands to facilitate this type of reaction monitoring.[39,45,68–70]

1.10 Reaction Monitoring with UV-Vis Spectroscopy

More recent work in the McIndoe group has focused on employing tandem orthogonal analytical techniques in order to obtain a more complete picture of what is happening in solution. From the examples above, it is clear that mass spectrometry is a very powerful tool for reaction monitoring. However, the application of orthogonal techniques is important for several reasons. MS is only capable of observing ions and while we can attempt to get around this with charge-tagging, there could possibly be analytes in solution which we are still not detecting with MS alone. Orthogonal techniques are synergistic and when applied to a single reaction vessel, make for a very compelling argument. We chose to use UV-Vis spectroscopy to complement our ESI-MS studies.

UV-Vis spectroscopy is an extremely well-tested form of molecular spectroscopy and an analytical technique that has been employed for several decades due to many benefits such as reliability of components and good limits-of-detection (which varies between instruments). Spectroscopy in the UV-Vis region is the absorption of UV-Vis light (wavelengths between about 190-800 nm for many absorption spectrometers) by analytes. The attenuated light is measured by a photodetector in order to determine the concentration of the analytes present. The degree of absorption and its correlation to the concentration of

an analyte is explained by the Beer-Lambert Law. Detection of an analyte depends on the molecular structure of the analyte. A chromophore, the component of a molecule which absorbs in the visible region of the electromagnetic spectrum, is coloured since there exists a particular separation between discrete molecular orbitals.

Photons in the UV-Vis range are absorbed and primarily associated with excitation from a π-orbital or non-bonding orbital to a π* anti-bonding orbital (and occasionally a sigma anti-bonding orbital). This is because the energy gap between these is congruent with the energy of the incident light and is therefore capable of inducing a transition. The energy gap between this set of orbitals explains why conjugated π systems and delocalized electrons (in non-bonding orbitals as well, including O and N lone pairs) are very important to an absorption. Further, the frequency of the light absorbed is related to the energy gap between molecular orbitals by Planck's equation ($E=h\nu$, where $\nu=c/\lambda$).

Exactly where a compound absorbs in the UV-Vis spectrum is due to how light of corresponding energy interacts with the material. Since absorption occurs when an electron transitions from a ground state to a higher energy excited state, the energy-level separation between the two molecular orbitals dictates the energy of light that can be absorbed by the molecule.

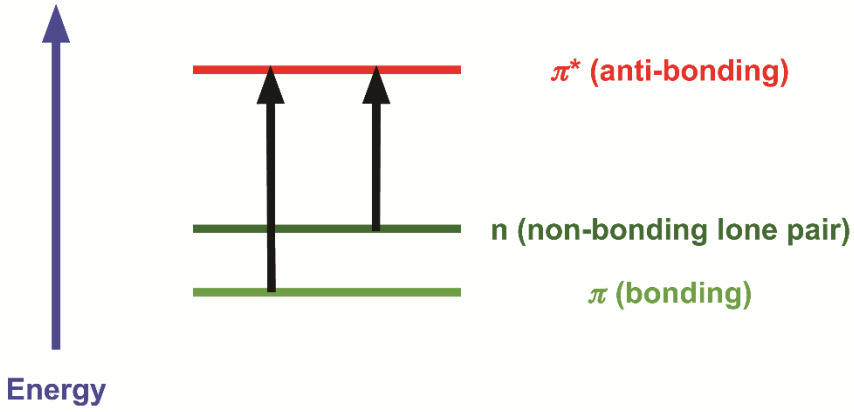

Figure 4. Simplified Jablonski diagram illustrating absorption and movement of an electron from the ground state to a higher energy excited state

This separation is theoretically a fixed quantity. Vibration and rotation of bonds within a molecule has a continuous effect on the relative energies of the molecular orbitals involved in the transition and affects the broadness of absorption spectra of molecules. This range of energy levels explains the broadness of peaks in the UV-Vis absorption spectrum. Ambient conditions including temperature and solvent are known to affect the shape and position of absorption spectra.

Functionality (chemical moieties and substitution) affects where in the spectrum the absorption occurs; though, to a lesser degree than the size of the conjugated system. A general trend is that larger, and more highly-conjugated systems tend to absorb more strongly at greater wavelengths while also exhibiting wider absorption bands. A classic example is the distinctive orange colour of carrots and other root vegetables due to the presence of the highly-conjugated beta-carotene molecule.

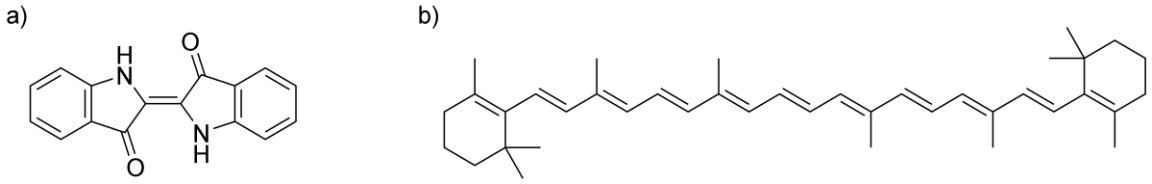

Figure 5. Examples of strongly coloured chromophore species featuring high levels of conjugation: indigo (a) and beta-Carotene (b)

Another excellent example is the dark blue colour of indigo which has been used as a dye from ancient times to present day for textiles.

A major benefit of UV-Vis spectroscopy for us was the simplicity of the instrumentation. Mass spectrometry is a much more complex analytical instrument and requires a great deal of upkeep and precautions compared to UV-Vis spectroscopy. In fact, a UV-Vis spectrometer can be assembled and implemented at very low cost. PublicLab[a] is a community of scientists committed to developing inexpensive spectroscopic tools primarily for environmental analysis. Their open source spectrometry project has developed a foldable spectrometer which can be constructed in a few minutes for the cost of a DVD and a small amount of cardstock. The foldable mini spectrometer is paired with a simple camera (the quality of which dictates the sensitivity and wavelength range of the resulting spectra) such as those found in an average smartphone. Incident light is separated by a simple diffraction grating formed from the transparent layer of a DVD and the image is uploaded into a free web-based application which quantifies the intensity of light across

[a] PublicLab (https://publiclab.org/) and their spectral processing API (https://spectralworkbench.org/) may be found online.

the UV-Vis spectrum. While it is a rudimentary solution, the device performs as well as can be expected with proper calibration.

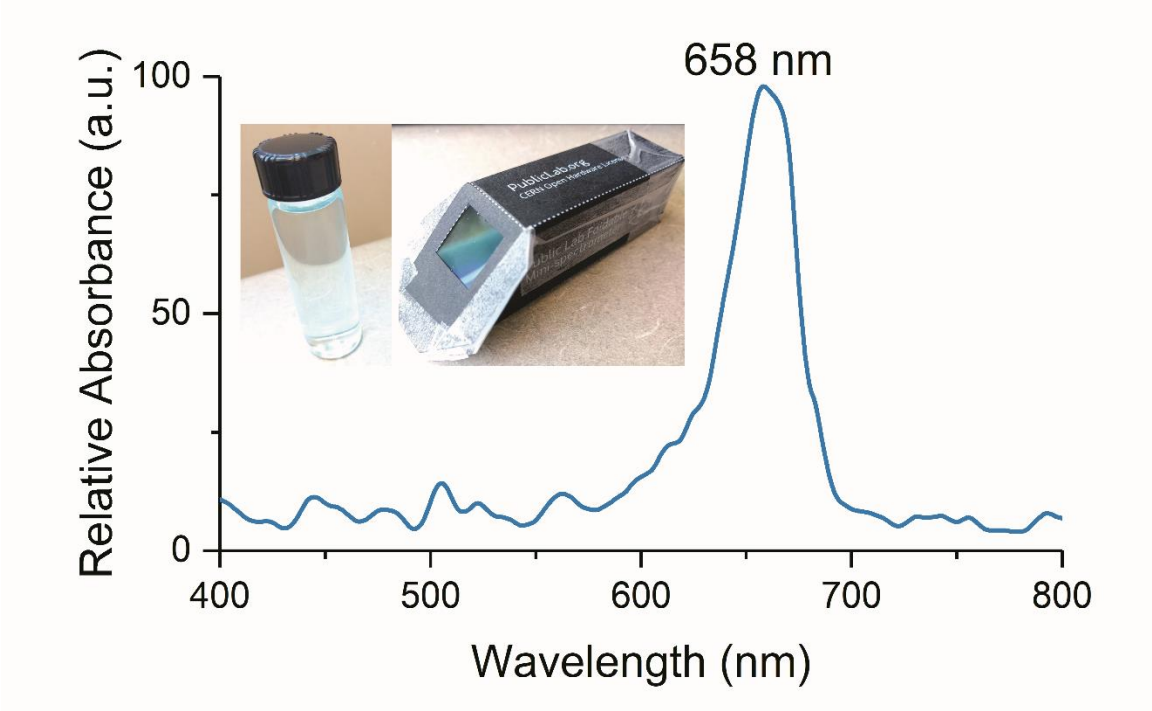

Figure 6. Absorption spectrum of a dilute copper(II) sulfate solution (inset: cardboard foldable spectrometer and copper(II) sulfate solution)

More pertinent is the prominent use of UV-Vis spectroscopy in the field of catalysis for characterization, *in situ* monitoring of reaction progress, identification of intermediate species, or in *in operando* spectroscopy when the aim is the identification of active catalytic sites.[28] Many examples of UV-Vis led investigations of homogenous catalytic systems appear in the literature. Examples include C-C cross coupling reactions (Suzuki, Heck, Sonogashira, Stille, etc.) of aryl halides,[71–75] catalytic oxidation of alkanes,[76] olefin

epoxidation,[77] Michael addition reactions,[78] cross-coupling reactions with Pd nanoparticles,[72–75,79,80] hydrogenation of olefins using supercritical CO_2,[81] and others.

In one example, UV-Vis was successful at monitoring the asymmetric hydrogenation of cyclooctadienyl as facilitated by the rhodium diphosphine catalyst.[82] This successfully demonstrates the usefulness of *in operando* spectroscopy. In this reaction, the reactive intermediate was presumed to be the rhodium-bound cyclooctene complex which was monitored through submersible optrode UV-Vis spectroscopy.

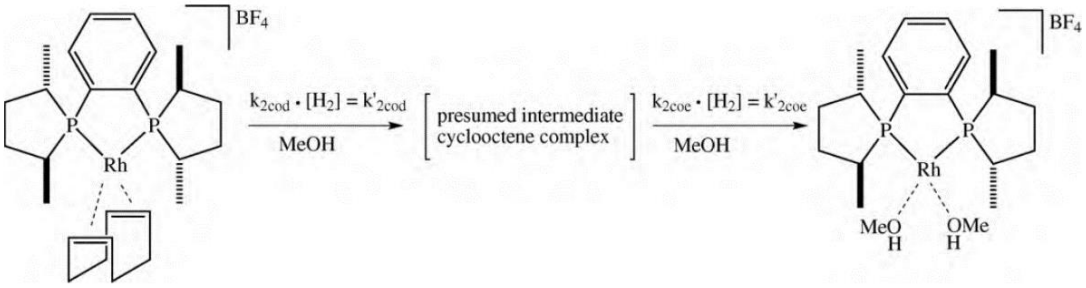

Scheme 1. Reaction scheme for the catalytic hydrogenation of cyclooctadiene[82]

This technique yielded kinetic information of the hydrogenation reaction through analysis of the extinction diagrams. On these plots, the change in absorbance of non-isosbestic points are plotted with respect to time and related to concentration by application of the Beer-Lambert law. The pseudo-rate constant k_{2cod} was determined to be 0.119 min^{-1} for the reaction. Several additional examples of these *in operando* techniques which employ UV-Vis to gather excellent mechanistic data appear in the literature, each of which with their own selectivity or sensitivity considerations.[82]

Further support for the value of spectroscopic techniques for the study of catalytic systems is evident in another example from a recent publication by Shi *et. al.* which presents a brief review of modern techniques used in the study of aqueous catalysis.[83] A noteworthy element of UV-Vis is time resolution which typically ranges between 0.1-1 milliseconds when monitoring a single wavelength (1-100 seconds when scanning many wavelengths with a monochromator). More modern diode array detectors (as in the instrumentation proposed below) may acquire full spectra in less than 10 ms which makes them ideal for rapid measurement of catalytic systems. Our fibre optic UV-Vis spectrometer is capable of a wide array of acquisition times based primarily on desired sensitivity (which is related to the exposure time with PDA instruments, for example) and rapidity of the analysis and will be described in more detail in Chapter 5.

Figure 7. Photo of custom PSI flask featuring openings for a fibre optic spectrometer and PEEK tubing

1.11 Practical Considerations

There are several factors to be aware of in order to study a catalytic reaction simultaneously with ESI-MS and UV-Vis spectroscopy. Despite both techniques having been proven as excellent techniques when applied to the study of homogeneous catalysis, the combination of the two techniques functioning smoothly and in-sync with each other generates its own issues. Indeed, a great deal of work is required to keep these very sensitive instruments in good working order.

For example, the current "UVMS" experimental setup involves the aforementioned fibre optic dip probe and a length of PEEK tubing extending to a Waters Triple Quadrupole Detector (TQD) mass spectrometer (figure 7). This setup means that the UV-Vis data appears immediately while the MS data is temporally offset based on the flow rate out of the PSI flask (affected by the overpressure applied to the flask as well as the length and diameter of the PEEK tubing used). Care must be taken to record this offset in acquisition and the data may be easily time-shifted as appropriate during the data work-up stage.

Operating parameters for ESI-MS have been very well documented throughout the years and many variables including source design, solvent composition, matrix effects and so on have been scrutinized for the analysis of a diverse array of analytes.[14,84–91] However, many catalytic reactions are typically carried out in organic solvents such as toluene, benzene, DMF, THF, dioxane, acetonitrile, and *tert*-butyl alcohol. The ESI amenability of these solvents range quite a bit; however, consideration should be put first toward dissolution of analytes since without homogeneity the analysis will fail. Since few of these solvents are

commonly used in ESI-MS, their behaviours can be unpredictable. Further, the choice of solvent may have an impact on UV-Vis. Not only does solvent affect absorption shifts, but the fibre optic dip probe cannot be exposed to particular solvents.

Additionally, both UV-Vis and MS are highly sensitive techniques and saturation effects must be considered. Several methods are available to sidestep saturation of either detector. The fibre optic probe has variable resolution. By adjusting the path length, the signal-to-noise (S/N) ratio can be adjusted to ensure any signals obtained are within an optimal absorbance range. For the mass spectrometer, there are several methods of adjusting S/N using the contemporary Waters Z-Spray source geometry including physically de-tuning the instrument or adjusting operating voltages and gas flow rates. The most obvious methods of minimizing saturating the MS is to reduce the concentration of analyte (either through splitting via T-joint, or in preparation) or reducing the MS detector power; nevertheless, initial experiments will be carefully tuned to ensure optimal S/N of all species present in the reaction system while avoiding saturation.

Finally, UV-Vis absorption bands are typically fairly wide and this UV-Vis yields no meaningful information regarding the structure of the compounds being sent through the instrument.[83] It is therefore important to differentiate by-products from expected products.

1.12 Conclusions

There is ample evidence to demonstrate the value of ESI-MS and UV-Vis investigations of chemical reactions as separate techniques. Surprisingly, these two have not been combined in the same reaction vessel to examine homogeneous catalytic reactions. Mass spectrometry is over 100 years old, and UV-Vis spectroscopy much older; however, much work is required in both camps to develop these for a combined approach. The study of organometallics with ESI-MS is relatively new and has grown dramatically in recent years. Continuing to enhance this tool for a general approach is needed to evaluate and improve chemical reactions. The aim of this dissertation, and the work presented herein, is to demonstrate that ESI-MS (as well as orthogonal analytical techniques) can be used to solve a plethora of chemical problems.

Chapter 2. Solvent Effects on Surface Activity of Aggregate Ions in Electrospray Ionization

Portions of this chapter have been previously published, and are reproduced in part with permission from "Solvent effects on surface activity of aggregate ions in electrospray ionization" J. Pape, K. L. Vikse, E. Janusson, N. Taylor and J. S. McIndoe, Int. J. Mass Spectrom., 2014, 373, 66–71.

Electrospray ionization is an appealing ionization source due to the retention of solution-phase information in the gas phase such that ions in solution are efficiently transferred into the gas-phase for analysis by mass spectrometry. However, the electrospray process is an intricate one and this must be contemplated when developing new procedures in order to optimize the quality of the data obtained.

The major stages of the electrospray process which carries an ion from solution into the gas phase are generally:

1. The generation of charged droplets at the tip of the charged capillary
2. Multiple charge induced fissions of the charged droplets leading to a reduction of droplet size and increase in droplet charge density
3. Discharge of ions from the charged droplet which proceeds via some mechanism. [92,93]

Several mechanisms for the transfer of ions in solution into the gas phase by ESI have been proposed, namely the Charged-Residue Model (CRM), the Ion Evaporation Model (IEM) and the Chain Ejection Model (CEM). These models seem to be given different weights depending on the situation. The mechanisms were meticulously explored by Konermann, et. al in 2013.[92] Low molecular weight species in particular seem to follow the IEM in which the charge on the analyte is produced via protonation. This model is based on the fact that the electric field of a Rayleigh-charged droplet is strong enough to promote ejection of small molecular weight ions from the droplet surface. The CRM follows more closely for the evaporation of larger, globular species (such as proteins) which are higher in molecular weight and often multiply charged. This model supposes that these analytes are sufficiently large that only a single analyte will evaporate into the gas phase following evaporation of the surrounding solvent layer. The evaporation of the solvent shell results in the ejection of the target, regardless of it's net charge. Finally, CEM has been proposed (with the help of molecular dynamics calculations) to effectively describe the sequential ejection of a large polymer chain or protein. In this model, the protein or polymer forms a compacted or folded structure which migrates toward the surface of the droplet following unfolding.

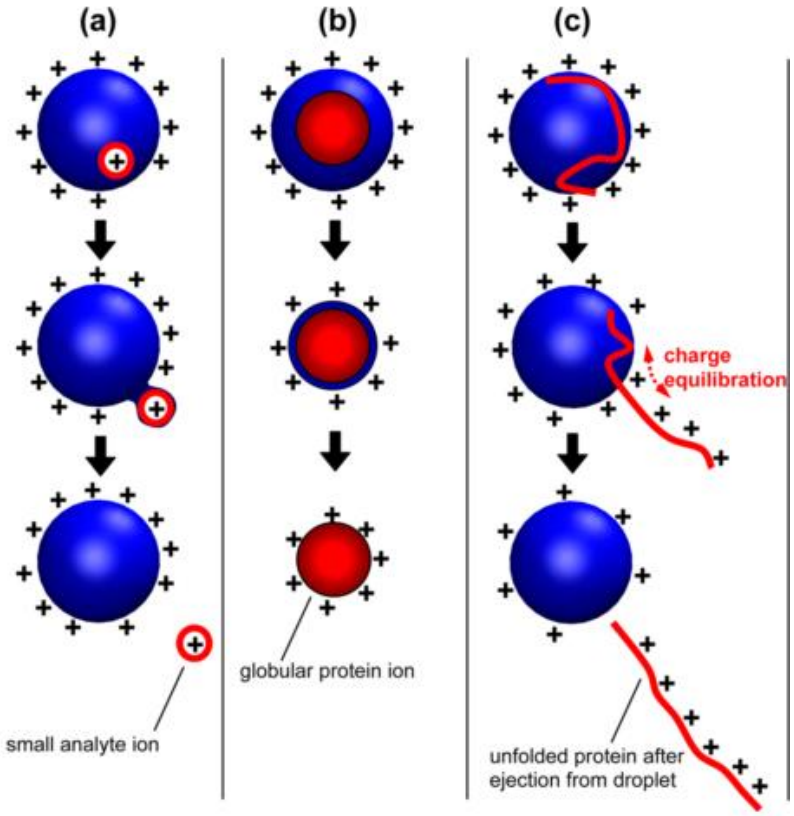

Figure 8. Examples of the three predominant theories for ESI mechanisms of analyte ejection from solvent into the gas-phase. a) IEM, b) CRM, c) CEM.[92]

Often overlooked is the surface activity of a given ion which plays a formidable role in the likelihood of evaporating from a droplet formed by the electrospray (the importance of which has been examined with laser ablation mass spectrometry).[94] The strong adsorption of a material at the interface between solvent and liquid is defined as the surface activity and can lead to preferential ion evaporation between very dissimilar analytes. The result of this effect is the propensity for ions to exhibit differential response over one another. That is, in equimolar quantities, a great difference in terms of absolute instrument counts may be observed. Consequently, an investigation of the response of a variety of ions in multiple solvents was warranted since it was expected that such an investigation could shed light on

both desolvation processes in ESI and the surface activity of the ions studied in the chosen solvent.

In general, ionic liquids (ILs) are salts composed of a heterocyclic cation such as imidazolium or pyridinium moieties which are often substituted. The inorganic counter-anion varies from halides to the non-coordinating anions tetrafluoroborate ($[BF_4]^-$) and hexafluorophosphate ($[PF_6]^-$), for example. As the name implies, ILs are a liquid at room temperature; however, the physical properties of the IL may vary substantially based on the properties and combination of cation, substitution, and anion. The archetypical ionic liquid is arguably 1-butyl-3-methylimidazolium hexafluorophosphate ($[BMIM]^+[PF_6]^-$);[95] the viscosity of this IL, for instance, can change considerably with a simple salt metathesis. Heavily substituted ionic liquids may exhibit an almost molasses-like viscosity at room temperature.

These compounds are useful and interesting for several reasons, some of which are especially appealing to us as ESI-MS users. Some interesting properties of ionic liquids include: [96]

1. ILs are effective in forming solvate complexes,
2. ILs exhibit relatively high conductivities and electrochemical stability (useful in developing supercapacitors),
3. ILs are reasonably thermally stable and,
4. ILs are exceptional at improving electrospray quality and exhibit profound electrospray activity on their own (of particular interest to us).[97]

Regarding point 4 above, the McIndoe group has been particularly interested in ILs in the past.[5,98] We wanted to explore the effect of solvent choice on differential response of ionic liquids in an electrospray. In the work discussed in this chapter, a cationic ionic liquid, butyl methylimidazolium (BMIM), was paired with a given counterion and mixed in various solvents in order to define the differential response observed in ESI-MS data. Subsequently, BMIM paired with a different counterion was added to the solution and analyzed by ESI-MS to determine the relative response ratio between two observable aggregates formed due to the mixture. The results obtained shed some light on differential surface activity of analytes in electrospray ionization when using a particular solvent. We initially postulated that analyte hydrophobicity had a profound effect on ion count of the analyte in question, depending on the solvent. As will be discussed, certain solvents are particularly suitable for the analysis of ILs and aggregates due to minimized differential effects whereas others serve to exacerbate this effect and produce potentially misleading spectra.

2.1 Introduction

2.1.1 Electrospray Compatible Solvents and Solvent Considerations

The choice of solvent for an ESI-MS analysis is typically based on solubility of the target analyte in that solvent as well as the compatibility of the solvent with electrospray. Solubility is extremely important since undissolved solids are extremely ineffective at

transferring to the gas phase via electrospray, are not inadequately drawn into the orifice of the mass spectrometer (pneumatically or electrostatically) and also serve to accumulate and obstruct the electrospray capillary or sampling cone, effectively terminating the analysis. Apart from analyte solubility, a range of criteria are used to designate a solvent as "ESI-compatible" and it is worth noting that "ESI-compatible" seems to mean different things to different research groups because of individual (or "case-to-case") purposes.[b] In general, however, the primary considerations for ESI-compatibility are the volatility (vapour pressure) of the solvent, the dielectric constant of the solvent, and, in some cases, the ability of the solvent to donate a proton thus facilitating production of the protonated ($[M + H]^+$) form of an analyte rendering it analysable by MS.

Solvent volatility, i.e. the rate of solvent evaporation, is imperative because it enhances the point at which droplets divide into smaller droplets which promotes the efficient production of gas phase ions in the ESI process.

The dielectric constant, or relative permittivity, is a decent gauge of a solvent's polarity. More specifically, the dielectric constant of a solvent is a measure of the tendency of that solvent to reduce the field strength of ions contained by the solvent. As a result, a solvent with a suitably high dielectric constant reduces the inter-ionic distance of ions within the solvent; that is, separation between charges in the solvent are minimized with increased dielectric constant (as per Coulomb's Law). Electrospray-generated droplets of this solvent

[b] This is especially true in my personal experience speaking with all sorts of ESI users and developers from research groups and manufacturer R&D personnel at MS focused conferences.

are continually reduced to smaller droplets via evaporation and as this process continues the ions contained within the microdroplets are packed closer together; in other words, the droplet radius shrinks while the charge within remains steady. Effectively, this increases Coulombic repulsion of surface ions to a point at which the ions are liberated from the microdroplets and thus promoting the generation of gas phase ions for MS analysis. The point at which the repulsive electrostatic forces become equal to, and subsequently exceed, the surface tension of the solvent is an interesting phenomenon and still closely studied.[92] As an additional note, a high dielectric constant is a reflection of the solvent's ability to dissolve ions and is therefore desirable not only to optimize ESI performance but to solubilize target analytes.

Spray stability of a solvent (or mixture) relies on the solvent meeting the aforementioned criteria. Water, perhaps the most widely used ESI solvent, is an excellent choice in this regard due to its high dielectric constant; however, it is less appealing for ESI considering its relatively low volatility. For this reason, water is commonly mixed with other organic solvents in order to maintain a reasonably high dielectric constant and enhance volatility for optimal spray stability. A 1:1 mixture of water and protic solvents (e.g. methanol) are extremely common to decrease surface tension. The added benefit of protic solvents is cationization of analytes via $[M + H]^+$ adduct formation; on the other hand, this adduct is also frequently, and oftentimes more efficiently, produced by the addition of low (0.1% v/v) concentrations of acid (e.g. formic or acetic acid). Aprotic solvents including acetonitrile and DMSO are very common and generally improve solubility as well as spray stability.

2.1.2 Ion suppression and less compatible solvents

Electrospray is a competitive process since there are limited surface sites available in an electrospray droplet. Ion suppression occurs when other more mobile ions or more surface-active constituents overwhelm the target analytes in an electrospray generated droplet through preferential evaporation. The result of ion suppression is diminished analyte signal and is therefore deleterious to quantitative ESI-MS experiments, if proper precautions are not carried out. This effect also limits the upper concentration range of ESI (though, it should be noted that the actual MS linear dynamic range is more completely described as a function of the sensitivity limits of the ion source, mass analyzer and detector, combined). At certain elevated concentrations, the complete occupation of droplet surface sites results in a nonlinear increase in signal with respect to rising analyte concentration.

Ion suppression is one of the more obvious issues that ESI users are well aware of and is something of particular concern among frequent users of intrinsically charge-tagged compounds (charged tags are discussed in more detail in Chapter 4). The issue of ion suppression is very frequently encountered with separation techniques such HPLC/ESI-MS in which matrix effects due to the presence of high buffer or salt concentration is deleterious to ESI spray quality and sensitivity through ion suppression as well as deposition or clogging. The composition of a sample (i.e. the sample matrix) is a more obvious source of matrix effects leading to altered instrument response most commonly via ion suppression. The sample matrix is especially problematic in quantitative ESI-MS

analyses of biological samples (plasma, urine, etc.) due to the substantial quantity of salts and lipids. Petroleum, another example of a complex matrix, is further complicated because of its exposure to various processes and additives through the course of extraction and refining (further discussed in Chapter 4).

Another means of ion suppression is ion pairing which can occur as a result of particular moieties present in solution or through the use of certain electrospray additives. Ion-pairing (or ion association) in solution effectively neutralizes the target compound and for this reason we typically use non-coordinating anions as counterions to our charged-tagged compounds in order to minimize this effect.

Finally, some solvents are exceptionally poor for ESI-MS use. Non-polar solvents, due to lack of conductivity, do not form stable electrosprays without the addition of electrolyte. In a (very) general sense, solvents less polar than dimethylsulfoxide are not appealing for use in quantitative ESI applications. Many ESI-MS setups, especially those with chromatographic separation techniques preceding the source, make use of polyether ether ketone (PEEK) tubing. Tetrahydrofuran reacts fairly quickly with PEEK rendering tubing made from this polymer swollen and unusable. Dimethylformamide, a useful organic solvent with a reasonably high boiling point, is tricky to purify, decomposes at room temperature, and leaves behind enduring contamination in the mass spectrometer. Spray quality, chemical compatibility, and contamination are certainly factors one should be aware of before considering a solvent for ESI-MS; however, many of these downsides can be subdued. Some of the worst ESI solvents, non-polar hydrocarbons such as hexane and

toluene, have been rendered usable through the addition of ionic liquids.[97] A close mimic of toluene, fluorobenzene, has been used with great success in the McIndoe group (and will be discussed in later chapters).[37] Chemical incompatibility with THF can be moderated through the use of fused silica or PTFE tubing, or slowed by employing a co-solvent. Instrument contamination due to solvent is a concern for maintaining an operable instrument; however, if some down-time is acceptable, the ion block and various source components can be stringently cleaned, polished, or replaced. While it is feasible to use a wide array of solvents, those presently used are chosen due to their relevance and commonplace in ESI analyses.

2.1.3 Surface activity and aggregation in ESI-MS

The term surface activity is used in a variety of disciplines and therefore somewhat context dependent. The concept is highlighted in catalysis,[99] adsorption,[100] host-guest interactions [101,102] and nanoparticles.[103,104] In ESI-MS, surface activity is an important process which describes how ions evaporate from ESI micro-droplets.[85,93,105–107] This mechanism assists in describing why particular analytes appear relatively overrepresented in an ESI-MS spectrum. Consider two chemically dissimilar cations, A^+ and B^+, which are both present in a solution to be analyzed by ESI-MS. The micro-droplets formed initially contain both A and B. If the solvent is most different in nature from A, then the overall solvation of A, relative to B, is minimized which promotes the presence of A at the air-to-vacuum interface of the droplet.[85] This renders A surface active while B remains preferentially solvated in the droplet.[85,108] Because ions that are the least well solvated or

ion-paired are most likely to be found on the surface of a droplet rather than in the core, they tend to appear over-represented in the ESI mass spectrum since they are more likely to evaporate from the droplet first.[109]

In a case where ions are more chemically similar, ESI-MS will yield a more reliable representation of the relative concentration of the analytes. This is an essential consideration when using an internal standard to determine analyte concentration; the relative concentration may not be accurate and is only a closer approximation if the internal standard and analyte(s) are more similar. For analytes that differ substantially in size or polarity, the ESI mass spectrum may produce an inaccurate picture of what is actually present in the analyzed solution.[108,110]

The nature of the solvent in ESI-MS plays a pivotal role in the absolute instrumental response of a given analyte. Between water and dichloromethane, we would expect a radically different result based purely on the physical properties of the solvent; whereas, methanol and acetonitrile might affect the results somewhere in between these two extremes.[108,110] For ESI-MS data to be reliably quantitative, situations in these (and other) common ESI solvents must be well understood.[111]

Aggregate ions are a common feature of ESI mass spectra, and are even exploited for calibration purposes. Mixtures of salts (sodium and cesium iodide, and sodium formate, for example) are often chosen for calibration because of the formation and appearance of regularly spaced aggregates due to strong ion pairing. Aggregates are of the form

$[(\text{cation}_{n+1}(\text{anion})_n]^+$ in the positive ion mode and $[(\text{cation})_n(\text{anion})_{n+1}]^-$ in the negative ion mode. For example, a solution of sodium iodide produces conveniently monoisotopic aggregates of the form $[(\text{Na})_{n+1}(\text{I})_{n+1}]^+$ which are used for mass spectrometer calibration in the positive ion mode. Ionic liquids exhibit this aggregation quite strongly,[112] and these "gaseous supramolecules" have been studied in detail.[34,113] Concentrated solutions (largely dependent on the experimental setup; however, "concentrated" here may be considered on the order of 10^{-4} mol·L^{-1}) are dominated by these aggregates, which become less prominent with decreasing concentration.

ESI-MS of dications with mixed counterions of the form [dication][I][NTf_2] exhibit positive ions of the type [dication + NTf_2]$^+$ preferentially over [dication + I]$^+$, but most markedly in water > methanol > acetone > acetonitrile.[98] However, there exists little to no experiments in the literature which compare the relative propensity of aggregate ions to appear depending on their molecular structure, nor have such experiments been conducted in various solvents.

2.1.4 The ionic liquids and their properties

For this investigation, we chose five different ionic liquids each containing the butylmethylimidazolium (BMIM) cation (see Table 1 for the physical properties of these ILs, along with the physical properties of water as a comparison), with anions ranging from the small and hydrophilic chloride ion to the large and hydrophobic bis(trifluoromethanesulfonyl)imide ion, $[N(SO_2CF_3)_2]^-$ (also known as bistriflimide and

abbreviated $[NTf_2]^-$). Table 2 details the size, surface area and volume of these anions, along with the standard molar Gibbs transfer energy for anions from water to 60:40 methanol/water (a measure of hydrophilicity).

Table 1: Physical properties of water and five butylmethylimidazolium salts.

Substance[114–119]	**Surface Tension (dyn cm^{-1} at 25°C)**	**Melting Point (°C)**	**Density (g mL^{-1} at 25°C)**	**Dipolarity / Polarizability (40°C)**	**Molar Mass (g/mol)**
Water	73	0.0	0.997	n/a	18.0
[BMIM]Cl	n/a (solid)	41	1.08	2.247	174.7
[BMIM]I	54.7	-72	1.44	n/a	266.1
[BMIM][BF_4]	46.6	-81†	1.12	1.647	226.0
[BMIM][PF_6]	48.8	10†	1.368	1.914	284.2
[BMIM][NTf_2]	37.5	-25‡	1.436	1.889	419.4

† Dried, ‡ water equilibrated. Note, "n/a" in this table represents unavailability of parameter.

Table 2: Properties of the anions.

Anion	**Structure**	**Molecular weight**	**Ionic Radius (pm)** [120–122]	**Surface Area†** **(Å²)**	**Volume†** **(Å³)**	**$\Delta_t G^{\circ\ddagger}$ (kJ/mol)**
Cl^-		35.45	184	39.9	23.7	7.0
I^-		126.90	220	51.5	34.8	2.6
[BF_4]$^-$		86.80	228	76.7	54.6	0.6
[PF_6]$^-$		144.96	254	100.7	73.1	-0.7
[NTf_2]$^-$	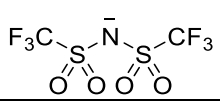	280.15	-	195.5	156.1	-

† Values calculated using Hartree-Fock at the 3-21G level of theory.
‡ Standard molar Gibbs transfer energy for anions from water to 60:40 methanol/water [123]

2.2 Effect of solvent on ionic liquid aggregate response

Each of the possible combinations of anions were mixed as their BMIM salts in a 1:1 molar ratio and the relative ratio of the peak areas of the two different aggregate ions (generally: $[(BMIM)_2 + anion]^+$) were measured in four different solvents: equal parts water/acetonitrile, methanol, acetonitrile, and dichloromethane (Table 3). [BMIM]Cl was not soluble in solvents less polar than dichloromethane, and $[BMIM][NTf_2]$ was not soluble in pure water, so these salts set the boundaries of what solvents we could reliably study.

The degree to which the hydrophobicity of an analyte influences ESI response may be estimated, and because of this, it is expected that more hydrophobic analytes in aqueous solvents will produce a greater ion count in a mass spectrum.[124] For example, chloride is the smallest of the anions examined and most likely to be strongly solvated by polar solvents, but least well solvated by non-polar solvents. Because of this, chloride containing aggregates are expected to be under-represented when compared to aggregates composed of larger, more hydrophobic anions in polar solvents. Conversely, this trend should be reversed in non-polar solvents.

Indeed, this effect is observed and is remarkably noticeable with pairs of $[PF_6]^-$ and $[NTf_2]^-$ aggregates. The response factor of the BMIM aggregates of chloride and other anions in acetonitrile are generally quite similar; however, in a water/acetonitrile mix and methanol the $[(BMIM)_2 + Cl]^+$ aggregate ion is barely measurable. This response is starkly juxtaposed with the response of the $[(BMIM)_2 + Cl]^+$ aggregate ion which is over-represented against all others in dichloromethane. This result suggests that the dichloromethane micro-droplets promote the surface activity of the chloride ions,

preferentially. Figure 9 shows the relative intensity comparison between aggregates containing Cl^- and $[NTf_2]^-$ in water/acetonitrile, methanol, acetonitrile, and dichloromethane.

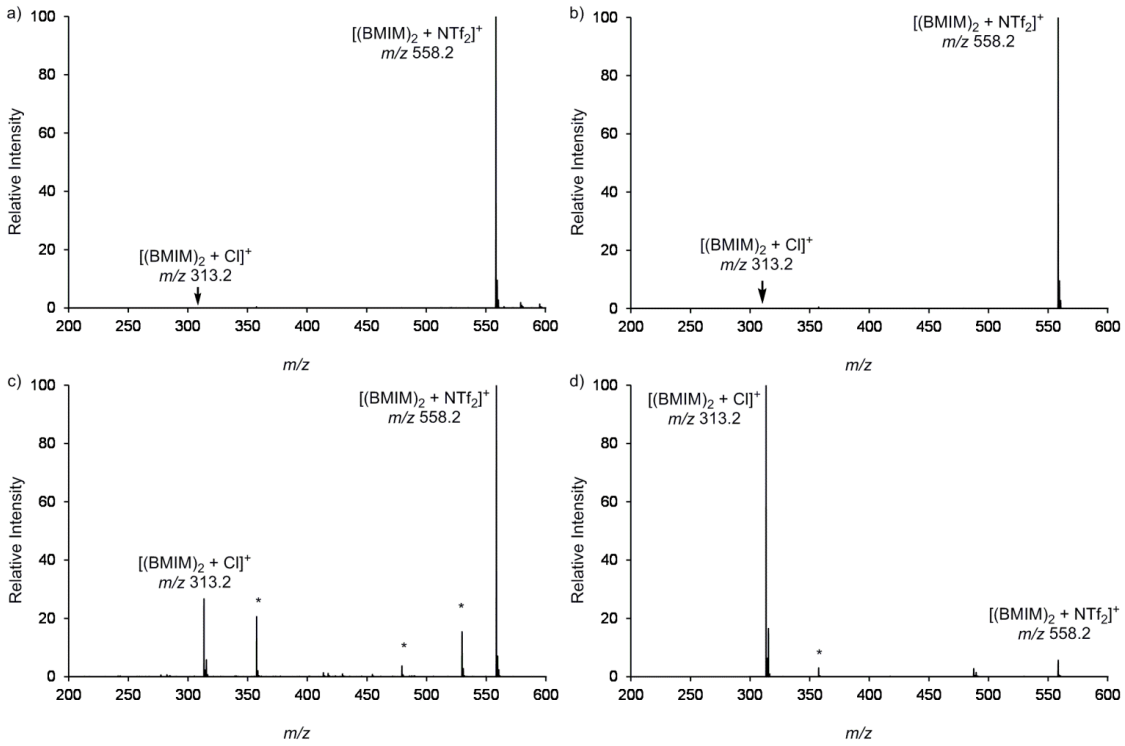

Figure 9: Positive ion ESI mass spectrum of a 1:1 mixture of [BMIM]Cl and [BMIM][NTf_2], showing the relative intensities of $[(BMIM)_2 + Cl]^+$ (*m/z* 313) vs $[(BMIM)_2 + [NTf_2]]^+$ (*m/z* 558) in a) 1:1 H_2O:MeCN, b) MeOH, c) MeCN, d) CH_2Cl_2.
Note: Peaks marked with a * are non-aggregate contaminants.

These experiments are representative of the trends in differential activity from one solvent to another. However, an important note on ESI sources must be considered in addition to these results. Electrospray source design varies from one manufacturer to another (and even between instruments from one manufacturer) and due to the abundance

of source designs a full quantitative investigation of ionic liquid aggregate activity is impractical.[90] As will be discussed in further detail in Chapter 3, the position of the spray head is also paramount in dictating differential response of analytes. The mass spectrometer used in these experiments (see Experimental) is equipped with a standard Waters Z-Spray ESI source. The nature of this particular electrospray source hinders this investigation somewhat due to the difficulty in controlling precise positioning of the capillary head relative to the source aperture. The spray head may be adjusted to the left, right, forward and away relative to the aperture of the instrument (but remains locked from moving above or below the aperture) by two knurled knobs with no indication or gauge of the absolute spray-head position without physical measurement. Because of this variance (and other practical considerations), large data sets are best acquired with as little delay or adjustments between experiments as possible. The spray head was kept in the same position for all experiments described herein and, where possible, datasets are collected on the same day. A follow-up study could be more quantitative if more stringent protocols are in place to guarantee that the source position is static and compared against multiple source designs.

The iodide counterion aggregate is overrepresented with respect to chloride-containing aggregates in water/acetonitrile, but underrepresented in the other solvents used. The most interesting difference with iodide is when it is matched up against other counterions. iodide, compared against the $[PF_6]^-$ and $[NTf_2]^-$ counterions in acetonitrile/water and methanol, is dramatically underrepresented. Compared to the $[BF_4]^-$ aggregate, the iodide aggregate is less abundant in all solvents; however, this trend is not as conspicuous in less polar solvents. Iodide and $[BF_4]^-$ behave similar to one another and this is most obvious when

these two are compared against the large and more hydrophobic anions $[PF_6]^-$ and $[NTf_2]^-$. The $[PF_6]^-$ and $[NTf_2]^-$ response factors are quite similar to each other but markedly different compared to other, smaller anions.

In water/acetonitrile, the overall relative surface activity is in the following order: $[NTf_2]^- \sim [PF_6]^- > [BF_4]^- \sim I^- > Cl^-$. The difference in magnitude of instrument response is greater than 500:1 in favour of $[NTf_2]^-$ compared to Cl^-. In methanol, the order is $[NTf_2]^- \sim [PF_6]^- > [BF_4]^- > I^- \sim Cl^-$, and the range of responses is similar to that observed in water/acetonitrile. In acetonitrile, all five anions provide similar responses, and there is no discernable order of preference. In dichloromethane, the most overrepresented ion is chloride (potentially from HCl contamination), and the overall order is the reverse of water/acetonitrile: $Cl^- > I^- \sim [BF_4]^- > [PF_6]^- > [NTf_2]^-$. The range of discrepancies, is less pronounced in water/acetonitrile or methanol, with a maximum difference of 6:1 in intensity between BMIM aggregates of chloride and $[NTf_2]^-$.

Higher order clusters are present only to a very small degree, and only in certain solvents. For example, the $[BMIM]_3Cl^{2+}$ cluster is present with reasonable intensity in DCM exclusively. In other solvents $[BMIM]_3Cl^{2+}$ is not above the limits of quantitation, as it is barely above background noise. This is also true for other higher order clusters containing $[NTf_2]^-$ which are generally not observed even with extended acquisition time (which improves the signal-to-noise ratio with increasing duration). There are several reasons why these particular higher order clusters are not seen. The most obvious reason is because the instrumental parameters which were used to collect all of the data for this project were not

optimized for the detection of these higher order clusters. A variety of parameters could be adjusted to facilitate the detection of these high order clusters including the position of the capillary to improve the response of particular aggregates (see Chapter 3), the potential applied to the skimmer cone which (at increased potentials) may fragment higher order aggregates, or the gas flow rates which may be optimized for a particular species. Adjusting and optimizing these parameters may help us observe higher order clusters; however, the appearance of larger aggregates is usually a function of the concentration of analyte introduced into the electrospray source. Consequently, the concentrations used in these experiments may not facilitate the formation of higher order aggregates. It is also possible that these larger cationic or anion aggregates are too fragile to endure the ESI process.

Expectedly, and in contrast to the high order aggregates, the free BMIM cation and anions of each ionic liquid are present in all spectra with high intensity. Ready dissociation of cation-anion pairs following dissolution is represented by the relative abundance of free ions in the spectra of these mixtures. Ions with particularly high charge density may reduce the absolute intensity of each other in ESI mass spectra via ion-pairing, a phenomenon which we generally try to avoid in order to improve signal-to-noise of the analytes. Ionic liquids are particularly suited to minimizing ion-pairing due to their relatively diffuse charge; therefore, it is of no surprise that the BMIM cation and associated counterions are prominent in all spectra. It is worth noting that the signal due to the free ions is sensitive to changes in instrumental parameters which promote fragmentation. In other words, increased ion energy readily separates clusters into simpler subunits which is indicative of the fragility of these aggregate species. The opposite is also true and instrument fine-tuning

is extremely important in producing an accurate representation of species in solution (an interesting case involving this issue is discussed further in Chapter 5).

Due to the differences observed in the mass spectra of identical mixtures of analyte in various solvents, we next contemplated what physical property (or properties) could predict the observed behaviour. Table 3 assembles the relative response ratio observed in a mass spectrum of each pairing of counteranions.

Table 3: Relative ratio of $[(BMIM)_2 + X]+$ vs $[(BMIM)_2 + Y]^+$ aggregates in four different solvents.

Matchups (X / Y)	1:1 H_2O: MeCN	MeOH	MeCN	CH_2Cl_2
Cl^- / I^-	**0.14**	**3.5**	1.8	**5.4**
Cl^- / $[BF_4]^-$	1.5	0.17	0.75	1.5
Cl^- / $[PF_6]^-$	***0.049***	***0.026***	0.74	**3.9**
Cl^- / $[NTf_2]^-$	***0.0017***	***0.021***	**0.15**	**19**
I^- / $[BF_4]^-$	0.41	0.69	0.88	0.92
I^- / $[PF_6]^-$	***0.061***	***0.023***	1.6	1.4
I^- / $[NTf_2]^-$	***0.025***	***0.018***	1.2	2.6
$[BF_4]^-$ / $[PF_6]^-$	***0.040***	**0.14**	0.34	1.1
$[BF_4]^-$ / $[NTf_2]^-$	***0.051***	***0.040***	0.88	3.0
$[PF_6]^-$ / $[NTf_2]^-$	0.41	0.37	1.3	0.96

Note: Response factors that are similar (differing by up to 3:1 in either direction) are represented normally. Those that differ by up to 10:1 are bolded, and those that differ by more than that are bolded and italicised.

Note that there are literally hundreds of different solvent polarity scales, [28] and selecting a representative one for consideration with these experiments was somewhat daunting. Table 4 includes the physical properties of the solvents used. Table 5 includes the Hansen solubility parameters,[125] which are advantageous as they are designed for solvent mixtures (and is therefore suited to deal with water/acetonitrile). The Hansen solubility parameters are based on the "like dissolves like" concept but categorize solvent properties (what they are "like") based on dispersion, polar and hydrogen bonding components. Effectively, this leads to a good discrimination between solvents such as methanol and acetonitrile due to consideration of their respective hydrogen bonding behaviours. On the contrary, other polarity scales such as the Snyder polarity index [126] and Hildebrand solubility parameter) [127] tend to lump these two solvents closely together.

Table 4. Properties of the solvents used in this study.

Solvent	Dielectric constant (ε_r)	Dipole moment (D)	Boiling point (°C)	Snyder polarity index (P')	Hildebrand solubility parameter (δ)
H_2O	80	1.85	100	10.2	21
H_2O: MeCN*	59	2.89	76	7.6	16.4
MeCN	37.5	3.92	81	5.8	11.7
MeOH	33	1.70	65	5.1	13.7
CH_2Cl_2	9.1	4.60	40	3.1	9.6

*All values are averaged, with the exception of the boiling point, which is that of the azeotrope.

Table 5. Hansen solubility parameters for the solvents used in this study.

Solvent	δD Dispersion	δP Polar	δH Hydrogen bonding

H_2O	15.5	16.0	42.3
H_2O: MeCN*	15.4	17.0	24.2
MeCN	15.3	18.0	6.1
MeOH	14.7	12.3	22.3
CH_2Cl_2	17.0	7.3	7.1

Considering the polarity of the solvents (Table 5) it became clear that solvent polarity alone does not sufficiently account for the ESI-MS observations and is potentially misleading since methanol and acetonitrile would be expected to behave similarly on this basis alone. The solvents that display the strongest selectivity between anions, water/acetonitrile and methanol, are both protic and hydrogen bonding solvents. Acetonitrile is a highly polar solvent; however, it is aprotic and exhibits substantially dissimilar behavior from the two protic solvents. This suggests that solvation of the anion may involve hydrogen bonding. Dichloromethane is relatively non-polar and aprotic, and the data collected using CH_2Cl_2 as a solvent suggests that the larger, diffuse, and hydrophobic anions are better solvated whereas the smaller and poorly solvated anions such as chloride are forced to the surface of the droplet and therefore overrepresented in the resulting mass spectrum. This is supported by data collected in both the positive and negative ion modes of the mass spectrometer. Both the solvent and the aggregate species are relatively small in size and because of this it is sensible to presume that these aggregates are formed in solution or within the microdroplets produced via electrospray. It also seems plausible that both the polarity of the solvent and its capacity for hydrogen bonding play a key role in the discharge of these aggregates from electrospray-generated droplets.

A comparison of the most dissimilar anions, Cl^- and $[NTf_2]^-$, in the most polar solvent, acetonitrile/water, demonstrates a strong suppression of the chloride anion (Figure 9a). This is true for solution in methanol (Figure 9b), and acetonitrile (Figure 9c); however, this completely inverts in dichloromethane (Figure 9d) in which the $[NTf_2]^-$ aggregate is suppressed. This is important for practical reasons and demonstrates the importance of solvent choice. That is, the results obtained via ESI-MS may span two orders of magnitude and change the primary species observed through a simple change in solvent.

Analogously, the less polar $[NTf_2]^-$ anion is drastically overrepresented in polar solvents. This anion favours the surface of the droplet due to decreased solvent interaction at the gas-liquid interface; hence, the anion is preferentially evaporated and borne into the gas phase facilitating its detection. This observation is consistent with the trend in the Gibbs energy of transfer ($\Delta_t G$) which is generally favourable (that is, a lower value) for the transfer of non-polar anions away from pure water and into a mixed methanol/water phase (Table 2). Relatively small anions, including those seen in this study, are expected to have a $\Delta_t G$ value which corresponds linearly to their volume; whereas, larger anions are more accurately related to their surface area.[128] Because the $[NTf_2]^-$ anion is relatively large, in terms of volume (6.6 times the volume of Cl^-), a small or potentially negative $\Delta_t G$ is expected which indicates a propensity for the anion to avoid aqueous solvation and, therefore, an inclination to migrate toward the surface of the droplet.

Around 90% of the response ratio results in acetonitrile demonstrate a 2× enhancement or a 1.5× suppression. This is in contrast to the results in an acetonitrile/water mixture in which only 10% of response ratios exhibit minimized suppression or enhancement. Also in the acetonitrile/water mixture, the larger and relatively non-polar $[NTf_2]^-$ anion was greatly enhanced in each combination of anions as were the majority of the results obtained with the $[PF_6]^-$ anion. In methanol, the anions behave similarly to that of the 1:1 acetonitrile/water solvent system. The anion behaviour in dichloromethane is most closely comparable to acetonitrile; however, the signal enhancement for chloride (the smallest anion used) is more pronounced. These trends appear to be linked to the protic/aprotic nature of the solvents. Water/acetonitrile versus acetonitrile are dissimilar in their anion aggregate responses due to the protic nature of water/acetonitrile and its ability to form an acetonitrile-rich azeotrope which possibly results in ESI-produced droplets largely composed of water.

Negative ion mode spectra were not thoroughly investigated as it was suspected that the negatively charged aggregates behave similarly to the positive aggregate species. Equimolar solutions of [BMIM]Cl and $[BMIM][NTf_2]$ demonstrate similar qualitative results. In dichloromethane, the negative $[(BMIM) + Cl_2]^-$ aggregate dominates over the $[(BMIM) + [NTf_2]_2]^-$ species; analogously, the reverse is true in methanol. This observation in the negative ion mode is consistent with the behavior seen in the positive ion mode and adds to the deduction that hydrogen-bonding solvent polarity is largely responsible for preferential ion evaporation. Not all pairings behave as expected, however. Equimolar solutions of [BMIM]I and $[BMIM][NTf_2]$ exhibit trends which are dissimilar to

what is seen in other anion pairings in the negative ion mode. For example, intermediate and high order aggregates including $[BMIM + I + NTf_2]^-$ and $[(BMIM)_2 + I_3]^-$ are detectable in certain solvents.

More importantly, the differential behaviours seen in the positive ion mode is not identical to what is seen in the negative mode. Free $[NTf_2]^-$ anion and aggregates of $[NTf_2]^-$ are the dominant species in all solvents used. In methanol and acetonitrile, the $[BMIM + (NTf_2)_2]^-$ aggregate behaves similarly to the trend noticed above, that is, it remains overrepresented compared to other anion aggregates in the positive ion mode. The dissimilarity arises in the negative ion mode when using dichloromethane or acetonitrile/water. In these solvents, the $[NTf_2]^-$ aggregates are overrepresented compared to the smaller iodide aggregates. It is worth noting that the negative ion mode work was performed separately from the positive ion mode experiments; that is, while the same procedure was used, instrumental variance over time and the precise positioning of the capillary are two major issues that may have affected the negative ion mode results. As will be discussed in the following chapter, capillary position can drastically alter the relative response of ions. Additionally, as a matter of experience, time can affect instrumental response due to the sensitive nature of the mass spectrometer. Within the interval of positive and negative mode experiments a variety of changes such as replacement of parts or variance in ambient conditions could have had an effect leading to the discrepancy with the negative ion mode results. While there is an imperfect agreement with some of the negative ion mode results, the positive mode trends remain explainable

and these experiments could be reproduced in a short course of time to further scrutinise the positive and negative ion mode results.

2.3 Conclusions

In measuring the relative responses of several ionic liquid-based aggregates in the positive ion mode, acetonitrile seemed to minimize the effects of differential surface activity and yield a more accurate representation of the concentrations used. The results in acetonitrile are still imperfect, however, the moderately polar aprotic solvent serves as the best choice for the analysis of dissimilar ions by diminishing the differential surface activity of dissimilar ions. These experiments also demonstrated a broader area of concern and prompted us to continue our investigation of differential response in the simultaneous analysis of chemically distinct ions with the electrospray source. The methodological approach taken to an ESI-MS analysis is seldom seriously scrutinized and the reasoning for a variety of important parameters – solvent choice, capillary voltage and position, cone voltage, gas flow rates, and so on – is rarely mentioned. Insufficient consideration of these effects could lead to misinterpreted results, especially in cases where matrix effects are likely or careful optimisation is not implemented.

2.4 Experimental

All salts were purchased from Sigma-Aldrich and used as received, except for [BMIM][NTf_2] whose preparation was based on a literature procedure.[129] Lithium

bis(trifluoromethanesulfonyl)imide (0.8 g, 0.003 mol, Aldrich) and 1-butyl-3-methylimidazolium chloride (0.5 g, 0.003 mol, TCI America) were each dissolved separately in 50 mL of deionized water. The lithium solution was added to the [BMIM]Cl solution with stirring. The solution became milky immediately and was allowed to sit for 45 minutes. The solution was heated at 55°C for 15 minutes after which point small oily droplets could be observed in the bottom of the flask. This material was extracted with dichloromethane (3 × 15 mL). The organic layer was washed with deionized water (5 × 10 mL) to remove any residual lithium chloride and starting material. The dichloromethane was removed via rotary evaporation resulting in 1.0 mL of liquid. The material was dried under vacuum for 48 hours prior to use.

For each test, a stable MS signal of a diluted ionic liquid (IL) was obtained (concentrations were 40 μM, 4×10^{-5} M). A second solution containing a different IL (in the same solvent) was then added in equal volume. The peaks monitored in this experiment were those representing the $[(BMIM)_2 + anion]^+$ cations. For comparison of IL signal intensity, a response ratio, defined as the peak area of the IL of interest to the second IL peak area, was calculated. In the absence of any signal response discrimination this procedure was expected to result in halving of the signal for the initial IL ions present while a secondary peak should also be observed at equal intensity for the IL added. If one signal is obviously favoured, it can be surmised that the ion-solvent interaction for that ion is less favourable resulting in surface enrichment and suppression of the other ion. The clusters were examined in the positive ionization mode using the full scan MS function on a

Micromass Q-Tof microTM mass spectrometer. Cone voltage was set low at 10V in order to minimize fragmentation of the aggregate ions.

Mass spectra were collected on a Micromass Q-ToF microTM mass spectrometer using pneumatically-assisted electrospray ionization. Capillary voltage: 2900 V. Cone voltage: 10 V. Extraction voltage: 0.5 V. Source temperature: 80 °C. Desolvation temperature: 150 °C. Cone gas flow: 100 L/h. Desolvation gas flow: 200 L/h. Scan time was 3 s and the inter scan time was 0.1 s.

Chapter 3. Spatial Effects on Electrospray Ionization Response

3.1 Introduction

We had demonstrated the impact of solvent choice on differential instrument response with ionic liquid aggregates (Chapter 2); therefore, we wanted to continue our investigation of the electrospray ionization source in order to better optimize ESI-MS for real-time monitoring. We were already aware that experimental parameters including the choice of solvent and the nature of the analytes of interest were highly important to the resulting spectra and were worth careful consideration before designing an ESI-MS procedure. However, missing from our prior investigation was a complete understanding of the plethora of other source conditions which potentially play a major role in what is observed. This seems to be a latent shortcoming in some of the literature involving ESI-MS analyses. Frequently, only the most experienced MS users fully understand the implications of a particular set of ESI conditions and instead rely on manufacturer recommended conditions or received wisdom to achieve quality results; therefore, we wanted to give a healthy amount of scrutiny to how we tuned the electrospray source to avoid any dangerous pitfalls. We were particularly interested in gaining a more quantitative picture of the effects of spray head position, as we have noticed the often dramatic effect

this can have on ion intensity. Surprisingly, optimization of the spray head position is usually not mentioned in user manuals or training programs from the vendors of ESI instruments.[130] More specifically, we were concerned with differential effects, that is, where moving the spray head affected one signal more than another.

A variety of instrumental parameters are involved in optimizing the electrospray source for the very general purpose of signal enhancement to facilitate detection and improve the signal-to-noise of a target analyte. With a conventional ESI source, the programmable source parameters include, but are not limited to, the following:

1. The capillary voltage – the potential at which the thin metal capillary of the ESI source is held at, relative to ground. This is used to produce the electrospray itself, generating highly charged droplets of the same polarity as the capillary voltage.
2. The cone voltage – the potential applied to the skimmer cone (relative to the extraction lens) employed in order to electrostatically draw gas-phase ions into the mass spectrometer.
3. Desolvation gas flow rate – generally a flow of nitrogen nebulizing gas which flows over the electrospray and promotes desolvation.
4. Cone gas flow rate – nitrogen gas flow out of the skimmer cone which is used primarily to protect the mass spectrometer source.
5. Desolvation temperature – temperature of the heater surrounding the spray head which promotes evaporation of the solvent.
6. Source temperature – temperature applied to cartridge heaters inside the ion block also used to promote solvent evaporation.

In addition to these important settings is the orientation (or position) of the capillary (spray head) relative to the sample cone. Many electrospray sources are equipped to move relative to the sample cone though the amount of control over capillary position varies heavily between instrument manufacturers and models.[90] We decided to examine how the parameters listed above could affect instrument response with respect to the capillary position using the common Waters Z-Spray ESI source. In the present work, the position of the spray-head, the solvent, and additional instrumental parameters were independently adjusted during the ESI-MS analysis of an equimolar mixture of two chemically distinct ions, bis(triphenylphosphine)iminium (PPN) and tetramethylammonium (TMA). Several of these parameters were found to have a profound impact on the distribution of signal intensity from one ion to the other, and therefore, the usefulness of the spectra acquired.

Each experimental parameter (such as temperature programming, gas flow rates and solvent choice) was individually adjusted prior to rastering the spray head across the operational plane in order to observe how adjustment to a particular parameter affected analyte signal in relation to the distance from the MS aperture. Following data acquisition, the intensities of PPN and TMA were plotted as ion contour maps which demonstrated the sharp contrast in ion intensity, and even differential ion activity, with relatively minor instrument changes. The data obtained from these experiments clearly established the importance of locating the optimal position for the ESI spray head for a high-quality analysis.

3.2 Electrospray Ionization Source Background

The electrospray process is sufficiently complex that despite several decades of widespread use, the exact mechanism of producing gas phase ions from condensed phase analytes in solution continues to be analyzed.[11] Adding to the intricacy involved in producing a more complete picture of the electrospray process is the development of various source designs and geometries. Common designs include the TurboV from MDS SCIEX, the Ion Max from Thermo Scientific, as well as the Waters/Micromass Z-Spray source design which is dealt with in the present work. Many of the modern designs from these manufacturers (e.g. Waters UniSpray Ion Source, Thermo Scientific EASY-Spray Source) build upon existing designs and are constantly improved with features such as Lockspray for enhanced calibration or "tool-free maintenance" for ease of use.

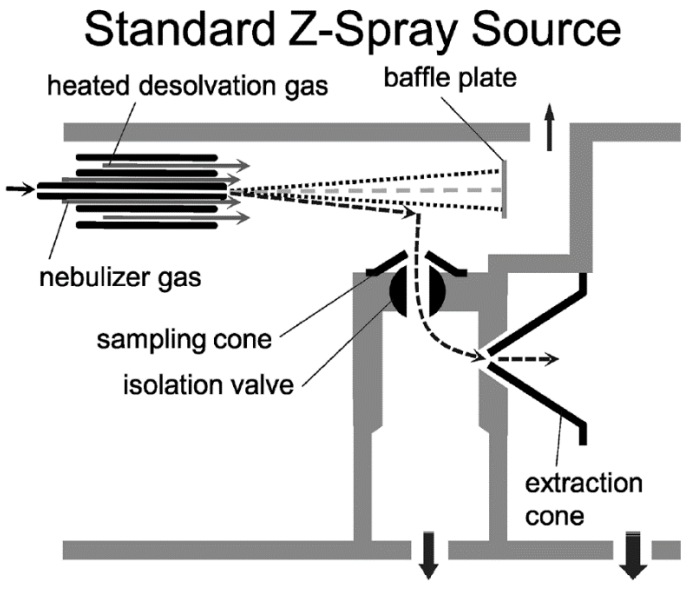

Figure 10. Schematic of the standard Waters Z-Spray source design

The spray head of an electrospray ionization (ESI) source contains the thin, highly charged metal capillary through which the solution to be analyzed is pumped. The spray head position is usually adjusted until an optimal intensity is achieved for the species under observation. While this method is generally effective, the lack of a systemic approach exemplified the need to study and understand how operating parameters factor into obtaining high-quality spectra.

Electrospray ionization mass spectra can be very sensitive to changes in source conditions, and there are several parameters that can be changed in order to optimize a particular experiment.[93] Electronically, the most significant settings are the capillary voltage and the voltage between skimmer cones which affects the electric field as the spray head position is adjusted which can have an effect on spray stability.[131] Thermally, the temperature of the source and of the desolvation gas can be independently adjusted over a wide range (typically from ambient to several hundred degrees Celsius). Volumetrically, the desolvation gas flow rate (as well as any auxiliary gas flows used to enhance desolvation) can be adjusted from tens to hundreds of litres per hour. Spatially, limited adjustments are available depending on the exact source employed.

Most conventional ESI sources are capable of some spatial adjustment of the coordinates and/or the azimuth of the spray head. Several of these designs, such as the Waters Z-Spray source used in this study, are oriented perpendicular to the skimmer cone of the mass spectrometer since sampling from this angle reduces MS contamination by electrostatically guiding ions into the instrument while neutrals are pumped away. The design of the Waters

Z-Spray source does not facilitate an accurate appraisal of where the capillary is positioned, that is, there is no built-in system for determining the exact placement of the capillary spray head relative to the sampling cone of the instrument. This is typically acceptable since the instrument is simply tuned to a particular analyte in many cases. For the purposes of these experiments, however, it was necessary to measure the limits of capillary positioning and subsequently implement a practical and simple method to determine where the capillary was at a given point in time. A set of calipers were used to accurately determine the extent of the attainable "*x*" and "*y*" coordinates. It was important to understand that the closest positions available were not conducive to ESI-MS analysis because of arcing (or corona discharge) between the highly charged capillary and the metal surface of the sampling cone. Corona discharge (CD) is an electrically generated plasma produced via ionization of the gas surrounding the highly-charged capillary which produces a characteristic light-blue glow.[132] In addition to this, the high voltage of the capillary can induce an electrical arc when brought in close proximity to a conductive surface. Corona discharge is a well-known phenomenon amongst mass spectrometrists as it is often exploited in another ambient ionisation technique, atmospheric pressure chemical ionisation (APCI), to produce gas-phase ions.[133] For electrospray users, CD and arcing are often an unwanted side effect since the high-energy plasma can break down target analytes and produce erroneous signals in the mass spectrometer. Indeed, with our test mixture there was a limit to how close the ESI probe could get to the sampling cone before arcing, and complete loss of signal, occurred. With this knowledge, we mapped out an area of sampling equal to 11.25 mm in the "*x*" direction (arbitrarily assigned as movement perpendicular to the sampling cone)

and 7.5 mm in the "*y*" direction (arbitrarily assigned as movement parallel to the sampling cone).

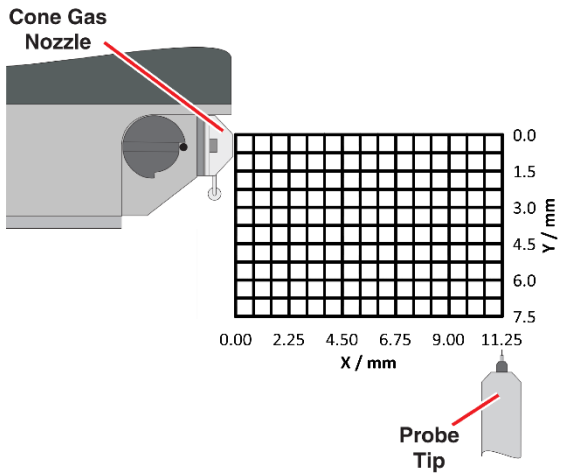

Figure 11. Illustration of the spray head in its most distant position with respect to the aperture. The grid defines the locations of each analysis.

The two knurled knobs used to control the position of the spray head yielded a change in either the *x* or the *y* axis of 1.5 mm with one full turn; therefore, we marked the knobs to determine a one-half turn of each of the two knobs corresponding to a change of 0.75 mm in either the *x* or *y* direction. Accurately marking the capillary facilitated many repeat experiments between multiple operators. Our sampling grid consisted of 176 points at which to acquire data for each experiment in order to produce a highly-detailed contour plot of ion intensities with respect to exact capillary position. The origin of this grid was assigned to the closest point the capillary could be set without resulting in arcing or corona discharge.

Typically, the electronic, temperature, and gas parameters are reported since these are expected to most significantly impact the data collected. The reported parameters very rarely include the physical geometry of the source. Generally, this position is left alone; however, there are cases in which the source position is tweaked in order to improve performance or moved more substantially if spray conditions are adjusted. For example, the McIndoe group frequently employs charged tags to highlight components of a reaction mixture.[45] Because these tags are specially designed to be highly lipophilic and are paired with non-coordinating counter ions, they are exceptionally surface-active and therefore provide tremendously intense spectra even at very low concentrations.[2,4,32,45,134] This is a very effective technique to detect species of interest because ionization efficiency is not a limiting factor; however, this consequently limits the upper concentration range available for an experiment and the McIndoe group often finds detuning of the ESI source necessary to reduce the sensitivity of the instrument to these charge tagged compounds. Reducing sensitivity by adjusting the spray head position is common procedure for ESI-MS analysis; however, the effect this has on analyte response is poorly understood and could end up adversely affecting results if one species becomes substantially overrepresented.[135]

Electrospray ionization has become increasingly popular as an investigatory tool in the study of reaction mechanisms [33,40] and its explorative capacity may be strengthened with a greater knowledge of instrument response with respect to the position of the capillary spray head, along with other experimentally-controlled conditions. In particular, it is important for reproducibility purposes across different concentration ranges that we

are not perturbing the relative response of different ions, because such effects may produce misleading kinetic data.

Because we mostly use permanently charged ions in our analyses of catalytic reactions by ESI-MS, [1,39,40] we chose to use two very dissimilar salts as analytes. The analytes used in this study were an equimolar mixture of bis(triphenylphosphine)iminium (PPN) chloride and tetramethylammonium (TMA) chloride (Figure 12). We selected two such dissimilar cations for two main reasons:

1. Mass and shape: TMA ($[NMe_4]^+$) is small (*m/z* 74) and near-spherical whereas $[(Ph_3P)_2N]^+$ is large (*m/z* 538) and dumbbell-shaped.

2. Chemical composition: chemically similar ions expectedly spray in a fairly similar fashion. In order to best examine the effects of differential ion response, somewhat disparate analytes are a necessity.

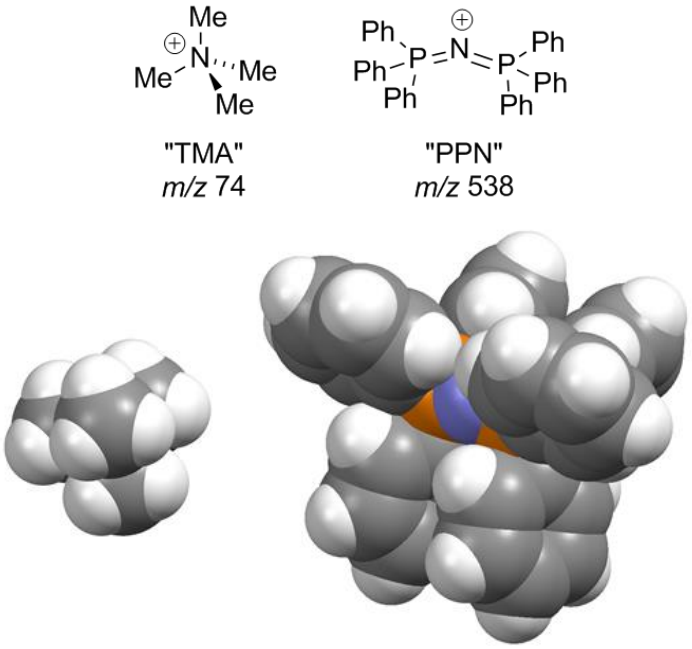

Figure 12. The two cations investigated in this study. Space-filling models were generated from published crystallographic data files.[136]

In polar solvents, PPN is less well solvated and therefore more likely to be found on the outside of a charged droplet, that is, due to the higher surface activity of PPN it is therefore generally over-represented in the spectrum.[107] It should be noted that the counterion for each cation is identical (Cl^-) so as to eliminate any variation due to ion-pairing; additionally, the two analytes used were ammonium salts so that an effective comparison of signal intensity could be made. Because the two cations are quaternary ammonium ions, both are fully dissociated in solution. Sufficiently high concentrations of such salts will cause the observation of aggregates of the form $[(\text{cation})_{n+1}(\text{anion})_n]^+$ in the positive ion mode,[34] but these experiments were run at sufficiently low concentration to avoid appreciable quantities of such aggregate ions. Furthermore, because both compounds are chloride salts, and *m/z* 50 is the lower limit of the mass range of the Q-ToF Micro mass spectrometer, investigations were carried out in the positive ion mode exclusively. Using the PPN chloride, $[(Ph_3P)_2N]Cl$, and TMA chloride, $[NMe_4]Cl$, test mixture we were able to thoroughly examine the issue of sampling efficiency and gather information regarding ESI probe spatial effects for the two analytes.

3.3 Methodology Development

Several important operating parameters should be noted prior to a discussion of our findings. $[NMe_4]Cl$ and $[(Ph_3P)_2N]Cl$ were mixed in a 1:1 molar ratio in several solvents, and run at a concentration of 26 $\mu mol \cdot L^{-1}$. This concentration was chosen after

experimenting with a range of values from an order of magnitude above and below, and this concentration avoided aggregation issues while preserving good intensity across the range of parameters investigated. In order to extract meaningful data across the majority of the source positions, it was necessary to use elevated salt concentrations. That being said, the highest observed intensity does not surpass the limit of saturation of the MCP detector of the instrument. Rate of infusion can alter relative ion intensities; thus, a constant infusion rate of 10 µL/min was employed for all experiments. A full table of experimental conditions is available in the appendix for this chapter (Table 10). Additionally, a cross section diagram of the Q-ToF Micro and Z-Spray source may be found in the appendix for this chapter. The spray head was rastered across an area 11.25 mm in the y direction and 7.5 mm in the x-direction in 0.75 mm increments. Data were collected throughout this process and manipulated in OriginPro 9.1 to generate a 3D surface of intensity vs. position for each ion which are presented throughout this chapter. These contour plots have been color-coded for interpretability such that PPN ion intensity is represented with a blue surface and TMA with green. Scan times were set between 1 and 5 seconds with an interscan time of 5 seconds to allow for repositioning of the capillary; all data were normalized to a 1 second acquisition time before plotting. Each 3D map involved the collection of 176 unique spectra, and a total of 352 intensity values (one for each of TMA and PPN in each spectrum).

3.4 Effect of capillary position on ESI-MS response

For our first set of experiments, we chose to work with acetonitrile under "normal" ESI operating conditions. "Normal" operating conditions are a set of manufacturer suggested conditions involving a source temperature at, or just slightly above the boiling point of the solvent used, a desolvation temperature equal to the source temperature plus 100° C, as well as a cone and desolvation gas flow rate of 100 $L \cdot hr^{-1}$. The reasoning for initially using acetonitrile was based on a multitude of factors, including our experience working with a variety of solvents for the ESI-MS analysis of intrinsically charged analytes (Chapter 2). Acetonitrile is one of the most frequently employed organic ESI-compatible solvents (the criteria for an "ESI-compatible" solvent is discussed in Chapter 2), along with small alcohols (methanol, ethanol, etc.). Methanol and water are also used in the following experiments, both of which are extremely common ESI-MS solvents. Pure water is an underwhelming ESI solvent primarily because it is limited in terms of its low vapour pressure. Because of this, it is common to see mixtures of water and some organic solvent (MeCN and MeOH especially) to ameliorate the shortcomings of pure water. Aqueous mixtures generally deliver a very stable ESI environment featuring high analyte solubility and efficient desolvation. For simplicity, we avoided aqueous mixtures in the present work and opted to examine the behaviour of pure water.

The general response to capillary position was largely as anticipated; that is, when the capillary was at its most remote, ion intensity was low, and as the capillary was moved closer, ion intensity increased. This behavior is illustrated in Figure 14, which is a contour map of ion intensity of the PPN and TMA cations versus capillary tip position, where the

x and *y* values are in millimetres away from the closest possible position to the cone aperture.

It was immediately obvious from the initial experiments that there was a large area in which ion intensity was consistently strong; near where the capillary and instrument aperture are closest. When the spray head is furthest from the skimmer cone, there was typically a large dead area of little to no intensity. In several experiments; however, the region of maximum intensity for PPN and TMA was observed at a far y-axis distance but a shallow x-axis distance. Presumably, this is indicative of an optimal point at which the electrospray plume has sufficiently evaporated and is very effectively drawn into the mass spectrometer.

Following a closer comparison of instantaneous spectra acquired in acetonitrile very near versus very far from the skimmer cone in the area sampled it became clear that the response for both TMA and PPN was not linear and was indicative of divergent behaviour (Figure 13).

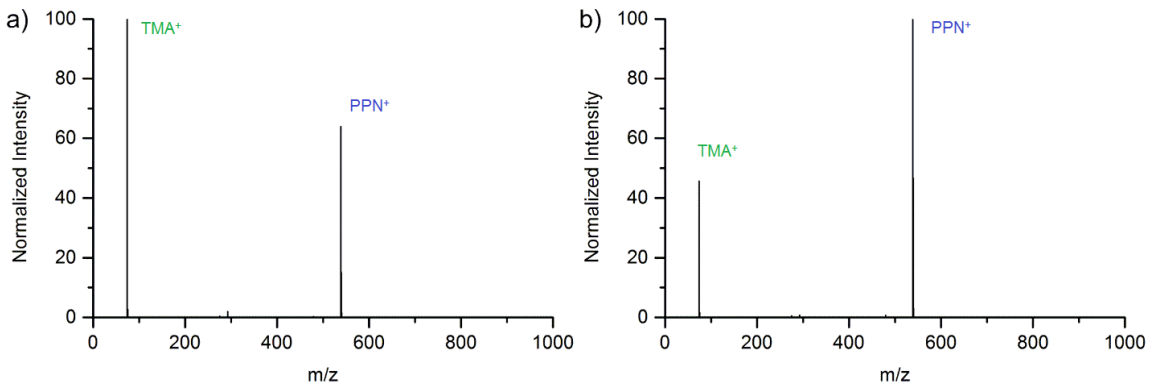

Figure 13. Mass spectra of 26 µM PPN (*m/z* 538.2) and TMA (*m/z* 74.1) in acetonitrile for capillary positions (a) far and (b) near the mass spectrometer aperture.

In order to better visualize this behaviour, we decided to plot the intensity of each ion as a contour map with the surfaces of the two ions plotted together, for simplicity (Figure 14). With most cone-to-capillary distances, the spectrum seems to consist almost entirely of PPN. This trend is especially true with shorter distances and the reverse is true at long distances, albeit in a narrower region.

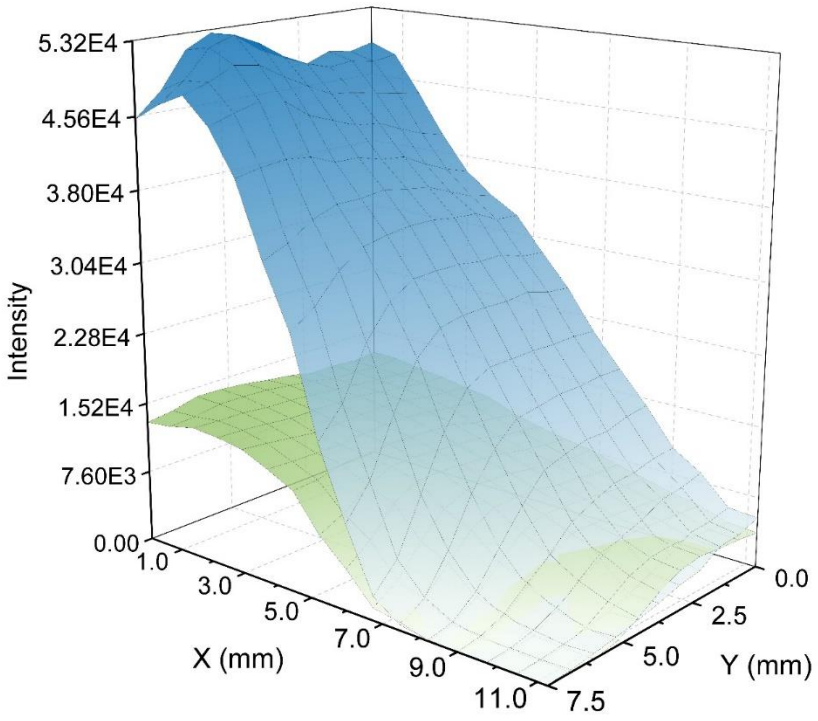

Figure 14. Overlaid ESI-MS intensities of an equimolar mixture of PPN and TMA at varying capillary positions. Note the divergent behaviour far from the MS aperture.

The physical properties of each cation must be considered in order to explain this behaviour. TMA is a small and nearly spherical cation with a substantially smaller cross section than PPN. The size of TMA relative to PPN may be an important factor in electrostatically drawing these ions into the instrument from a longer distance. A greater

ion mobility may mean it is more efficiently transferred into the mass spectrometer. In contrast, PPN dominates the spectrum at closer distances. Because PPN is a relatively bulky and hydrophobic cation, it possesses a high surface activity; therefore, this trend may be due to a greater affinity for the surface of the droplet and a preferential "early" ion evaporation from the electrospray.

In a more prosaic sense, these preliminary results demonstrated to us just how sensitive the ESI mass spectrum is to instrumental settings, especially in cases where the ions are dramatically different in nature. Simply applying a response variation factor to two different ions without ensuring that other parameters are equivalent is a recipe for results that are misleading at best. Given the dramatic differences in response factor that we saw with probe position, we then decided to determine if these differences were consistent when other parameters such as solvent, desolvation and cone gas flow rate, and source and desolvation gas temperature were varied.

3.4.1 The effect of solvent

The relationship between surface activity, solvent and ion signal in electrospray has been investigated previously in the McIndoe group and several others;[88,91,92,108,110,137,138] however, the importance of capillary position relative to the sample cone has only limited detail in the literature.[89,139–142] Zenobi demonstrated that solvent polarity increases when the droplets become smaller at the periphery of the plume or further away from the emitter.[143] Though a great variety of solvents and ESI source arrangements have been

utilized, the relationship of these two parameters together has not been rigorously investigated.[84,90,144,145] Our investigations using multiple solvents clearly demonstrates capillary position plays an important role in ion selectivity.[91] The effect on ion intensity from one solvent to another can be dramatic and should be taken into account for any quantitative experiments.

Running the experiment in methanol led to almost complete suppression of the TMA signal by PPN by a factor of greater than 1500:1 across the entire area examined (Figure 15). In fact, the only region where TMA had any appreciable intensity at all was when the capillary was near the cone in the *x* direction, but far from it in the *y* direction. This increased discrimination between ions is presumably a function of the enhanced solvation of TMA vs. PPN in methanol, which encourages PPN to occupy the surface sites of the droplets and accordingly over-representing the signal due to PPN ions. So-called "offspring droplets" are thought to contain disproportionate quantities of the excess charge (~15%) compared to the total mass (~2%) of their precursors,[107,122] and hence we may expect that sampling the plume at distance may increase the amount of the most surface-active ion observed.

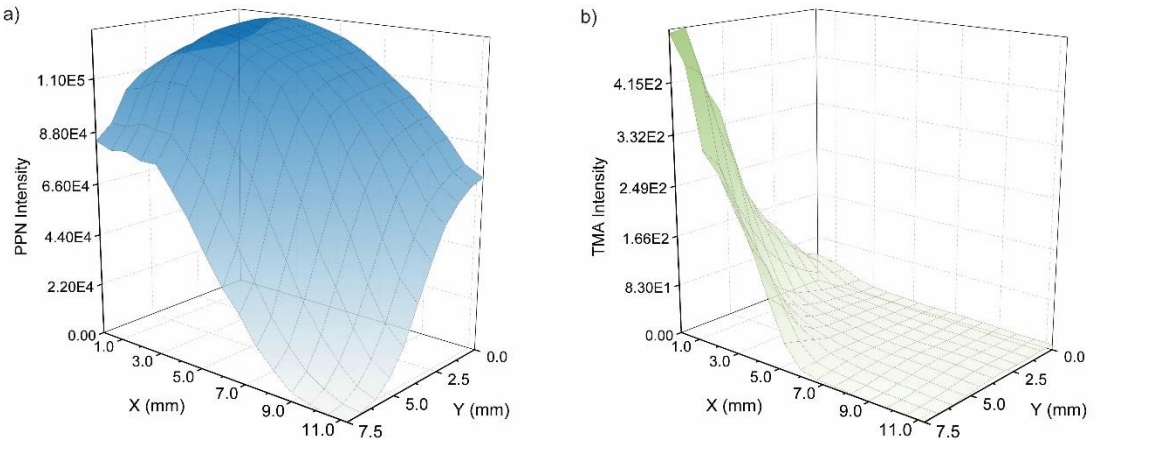

Figure 15. Intensity vs. capillary position for a) PPN vs. b) TMA in methanol. Note the difference in the vertical axes in the two plots (0-150,000 vs. 0-500).

Using water as a solvent, the spectra acquired demonstrated similar behaviour to those acquired in methanol (Figure 16). PPN dominated in the majority of the sampling area; however, these regions of high intensity were much more localised. The dead zone for PPN was sizeable, and notably extended into the area where the capillary was very close to the cone. This behaviour is almost certainly a function of the fact that the "normal" desolvation conditions used were not optimized for water, and the degree of droplet desolvation was insufficient at shorter distances. Through the course of the experiment, condensed water was observed on the baffle opposite the capillary tip which is evidence of insufficiently vigorous desolvation conditions.

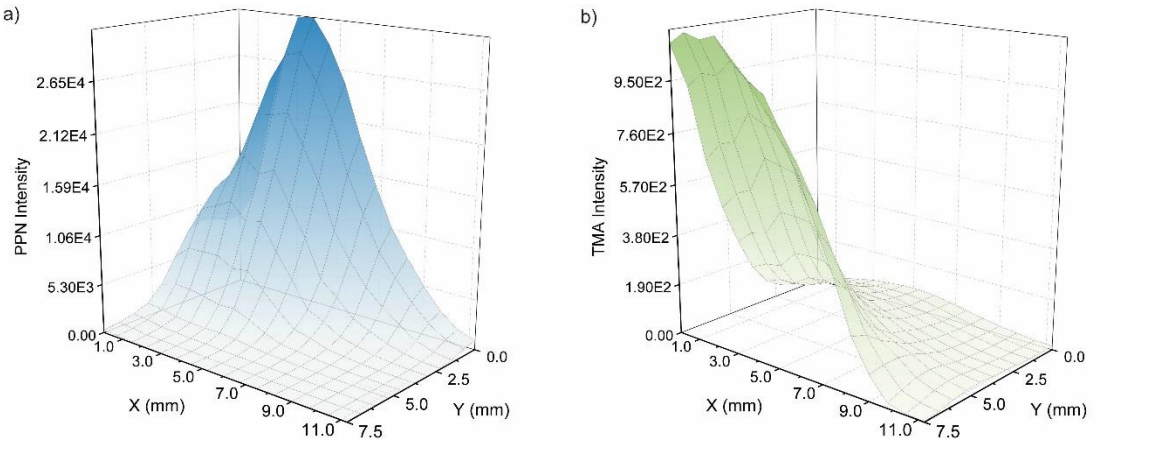

Figure 16. Intensity vs. capillary position for a) PPN vs. b) TMA in water. Note the orders-of-magnitude difference in the vertical axes in the two plots.

The nature of the ESI process supports the variation observed from one solvent to another. The nebulization of solvent droplets with high charge density promotes the liberation of highly mobile ions from the droplets. We would expect, therefore, that because of the differential ion mobility between TMA and PPN one ion may be given preference for desolvation from these droplets and therefore appear overrepresented in the spectrum.[85,106,122,146–148] In most solvents, PPN overwhelmingly dominates the spectrum which is indicative of the high surface activity of the bulky cation. Despite this affinity for the droplet surface, the position of the capillary is a critical factor in signal optimization as evidenced by the poor desolvation of PPN in the majority of the two-dimensional sampling plane when using water as the solvent. Movement of the capillary outside of the "sweet spot" for a particular analyte throughout the course of an analysis could lead to substantial quantitative error.

3.4.2 Gas flow rates

Aiding in desolvation are the streams of (generally an inert gas such as nitrogen) sheath gas emerging from the spray head as well as the sampling cone referred to as the desolvation gas and cone gas, respectively. The cone gas and desolvation gas flow rates may be manually adjusted across a wide range, contingent on application and instrument capabilities, and are known to alter the response of the instrument. It was therefore important to perform the experiment with varying nitrogen gas flow rates in order to investigate the effect this had on instrument response across the operational plane.

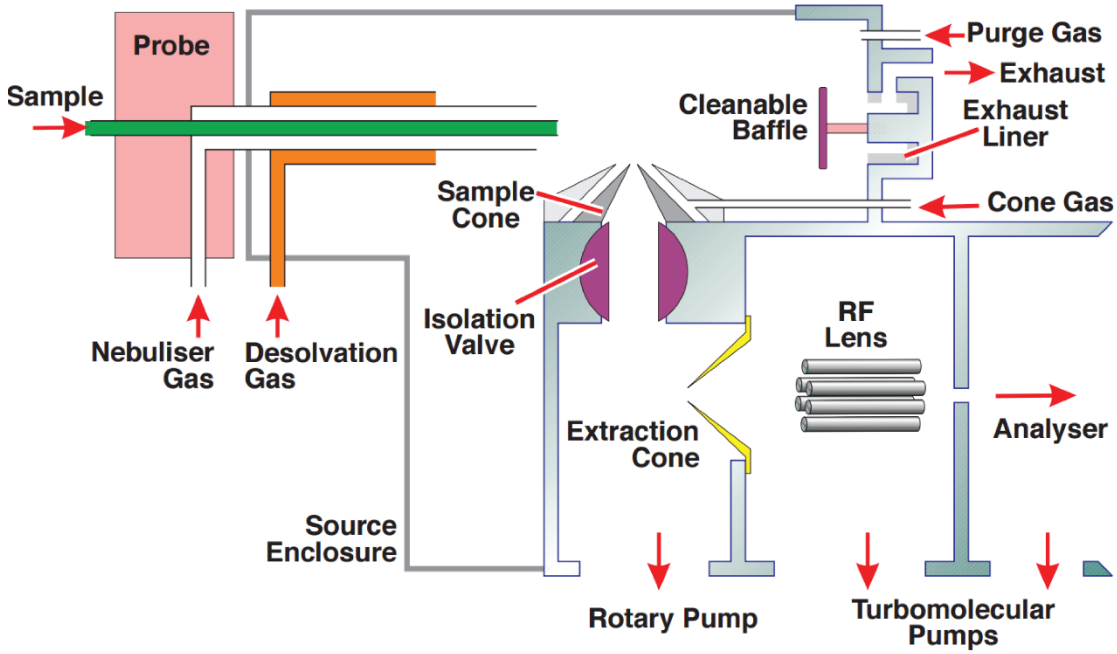

Figure 17. Waters Z-Spray Source Cross Section (adapted from Waters Q-ToF Micro User's Guide)

The purpose of the sampling cones (or skimmer cones) is to provide a smooth transition from the atmospheric pressure of the source to the high vacuum of the mass analyzer (see Figure 17 for a schematic). While the sampling cone is positioned perpendicular to the spray head (in a typical Water Z-Spray ion source and other similar source geometries), the cone gas provides additional protection from contamination for the mass spectrometer

while at the same time enhancing analyte desolvation. Increasing this flow rate in certain situations includes the added consequence of preventing larger aggregate species from entering the source. Based on a variety of factors, the cone flow rate is generally set somewhere between 100 to 300 $L \cdot hr^{-1}$. Plots were collected with low cone gas flow rates of 100 and 50 $L \cdot hr^{-1}$ for the sake of comparison. As seen in Figure 18 (a and b), the difference in flow rates was observed to have minimal effect on the intensities of either of the two ions across the area sampled. The profile and intensity of both plots (for 50 and 100 $L \cdot hr^{-1}$ cone gas flow rate) are very similar across the entire plane, suggesting a higher flow rate may be an unnecessary strain on gas reserves unless solvent adducts or cluster ions are observed.

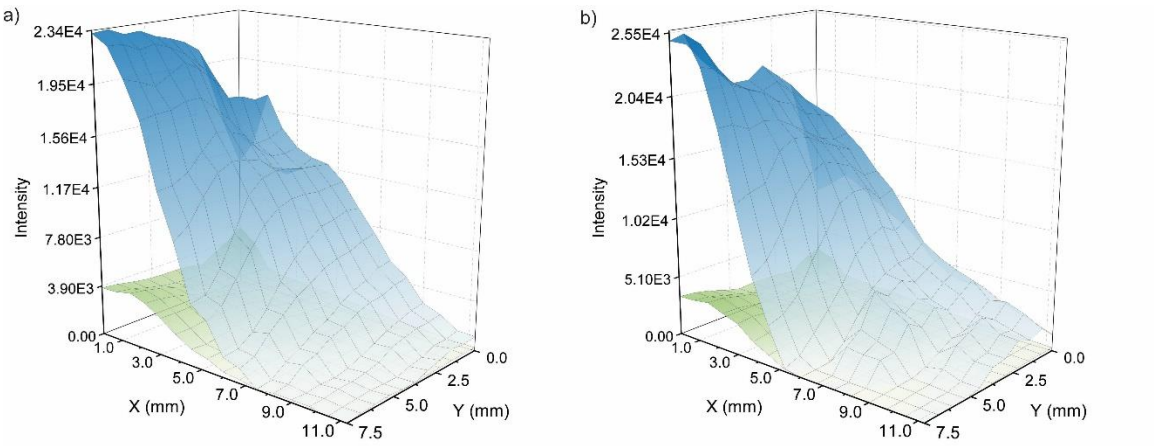

Figure 18. PPN (blue) and TMA (green) ion intensity at 26 µM in MeCN with a) 50 $L \cdot hr^{-1}$ cone gas flow rate and b) 100 $L \cdot hr^{-1}$

Conversely, changes in desolvation gas flow rate result in dramatic changes to signal intensity and profile (Figure 19). The considerable effect on the signal intensity of each ion with respect to adjustment of the desolvation gas flow rate demonstrates the importance of this parameter in facilitating the transfer of ions to the gas phase. Although, it appears that

there is a “sweet spot”. Desolvation gas flow rates of 50 and 200 L·hr^{-1} yielded similar results for TMA. The limited enhancement of PPN intensity observed at a medium flow rate of 50 L·hr^{-1} is possibly influenced by instrumental variance; however, it may be true that a decreased gas flow rate is optimal for this analysis.

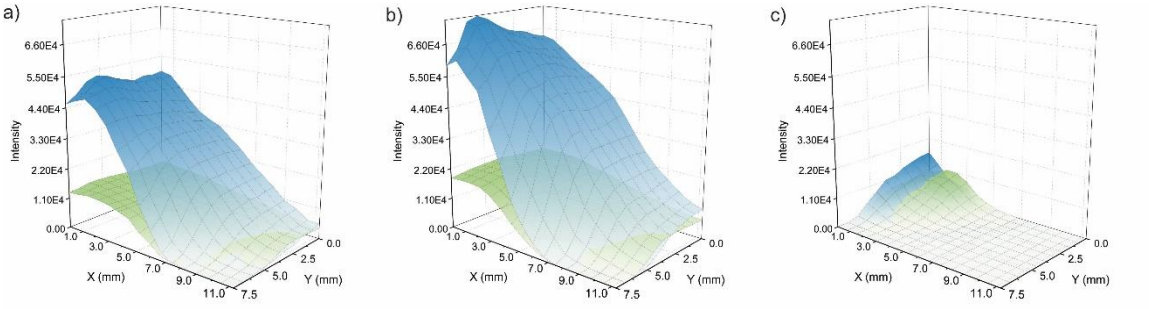

Figure 19. PPN and TMA Ion Intensity at 26 µM in MeCN with a) 200 L·hr^{-1} desolvation gas flow rate, b) 50 L·hr^{-1} and c) 25 L·hr^{-1}

One can imagine that a turbulent gas flow within the source could reduce effective ion transfer; however, it is also important to understand that the flow rates used in these experiments are on the lower-end of gas flow rates used in some routine ESI-MS analyses (which may surpass 1000 L·hr^{-1}) and it is unlikely that the differences here are due to an unstable ESI spray as a result of extreme desolvation gas flow rate. At a very low flow rate of 25 L·hr^{-1}, the intensity of the PPN ion in particular dropped off considerably which suggests inadequate desolvation except perhaps near the center of the plume (i.e. where the capillary is close to the cone). The increase in intensity near the origin (0 mm, 0 mm) for the lowest gas flow rate is very likely due to the increase in field strength as the capillary approaches the sampling cone. All source voltages are kept constant throughout all experiments and it is worth noting that a study of field strength effects with respect to

capillary orientation could produce an additional chapter of a similar length. A future investigation of capillary position should examine the effect of spray head position with respect to variance in field at the probe tip to further improve the ESI source. Predominantly, the results obtained for changes in desolvation gas flow rate are sensible and but may contribute to differential analyte response in some cases. In general, an increased desolvation gas flow rate enhances desolvation and improves signal; however, there also exists a practical upper limit at which considerable increases in gas flow rate do not appreciably enhance analyte response. As expected, either ion has a distinct range in which its response is maximized which may be exploited depending on the nature of the analyte. Finally, unwanted suppression of an analyte could be minimized by adjusting not only the capillary position, but also optimizing the desolvation gas flow rate.

3.4.3 Temperature Programming

Temperature programming for a typical electrospray ionization setup involves two parts of the ESI source. The “source temperature” parameter adjusts the temperature of the heater encircling the probe which facilitates desolvation at the early stage of the electrospray. The metal housing to which the sampling cones are attached and where the extractor cone may be found is referred to as the ion block. Inside the ion block is a pair of cartridge heaters which warm the bath gas emerging from the sampling cone. The cartridge heaters are controlled by the “desolvation temperature” parameter. These two heaters are crucial for solvent evaporation and therefore the effects of temperature programming have been studied in some detail;[149] however, their effects with respect to capillary position had not

yet been examined. These previous studies demonstrated the importance of temperature programming and the profound effect of source temperature on the electrospray process.[150,151] As an example of the consequence of temperature optimization, the source temperature has been shown to have considerable effects in ESI-MS by facilitating desolvation with the unwanted consequence of thermal denaturation of proteins during analysis.[152,153] Source and desolvation temperature are independently controlled and they affect the transfer of solvated analytes to gas phase ions in slightly different ways. Because of this, the effects of each temperature parameter will be discussed separately.

3.4.4 Source Temperature

The temperature of the source is generally set at or slightly above the boiling point of the solvent used in order to promote desolvation. Increasing this temperature above the boiling point is usually necessary in order to offset the low vapour pressure of certain solvents (aqueous solutions, for example) or compensate for high solvent flow rates (greater than 500 $\mu L \cdot min^{-1}$). Three source temperatures were used for the analysis of an equimolar mixture of PPN and TMA in acetonitrile (b.p. 82°C): 39°C (low temperature), 89°C (medium), and 150°C (high). During these experiments, the desolvation temperature (and all other parameters) were held constant.

Source temperature variation yielded effects that were reminiscent of changes to desolvation gas flow rate. At a lower source temperature, the ion count is zero across much of the plane and is present in appreciable counts when the capillary is very close to the

aperture of the instrument (Figure 20). Notably, PPN does not dominate across the majority of plane while the source temperature is low; instead, the signal for PPN is much sharper and localized near the source. In contrast, TMA is overrepresented across a broader area (than PPN) when capillary is extremely close to the sampling cone and a short distance away. This is a demonstration that small and more mobile ions are readily evaporated from the electrospray plume even at reduced temperatures.

Increasing the source temperature to 89°C promotes desolvation and therefore signal intensity as more ions are liberated from the electrospray. Moreover, the increased source temperature vastly improves analyte response over the majority of the capillary plane when compared to a lower source temperature. A wide region of high-intensity signal that appears at high temperature is shared by both PPN and TMA, especially closer to the sampling cone; however, much of the sampling area features an overwhelming response from PPN over TMA.

Notably, the increase in temperature from 89°C to 150°C gave rise to only minor changes in the contour plots for both PPN and TMA. The maximum response, for TMA in particular, is nearly identical at both 89°C and 150°C while a small enhancement is observed for the upper limit of PPN counts near the sampling cones. High signal intensity persisted for greater "Y" distances from the MS aperture at a source temperature of 89°C than at an elevated temperature of 150°C (the sharp drop in signal is particularly noteworthy for PPN) (Figure 20). This indicates that optimizing sensitivity by adjusting the source temperature greatly above a solvent's boiling point is slightly beneficial

especially in cases where even small signal-to-noise enhancement is important. For small and hydrophobic ions, such as PPN and TMA, the benefit of increased source temperature is underwhelming. However, well-solvated and highly functionalized molecules such as peptides could greatly benefit from an increased source temperature. In addition to notable differences in which the signal from one ion dominates the spectrum, the gradient of intensity across the X direction between temperatures is interesting. A sharp change in intensity is observed with both PPN and TMA signal with small changes to the X position; whereas, changes to the Y direction result in relatively minor intensity differences.

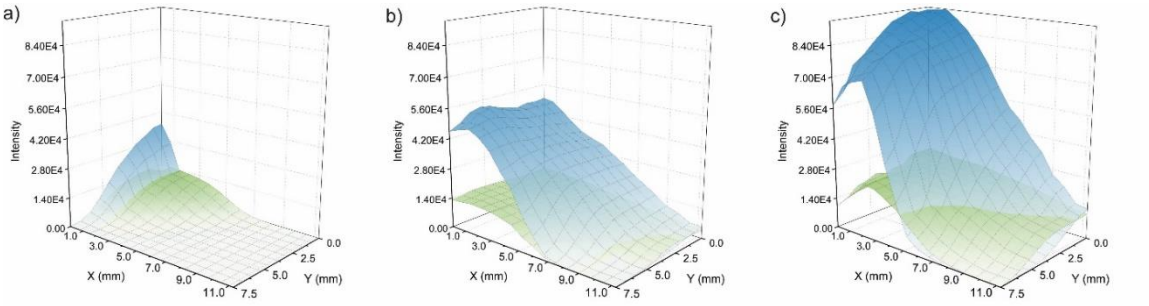

Figure 20. PPN and TMA ion intensity at 26 uM in MeCN with a source temperature of a) 39°C, b) 89°C, and c) 150°C

3.4.5 **Desolvation Temperature**

The source temperature was left constant just above the boiling point of acetonitrile for investigations of the desolvation temperature parameter. In contrast to the source temperature, desolvation temperature has little influence on instrument response across the temperatures used. The contour plots for a desolvation temperature of 89°C and 189°C are very similar in terms of overall shape and intensity (Figure 21); therefore, the temperature

of the warm bath gas emerging from the aperture of the instrument is less important than other parameters in optimizing signal intensity. Notably, the maximum intensity for both PPN and TMA are insensitive to a 100°C difference in desolvation temperature.

That being said, the profile for TMA and PPN intensity both demonstrate an extended area of high sensitivity as the capillary is moved away from the MS aperture. Extended Y positions are attainable with higher sensitivity at elevated desolvation temperature, though the favourable X positioning is narrowed perpendicular to the aperture. Interestingly, the higher temperature preserves the advantageous surface activity-driven advantage of PPN over a wider range of capillary positions. At lower temperature and furthest extents of capillary position, TMA is relatively competitive with PPN and divergent behaviour between ions is evident. Sensibly, a reduced desolvation temperature should decrease the rate of solvent evaporation, which inhibits droplet fissioning events; however, the data obtained for this specific experiment seems to suggest that ion evaporation is the dominant process as small and highly mobile ions are readily evaporated from the electrospray plume, even at reduced temperatures. In other words, at lower desolvation temperatures, the small and highly mobile TMA ion is more efficiently transported across the long distance from capillary to skimmer cone.

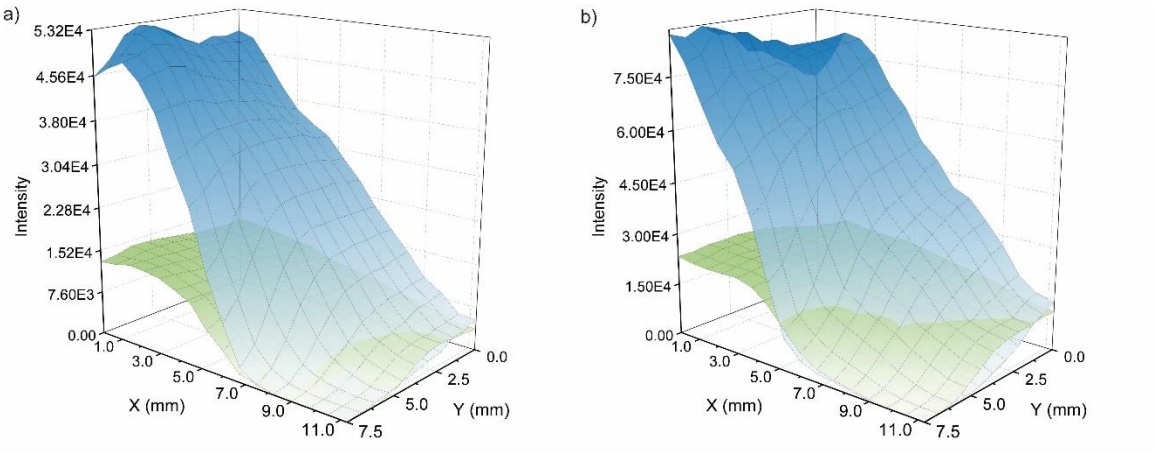

Figure 21. PPN and TMA ion intensity at 26 uM in MeCN with a desolvation temperature of a) 189°C and b) 89°C

3.4 Conclusion

The relative and absolute ion abundances of PPN and TMA cations were examined with respect to capillary position for a range of common experimental parameters for ESI-MS. ESI is an excellent sample-introduction mechanism as it provides effective liquid-to-gas phase transfer for the effective analysis of ions in solution by mass spectrometry. However, due to the variability of source parameters, a more rigorous investigation was needed. The observation and reporting of ionization suppression using a Z-spray mass spectrometer front-end was an important and much-needed contribution to the field; additionally, the study was unique in that it highlights the possibility that relative response of different analytes can shift depending on source geometry. In general, the evidence obtained suggests variation in the x-axis distance between the MS aperture and the spray head have a greater impact on signal intensity than do changes in the y-axis. Discrepancies in ESI-MS response to different analytes is a well-known phenomenon, which can be affected

greatly by experimental conditions as evidenced by the data collected. However, the geometry of the source not only affects the overall sensitivity of the technique, but in extreme cases, the relative response of two ions can even reverse. It is important to keep this divergent behaviour in mind when implementing ESI-MS due to the great deal of tunable parameters, variations in sample preparation, source geometries and designs, and supplementary variables associated with ESI-MS analysis.

3.5 Experimental

Solvents and chemicals were purchased from Sigma-Aldrich. Anhydrous and air-free acetonitrile and methanol were purified with an MBraun solvent purification system before use. Deionized water was obtained from a Millipore Milli-DI water purification system. Equimolar 100 mL solutions of bis(triphenylphosphine)iminium chloride and tetramethylammonium chloride were separately prepared in a variety of solvents at a concentration of 26 $\mu mol \cdot L^{-1}$. This solution was fed into the ESI source through the use of a syringe pump and a Hamilton GASTIGHT® analytical syringe connected to a fixed length of PEEK tubing. The flow rate was set to 10 $uL \cdot min^{-1}$ for all experiments. Prior to each run, instrument cleanliness and stability was ensured through rinsing with the appropriate solvent and acquisition of stable analyte signal from the subsequent sample solution. After achieving a steady signal the spray head was moved to a known position, furthest from the mass spectrometer aperture. Data points were acquired with 1-5 seconds of scan time and 1-5 seconds of interscan time. The relatively high scan and interscan times ensured that high quality data was obtained and plenty of time was allotted for

smooth movement of the spray head to each desired position in the xy plane. Movement in the xy plane was tracked by markers affixed to the ESI probe adjustment collars, corresponding to a distance of 0.75 mm in the x-direction and 0.75 mm in the y-direction. Five runs were repeated in the forward and reverse direction, then compared to ensure reproducibility of the data acquired. Furthermore, the experiment was found to have excellent reproducibility through the comparison of several trials performed with the same experimental parameters. Data analysis was assisted by Chemcalc.org.[154]

All electrospray ionization mass spectra were collected in the positive ion mode on a Waters Micromass Q-TOF Micro mass spectrometer. While many settings were adjusted throughout the course of the experiments, the following parameters were left constant throughout. The capillary voltage was held at 2.9 kV, cone voltage at 15.0 V, and extraction cone at 0.5 V. The collision energy was left quite low at 2.0V since the intrinsic charge of the analytes used effected an excellent signal. The MCP detector on the instrument was set to 2.7 kV. Most other parameters varied according to what was being investigated during that particular experiment. Inter-scan time varied according to the operator's preference, as each operator may require more or less time to reach the desired acquisition point. Accordingly, inter-scan time is not expected to have any effect on data acquisition. Several trials were run with similar conditions and combined to form an average of several runs. In the event that the scan time differed, the runs were weighted based on scan time before averaging. Once completed the data from the run was extracted through selected ion monitoring (SIM) of *m/z* 538.2 for PPN and *m/z* 74.1 for TMA and

was subsequently plotted by relating the acquisition time of individual points to the position of the spray-head.

Chapter 4. Selective Mass Spectrometric Analysis using Charge-Tagged Reagents

Portions of this chapter have been previously published, and are reproduced in part with permission from "Janusson, E.; McGarvey, G. B.; Islam, F.; Rowan, C.; McIndoe, J. S. Selective mass spectrometric analysis of thiols using charge-tagged disulfides. *Analyst.* **2016**.

Other portions of this chapter have been submitted for publication, and are reproduced in part with permission from "Zhu, H.; Janusson, E.; Luo, J.; Piers, J.; Islam, F.; McGarvey, G. B.; Oliver, A.; Granot, O.; McIndoe, J. S. Phenol-selective mass spectrometric analysis of petroleum fractions. *Analyst.* **2017**.

4.1 Introduction and Background

Petroleum is an accumulation of hydrocarbons beneath the ocean or ground, which range from simple to highly complex compounds composed of hydrogen and carbon which, at standard temperature and pressure, may be gaseous, liquid, solid, or in a mixture of states.[155] As a decomposition product of flora and fauna remains, it is naturally an incredibly complex matrix containing thousands of diverse compounds which primarily consists of high concentrations of olefinic and aromatic hydrocarbons. Petroleum also contains small quantities of complex heteroatomic compounds containing sulfur, nitrogen and oxygen, in addition to trace amounts of metals.[155] Furthermore, petroleum is a non-

uniform substance and may vary widely in chemical composition between wells, or even within the same well.

There is no doubt that petroleum is an extremely valuable resource used in numerous applications. Following 1940, roughly 6 million barrels were consumed per day which drastically increased to approximately 97 million barrels per day in 2016.[156–158] Due to growth in usage of this resource, much research is directed at the reduction of environmental impact, and improving extraction and exploitation of this resource while avoiding a multitude of foreseeable complications. In order to facilitate this, there is a need to develop processes for the extraction of harmful compounds which requires a clear understanding of the chemical composition of crude oil and its fractions.

4.2 Unwanted chemical components

Several impurities, containing a variety of chemical moieties, exist within petroleum products and many of these species are hazards to the environment or a health concern. One of the most important factors during processing and refinement of petroleum is ensuring such contaminants are effectively removed or reduced to acceptable levels. Some exemplary natural contaminants of petroleum products are sulfur-containing molecules which can be corrosive, lethal if inhaled, and environmentally harmful without proper sulfur removal process (also known as “gas sweetening”).

In addition to naturally occurring contaminants, it is well known that petroleum distillate streams contain both naturally occurring contaminants in addition to added chemicals used in a variety of recovery and refinement processes. For example, emulsifiers, wetting agents, foaming agents and surfactants may all be used in the extraction of crude oil. It is therefore not surprising that some of these processes play a role in contamination of the resource before it reaches the refinery and that this contamination persists into the final products. Knowledge of these treatments and processes is crucial as this may provide some insight toward the identification of contaminants in a particular sample. The following is a brief introduction to the extraction processes used and the reason they are of concern to the petrochemical industry as a source of potential contamination.

4.3 Petroleum Extraction and Enhanced Oil Recovery

In many cases the intrinsic pressure of a petroleum reservoir is sufficient to initially produce some oil from the well; however, as the natural pressure of the reservoir is decreased other mechanisms must be implemented to recover the remaining crude oil. These supplementary techniques are referred to as “enhanced oil recovery” (EOR). EOR encompasses non-conventional techniques such as thermal, miscible and chemical recovery techniques.[155]

Chemical EOR processes comprise the more expensive (and possibly more effective) methods at the frontier of research efforts. These increasingly elaborate petroleum extraction processes add to the complexity of the petroleum matrix which can complicate

refinement. Enhanced oil recovery techniques are employed with increasing frequency especially as displacement techniques such as polymer, microbial and alkaline surfactant flooding become more efficient.[159,160] The principal goal of chemical recovery methods is the reduction of capillary forces within the well as well as increasing the viscosity of fluids used to pump the oil out of the reservoir.[161] This involves the addition of polymers, surfactants or other chemicals to the reservoir. Polymers are added to the displacing fluid (typically water) if the oil is much less mobile than the fluid, otherwise the fluid may overtake the oil. Surfactant flooding (also known as "micellar flooding" or "micro emulsion flooding") is used to collect droplets of oil still contained in capillaries of the reservoir after water-based drives have been used.[155] The amphiphilic nature of surfactants allows them to emulsify very small amounts of oil by this reduction in tension between the aqueous and oil phases.[162] When a refinery receives crude/unrefined product they do not necessarily know the processes used at a particular site or reservoir. This is because process additives are typically not disclosed such that the retailer retains a competitive advantage.

While chemical additives facilitate enhanced recovery of petroleum, this practice has the potential to lead towards adverse product conditions downstream because of the potential for unexpected interactions of additives. Thus, the eventual product output from the refinery may contain toxic or poisonous impurities that lead to poor product quality. Examples of unknown contaminants resulting in refining problems upstream have been communicated to us by our collaborators at Imperial Oil. In one case, a particular stream tended to develop discolouration at some point in the refining process. It has been

suggested (by our industry contacts) that this discoloration is indicative of the presence of phenolic compounds. The exact concentration, composition, and source of these phenolic compounds is as yet unknown. Another example from Imperial Oil is the discovery of low levels of fluorinated compounds in some streams. This may be the result of certain fluorinated surfactants or foaming agents having been used in EOR techniques in some reservoirs. Additional examples of worrisome contaminants upstream are polyphosphate esters which are used to prevent corrosion and scale formation, as well as nitrogen containing additives which may interact with refinery equipment resulting in degradation (and costly maintenance).[163]

Figure 22. Discoloured Salt-Filtered Jet Fuel Sample (ideally, this sample should be clear and colourless)

Raw and unprocessed petroleum is not useful in any kind of commercial application and is therefore generally sent to a refinery after extraction. Following extraction from the subterranean or sub oceanic well, the crude oil is processed and refined into several fractions such as kerosene, naphtha, and petrol. These fractions are then refined into several quality grades through a variety of processes which are contingent on market

demands. Crude oil distillate fractions are used primarily as a source of fuel or in the production of primary chemicals such as ethylene, propylene, butadiene, BTEX, and several other important chemical precursors.[155]

This refining process entails a complex series of downstream treatments, some of which involve chemical treatment. The key downstream stages are the initial atmospheric and vacuum distillation, hydro treating, desalting, amine treating, hydrocracking, coking, and desulfurization. During desalting, for example, emulsification agents are added. Throughout several of these stages, other compounds may be used to prevent corrosion. High-sulfur fractions are treated downstream with amines for the removal of hydrogen sulfide gas (also known as gas-sweetening or acid gas removal). As well, biocides are added to aid in the removal of bacteria that may crop up in some streams. Unwanted contamination following the refining process may be due in part to this array of treatments at the refinery in addition to the naturally occurring species which persist through to finished product.

For the petroleum industry, it is imperative to develop analytical techniques to facilitate the detection and characterization of contamination. Knowledge of the identity and quantity of particular compounds that exist within petroleum is essential, not only for mitigating the negative environmental effects of such compounds, but also for developing effective strategies for their removal. This is a priority for the petroleum industry as it ensures a clean commodity for trade or as an energy source; therefore, several advanced analytical techniques have been developed and employed for petroleum analysis.

4.4 Current Methods of Petroleum Analysis

The chemical characterization of petroleum and its fractions, petroleomics, is a complex field of study.[164] There are many unique molecules in a given sample of petroleum ranging from very simple hydrocarbons to extremely complex constituents with multiple functionalities. Therefore, an ideal method of identifying by-products, impurities, or other molecules of interest in a sample of petroleum must be both sensitive and selective. Typically, the molecular characterization of petroleum is accomplished using a handful of advanced analytical techniques. The need to develop these analytical approaches to investigate speciation in petroleum products is well-recognized, whether to enable efficient usage of all the fractions or to establish the extent to which these products may affect the environment. Analytical techniques that are both accessible and inexpensive are desirable for use in industry, since a rapid and simple analysis with common equipment is the most economically justifiable angle to approach this problem. Functional group specific analyses are valuable since they aid in tracking down problematic species and simplify the analysis.

Modern petroleum characterization techniques include powerful separations using Fourier-transform ion cyclotron resonance mass spectrometry (FT-ICR MS) and two-dimensional gas chromatography (GC×GC).[164–171] Each unique elemental composition has a different exact mass; however, differentiation between the many compounds present in a highly complex matrix such as crude oil is possible only with incredibly high mass

resolving power. Fourier-transform ion cyclotron resonance mass spectrometry (FT-ICR MS) is commonly used because of its extremely high resolving power.[164] This mass analyzer is capable of resolving thousands of unique molecules in petroleum. Molecular formula determination is made simple due to the extremely high mass accuracy of FT-ICR. It is able to sort compounds by their class: heteroatomic or hydrocarbon, the number of double bond equivalents, the number of carbons, and so on. FT-ICR MS is frequently paired with an electrospray ionization (ESI) ion source for the analysis of more polar or functionalized compounds. ESI is a popular ion source choice because many of the problematic species present in petroleum, specifically those species containing heteroatoms, tend to be sufficiently polar to be amenable to ESI-facilitated analysis. Due to the soft nature of the ionization method, ionization of neutrals is typically achieved via protonation of basic functionalities or deprotonation of acidic functionalities. This very common deprotonation/protonation derivatization methodology further adds to the attractiveness of ESI as this derivatization is somewhat selective for the more interesting functionalities that lead to common problems in the refinery.[164] The powerful technique ESI FT-ICR MS, according to Marshall and Rodgers, can successfully resolve and identify over 20,000 chemically distinct species in a crude oil sample.[172]

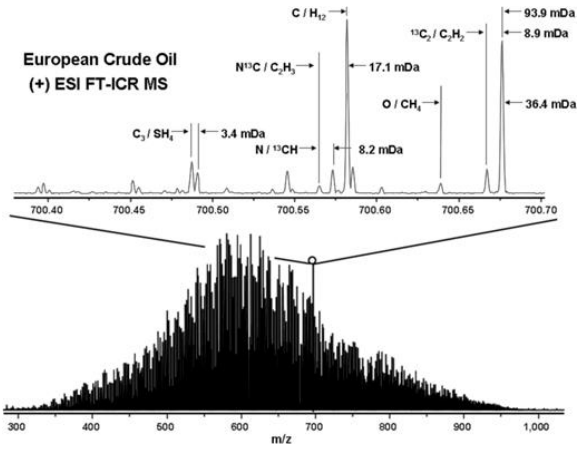

Figure 23. An FT-ICR mass spectrum of a crude oil sample. Note the inset which demonstrates the resolving power of FT-ICR.[164]

Two-dimensional gas chromatography (GC×GC) is a powerful modern separation technique used in industry and among petroleomics research groups.[169] Standard chromatographic separations of complex matrices are occasionally difficult and do not yield sufficient resolution to distinguish every unique species present. The advantage of GC×GC in such a case is its ability to separate compounds by two independent physicochemical properties. One column retains eluted species via one mechanism and the second column retains via a separate mechanism. In this way, GC×GC provides powerful contour images that correlate peak position with the type of compounds in a multi-component mixture. GC×GC is limited in that it is incapable of analyzing non-volatile compounds. Furthermore, while GC×GC mass spectrometry is possible and provides valuable spectra, the drawback is the lengthy time of analysis and lack of selectivity without sufficient pre-treatment.

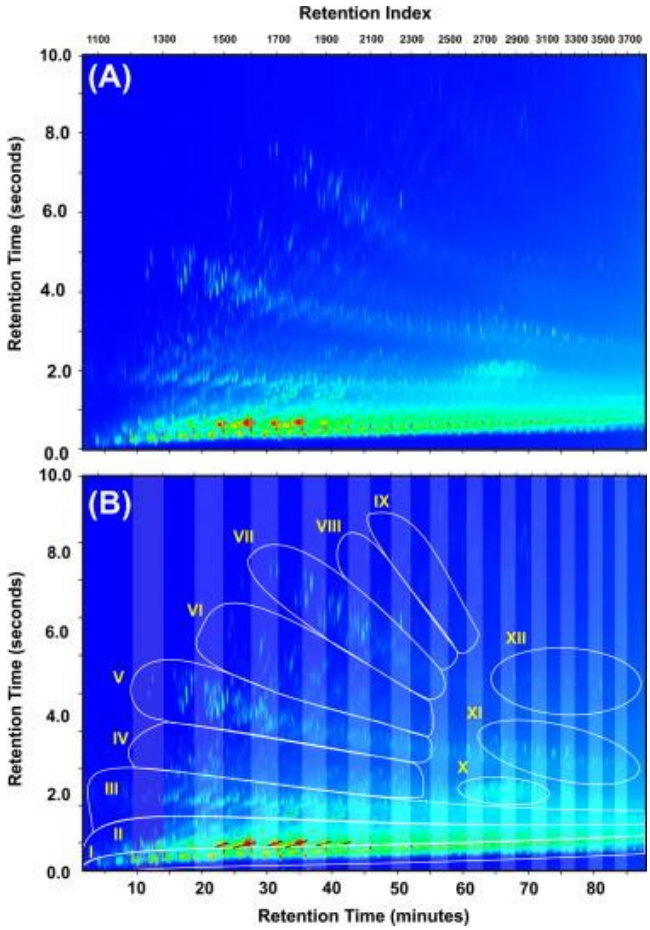

Figure 24. A two-dimensional GC chromatogram of a crude oil sample[173]

Some research has been directed towards distinguishing specific types of compounds in oil fractions. Sulfides have been analyzed in vacuum gas oil using positive ion ESI coupled with FT-ICR mass spectrometry through selective oxidation and methylation.[170] Two-dimensional gas chromatography has been used in the past to identify organohalogenated contaminants (OHCs) such as polychlorinated biphenyls and organohalogenated pesticides.[174] Additionally, GC×GC has demonstrated some potential in separating individual OHC congeners.[171] Unfortunately, these techniques are not exceptionally suited to separating and analyzing molecules by specific functional groups. This is a feature which would be ideal for hunting down problematic species and simplifying the analysis

and interpretation. Furthermore, FT-ICR MS is plagued by high up-front instrumentation costs. As one of the most expensive pieces of analytical equipment on the market, it is of little surprise that acquisition of this powerful mass spectrometer includes high maintenance and infrastructure overheads. Two-dimensional GC, while not exceptionally expensive, involves two slow chromatography steps in addition to laborious setup. A simple, and inexpensive selective analysis would be the most desirable to industry, since it will better cater to the treatment of specific upstream and downstream processes or problems.

We wanted to develop a method which effects a selective analysis while avoiding chromatography altogether. Additionally, we were aiming to make use of relatively simple equipment, syntheses, and reactions. Following consultation with Imperial Oil, we recognised that a simple analysis, one which is selective for sulfur, oxygen and nitrogen containing compounds (e.g. mercaptans, disulfides, ketones, naphthenic acids, amines) in a complex matrix such as downstream petroleum fractions, was potentially rather valuable. We set out to solve this problem using our experience with charge-tagged compounds and electrospray-ionization mass spectrometry. We expected the analysis would be somewhat difficult due to the nature of the highly complex hydrocarbon matrix; however, this issue was somewhat ameliorated since the initial target samples were downstream distillate fractions, rather than crude petroleum itself. We decided that an ideal solution to this problem was to consider the selective reactivity analytical targets with a charge tagged compound. The derivatized analytes could then easily be detected via electrospray-ionization mass spectrometry.

4.5 Electrospray Ionization, Derivatization, and the Charge Tagging methodology

Solvent adduct and metal ion aggregation has seen use with desorption electrospray ionization in order to promote the detection of polar constituents of petroleum samples.[175] Sulfur compounds have also been detected with some success through methylation and oxidation as alternative chemical derivatization techniques.[176] More exotic chemical derivatization techniques have also enjoyed success in derivatization of thiols including the addition of dansylaziridine, a reagent typically used as a fluorescent probe for proteins.[64] Atmospheric pressure photoionization (APPI) mass spectrometry is a complimentary soft-ionization technique to ESI-MS since it specializes in the speciation of nonpolar compounds that are less accessible to typical ESI-MS analyses.[8] When paired with a toluene dopant, APPI has been proven useful in the speciation of sulfur compounds in crude oil when paired to an ultrahigh resolution FT-ICR mass spectrometer.[177–179]

The McIndoe group has previously employed the addition of a charged tag, such as a phosphonium ($-PR_3^+$), ammonium ($-NR_3^+$) or sulfonate ($-SO_3^-$) group to facilitate the detection of specific analytes.[4,42,180] Charged tags are useful in the detection of species not normally detectable by ESI-MS due to an absence of polarity (or functionality) which inhibits ionization efficiency via commonly used mechanisms (e.g. adventitious protonation by solvent). Charged substrates have proven very useful in mechanistic investigations when combined with ESI-MS by allowing us to monitor the behaviour of tagged intermediate species.[2] The charge-tagging methodology is particularly useful when

combined with the soft ionization of ESI, since much of the background is eliminated while intrinsically charged species (i.e. those which we have tagged) are pronounced in the spectrum. In other words, selectively affixing a charged tag eliminates ionization efficiency as a barrier to detection and promotes signal intensity for desired analytes.

Every functional group has unique reactivity, and selective reactions exist that are highly favourable for a particular class of compound while leaving others untouched. This fact is most obviously used in organic synthesis where protecting groups are used to modify particular functionalities. Bioconjugation reactions have also been a source of inspiration for our selective charge-tagging methodology since this class of reaction is necessarily highly selective, high yielding, easy to execute, and are well-studied.[181] An example of this type of reaction (and the main focus of this chapter) is our approach to characterization of mercaptans in petroleum distillate fractions using a well-known bioconjugation reaction, thiol-disulfide exchange, in order to selectively tag thiols for analysis by electrospray ionization mass spectrometry.[45,182,183] The charge-tagging and derivatization approach was extended and proposed for several classes of compounds for our industry partners. Each of the following sections detail the sources of some contaminants of interest, in addition to a candidate reaction for their identification.

4.6 Charge Tagging of Alkylphenols in Petroleum

Imperial Oil was concerned with phenolic constituents as it is suspected that the presence of these lead to discolouration in some streams. Alkylphenols are a class of compound

found within crude oil with variable concentration, depending on several factors such as biodegradation.[184] Low molecular weight alkylphenols are abundant in some fractions of crude oil though the actual concentration is constantly modified. The presence of somewhat hydrophilic compounds of crude oil such as carboxylic acids and alkylphenols is heavily altered due to interaction with natural mineral deposits and groundwater during secondary migration, the movement of the petroleum through reservoir rock.

One method of derivatization involves the use of 5-(dimethylamino)naphthalene-1-sulfonyl chloride (also known as dansyl chloride) in order to form a sulfonate which may then be protonated in slightly acidic conditions.[64] While effective, dansyl chloride will also react with thiols and this lack of selectivity was found to be of limited use for us during the analysis of petroleum fractions.

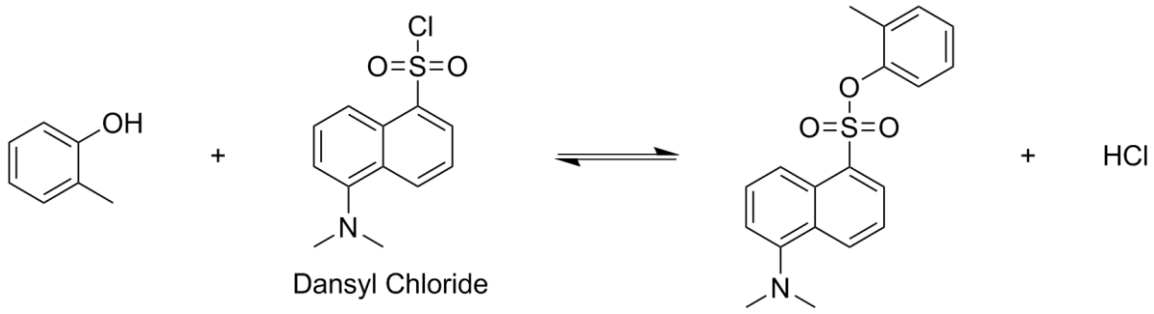

Scheme 2. Reaction of *o*-cresol with Dansyl Chloride[64]

A simpler method of detecting phenols is through the acidic proton. Use of a strong base effects deprotonation in solution, producing a phenolate which is easily detectable by negative ion mode ESI-MS. This technique, while cheap and effective, will also deprotonate other acidic functionalities (such as thiols and especially carboxylic acids) and

therefore suffers from a lack of selectivity. That being said, the mass spectra obtained of the two jet fuel fractions studied in this chapter following caustic treatment are relatively simple (Figure 25, Figure 26). This is not always the case, especially in less refined samples. The appendix for this chapter contains several examples of more complicated spectra obtainable following caustic treatment of certain petroleum fractions containing considerable amounts of acidic moieties.

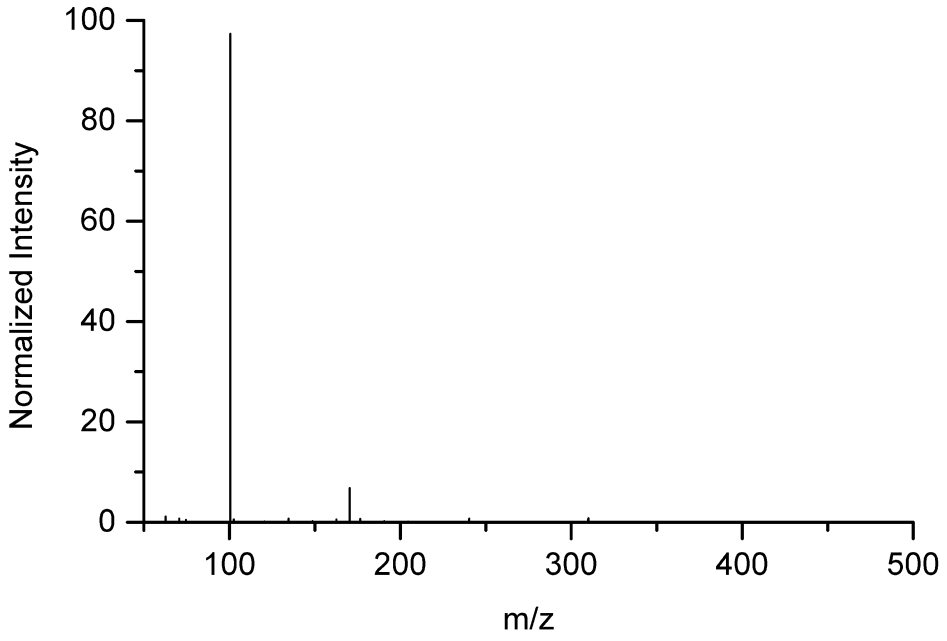

Figure 25. IO Jet Sample 77229 (0.1mM KOH, 10%v/v sample in MeOH)

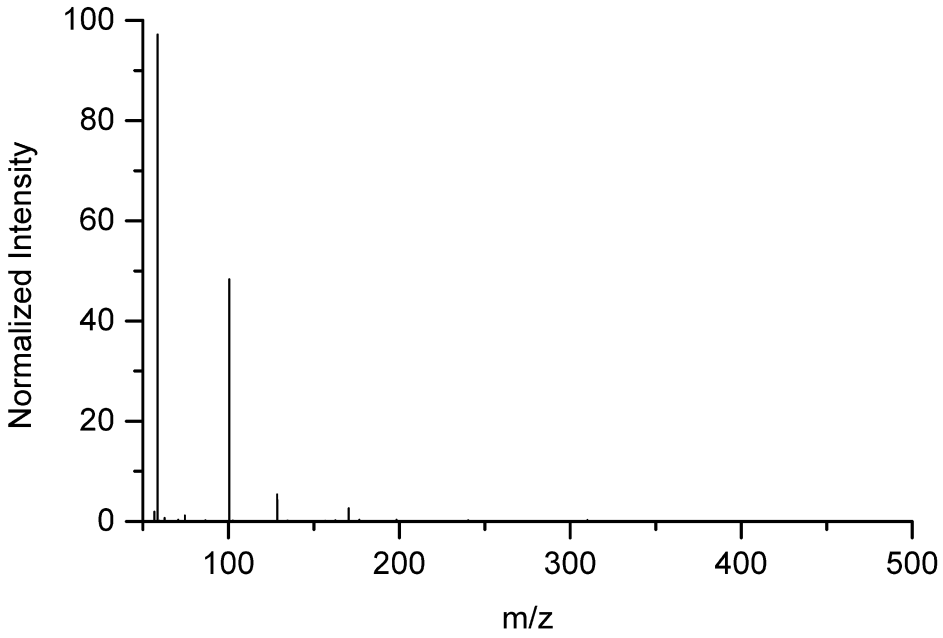

Figure 26. IO Jet Sample 77234 (0.1mM KOH, 10%v/v sample in MeOH)

Because of this lack of selectivity (and sensitivity to phenolic constituents), we opted to develop our charge-tagging methodology for this application. This work centered on an S_N2 reaction between an alkoxide and an imidazolium-based charge-tagged alkyl halide to form a charged ether, enabling the detection of phenolic constituents in a complex matrix via ESI-MS (examples of Ms. Zhu's work seen in Scheme 3, Figure 27, and Figure 28).[134]

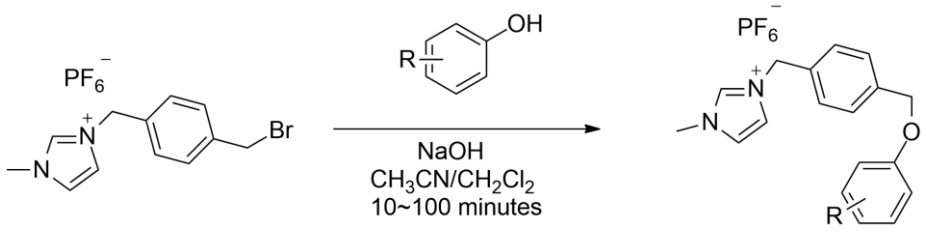

Scheme 3. Reaction conditions for *o*-alkylation of phenolic constituents using charge-tagged imidazolium complex

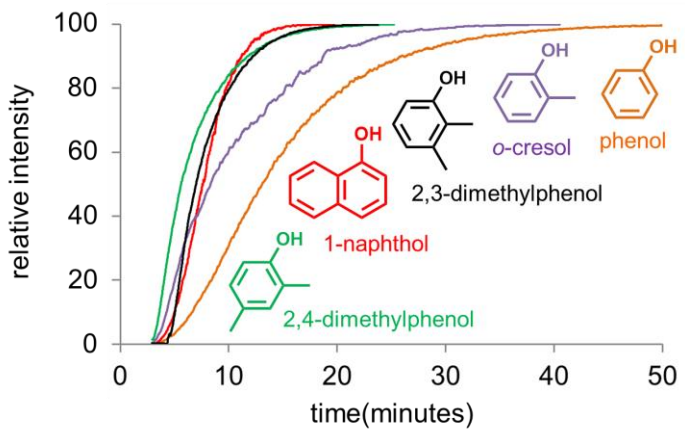

Figure 27. Online reaction monitoring of various alkylphenols with charge-tagged imidazolium complex using Pressurized Sample Infusion (PSI) ESI-MS

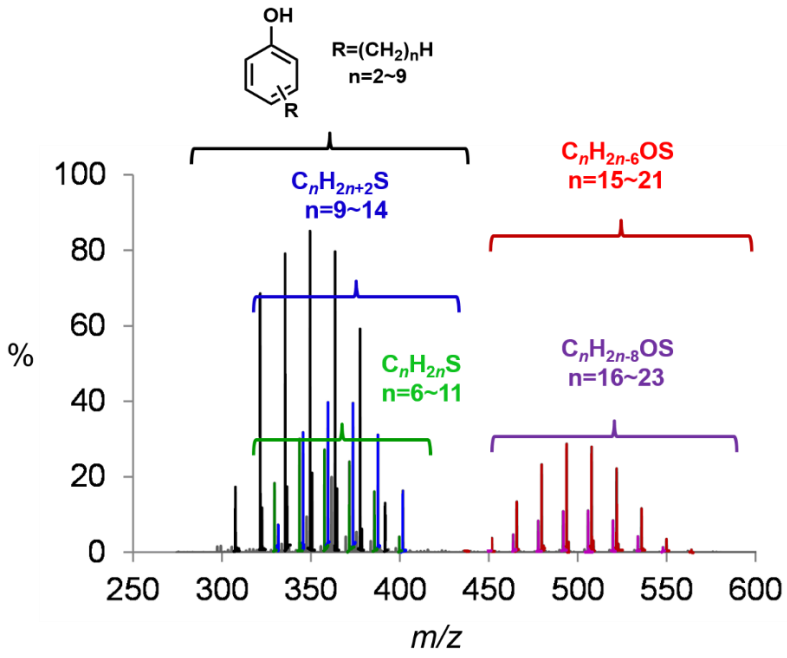

Figure 28. ESI-MS mass spectrum of jet fuel fraction following treatment with charge-tagged imidazolium complex. Note the numerous distributions of alkylphenols of varied unsaturation and chain length.

4.7 The Acidic Constituents of Petroleum

A significant component in crude oil to consider and investigate are naphthenic acids. Acids present in crude oil are termed naphthenic acids for historical reasons since the carboxylic acids found in crude oil primarily stem from the oxidation of naphtha, one of the lowest boiling point fractions of crude oil.[185] Naphthenic acid is a complex class of mixed compounds containing a carboxylic acid moiety with long chain hydrocarbon backbones consisting of approximately 9 to 20 carbon atoms and features a diverse array of cyclopentyl and cyclohexyl groups.[186] The molecular weight of these compounds varies but is generally in the range of 120-700 amu. The acidity that these complexes imparts on petroleum fractions is important to monitor as high acidity can cause corrosion and refinement concerns.[185] Due to recent detection of crude oils containing significant quantities of naphthenic acids this compositional investigation is in high demand.[187] Biodegradation has been shown to correlate directly with the production of significant concentrations of carboxylic acids which leads to an increase in the total acid number (TAN) of several crude oils (along with other components such as total sulfur content).[185] TAN is the metric by which the acidity of crude oil is measured and is expressed as the mass of potassium hydroxide required to neutralize a given mass of crude oil. The TAN varies widely in crude oils, ranging from less than 0.1 $mg \cdot g^{-1}$ to 8 $mg \cdot g^{-1}$ and high TAN oils are pervasive.[187] The confounding nature of petroleum has led to the use of several analytical techniques such as Fourier transform infrared spectroscopy, high-performance liquid chromatography, gas chromatography, and mass spectrometric techniques to perform the compositional analysis of naphthenic acids; however, the results of these techniques are mixed and occasionally disappointing.[187]

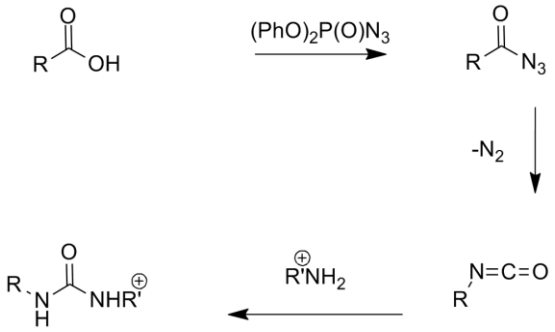

Scheme 4. General scheme of carboxylic acid derivatization via the Curtius Rearrangement and the use of DPPA [188]

Our proposed selective charge-tagging methodology for naphthenic acids involved a reaction between the carboxylic acid functionality and an azide. Known as the Curtius rearrangement, the well-studied reaction is applicable to a diverse range of carboxylic acids. The reaction produces an acyl azide and is commonly effected through the use of diphenyl phosphorazidate (DPPA), a common azide reagent for the Curtius rearrangement.[189–191] Thermal decomposition of the acyl azide derivative yields an isocyanate through the loss of dinitrogen. This thermal decomposition is likely a concerted process, since the intermediates expected from a nitrene are non-isolable. Isocyanates (R–N=C=O) are a highly reactive compound and if formed in the presence of primary amines the urea derivative is formed.[192] In this example, the charged tag could be any primary amine featuring a carbon backbone with a cationic functionality.

Because of the high reactivity of the isocyanate intermediate, some unwanted side reactions could occur. The presence of water and primary alcohols yields primary amines and carbamates, respectively, though this side reaction could be mediated through increased charge tag concentration in the crude oil containing solution. Non-nucleophilic

solvents must therefore be used when performing charge-tagging. An increased concentration of amine charge-tag is required to ensure the isocyanate intermediate species has a greater opportunity to be tagged. The proposed analysis of a petroleum sample involves treatment with DPPA and amine charge tag in toluene with heating applied over several hours. Following this reaction, a diluted aliquot of the mixture may be analyzed via ESI-MS and derivatized naphthenic acids detected.

4.8 Nitrogen-Containing Species and Quaternization to Ammonium Salts

Heteroatomic, nitrogen-containing compounds are another component of crude oil which, in some shale oils, can be present at concentrations as high as 1.27% (w/w).[193] Removal of these unwanted contaminants in distillate fractions is important for several reasons. Despite being a relatively minor constituent, the nitrogen-containing compounds may increase to worrisome concentrations in distillate fractions during the refinement process. The increase in nitrogen compounds can lead to refining and usage issues including deposition, color formation, pollution, unpleasant odour, increased carcinogenicity, and contribution to gum formation in the finished product.[194,195] The presence of nitrogen compounds is also a concern when treating distillate fractions through catalytic processes such as hydrodesulfurization, as they may poison and deactivate the catalysts used.[194] Nitrogen compounds in crude oil can be classified as basic or non-basic; the non-basic nitrogen compounds are the most prevalent in crude petroleum and consist of pyrroles, indoles, and carbazoles.[195,196] The basic nitrogen components are generally

found in lighter fractions of crude oil and primarily consist of pyridines and quinolines such as benzoquinolines.[195,196]

A tertiary amine (R_3N) will react with an alkyl halide (R′-X) to rapidly produce [R_3N-R′]$^+X^-$, in an historically important transformation known as the Menshutkin reaction.[197] Amine quaternization may also be achieved from a primary or secondary amine by methylation using a methylated halide reagent. Iodides are the most reactive of the methyl halides, and the reaction is accelerated at high temperature and in polar aprotic solvents.

We have exploited this reaction for the detection of amines in petroleum fractions. The addition of a small amount of methyl iodide (0.1% v/v) is added directly to an aliquot of a sample. The diluted mixture was analyzed by ESI-MS to detect the derivatized products. Equivalently, treatment with iodomethane will methylate primary and secondary amines in succession to produce the tri- or dimethylammonium salt. Favourably, these quaternary ammonium salts are quite stable and do not undergo conversion back to the parent amine.

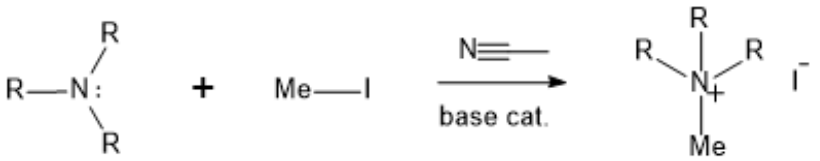

Scheme 5. General Scheme of amine methylation using iodomethane

Several samples of petroleum distillate fractions were collected at various points throughout an Imperial Oil refinery. We used the simple methylation procedure described here to characterize the amines present in several of these samples. For these samples, 50

μL of iodomethane was added to 5 mL of 10% (v/v) sample in acetonitrile and allowed to stir at room temperature for 30 minutes. The rapidly produced methylated amine species are easily identified by ESI-MS analysis, and the assignments supported with MSMS and acidification data. An example of the advantage of this kind of derivatization is seen in Figure 29. The overly complex spectrum (a) is greatly simplified following methylation (b) enabling efficient amine speciation.

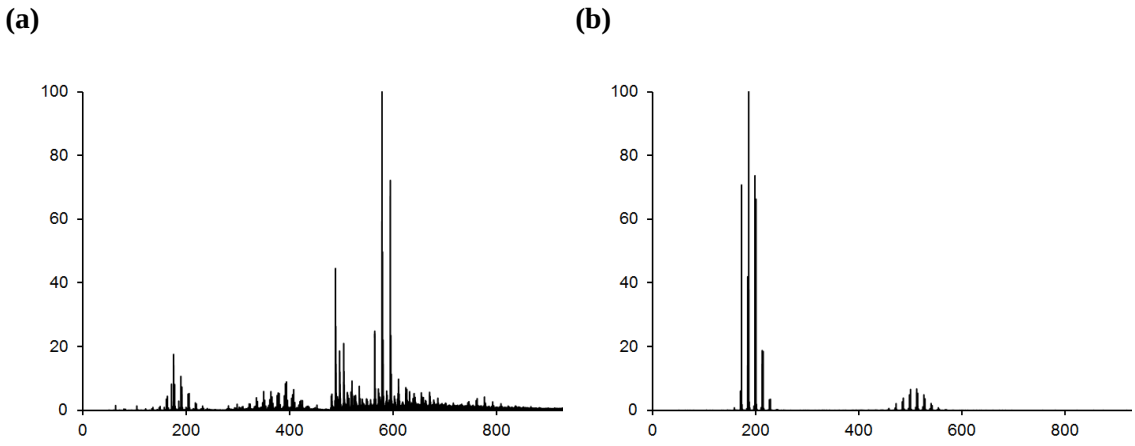

Figure 29. Mass spectrum of salt-filtered jet fuel treated with (a) 1% formic acid and (b) after treatment with 1% iodomethane. Both solutions composed of 10% (v/v) oil fraction in MeCN

In many of these samples, there is clearly an interesting bimodal distribution in which signals are 14 Da apart due to hydrocarbon chains of varying length, each signal differing by a methylene group. Another interesting feature of these spectra are notable 2 Da separations between many signals, indicative of unsaturation. Both of these are common features in other samples because the samples are separated by vacuum distillation. This results in a statistical distribution of species based on the boiling point range at which the fraction was collected.

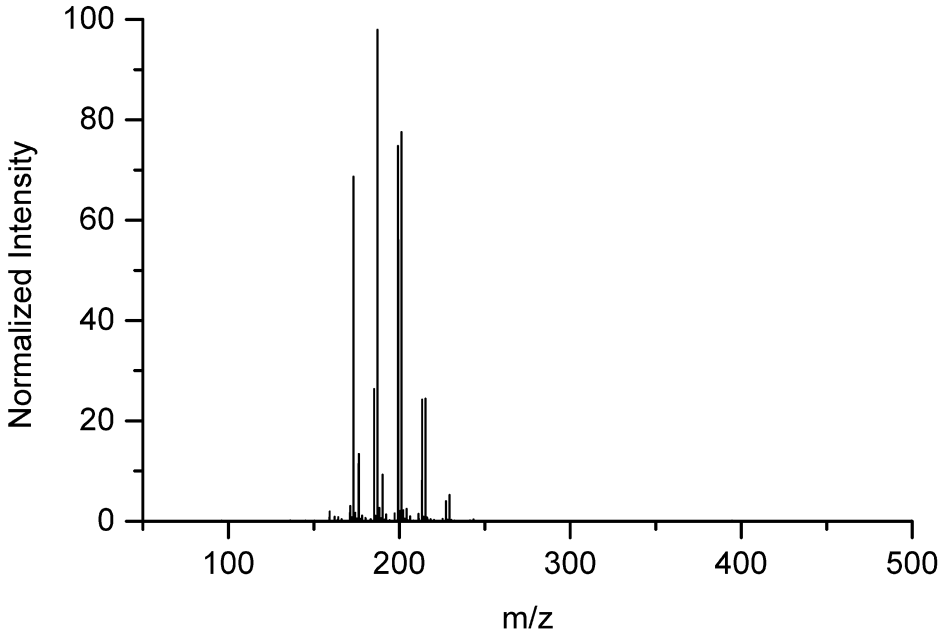

Figure 30. IO Jet Sample 77229 (0.1%v/v Iodomethane, 10%v/v sample in MeCN)

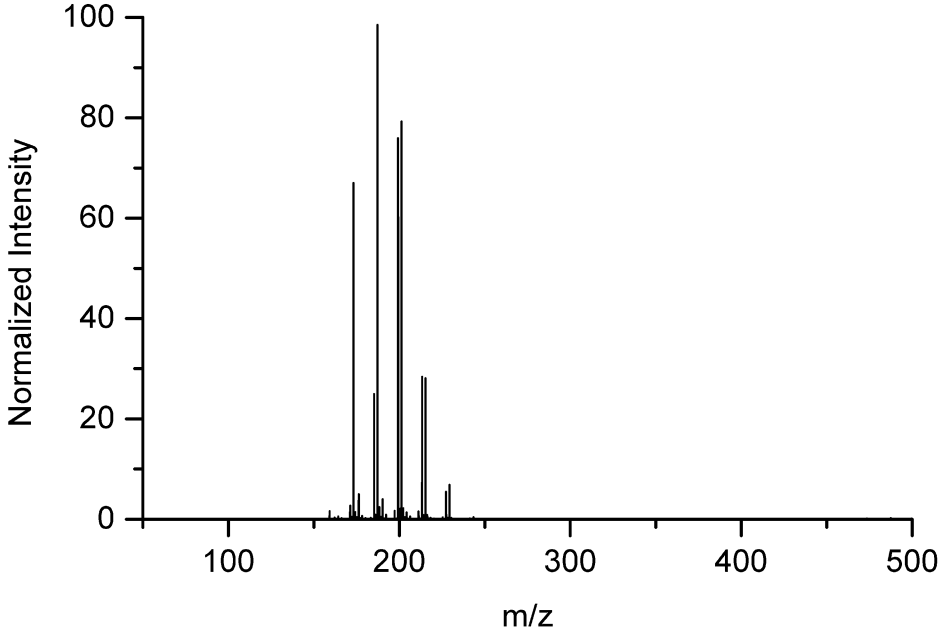

Figure 31. IO Jet Sample 77234 (0.1%v/v Iodomethane, 10%v/v sample in MeCN)

Alternative derivatization strategies methods may be explored in the future to discriminate between primary, secondary, and tertiary amines. An example of one of these

derivatizing agents is 2,4-diphenyl-6-ethylpyrylium tetrafluoroborate which has been used in conjunction with fast atom bombardment MS for the analysis of primary amines, exclusively.[64]

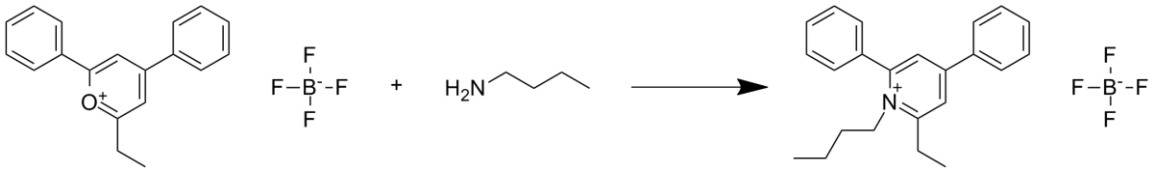

Scheme 6. Reaction of butylamine with 2,4-diphenyl-6-ethylpyrylium tetrafluoroborate

4.9 Sulfur in Petroleum

The main focus of this chapter is focused on the detection and characterization of sulfur compounds in petroleum fractions. This impurity was of concern to Imperial Oil, so we applied our charge-tagging methodology toward the selective derivatization of mercaptans. The total sulfur content of petroleum can vary widely from low-sulfur sweet oils to high-sulfur crude oils.[155,164,198–201] Refined petroleum products are required to meet strict low-sulfur content standards and are subjected to a variety of treatments in order to meet these standards. Despite advances in desulfurization methods, some deep desulfurization goals (such as the US EPA Tier 3 gasoline sulfur standard) have not yet been met due to the presence of trace quantities of mercaptans.[202] At the refinery, distillate fractions of petroleum are refined into several products such as fuels, lubricants, solvents, and primary chemicals. High-sulfur fractions are generally treated downstream with amines for the removal of hydrogen sulfide gas (often referred to as gas-sweetening or amine scrubbing).[203] Many other sulfur-containing species are removed from petroleum through

catalytic desulfurization processes such as SCANfining and catalytic mercaptan oxidation (Merox).[204] New deep desulfurization (less than one part-per-million) methods must go beyond hydrodesulfurization processing schemes and adsorbents to economically produce fuel that meets increasingly strict government regulations on sulfur content in these fuels, whilst keeping in mind the stricter protocols emplaced by fuel cell driven vehicles.[205] The future of crude oil sulfur removal processes is heading toward "near-zero" sulfur content which will likely require a great deal of catalysis research and development to meet this goal.[27]

Of the sulfur compounds present in petroleum, we were interested in selective thiol speciation in particular since this class of compound leads to odour issues as well as certain types of corrosion in fuel products (resulting in a failure of the traditional industrial copper corrosion specification for gasoline) and are of more concern to industry than non-acidic sulfur functionalities. It was therefore desirable to invent a method which would not charge tag aliphatic or basic sulfur constituents since we were targeting the greater contributors to high-temperature sulfidation corrosion. Total sulfur analysis of lighter stream petroleum products is typically achieved via X-ray or GC methods (coupled with a sulfur-selective detector). Sulfur analysis of heavier streams and crude petroleum is more easily facilitated by high resolution mass spectrometry. Keeping these techniques in mind, our most important goal in developing the charge-tagging methodology was the ability to detect low levels of mercaptans, specifically, in a complex matrix using relatively simple techniques and preparation.

The total sulfur content of crude oil is as high as approximately 3% sulfur in some sour (high sulfur) crude oils such as Basra crude or 0.3% (w/w) in sweet (low sulfur) crude oils such as White Rose crude; however, the actual mercaptan content of the sulfur found in these crude oils is as low as 0.011% (w/w).[155,164,198–201] Jet fuel (or kerosene) is a higher boiling point fraction of crude oil (approximately 190-250°C) with a typical total sulfur content of less than 0.3% (w/w) and about 0.0015% (w/w) of this sulfur content is mercaptans. The identification of mercaptans in petroleum fractions is an analytical challenge, not only due to the generally confounding matrix of petroleum, but also because of the diminutive quantities involved.

4.9.1 Derivatization of Thiols with Charge Tagged Disulfides

Our approach to this analysis was to exploit thiol-disulfide exchange, a well-known metathesis-like reaction important in several biological processes, to charge tag mercaptans.[206,207] We felt this bioconjugation reaction could be employed to selectively charge-tag thiols in crude oil or other complex matrices.

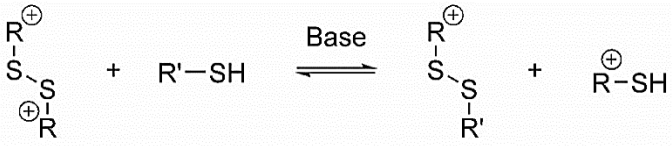

Scheme 7. Representation of a thiol-disulfide exchange reaction and the charge-tagging methodology

A charge-tagged disulfide (R^+SSR^+) will react selectively with a thiol (RSH) via thiol-disulfide exchange to form $RSSR^+$ and R^+SH.[208,209] The general reaction proceeds by

nucleophilic attack of a thiolate anion (RS^-), formed by deprotonation, on one of the two sulfur atoms present in a disulfide (RS-SR). This net reaction "tags" the target functional group yielding a new disulfide and a new thiolate, the latter of which is easily characterized by ESI-MS.

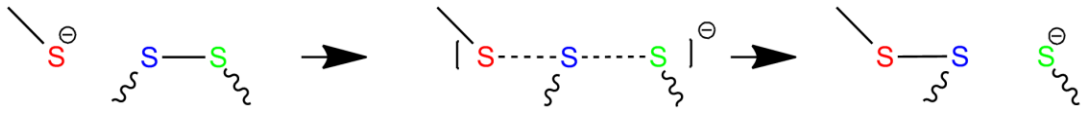

Figure 32. Representation of a thiol-disulfide exchange reaction

Several charged groups were investigated for the charged disulfide including ammonium, imidazolium and phosphonium functionalities. Our successful synthesis of an early prototype charged disulfide proceeded as demonstrated in Scheme 8.

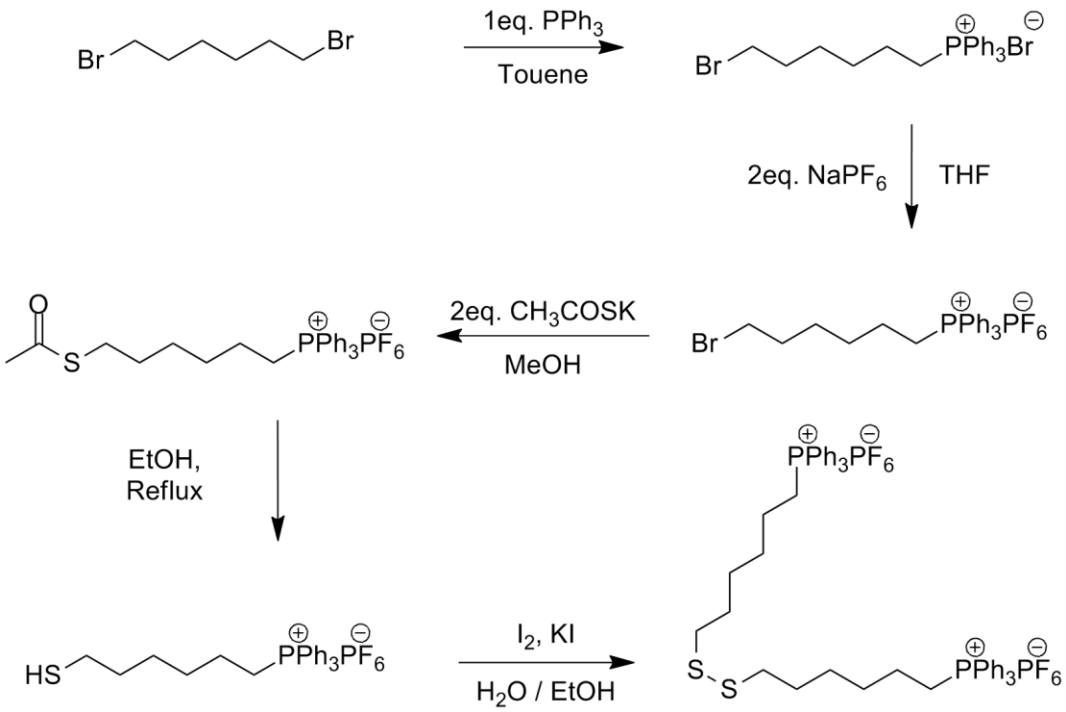

Scheme 8. One of several charge-tagged disulfide synthetic pathways explored

Triphenylphosphine was alkylated with excess 1,6-dibromohexane to generate the phosphonium bromide salt. Salt metathesis with sodium hexafluorophosphate improved the solubility of the salt in non-polar solvents (but is also favourable for ESI-MS as it reduces ion pairing and therefore enhances signal intensity). Substitution of the bromide was achieved using potassium thioacetate while transesterification and hydrolysis of the thioester in methanol formed the thiol. The thiol oxidizes spontaneously in air to the disulfide. We experimented with a variety of oxidants such as tincture of iodine and bubbling with oxygen, but found this largely unnecessary.

Several phosphonium-, ammonium-, and imidazolium-tagged disulfide prototypes were tested with a dilute solution of 4-methylbenzene thiol. When the reaction was performed simply through stirring (without heating or the assistance of other chemicals), the desired charge-tagged product was seen in just a few minutes, proving the technique was both rapid and uncomplicated. Subsequent optimization of reaction conditions, disulfide tag synthesis, and trials with petroleum fractions justified the efficacy of the method.

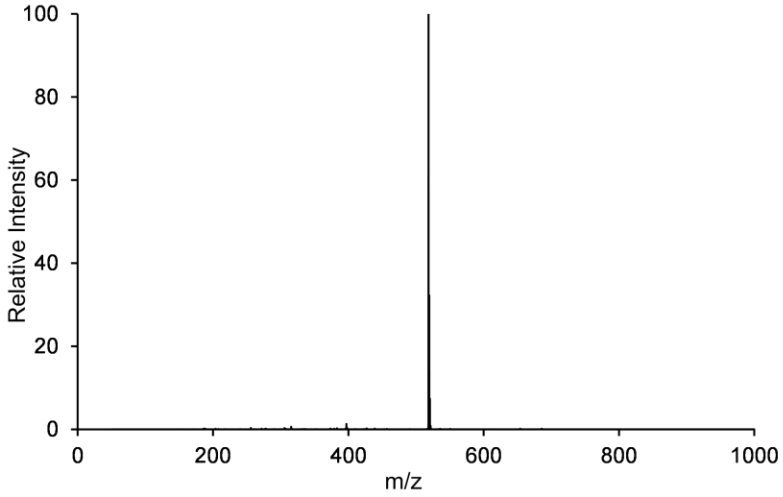

Figure 33. Positive-ion ESI-MS of the mixture of charge-tag and 4-methylbenzenethiol

Ultimately, we decided to use one particular phosphonium-tagged disulfide seen in Scheme 9 as compound (**4**) (full synthetic details in experimental section) for our work with salt-filtered jet fuel fractions provided by our industry partners. This decision was driven largely due to the simple synthesis, easy purification, high spray-quality of the tag in ESI, and resiliency of the tag to harsh chemical environments.

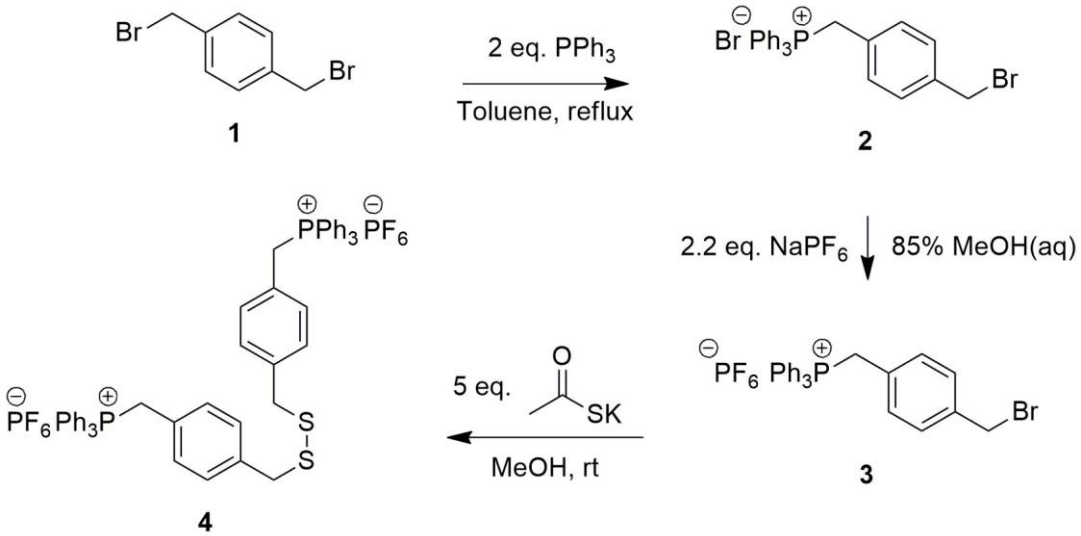

Scheme 9. Charge-tagged disulfide (4) synthetic pathway

In the discussion of our results with this charged tag, we will deal with the analysis of two specific jet fuel samples. These two jet fuel samples originated from two different points in the refinement process. Sample A is an untreated light distillate stream from the atmospheric distillation of a refinery crude oil blend. This sample is considered an "upstream" fraction since it had not been exposed to the full suite of treatment processes required to produce a finished product. On the other hand, Sample B has been subject (at least) to caustic washing, catalytic mercaptan oxidation, water washing, salt drying and clay treating. In other words, Sample B is much nearer to finished product. In general, we expect that the relative mercaptan concentration of samples obtained further downstream (Sample B) should be consistently reduced when compared to samples retrieved from further upstream (Sample A).

4.9.2 GC-MS characterization of jet fuel samples

Very little was known (or divulged) about the samples which were provided to us. Therefore, we first needed to acquire a picture of what type of species we were dealing with. We chose to perform Cold-EI gas chromatography-mass spectrometry in order to determine the distribution of species by determining the carbon numbers of the hydrocarbons seen in the chromatogram. From the GC-MS chromatographic distribution, we determined that the samples were distillate fractions acquired in the approximate boiling point range of 150-290°C (Figure 34), which was expected based on other jet fuel boiling point ranges.[210] The complexity of the samples meant we could determine only

the much more abundant species while less intense species were swamped out due to large overlap of signals; therefore, no thiols were distinguishable in the mixture.

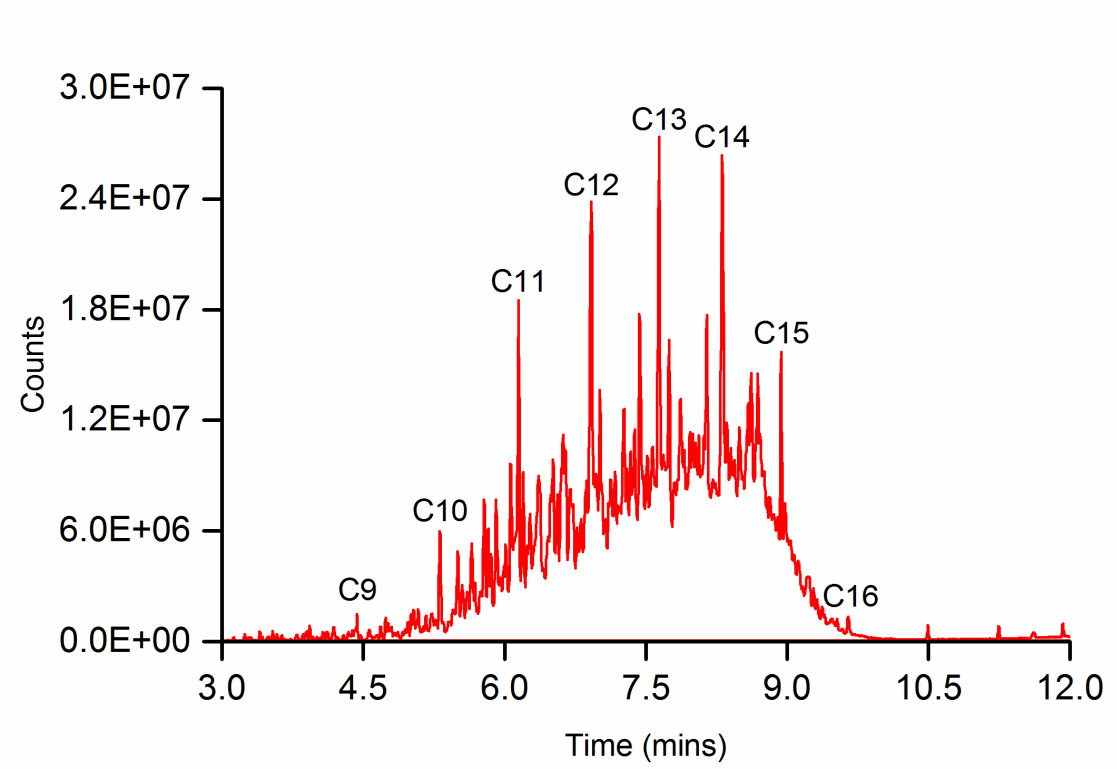

Figure 34. Cold-EI GC-MS chromatogram of jet sample A. Major peaks are labelled with carbon number and correspond to the alkane. Peak assignments were made using library matching. Thiols could not be identified in either sample A or B.

4.9.3 Effect of Base on Thiol-Disulfide Exchange Reaction

The rate of thiol-disulfide exchange is very well-studied and is considered first-order in both disulfide and thiolate. The reactions is therefore catalyzed by base since the thiolate must be formed for the reaction to initiate.[211,212] The overall rate of the reaction must therefore incorporate deprotonation and the thiolate-disulfide S_N2 reaction separately. We expected the rate of charge tagging should be greatly affected by the concentration of base and therefore investigated the results of varying solution pH. It is worth noting that this ability to easily control rate is useful, since the concentration of charged tag (**4**) added to

an unknown sample needs to be limited in order to avoid instrument saturation. We evaluated the rate of our charge tagging methodology via thiol-disulfide exchange and the base-dependence of the reaction using a model reaction between the tag (**4**) and 4-methylbenzenethiol (MBT) standard solutions. MBT was chosen as a model thiol species since its boiling point of 195°C is a close fit to the median of the 150-240°C distillation boiling point range for the jet fuel samples we were investigating (and was, in fact, present in these two jet fuel samples, as discovered later). The general reaction between MBT and our disulfide charge tag, as well as the effect of increasing sodium hydroxide concentration may be seen in Scheme 10 and Figure 35 which shows the abundance of the product disulfide (5) over time.

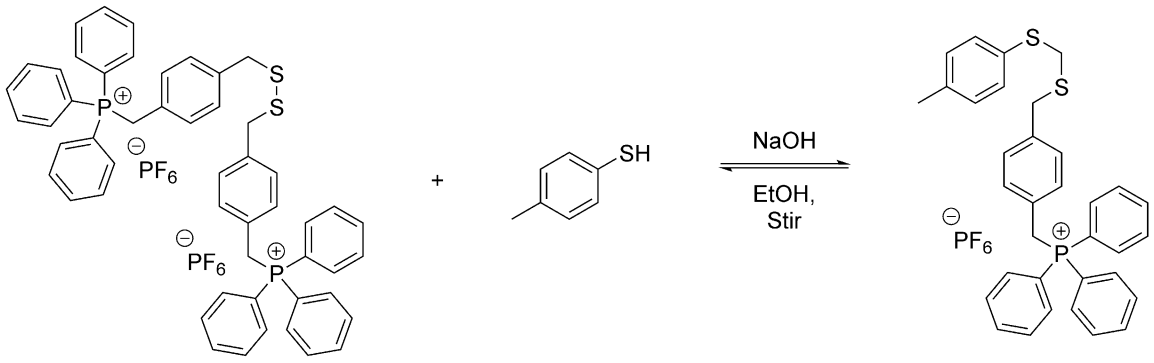

Scheme 10. Derivatization of 4-methylbenzenethiol with a charge-tagged disulfide reagent (full details in experimental)

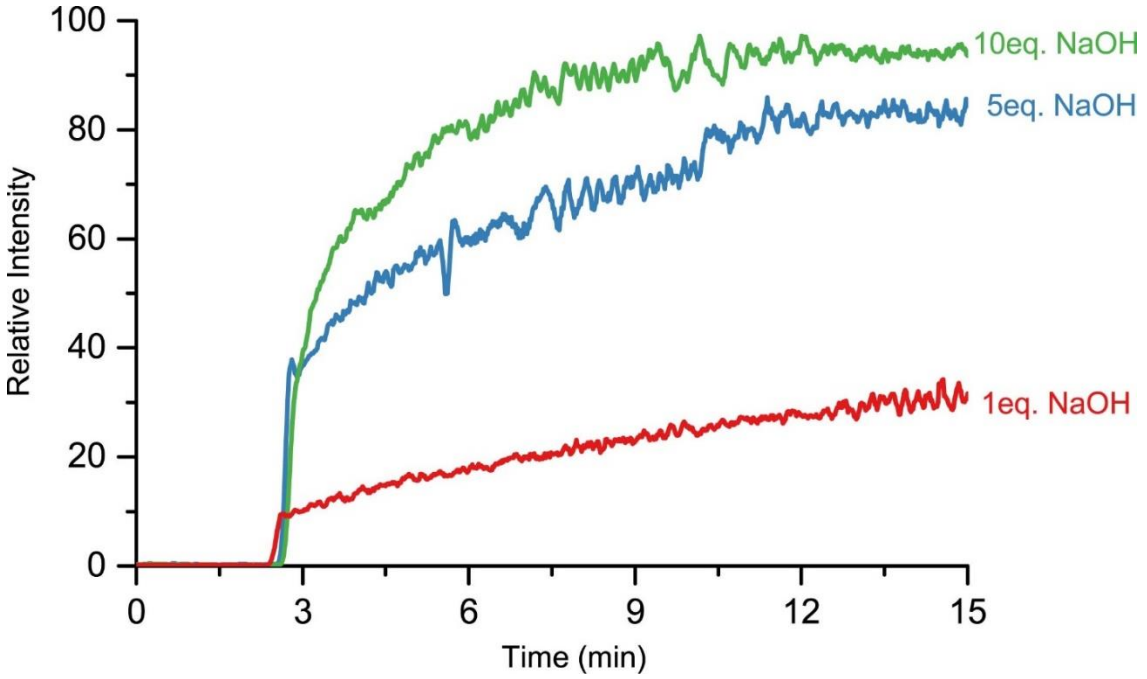

Figure 35. TDSE reaction dependence on base concentration. Traces show the abundance of the product disulfide (5) over time

For each of these reactions, 20 µM (10 eq.) of MBT was injected into a stirring mixture of 2.0 µM of charged disulfide (**4**) in ethanol and 1, 5, or 10 equivalents of sodium hydroxide, at room temperature, independently. In addition to the rate of the thiol-disulfide exchange, the degree of conversion of the reaction is largely dependent on the concentration of base. The reaction is sufficiently rapid that information regarding the initial stage of the reaction is lost; however, the equilibrium time is extended to approximately 40 minutes in the case of one equivalent of base. For practical use as a derivatization agent, an elevated concentration of base relative to the expected thiol concentration is recommended to thoroughly deprotonate any thiols present in the sample and expedite analysis time.

4.9.4 Petroleum Sample Mercaptan Analysis

Jet fuel samples A and B were treated with our charge-tag disulfide for a selective mercaptan analysis in an effort to establish the efficacy of our methodology. It should be noted that several crude oil samples were investigated using this charge tagging methodology; however, the analysis of these samples was hindered largely due to the complexity of the matrix, and the much higher concentration of thiols present. Conversely, the work presented here on jet fuel fractions yielded excellent results. Additionally, the objective of these petroleum fraction experiments was purely a qualitative venture as our industry partners required chemical information about the varieties of mercaptans present in pipeline streams prior to, and following, certain refinery treatments.

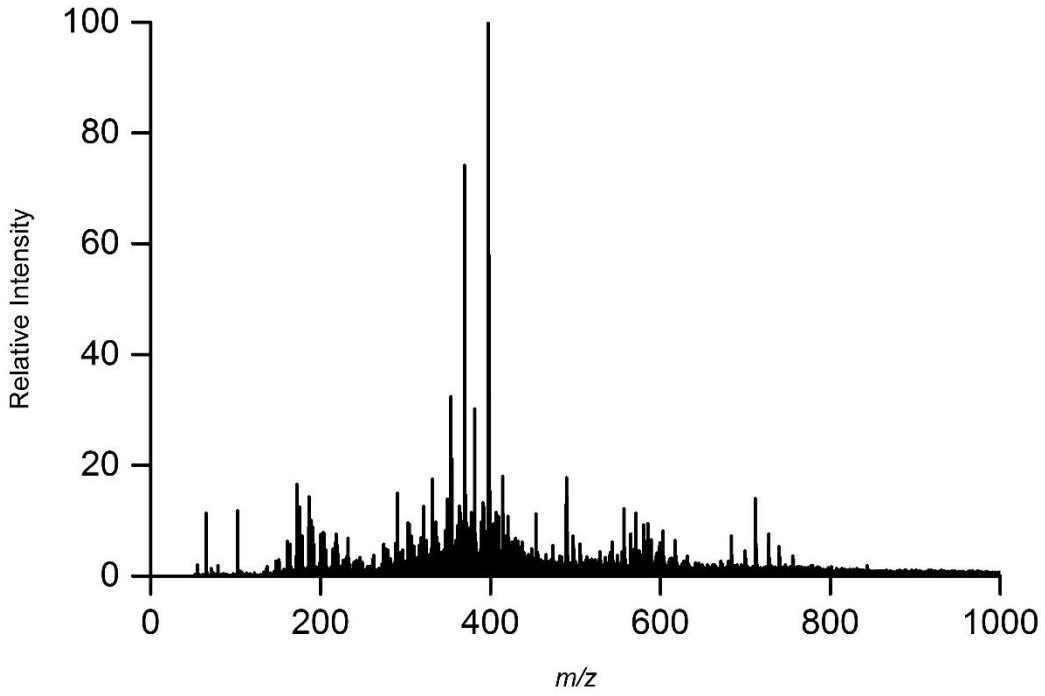

Figure 36. Positive ion ESI-MS of the mixture of charge-tagged disulfide and Basra crude petroleum

The general procedure was as follows: dilute solutions of charge-tagged disulfide (**4**) and sodium hydroxide were prepared separately in ethanol and subsequently injected into a stirred ethanolic solution of 1-10% (v/v) petroleum sample, at room temperature. The reaction was found to come to equilibrium within approximately 10-30 minutes. The reaction time varies depending on the amount of base used and analyte and therefore a general protocol should call for extended stirring times to ensure the system has come to equilibrium, especially considering the derivatized products are stable in solution over many days. Along with stability of the derivatized products, the charge tagged disulfide itself is stable when exposed to very high concentrations (over 500 equivalents) of sodium hydroxide; thus, the reaction may easily be accelerated through the use of additional base (while keeping possible instrument contamination in mind). Further, long stirring times (48 hours) with all reagents present did not result in tag decomposition or by-products. An excess of charge tag was used to ensure tag decomposition as a result of the matrix did not occur without sufficient exchange with in-solution mercaptans and to enhance the rate of exchange; however, to avoid instrument saturation and to facilitate direct injection of the mixture into the instrument, the disulfide concentration was kept below 20 μM. Finally, the samples were not filtered, concentrated, or otherwise manipulated in any way prior to analysis other than what is described here.

Prior to derivatization with our disulfide (**4**), untreated control samples were infused into the ESI-MS. The spectra from these were very simple and low intensity. The observable signals were likely due to a small amount of adventitious sodiation or protonation due to impurities in the sample; however, the majority of the signal is too shallow for an accurate

assignment. These control samples (method blanks) were used to establish a background for each sample analyzed. The two samples discussed here (A and B) did not exhibit significant background noise at the region of interest (that is, above *m/z* 400 and below *m/z* 2000). In addition to this, a method detection limit (MDL) was established for our reaction. A method blank, along with an MDL, allows us to precisely define the minimum signal required for us to accurately assign a species. This is a necessary precaution since the derivatization process is limited by the reactivity of the target analytes as well as dissimilarity between sample matrices. That being said, our definition here for a method detection limit is an approximation only and will vary slightly between samples, as an MDL was not independently established for each sample. The MDL in complex matrices such as petroleum fractions can vary widely, depending on their treatment and source; therefore, our method detection limit was set very high (at a signal-to-noise ratio equal to 10) for more confidence in our assignments.

The general method detection limit was established based on a reaction with 2.0 uM of compound **(4)** and 4-methylbenzenethiol as an archetypal thiol. First, the average baseline noise of a simulated petroleum sample composed of 10% hexane (v/v) in ethanol and 2.0 uM of compound **(4)** was determined. The response of the derivative compound **(5)** was determined for varying MBT concentrations and found to be reasonably linear for nano- to micromolar quantities of thiol.

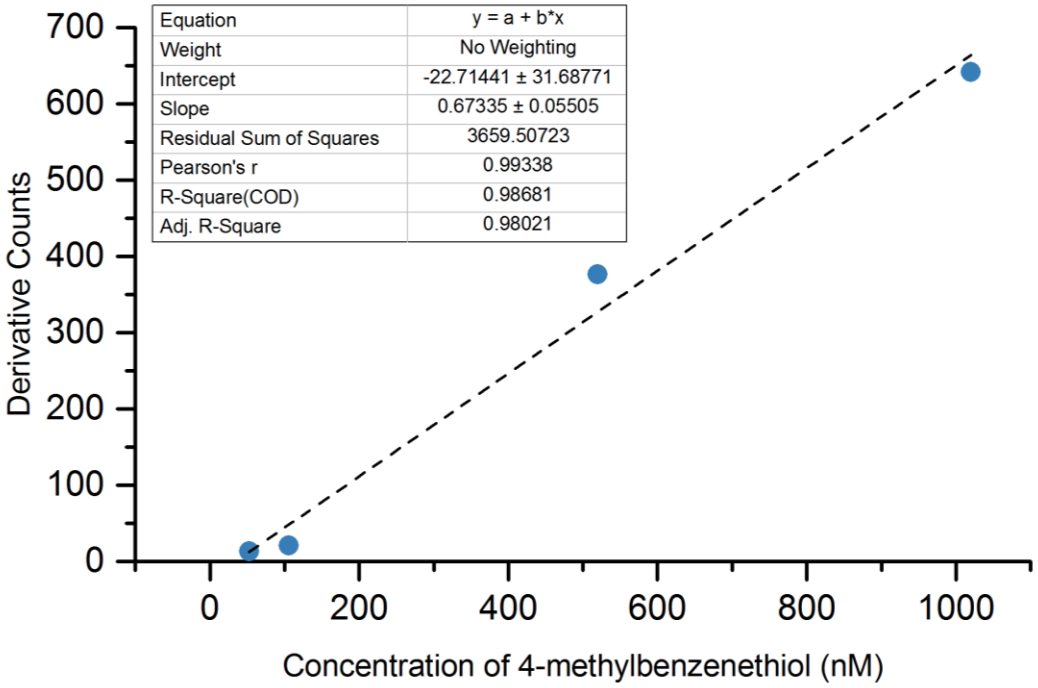

Figure 37. Response of derivative (5) following thiol-disulfide exchange reaction with 2.0 uM compound (4)

The response of the lowest identifiable derivative, **(5)**, was then used to establish the limit of detection (defined here as 3 times the signal-to-noise ratio) and quantitation (10 times the signal-to-noise ratio) for the jet fuel samples to be analyzed. The limit of detection for **(5)** was determined to be 39 counts (1.2 ng/L MBT) with a limit of quantitation of 130 counts (4.0 ng/L MBT). Our MDL for this analysis was therefore set at 130 counts for derivative assignment.

Following derivatization with the selective charged tag the response from thiol species was found to be greatly enhanced due to the fixed charge (i.e. 100% ionization efficiency) and spray quality of the phosphonium tag. The spectra of treated samples of A and B

demonstrate a wide distribution of mercaptans having different carbon number and double bond equivalents (DBE).

In sample A, several tagged thiols were apparent, from *m/z* 445-739. These were assigned as C1 unsaturated thiols (CH_3SH) to C22 thiols ($C_{22}H_{25}SH$) with 0-2 DBE. Also in this region was a more pronounced Gaussian-like distribution between *m/z* 520-620 composed of C4 unsaturated thiols to C14 (0 DBE) thiols. There were several degrees of unsaturation among this series, with species having between 0 and 4 DBE. The exact isomeric forms are not distinguishable with our Q-ToF mass spectrometer alone.

Table 6. Thiol derivatives signal response detected in salt-filtered jet fuel sample A and corresponding signal in sample B

m/z	**Thiol C#**	**DBE**	**Sample "A" MS Abundance (counts)**	**Sample "B" MS Abundance (counts)**
487.3	4	0	338	5
501.3	5	0	898	9
513.3	6	1	3037	14
515.3	6	0	1896	9
521.3	7	4	1436	15
525.3	7	2	418	14
527.3	7	1	4689	5
529.3	7	0	3334	7
541.3	8	1	8218	37
543.4	8	0	9703	24

553.4	9	2	1493	6
555.4	9	1	6874	64
557.4	9	0	8976	98
567.4	10	2	1677	38
569.4	10	1	4643	42
571.4	10	0	7069	111
581.4	11	2	1482	83
583.4	11	1	3238	45
585.4	11	0	4928	85
595.4	12	2	731	67
597.4	12	1	1709	30
599.4	12	0	2920	47
607.4	13	3	180	3
609.4	13	2	368	13
611.4	13	1	692	18
613.5	13	0	992	19
621.4	14	3	180	3
623.5	14	2	169	2
625.5	14	1	236	3
627.5	14	0	324	6

The distribution of non-derivatized mercaptans is consistent with the boiling point range of the distillate fraction. The handful of those mercaptans which lie under the boiling point

range are very likely due to the derivatization of disulfides in the sample. Following thiol-disulfide exchange of (**4**), the tagged thiolate is free to react with disulfides present in the sample. Table 6 lists the derivatized mercaptans detectable above the method detection limit in sample A, along with the abundances (counts) of each species in both samples. Below our method detection limit were several signals which appeared to be due to derivatized thiols since they were reasonably above the limit of detection for the sample. The derivatized mercaptans are easily identified as derivatives via MS/MS, and indeed several derivatives were discovered outside the MDL using MS/MS for both samples but not reported.

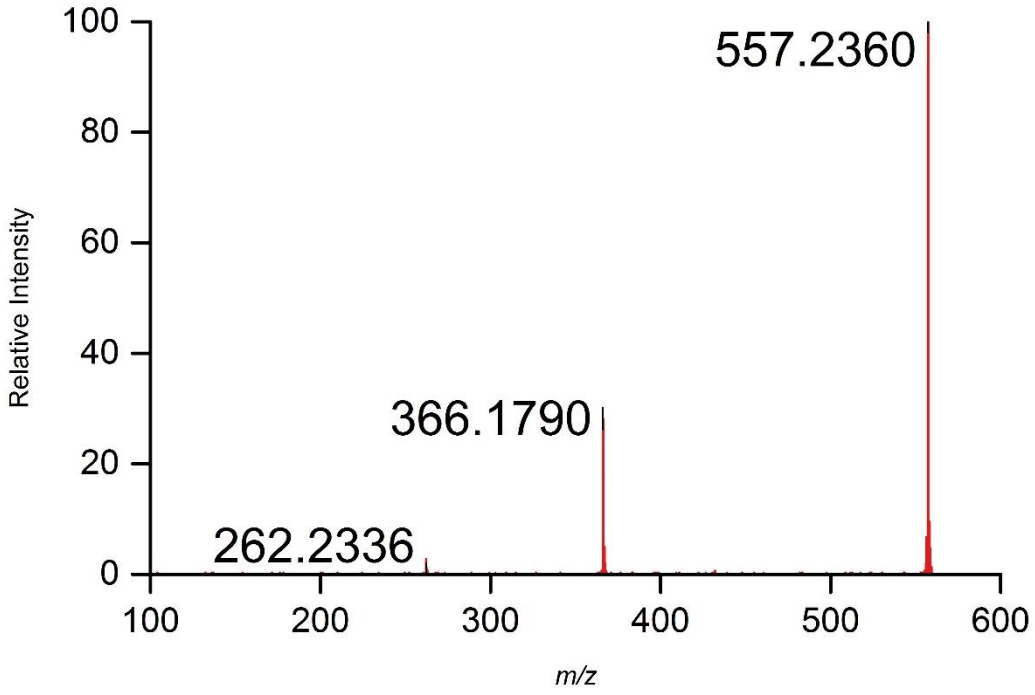

Figure 38. MSMS of nonane-1-thiol derivative with (4) in "Sample A" (NAN-130 77229)

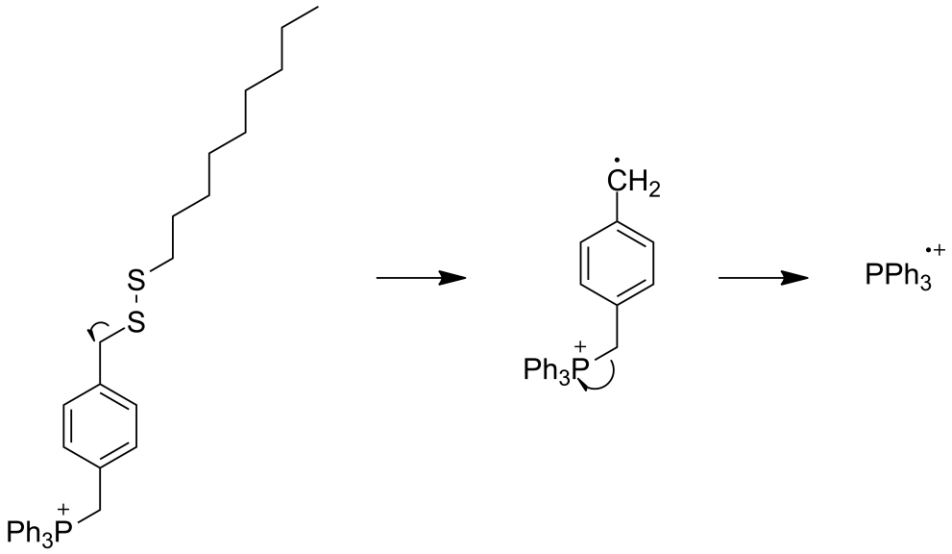

Figure 39. Fragmentation pattern example using nonane-1-thiol derivative of (4)

Because the derivatized thiols fragment in a characteristic manner, treated samples were analyzed with great effectiveness using the precursor ion scan function of a triple-quadrupole mass spectrometer. This led to enhanced selectivity, ease of analysis and sensitivity of the method, but will not described here; instead, this will be further explored in future work.

4.9.5 Online Thiol-Disulfide Exchange Reaction Monitoring and Sample Comparison

We wanted an idea of how this charge tagging methodology occurred in real-time with the jet fuel samples. We explored this with our pressurized sample infusion method to facilitate on-line monitoring of the reaction with jet fuel sample A (Figure 40). The traces of several derivatives demonstrate the reaction progress over a short period of time

following injection of 10 µM of compound (4). The reaction time was lengthier due to the low concentration of thiols present in sample A.

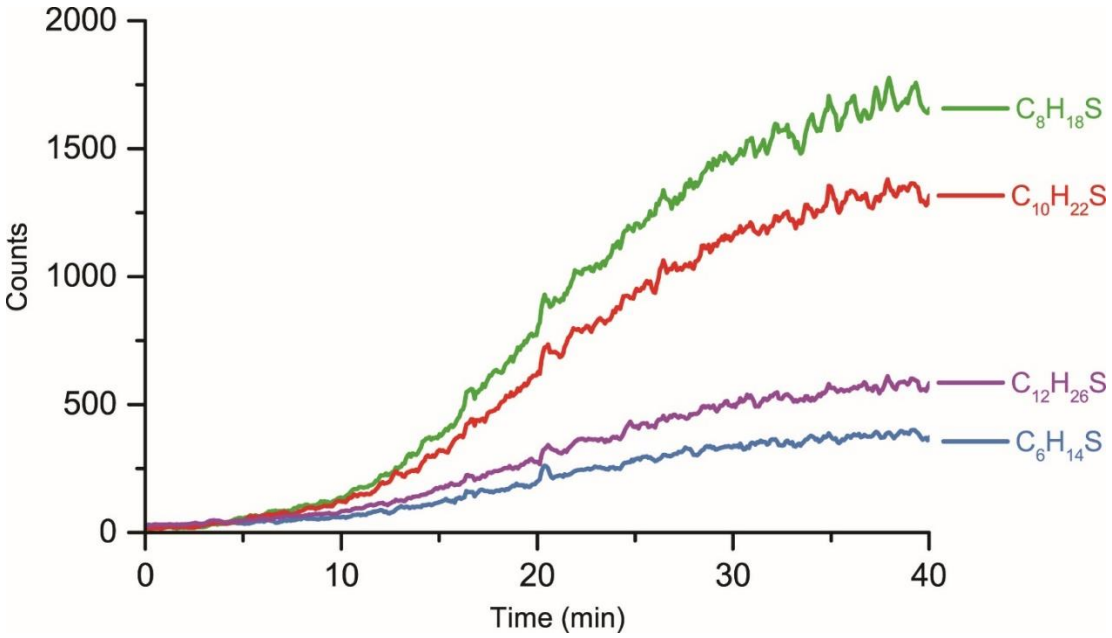

Figure 40. Online derivatization reaction of jet fuel sample A demonstrating the rate of appearance of four of the most abundant derivatized thiols present within the sample

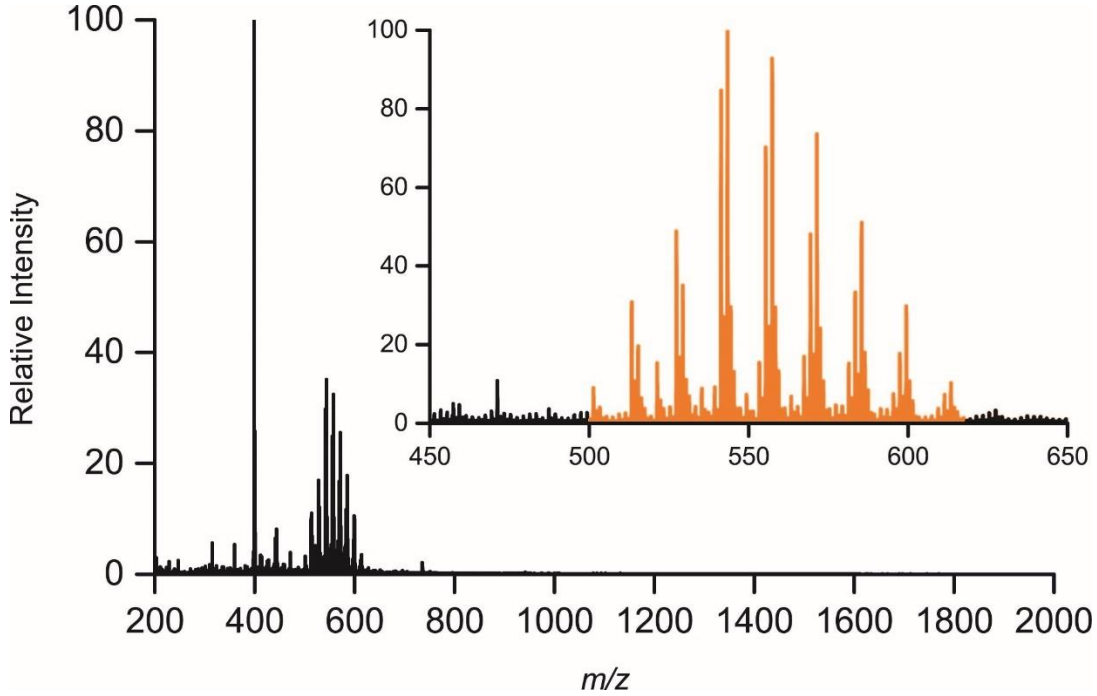

Figure 41. Treated jet fuel sample A (10 µM compound (4), 10%v/v sample in EtOH)

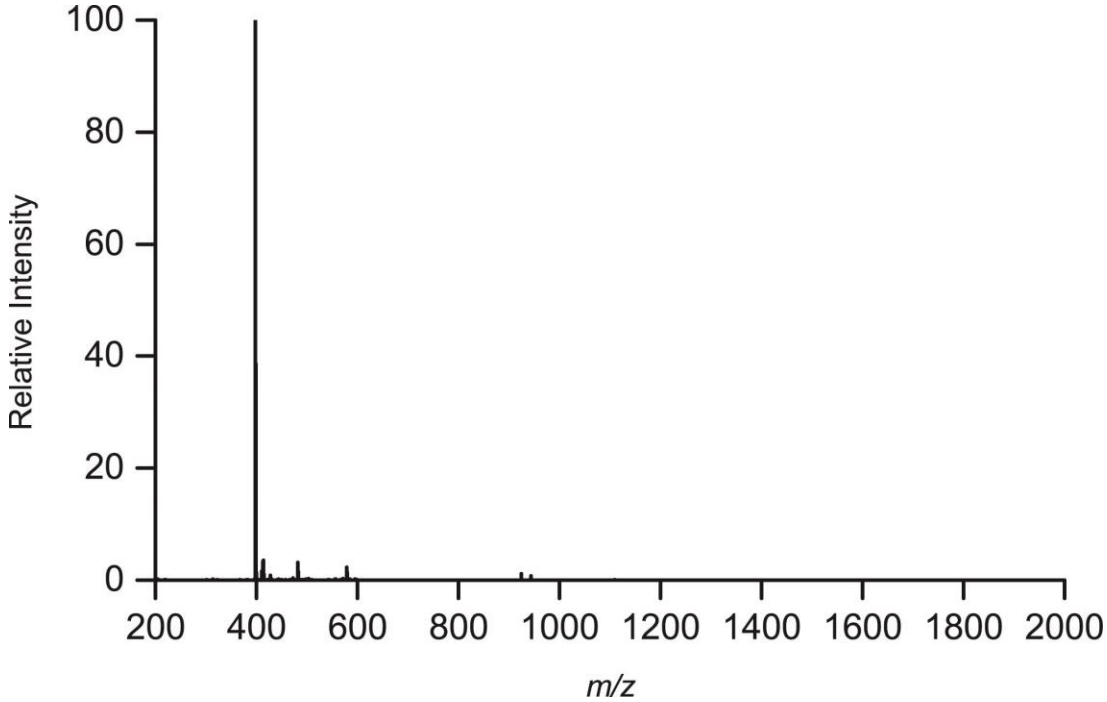

Figure 42. Treated jet Sample B (10 µM compound (4), 10%v/v sample in EtOH).

A dramatic difference was observed between the salt-filtered jet fuel samples A and B. Sample A, originating from further upstream and therefore exposed to fewer refining processes, exhibits a more significant background than sample B. Sensibly, the detectable thiols in sample B are scarce, having been exposed to thiol scrubbing processes such as SCANfining. The mercaptans in sample B are sparse and low in concentration, consisting primarily of short (3-4 C) and moderate (8-11 C) carbon chain length. Judging by the low relative response of these compounds, it is safe to assume these species are very low in concentration. While we cannot definitively comment on concentration due to effects such as spray-quality and completeness of reaction, the thiols in these fuels, and several others with similar treatment (Appendix), appear to have a concentration in the low micromolar range. This is expected and favourable, as it demonstrates the one or more of the refining processes (caustic washing, Merox treating, water washing, salt drying and clay treating) result in dramatic reduction of mercaptans in the jet fuel stream.

4.10 Experimental

All mass spectrometry experiments were collected in the positive ion mode on a Waters Micromass Q-TOF Micro mass spectrometer equipped with a standard Waters Z-spray ESI source. The following parameters were left constant for all experiments: capillary voltage, 3000 V; cone voltage: 15 V; extraction voltage, 0.5 V. Source temperature was set to the boiling point of the solvent used and desolvation temperature was set 100 degrees higher than the source temperature. Cone gas flow rate: 100 L/h. Desolvation gas flow: 200 L/h. Scan time was set to 1 with an inter-scan time of 0.1 s. The MCP detector on the instrument was set to 2.7 kV. Tables of complete instrumental parameters, including quadrupole, TOF settings and TDC (time to digital converter) settings, may be found in the appendix for this chapter (Table 11, Table 12, Table 13).

For PSI experiments, the custom reaction vessel was pressurized using 3 psi of argon gas and solution was fed into the ESI source using 0.178 mm inner diameter PEEK tubing with a length of 50 cm. Mechanical stirring was provided by magnetic stirring hot plate and stir bar. In a typical experiment, a Schlenk flask was charged with a 10% (v/v) solution of a petroleum fraction, and 1-10 eq. of NaOH in 25mL of ethanol. Subsequently, a 100 uL of charged disulfide (4) solution was injected to the mixture, giving a 10-20 μM concentration of (4).

For non-PSI experiments, solutions were fed into the ESI source through the use of a syringe pump and a Hamilton GASTIGHT® analytical syringe connected to PEEK tubing (0.1778±0.0127 mm inner diameter, 50 cm length). Prior to each run, instrument

cleanliness and stability and was ensured through rinsing with the appropriate solvent and acquisition of stable analyte signal from the subsequent sample solution. After achieving a steady signal, the spray head was moved to a position with optimal intensity and was locked to this position for every experiment.

MS/MS experiments were conducted using the following parameters to acquire structural information. The collision cell energy was set to 32 V, with the high mass and low mass resolution maintained at 15 V each. Argon was used as the collision gas with an internal collision cell pressure of 2.0e-5 psi.

Mass spectrometric data interpretation was aided with online tools available from chemcalc.org.[154]

GC-MS data was collected on a PerkinElmer Clarus 680 with a PerkinElmer Axion iQT MS/MS. The injector used was a programmable split/splitless injector with a 0.5 µL injection volume set to 220°C. The analytical column used was a PerkinElmer EliteTM-5MS (30 m × 0.25 mmID × 0.25 µm). Carrier gas flowrate was set to 1 mL/min. The oven was programmed initially to hold at 40°C for 1 minute, with a final ramp of 20°C to 260°C held for one minute. The cold EI source conditions were as follows: GC transfer line was set to 250°C, ion source temperature 200°C, acquisition range *m/z* 50-500, acquisition time 0.2 s, solvent delay 3.0 mins for split 10, cold EI makeup gas 50 mL/min, and filament set to 5 µA.

The ^{1}H and ^{31}P NMR were recorded on a Bruker Avance 300 MHz spectrometer as solutions prepared in $CDCl_3$.

Solvents and chemicals were purchased from Sigma-Aldrich. All anhydrous and air-free solvents were purified with an MBraun solvent purification system before use unless otherwise noted. Deionized water was obtained from a Millipore Milli-DI water purification system. All petroleum and petroleum fractions samples (including samples "A" and "B") were supplied courtesy of Imperial Oil.

Synthesis of (3) (4-(bromomethyl)benzyl)triphenylphosphonium hexafluorophosphate

Triphenylphosphine (1.58 g, 6.02 mmol) was alkylated with excess α,α′-dibromo-p-xylene (2.00 g, 7.58 mmol) through gentle reflux under argon over 12 hours in 50 mL of toluene in order to generate the phosphonium bromide salt. A white powder was recovered from toluene through filtration and dried under reduced pressure overnight (3.10 g, 5.89 mmol 98% yield). Salt metathesis with sodium hexafluorophosphate improved the solubility of the salt in non-polar solvents, proving helpful for subsequent steps. Several anions were used to substitute the bromide counterion; however, a good mix of cost-effectiveness and increased solubility in polar solvents was achieved through substitution with hexafluorophosphate. The phosphonium salt (3.10 g, 5.89 mmol) was dissolved in a minimum of 85% MeOH and 15% deionized water, by volume. To this, 2.0 equivalents (1.98 g, 11.8 mmol) of sodium hexafluorophosphate were added and stirred for one hour. A white precipitate formed quickly and the powder was recovered through vacuum

filtration and, following three washes with 30 mL aliquots of deionized water to remove excess sodium hexafluorophosphate, was recovered and dried under reduced pressure overnight (99% yield). This step also served to greatly increase the purity of the compound as vacuum filtration of the hexafluorophosphate substituted product yielded ionic compounds exclusively.

No detectable double-substitution product was formed in the first step which resulted in a high-yield of a very pure and versatile precursor charge-tag compound which may be used in a variety of applications.[134]

^{1}H NMR (300 MHz, $CDCl_3$): δ_H 4.39 (2H, d, J=0.9 Hz), 4.53 (2H, d, J=14.1 Hz), 6.88 (2H, dd, J=8.3, 2.5 Hz), 7.16 (2H, d, J=7.9 Hz), 7.40-7.88 (15H, m), ^{31}P{^{1}H} NMR (300 MHz, $CDCl_3$): δ_P -144.25 (spt, $J_{P\text{-}F}$ = 712.1 Hz), 22.65 (s). QTOF ESI+: *m/z*: $[M]^+$ 445.3.

Synthesis of Charge-tagged Disulfide (4)

Complete synthesis of the charged disulfide proceeded as shown in Scheme 1. The phosphonium-hexafluorophosphate salt, (4-(bromomethyl)benzyl)triphenylphosphonium hexafluorophosphate, (0.70 g, 1.2 mmol) was dissolved in 25 mL methanol. To this solution, potassium thioacetate was added (0.65 g, 5.7 mmol, 5 eq.) and stirred at gentle reflux for two hours. This solution was initially light tan and developed a deep red colour within 30 minutes of reflux as the compound is thioacetylated. Continued reflux resulted in a subsequent change in colour to a light tan solution indicating formation of the thiol and continued stirring in air provides oxidation to the disulfide. Extended, aggressive reflux

at this step resulted in moderate decomposition and should be avoided for best yield. This step provided transesterification and hydrolysis of the thioester, forming the thiol which oxidizes spontaneously in air to the disulfide. The thiol may be recovered if reflux was done under an inert atmosphere. A variety of oxidants may be used to induce formation of the disulfide from the thiol. Further, the thioester may be recovered if the solution was simply stirred overnight without heat. Reflux of the methanolic solution while exposed to air, or stirring while bubbling air through the solution both provided sufficiently oxidizing conditions to produce the disulfide. The disulfide was recovered from methanol through rotary evaporation under reduced pressure. Excess potassium thioacetate was removed following three washes of deionized water, and the light tan solid was recrystallized from methanol to achieve high purity. The disulfide crystals were dried under vacuum overnight.

^{1}H NMR (300 MHz, $CDCl_3$): δ_H 3.83 (4H, s), 4.53 (4H, d, J=14.30 Hz), 6.81 (8H, s), 7.44-7.85 (30H, m), $^{31}P\{^{1}H\}$ NMR (300 MHz, $CDCl_3$): δ_P -144.17 (spt, $J_{P\text{-}F}$ = 713.57 Hz), 22.48 (s). QTOF ESI+: *m/z*: $[M]^{2+}$ 398.1.

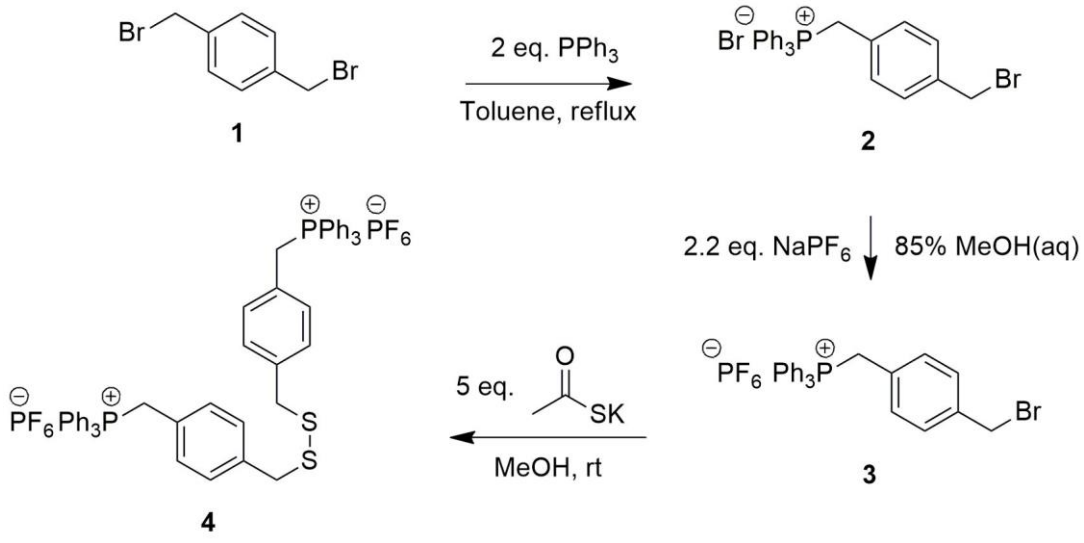

Figure 43. Charge-tagged disulfide (4) synthetic pathway

Data and plots were processed using OriginPro 2016. MS and NMR data was exported directly from files acquired using MassLynx 4.1 and TopSpin 3.5, respectively.

4.11 Conclusions

A chemical derivatization technique using the principles of thiol-disulfide exchange and charge tagging was developed for ESI-MS for the detection and characterization of thiols and disulfides in petroleum fractions. This reagent, and other similar tags, greatly enhance the detection of the target analyte for a rapid and simple analysis. This is in large part owing to the high spray quality of the tag and its derivatives, along with the fixed charge appended to the target. Some advantages of this are that expensive isotopically labelled substrates to identify analytes are not required, we can perform the analysis in a very complex and impurity-ridden matrix without pre-treatment such as filtering or chromatography techniques, and that the total analysis time is quite short. The synthesis of these reagents, and similar charge tags, is simple and very easy to prepare with high purity. The effectiveness of this methodology was demonstrated with a variety of petroleum samples provided by Imperial Oil.

Due to the nature of our industrial partnership, this research is highly focused for one specific application: the qualitative characterization of thiols in petroleum samples. While selective chemical derivatization of chemical compounds for electrospray ionization mass spectrometry is not new, its application in petroleomics has not been extensively studied.

The selective detection and characterization of undesirable components in petroleum fractions is an incredibly valuable task due to important economic and environmental motives; however, this remains a challenge despite considerable effort. This research focuses on the characterization of petroleum (and deals largely with the difficulty of this specific matrix) and while this was developed as a technique for the petroleum industry, it is very possible that this research and methodology could prove useful in many other areas of research. This supported due to the fact that ESI-MS enjoys a wide range of applicability in analyzing complex and often "dirty" samples (very commonly seen in biological applications). The "softness" of ESI-MS ionization can turn into a downside when the analyte of interest is not readily, or adventitiously, ionizable. Our charge tagging methodology, an extension upon traditional ionization techniques in ESI-MS, greatly enhances our ability to target neutrals in a mixture and allows us to characterize diverse matrices or follow a reaction without overly complex preparation or planning. The main advantage for the analysis is the resulting spectra are generally much cleaner and easily interpretable than in less-selective approaches where derivatization is either non-specific or inefficient. In this specific application, we enjoy a rapid and effective reaction which requires no chromatographic steps and can be executed using readily available instrumentation and chemicals. Because of the simplicity and ease of use and analysis it is expected that the method employed here will extend to other areas of research. We have been focused on the analysis of petroleum; however, this research should easily extend to other applications in fields of high interest such as the analysis of biological environmental samples.

Chapter 5. Activation of Palladium Catalyst Precursors

5.1 Abstract

This work describes methods for the real-time investigation of palladium catalyst activation reactions through the use of combined, orthogonal analytical techniques: electrospray ionization mass spectrometry (ESI-MS) and ultraviolet-visible (UV-Vis) spectroscopy. In order to study the reaction as it occurs we used Pressurized Sample Infusion (PSI).[41] For the first time, we used the cannula transfer-like mechanism to monitor a reaction mixture by both a flow UV-Vis and ESI-MS with great success. We used the popular precatalyst tris(dibenzylideneacetone)dipalladium(0) ($Pd_2(dba)_3$) for the activation, along with sulfonated versions of PPh_3 and a Buchwald-type ligand. This provided insight into the effect of ligand and preparation conditions on palladium activation.

5.2 Introduction

Catalyst activation shares some similarity to the culinary arts. Several experts claim to have the best recipe; however, this claim is not necessarily backed with hard science but is

instead grounded in traditional methods. It is often complicated due to these inscrutable recommendations concerning reaction conditions which, apparently, few chemists seriously investigate. The solvent, temperature, mixing time, addition order, and exposure to various activators and additives are all possible components of a procedure. However, the reasoning for a particular set of conditions is often obscure and grounded mostly in received wisdom. While this approach is somewhat effective, potential for improvement is hampered by a lack of understanding of what is going on. There exists a need for the application of high quality instrumental analyses of these reactions to better describe homogeneous catalytic reactions and to expand on important details such as catalyst deactivation routes. We decided to address this by inspecting the effect of various conditions on catalyst activation using a well-known precursor in palladium-catalyzed cross-coupling, tris(dibenzylideneacetonedipalladium) (abbreviated as $Pd_2(dba)_3$), and monitoring the reaction in real time using two orthogonal analytical techniques: UV-Vis spectroscopy and electrospray ionization mass spectrometry (ESI-MS). To the best of our knowledge, the two very common pieces of analytical equipment have not been used simultaneously on a single vessel to study catalytic systems in detail.

Palladium-based catalysts are some of the most important and widely used transition-metal complexes in catalysis and are frequently employed in organic synthesis to facilitate a number of coupling reactions.[213] Preparing the active catalyst is very often performed *in situ* through mixing of a palladium source with a ligand to enhance catalytic activity of the metal. The result of the activation process depends on a variety of conditions such as the precatalyst source,[214] order of addition, choice of ligand, and application or duration

of heat or mixing.[215] Precatalyst activation is one of the main considerations in determining the efficiency and scope of many catalytic reactions.

Palladium acetate, a common source of Pd(II) used in palladium catalysed reactions, has received a large amount of attention which is nicely summarized in a recent review by Carole and Colacot.[216] Within, the authors critically assess the catalytic activity and activation pathways of palladium acetate in excellent detail. On the other hand, investigations regarding the activation of zero valent Pd precursors remains limited.[217–224]

Tris(dibenzylideneacetone)dipalladium(0) ($Pd_2(dba)_3$) is the most popular source of zerovalent palladium and is used in several highly important bond-forming reactions such as the Heck reaction,[225,226] the Buchwald-Hartwig amination,[227–229] the Suzuki-Miyaura coupling,[230] and ketone arylation.[231,232] The palladium source has been used to produce diverse compounds such as pharmaceuticals,[233,234] natural products,[235,236] organic light emitting diode materials,[237] solar cells,[238] and photovoltaic polymers.[239] However, there is some contrast between the popularity of $Pd_2(dba)_3$ as a precatalyst and the detail with which users recognize the fine details of priming the complex for a catalytic coupling reaction. Indeed, only very recently has $Pd_2(dba)_3$ been seriously examined with respect to purity, nanoparticle formation and its potential effect on catalytic activity by Ananikov and Zalesskiy.[214] Despite this, the actual nature of the catalytically relevant species and the influence of reaction conditions on its activation are incompletely understood. The precatalyst is surprisingly complex, resulting in much effort required in order to accurately

characterize the complex, detailed in an isotopic labelling investigation by Fairlamb *et.al*.[232]

In situ activation with this precursor is most often carried out by the addition of two equivalents of phosphine ligand to a $Pd_2(dba)_3$ solution which is either preheated or stirred for an extended period of time.[217–219,227] The process is often depicted as a simple ligand exchange (see Scheme 11) but this process is more complicated since the displaced dibenzylideneacetone (dba) ligand in solution competes with the phosphine ligand (L) for coordination to palladium.

$$Pd_2(dba)_3 + 4L \rightleftharpoons 2Pd(\eta^2\text{-}dba)L_2 + 2dba$$

Scheme 11. Common portrayal of $Pd_2(dba)_3$ activation

Previous work on the activation process involving simple phosphine ligands has explored the non-innocence of the dibenzylideneacetone ligand under particular conditions.[217–220]

The activation processes of an analogous complex, bis(dibenzylideneacetone)palladium(0) ($Pd(dba)_2$), has been studied in some detail previously. For example, Amatore and Jutand explored the reactivity of mono- and bidentate phosphine-activated $Pd(dba)_2$ (using a combination of UV-Vis, NMR and electrochemistry) and found that the nature of the phosphine ligand used resulted in several stable dba-containing catalysts in solution which diminished oxidative addition activity.[217] By extension, non-innocence of the dba ligands in $Pd_2(dba)_3$ activation will result in complications forming the active catalytic species, instead forming the less

reactive $Pd(L)_x(dba)_y$ compounds which reduces the efficiency of catalytic reactions.[217–220,240] Interestingly, in a study involving *in-situ* precatalyst activation using 1,1‘-binaphthalene-2,2‘-diylbis(diphenylphosphine), Buchwald, Blackmond, and Hartwig found that some of these $Pd(L)_x(dba)_y$ species may actually be involved in the generation of catalytically active species. The occurrence of these species in different solvents systems during activation has not yet been investigated in detail and may play a significant role in the catalytic process.[241–243]

Fairlamb *et.al.* demonstrated the importance of dibenzylideneacetone ligand substituents and their effects in modulating the activity of Suzuki-Miyaura coupling reactions.[220] Importantly, the speciation of *in-situ* activated $Pd_2(dba)_3$ in various solvent systems remains somewhat ambiguous, leading to some uncertainty regarding the reactivity of isolated catalysts versus those prepared *in situ*.[215]

Furthermore, several examples appear in the literature in which *in situ* precatalyst activation is carried out using either a relatively large amount of $Pd_2(dba)_3$, elevated temperatures, or extended stirring times following the addition of phosphine ligand, potentially spurring oxidation of the phosphine ligand and wasting a significant portion of the catalytic precursor.[214,244] Preheating has been suggested as a means to ensure reproducible reaction rates;[227,245–247] however, it is unclear if this is truly beneficial and others question the benefits of this step in catalyst activation.[214,215,248] For example, preheating may simply promote the loss of phosphine ligand to the oxidized product due to catalytic decomposition.[180] These kinds of losses are typically acceptable when

producing microscale quantities of a synthetically challenging complex; however, the loss may ultimately be unnecessary in the majority of applications.

Depending on the ligand and the reaction conditions chosen, the activity appears to vary substantially.[249] Perplexingly, the effect of certain changes in parameters during activation are occasionally contradictory.[250] Unsurprisingly, the choice of supplier, handling of the precatalyst, or storage may influence the activation and catalytic activity of $Pd_2(dba)_3$. Possible reasons for this include the presence of minor impurities or palladium nanoparticles in individual samples of $Pd_2(dba)_3$.[214,251]

The McIndoe group has previously investigated several organometallic and catalytic systems through the use of electrospray ionization mass spectrometry (ESI-MS) and so we are very comfortable with the technique.[1,3,4,32–40] ESI-MS is uniquely well-suited to study these types of systems, including homogeneous catalytic systems, due the wide dynamic range and low degree of fragmentation.[46] Coupled with charge tagged ligands, ESI-MS has been established as a useful means of enabling real-time monitoring of a normally neutral system.[2,43,65] To develop a more complete analysis, we have more recently begun examining the potential of tandem orthogonal analytical techniques, including UV-Vis. Ultraviolet-visible (UV-Vis) spectroscopy is an exceedingly well-tested form of molecular spectroscopy and an analytical technique that has been employed for several decades due to high reliability and sensitivity. Because of the synergistic nature of orthogonal analytical techniques, we chose to use UV-Vis coupled to ESI-MS evaluate the activation process. This also allows us to observe neutral species which are invisible to mass spectrometry

alone. This methodology provided us with a deeper understanding of the activation of $Pd_2(dba)_3$ under various conditions and allowed us to optimize the formation of active catalyst.

5.3 UV-Vis/ESI-MS methodology for $Pd_2(dba)_3$ activation

We expected to further extend our grasp on what was occurring in solution beyond ESI-MS with the application of UV-Vis for this study and future investigations. Solutions of $Pd_2(dba)_3$ exhibit a strong purple colour due to palladium-bound dibenzylideneacetone ligand which, when uncoordinated, is a strong yellow colour. This strong colour persists even at low (catalytic) concentrations. The addition of neutral $Pd_2(dba)_3$ to certain solvents results in a persistent, strong purple colour. While the UV-Vis signal demonstrates a characteristic absorption profile, the mass spectrometer is silent. In methanol, $Pd_2(dba)_3$ possesses a strong absorbance at 532 nm (d-d) along with another, stronger absorbance at 345 nm (n-π*) owing to the presence of free dba ligand which is exceedingly common in commercial samples.[214,220] The colour of the solution changes from light purple to bright yellow following the addition of ligand due to the release of free dba into solution as it is displaced from Pd.

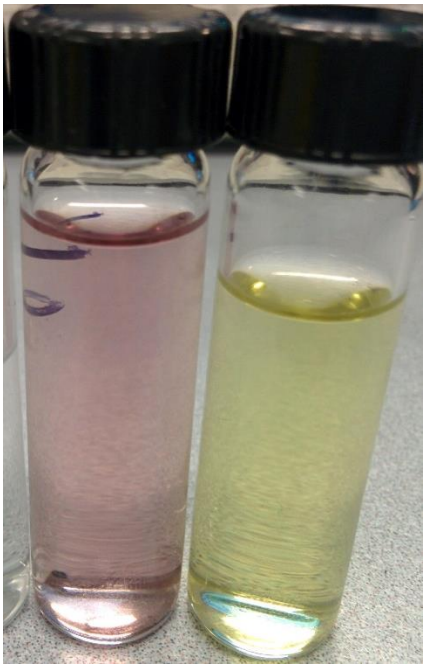

Figure 44. The distinctive colours of dilute tris(dibenzylideneacetone)dipalladium (left, purple) and dibenzylideneacetone (right, yellow) solutions in methanol

Our preliminary experiments were performed using an in-line UV-Vis detector. The Waters 996 photodiode array (PDA) detector is equipped with a flow-cell and is typically employed in conjunction with a high-pressure liquid chromatography (HPLC) setup. The flow cell design allows for continuous infusion of solution from a pressurized vessel directly to the UV-Vis then to the ESI-MS probe. Because the UV-Vis used is equipped with a PDA detector, we were able to obtain one full spectrum from 190-800 nm each second and monitor the dynamics of individual wavelengths in this region with a resolution of 1.2 nm.

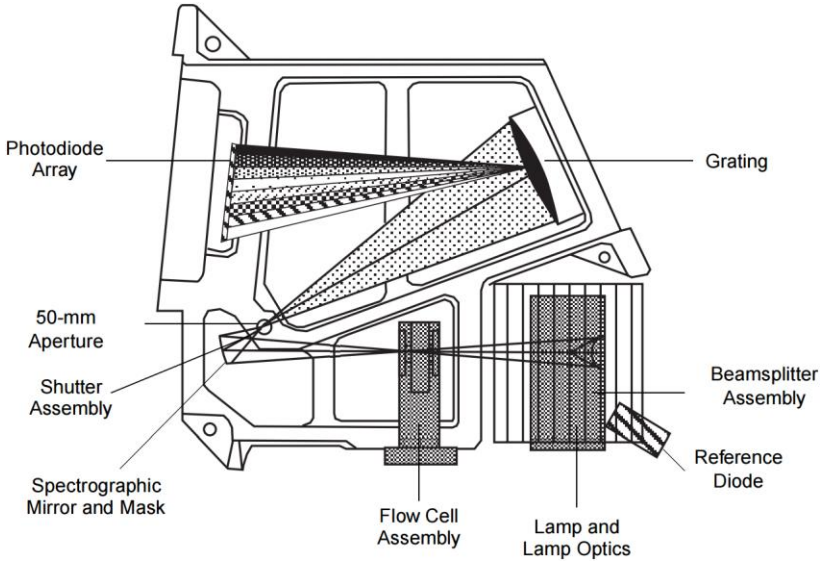

Figure 45. Optic Diagram of the Waters 996 Diode Array Detector[252]

These initial experiments facilitated identification and monitoring signals of interest for the activation process or $Pd_2(dba)_3$. This detector seemed an ideal choice due to its wide solvent compatibility and fairly simple setup for the reason that we could use our existing hardware (such as our custom Schlenk flasks termed "PSI flasks") and PSI methodology. Figure 46 is a schematic of the in-line setup. The setup was similar to a typical PSI experiment in which an overpressure of inert gas is applied to a custom built Schlenk flask with an in-line condenser containing a reaction mixture. Much like a cannula transfer, the reaction mixture in the PSI flask is forced through PEEK tubing. This solution first passed through the Waters 996 PDA before carrying on to the ESI-MS source. To prevent an extended lag time from the PDA detector to the ESI source, all PEEK tubing lengths were kept at a minimum and the flow rate was optimized. Prior to an experiment, the lag time between detection by the UV-Vis PDA and appearance in the MS was calculated with a dilute standard of caffeine and this time was corrected in post-processing. With proper length and diameter of PEEK tubing as well as sufficiently high (4 psi) Argon gas

overpressure, the lag time was generally under 10 seconds. This was acceptable for our purposes since most of the reactions we study are sufficiently slowed (both by cooling and lack of mixing) within the PEEK tubing and we obtained a true "snapshot" of the reaction at a specific point in time with excellent dynamic data. Further, the important transient species in many catalytic reactions survive and accumulate for a great deal longer than 10 seconds. That being said, it is worth noting that this technique may not be desirable for detecting ephemeral species where a rapid *in situ* approach excels.

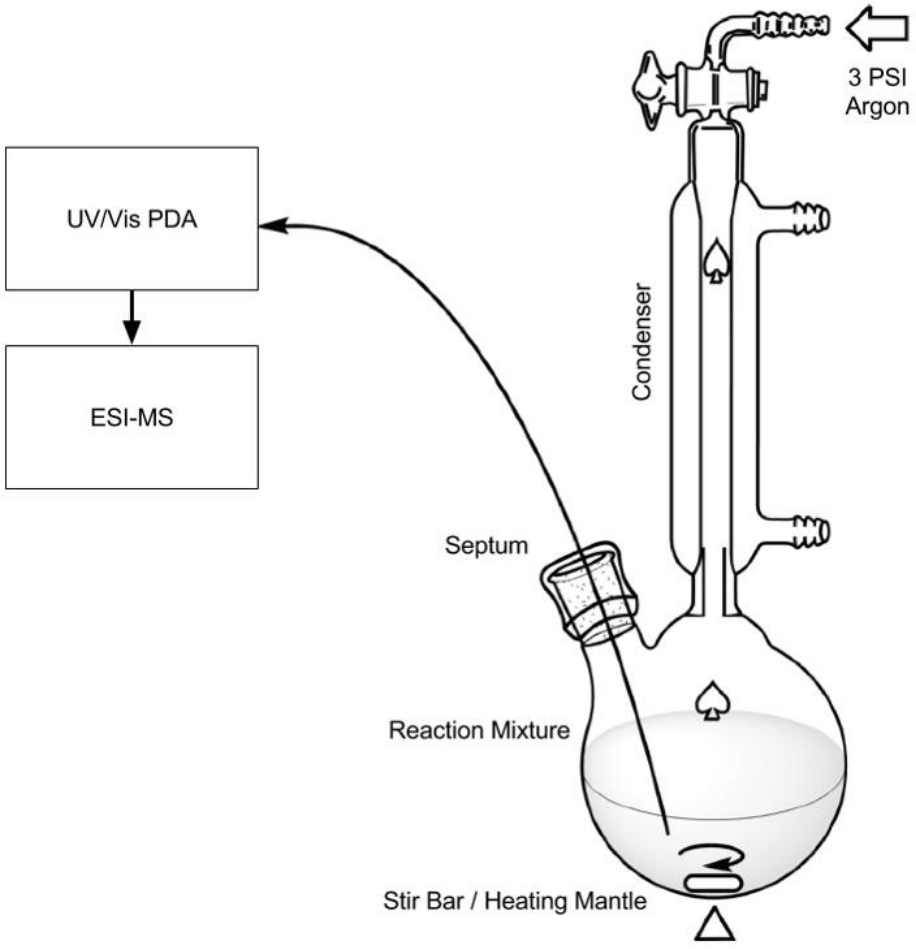

Figure 46. Schematic diagram of initial PSI UV-Vis/ESI-MS setup using the Waters 996 UV-Vis PDA detector

Figure 47 is a series of UV-Vis spectra taken over approximately 1.5 minutes during the activation of $Pd_2(dba)_3$ with TPPMS in methanol with the Waters 996 PDA. It is immediately apparent from the signal at 328 nm that some free dba is present prior to the addition of $Pd_2(dba)_3$ to methanol, likely due to the purity of $Pd_2(dba)_3$ from a commercial source which was used as is.[214] This intensity of this absorbance grows over time as TPPMS displaces the dba from palladium. During this reaction, the signal at 528 nm corresponding to bound dba ($Pd_2(dba)_3$) disappears following the addition of phosphine ligand along while a signal specific to the active catalytic species, $[Pd(TPPMS)_2(dba)]^{2-}$, appears at 402 nm.

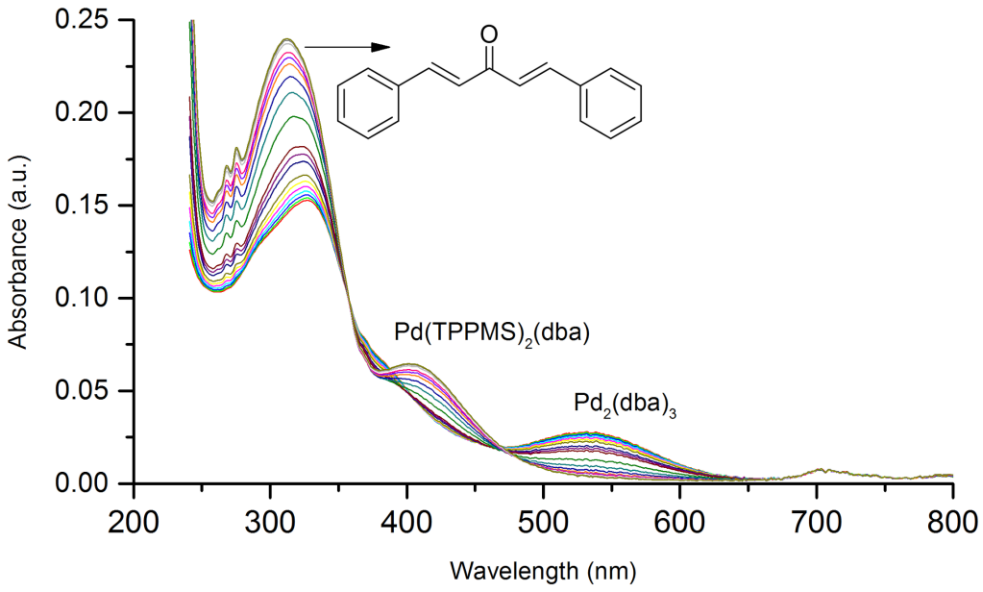

Figure 47. Illustrative example of spectral shifts during activation of $Pd_2(dba)_3$ with 4 eq. TPPMS in methanol

While it served to lay the foundation of future experiments, this detector yielded highly irreproducible results due to technical issues. Because the flow-cell in this instrument is typically used as a detector for high performance liquid chromatography systems, the pressure and volume within the flow-cell cell was inadequate when paired with our PSI technique which operates at a substantially lower pressure than the typical operating pressure of around 400 bar supplied by an HPLC pump. The internal volume of the flow cell is of fixed size as it is primarily a single machined cell with non-adjustable stainless-steel tubing; this resulted in frequent clogging which resulted in extremely time consuming (delicate) cleaning, along with the loss of useful data.

The majority of the experiments discussed in this chapter were performed with a much more reliable transflectance fiber optic dip probe (see experimental section for full details) and ASEQ instruments LR-1 broad range spectrometer (also equipped with a PDA detector) which enabled *in situ* UV-Vis monitoring. This setup for monitoring of catalytic systems – the first of its kind as far as we could determine - retains the benefits of sensitivity and speed of analysis while being a more direct approach since the probe is submerged directly into the solution.

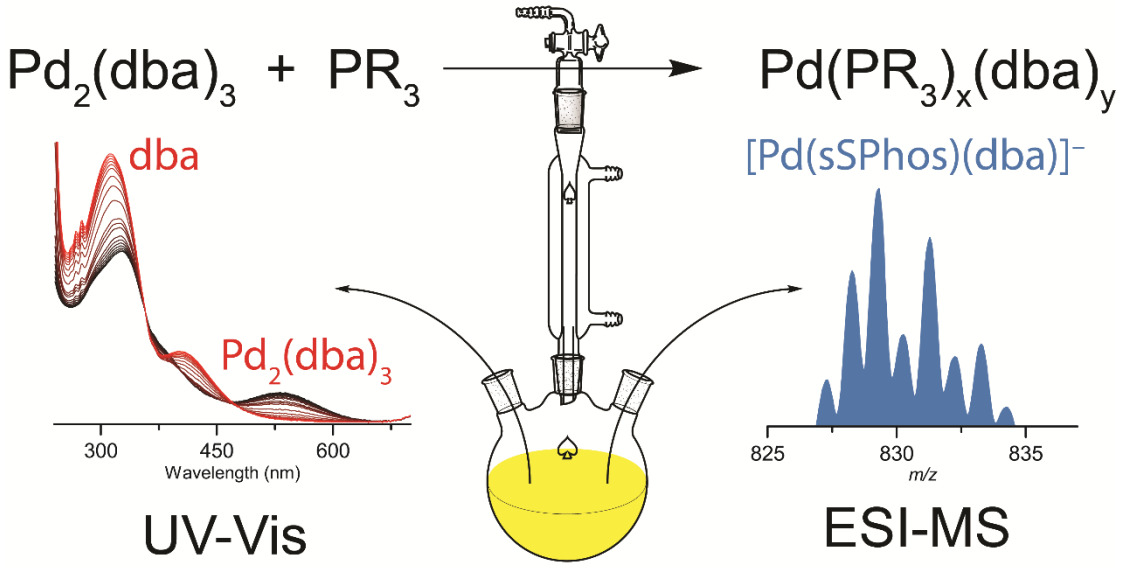

Figure 48. General schematic of $Pd_2(dba)_3$ activation using combined UV-Vis, ESI-MS methodology

5.4 Effect of cone voltage on speciation in ESI-MS

The relatively weak bonds of the active catalytic species required careful optimization of the mass spectrometer to prevent significant fragmentation of these delicate species. The potential between the capillary and the sampling cone on an ESI-MS instrument is referred to as the cone voltage. Increasing this value has been shown to promote in-source collision-induced dissociation (CID) due to the higher kinetic energy applied to ions generated from the electrospray process.[253]

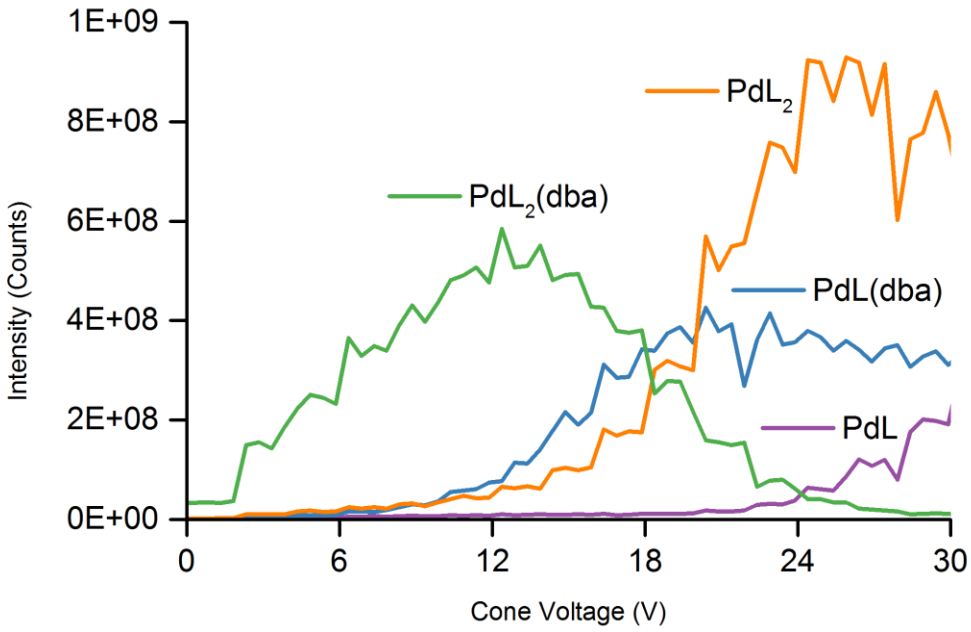

Figure 49. Observed speciation over a range of applied cone voltages following activation of $Pd_2(dba)_3$ with 4eq. TPPMS (L) in methanol at room temperature (21°C)

The increased kinetic energy results in CID with the bath gas which is used to promote desolvation. In order to probe the effect cone voltage has on apparent speciation we decided to increase the cone voltage over time and observe changes in the mass spectrum. It was determined that the compounds present above a cone voltage of 10 V are actually fragments formed out of higher-order species such as $[Pd(TPPMS)_2(dba)]^{2-}$; therefore, we opted to leave the cone voltage very low for all solvents to report the proper speciation because of the fragile species involved.

5.5 *In-situ* precatalyst activation

To observe the formation of catalytically active products with both ESI-MS and UV-Vis, charged phosphine ligands were used in conjunction with $Pd_2(dba)_3$ as a source of palladium. Both of the ligands used in this study were sulfonated, enabling their detection in the negative ion mode (see Figure 50). The simplest phosphine ligand used was bis(triphenylphosphine)iminium ($[PPN]^+$) triphenylphosphine-*meta*-sulfonate ($[TPPMS]^-$) **(1)** which was chosen as an analogue of triarylphospines (PAr_3), the most commonly used phosphine ligands. A bulkier biaryl phosphine ligand, sodium 2′-dicyclohexylphosphino-2,6-dimethoxy-1,1′-biphenyl-3-sulfonate hydrate ($Na^+[sSPhos]^-$, also referred to as sSPhos) (**2**), was also used to determine any differences in speciation. Stephen L. Buchwald made famous this eponymous series of ligands known as Buchwald ligands. These ligands, including $Na^+[sSPhos]^-$ (**2**), are noteworthy because they are extraordinarily versatile reagents, especially useful in many coupling reactions, and well known for their resiliency against oxidation.[227,254–256]

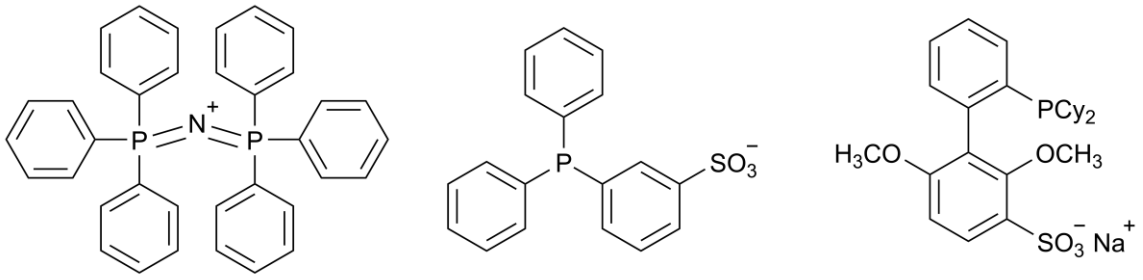

Figure 50. Sulfonated phosphine ligands used in this work: $[PPN]^+[TPPMS]^-$ (1); $Na^+[sSPhos]^-$ (2)

The *in-situ* catalyst activation process is technically simple. A custom Schlenk flask was evacuated and filled with degassed solvent. To this, a mixture of either phosphine ligand

was added in a 4:1 ligand to $Pd_2(dba)_3$ ratio while stirring (generally at room temperature). This rapidly generated a series of active catalytic species, depending on the solvent used. This reaction mixture was introduced to the mass spectrometer via our pressurized sample infusion (PSI) methodology,[41,42] passing first through the UV-Vis photodiode array detector.

Once setup, the ligand or palladium was injected through the septum of the vessel and the activation process was monitored. Following the addition of charged ligand, both free ligand and ligated palladium complexes were easily identifiable using ESI-MS. The combination of these two techniques allowed us to monitor the conversion of $Pd_2(dba)_3$ into the charged catalyst under a variety of conditions. Initial results in methanol yielded a variety of species, with the major palladium species present containing two ligands as well as dibenzylideneacetone (dba); in fact, $[Pd(TPPMS)_2(dba)]^{2-}$ appeared to be the sole catalytically active compound present and other, less intense complexes which formed seemed to be slight fragmentation of the primary palladium complex; however, we need to investigate this effect further.

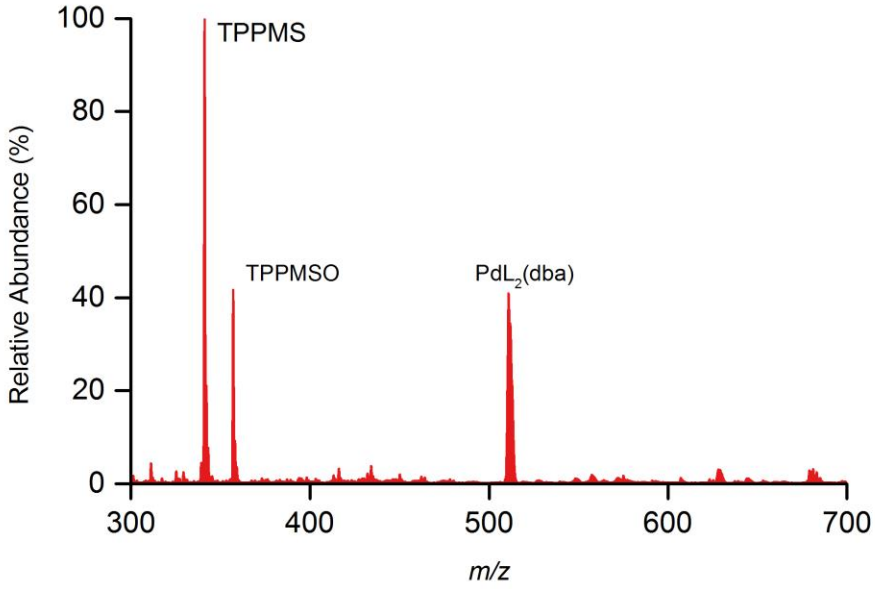

Figure 51. Mass spectrum of the mixture of 4 eq. $[PPN]^+[TPPMS]^-$ with 1 eq. $Pd_2(dba)_3$ in methanol at 10 V cone voltage

5.5.1 Activation of $Pd_2(dba)_3$ in methanol

Following methodology optimization for simultaneous ESI-MS and UV-Vis monitoring, the setup was used to simultaneously monitor the activation process of $Pd_2(dba)_3$ using both ESI-MS and UV-Vis in a variety of solvents and reaction conditions. The use of the technique to monitor the activation process with TPPMS in room temperature methanol may be seen in Figure 52. In this plot, 402 nm is assigned as the newly formed $[Pd(TPPMS)_2(dba)]^{2-}$; however, some overlap exists with free dba as seen by the jump in intensity of the signal prior to addition of precatalyst. The advantage of the technique was immediately obvious, especially during the period in which no signal was observed by ESI-MS (~3-7 minutes in Figure 52), as well as the complementary MS information obtained following the addition of ligand (see Figure 52 after roughly 7.5 minutes).

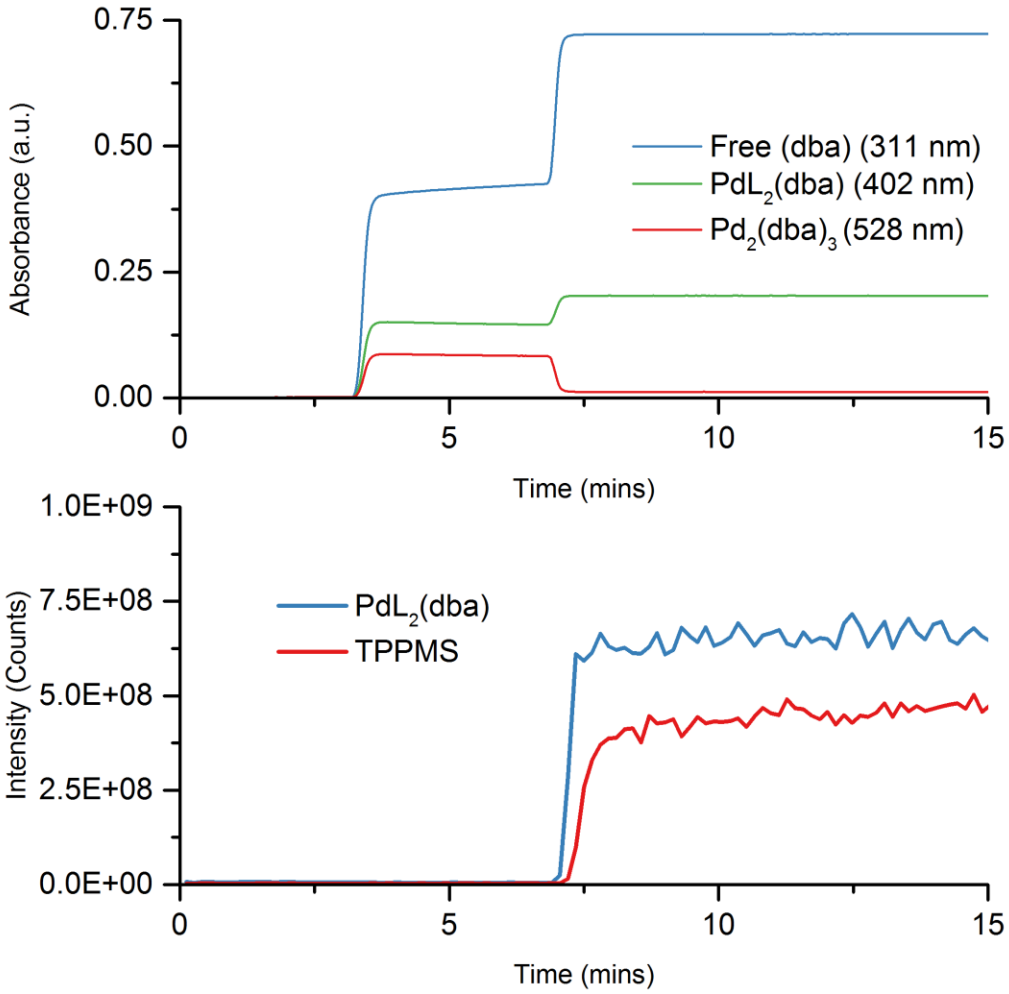

Figure 52. Activation of $Pd_2(dba)_3$ precatalyst with 4 eq. TPPMS in room temperature methanol monitored using the Waters 996 UV-Vis and ESI-MS

It was immediately obvious that dibenzylideneacetone is a non-innocent ligand in the activation process in methanol. In order to probe the reactivity of the complex formed in methanol, 50 eq. of iodobenzene was added following the activation with 16 μM $Pd_2(dba)_3$ and 64 μM TPPMS. This resulted in a fast conversion (2.5 mins) of $[Pd(TPPMS)_2(dba)]^{2-}$ in solution into the oxidative addition products, $[Pd(TPPMS)(Ph)I]^{-}$ and

$[Pd(TPPMS)(Ph)I(dba)]^-$ (Figure 53). The rapid reaction was somewhat surprising, considering the propensity of the dba ligand to interfere with oxidative addition.

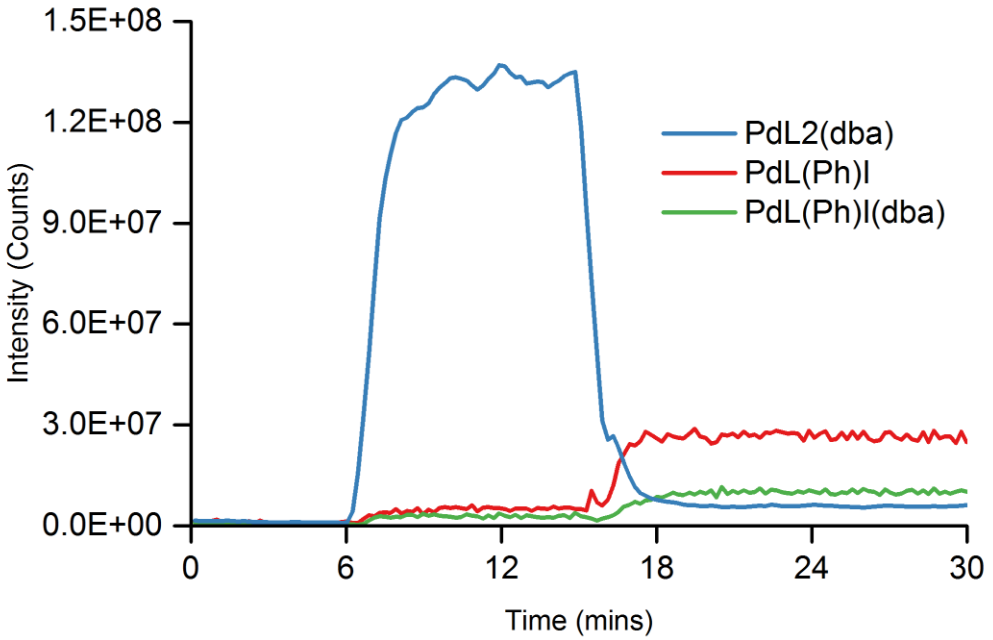

Figure 53. ESI-MS Chromatograms of key species formed following oxidative addition of catalyst with iodobenzene in methanol at room temperature (L = TPPMS)

Activation of $Pd_2(dba)_3$ in MeOH at room temperature (21°C) with (**1**) yields $[Pd(TPPMS)_2(dba)]^{2-}$ as the major product, along with the two minor species $[Pd(TPPMS)_2(dba)_2]^{2-}$ and $[Pd(TPPMS)(dba)]^-$ (see Figure 54). The speciation is similar to that observed previously using DMF or THF and $Pd(dba)_2/PPh_3$.[219] It is interesting to note that the sensitivity of ESI-MS also allows for observation of species not registered by other methods.

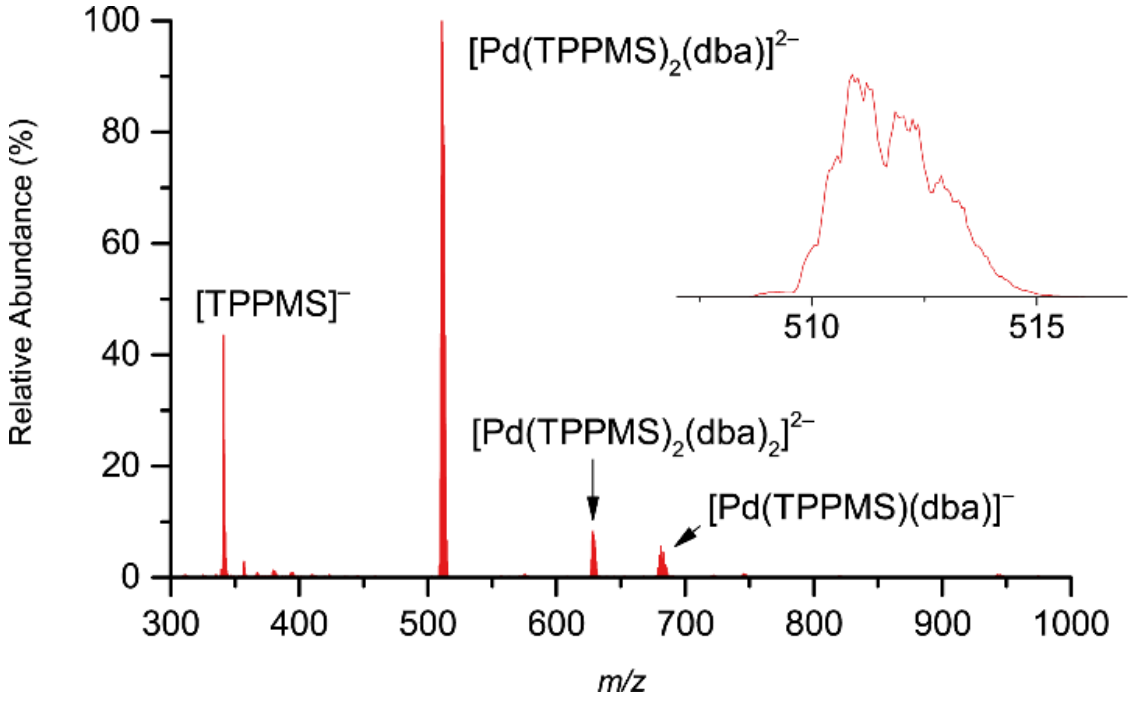

Figure 54. ESI-MS spectrum of activation of $Pd_2(dba)_3$ with 4eq. $[TPPMS]^-$ in methanol at room temperature

A closer look at the real-time UV-Vis and ESI-MS data shows that the reaction takes only about 1.5 minutes to reach equilibrium (Figure 55), despite activation procedures often calling for much longer stirring times or heat in other solvents.[227,257] If the precatalyst/ligand mixture was heated instead of stirred at room temperature, catalytic oxidation of $[TPPMS]^-$ was observed. Oxidation of the phosphine ligand has been reported to reduce the activity of Pd-based catalysts and is therefore undesirable.[180,258] While often present in small quantities despite rigorous solvent degasification, heat served to accelerate this decomposition and effectively reduces the concentration of active catalyst in solution. Phosphine oxidation should be considered when preheating is employed while using simple phosphine ligands, though this side reaction can be avoided with oxidation-resistant ligands.

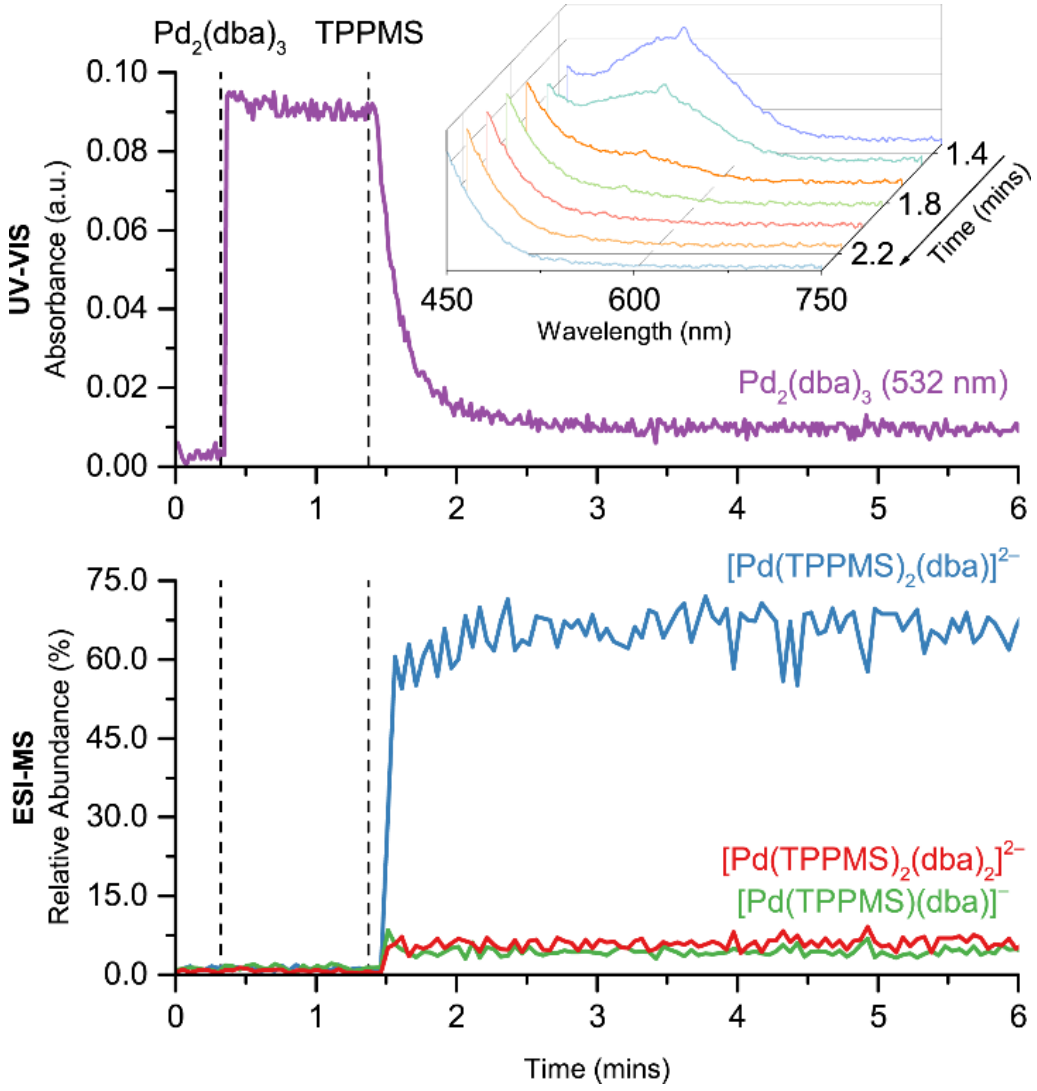

Figure 55. UV-Vis (top and inset) and ESI-MS (bottom) chromatograms of activation of $Pd_2(dba)_3$ with $[TPPMS]^-$ in MeOH at room temperature

Use of the Buchwald-type ligand, $[sSPhos]^-$ (**2**), also yielded a single palladium species in the form $[Pd(sSPhos)(dba)]^-$ and exhibited no oxidation following activation. In fact, when using HPLC grade MeOH and no degasification steps, extremely little ligand oxidation is seen. In contrast to TPPMS, the bulkier sSPhos phosphine ligand forms the active $[Pd(sSPhos)(dba)]^-$ species much more slowly.

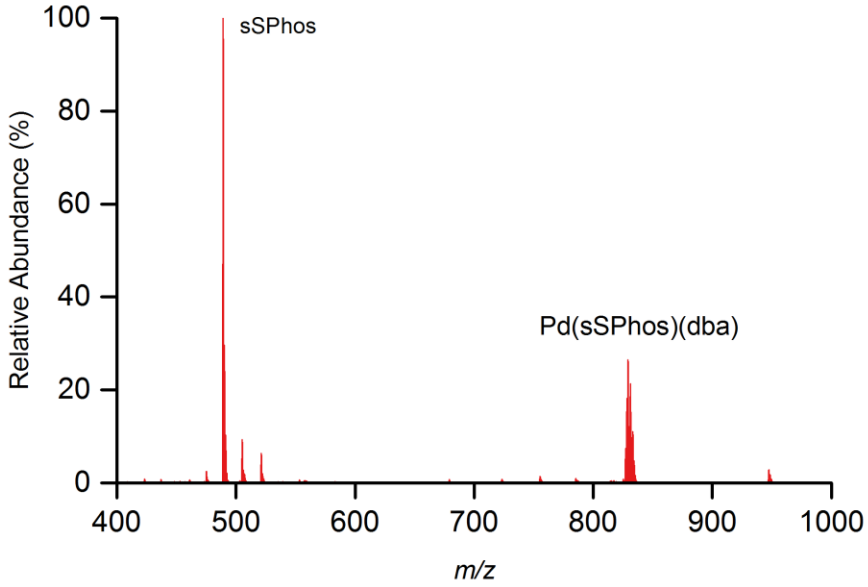

Figure 56. Mass spectrum of $Pd_2(dba)_3$ activation product using 4 eq. sSPhos in room temperature methanol

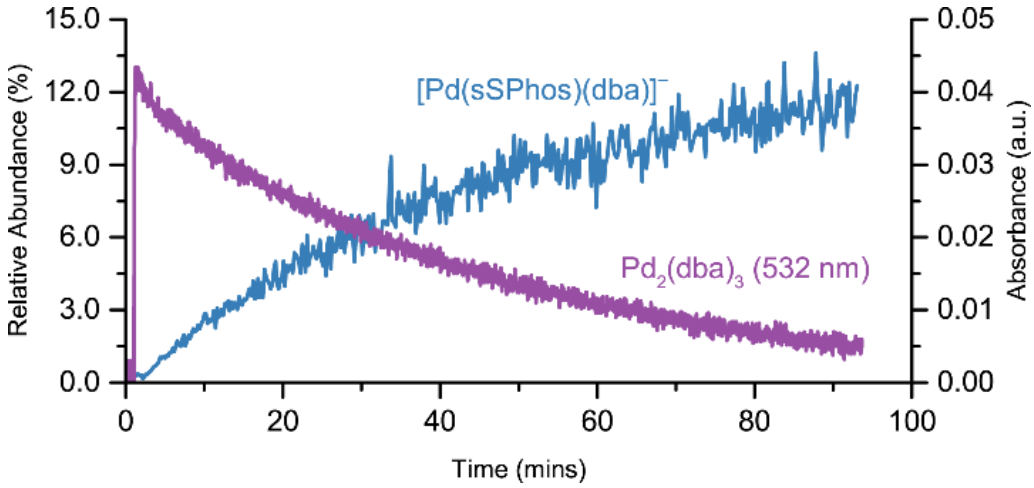

Figure 57. Activation of $Pd_2(dba)_3$ with $[sSPhos]^-$ in MeOH at room temperature

5.5.2 Activation of $Pd_2(dba)_3$ in dimethylformamide

N, N-Dimethylformamide (DMF) is a widely-used solvent partly due to its similarity to water. While it shares a similar boiling point, DMF is superior to water because of its ability

to dissolve an extended range of organic molecules or analytes. It is also desirable due to a high miscibility with water and other organic solvents. That being said, the solvent has some serious downsides; especially for ESI-MS users. Firstly, it is linked to several concerning health and safety issues. From a practical stance, the solvent is notoriously difficult to purify since it readily decomposes at room temperature (possibly due to trace water, metals or other impurities common in the solvent) into methylformamide (MF), dimethylamine, and (most troubling for MS users) formate anion; all of which yield serious impurities to mass spectra.[259] The rare cases of DMF used with ESI-MS in the literature are generally met with very poor results, even when using optimal analyte combinations and forcing source conditions.[260,261] In other words, while it is theoretically possible to use DMF (and may even yield better results than other solvents in extremely rare cases) with ESI-MS, it should generally be considered on the bottom of the list of usable solvents because of major contamination and sensitivity issues. Regardless, we opted to use the solvent since many palladium-mediated coupling reactions employ the solvent.

While the activation of $Pd_2(dba)_3$ precatalyst in methanol produces a single palladium complex, the same is not true for dimethylformamide (DMF). $[Pd(TPPMS)_2]^{2-}$ is the major species observed in DMF following the addition of both ligand and palladium, along with a second dimeric complex, $[Pd_2(TPPMS)(dba)(DMF)]^-$, and the species $[Pd_2(TPPMS)(dba)(MF)]^-$ is also observed in small quantities due to impurities present in DMF.

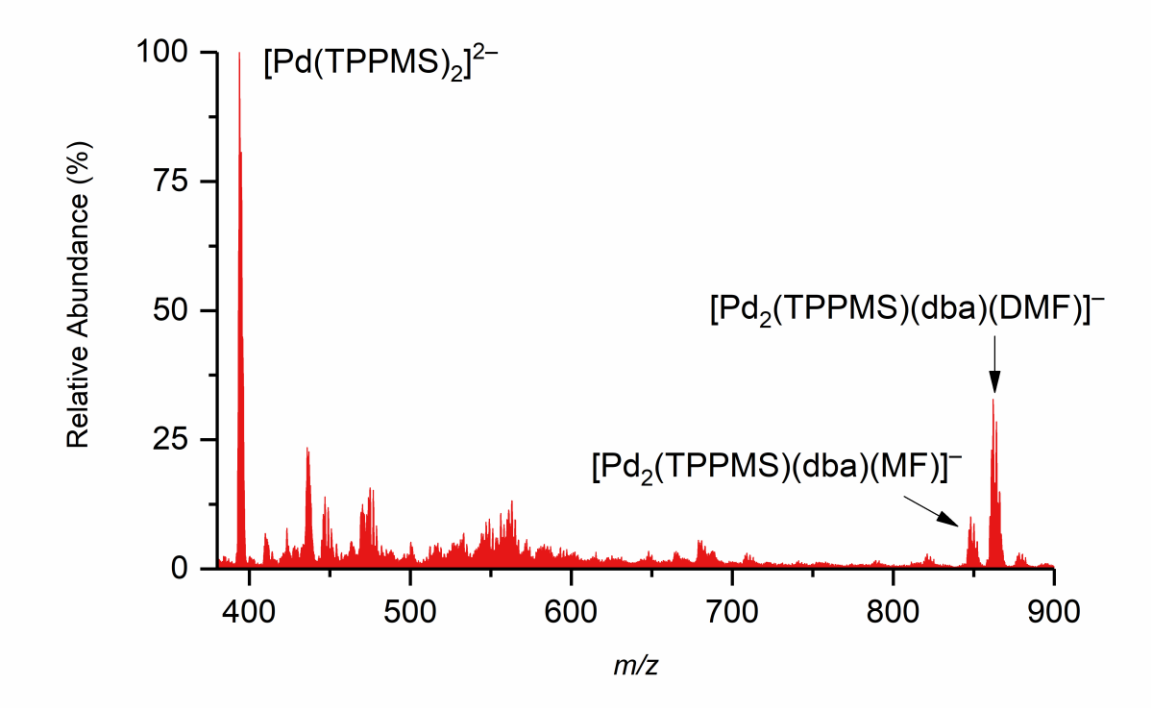

Figure 58. ESI mass spectrum of activation of $Pd_2(dba)_3$ with 4eq. [TPPMS]− in room temperature DMF

The speciation in DMF differs to what has previously been reported which found that the species present, when using the analogous complex $Pd(dba)_2$, are primarily $Pd(dba)(PPh_3)_2$ and $Pd(PPh)_3(DMF)$ (when triphenylphosphine is used as a ligand).[219] No solvent adducts, such as $[Pd(TPPMS)_3(DMF)]^{3-}$, were observed by ESI-MS which indicated that the tricoordinate complex is not present in detectable quantities using TPPMS. The lack of $[Pd(TPPMS)_3(DMF)]^{3-}$ is possibly due to the nature of the charged ligand; however, mixed ligand substitution experiments did not confirm the assumption that Coulombic interactions prevent formation of a tricoordinate-TPPMS complex under these conditions. When the substitution experiment is run with a mixture of 1:1 TPPMS:PPh_3, the major species appear to be a mixture of $[Pd(TPPMS)_2]^{2-}$, $[Pd(TPPMS)(dba)]^-$, $[Pd(TPPMS)(PPh_3)(dba)]^-$ rather than any tricoordinate complexes.

In order to make any strong assertions about the presence (or absence) of tri-coordinate palladium phosphines in solution, further experiments are required.

We explored the effect of the ESI-MS cone voltage when the activation was performed in DMF and found that the speciation did not change appreciably with increased cone voltages; instead only the fragment Pd(TPPMS) was formed from $Pd(TPPMS)_2$.

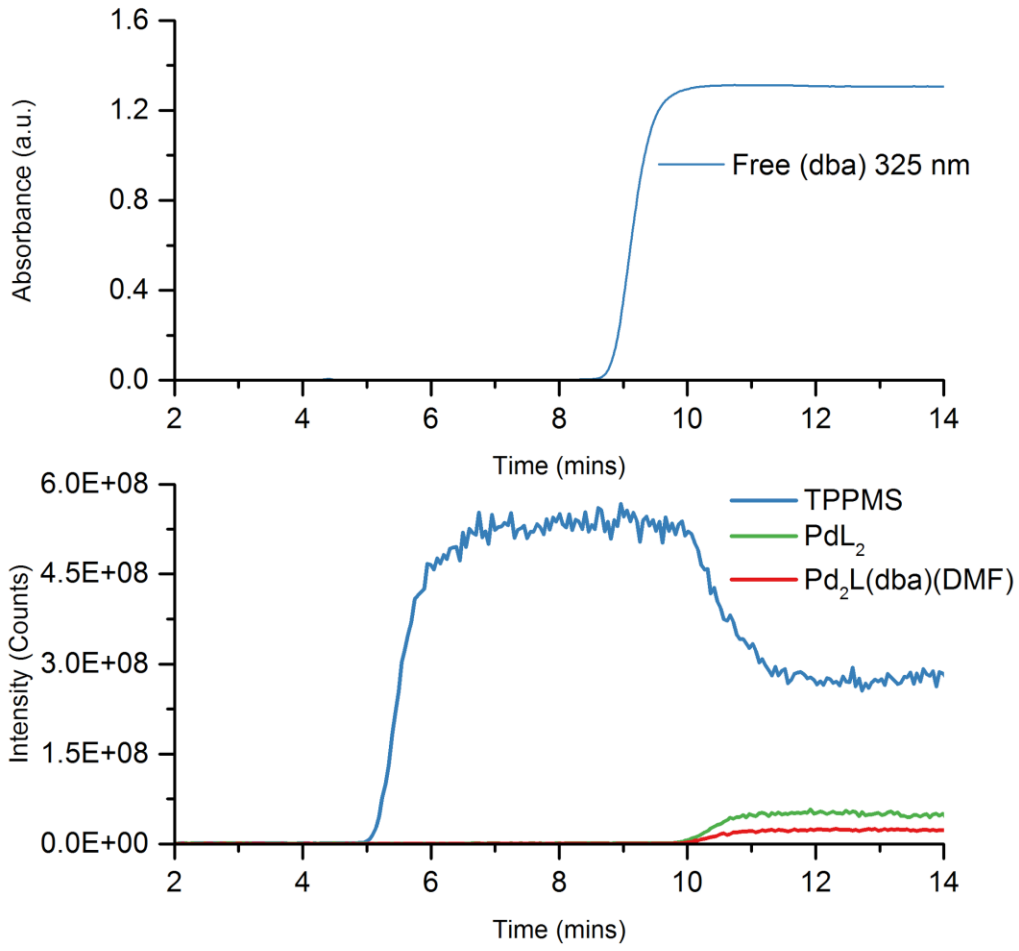

Figure 59. Activation of $Pd_2(dba)_3$ precatalyst with 4 eq. TPPMS in room temperature DMF monitored using both UV-Vis and ESI-MS

The order of addition is critical in DMF, since DMF is a coordinating solvent and will displace the Pd-bound dba in $Pd_2(dba)_3$ which renders the metal unavailable for coordination when using a 4:1 ligand to $Pd_2(dba)_3$ ratio.[262] Theoretically, it may be possible to overwhelm the system with ligand to liberate the sequestered metal but with the increased use of expensive ligands this is generally an unacceptable solution. Figure 60 demonstrates the release of dba and loss of $Pd_2(dba)_3$ over a period of 80 minutes when 16 μM precatalyst is added to a stirring room temperature solution of DMF. To minimize this competition and optimize the amount of active catalyst the phosphine ligand should be present in solution before addition of $Pd_2(dba)_3$. If the simple phosphine ligand TPPMS is added prior to the $Pd_2(dba)_3$ precatalyst, this effect is not observed and the catalyst is formed rapidly and efficiently. This proves that the phosphine ligand has sufficiently high binding affinity compared to DMF (Figure 61) and that proper addition order protocol will potentially save a significant portion of precatalyst. The importance of various additives, preheating, or pre-treatment with these activations cannot be understated, especially in transformations mediated by expensive metals and expensive ligands.

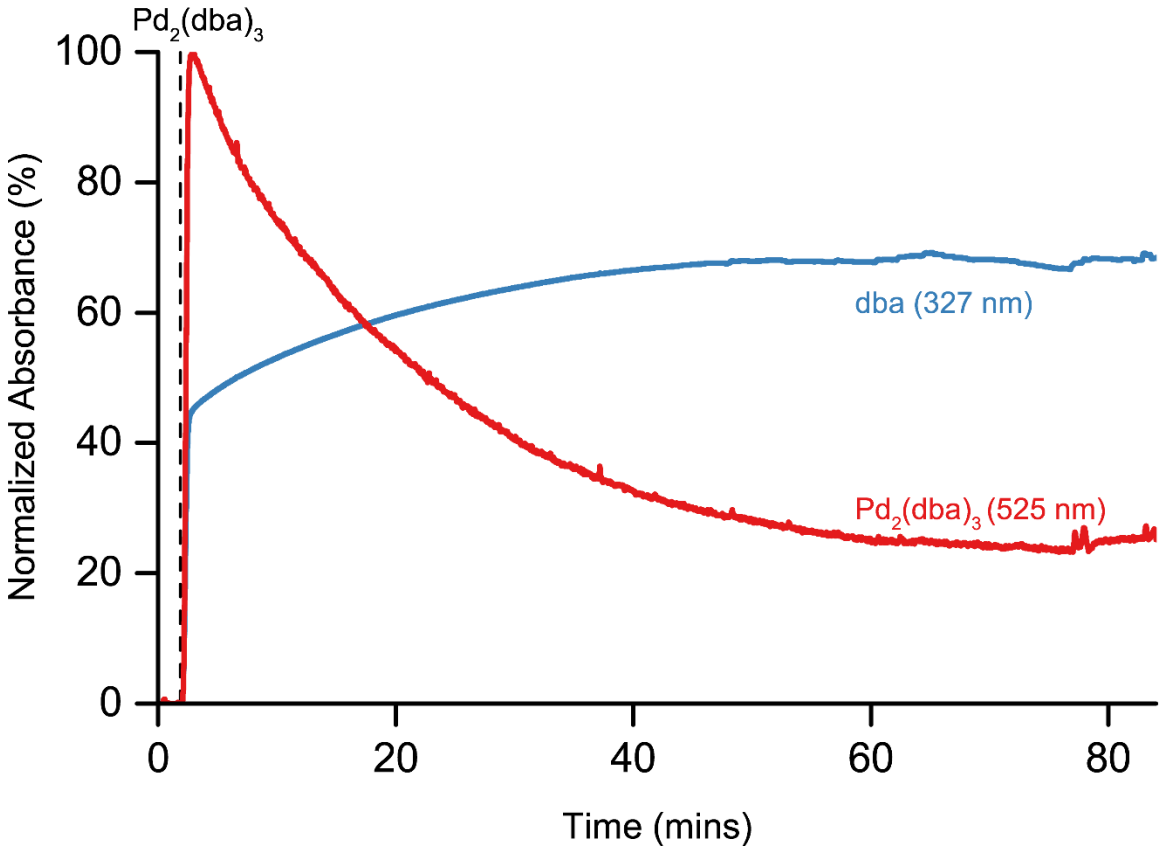

Figure 60. Decomposition of $Pd_2(dba)_3$ in room temperature N,N-dimethylformamide as monitored by UV-Vis

Compared to the results in DMF, $Pd_2(dba)_3$ is quite stable in other common solvents such as methanol and toluene, provided both solvents are of high purity. Therefore, no such precautions need to be taken.

Activation of $Pd_2(dba)_3$ with a modest 2 equivalents of TPPMS in DMF yields $[Pd(TPPMS)_2]^{2-}$ instead of $[Pd(TPPMS)_2(dba)]^{2-}$ as the primary species (Fig. 4), though others have reported that as many as 100 equivalents of ligand are needed to fully replace dba with PPh_3 in DMF as compared to MeOH.[217,218] Previously, a Pd:L ratio of 1:2 was reported to yield only $Pd(dba)(PPh_3)_2$, $Pd(PPh)_3(DMF)$ and/or $Pd(PPh_3)_2$.[219] This

discrepancy reveals that activation procedures are an exact recipe and even subtle changes may inadvertently affect the overall reaction (adversely or positively) in unexpected ways.

Activation of $Pd_2(dba)_3$ at room temperature in MeOH or DMF using $[sSPhos]^-$ yields the same species, $[Pd(sSPhos)(dba)]^-$, as the only Pd-containing species observable by ESI-MS at our detection limit. The ligand exhibits negligible oxidation following activation even after heating of the mixture demonstrating the robustness of the ligand, as illustrated previously.[256] In room temperature (22°C) MeOH, the catalytically active species is formed relatively slowly, requiring approximately 90 minutes to come to equilibrium. This can be shortened to one minute if the reagents are added to refluxing MeOH, without any change to the speciation observed at lower temperature. Conversely, the activation with $[sSPhos]^-$ in DMF proceeds very quickly, forming a maximum quantity of $[Pd(sSPhos)(dba)]^-$ in three minutes. As previously noted, the order of addition is critical and the ligand should be introduced before $Pd_2(dba)_3$ to optimize the amount of active catalyst produced. The speciation observed with $[sSPhos]^-$ is similar to the active species, "L_1Pd", reported for Buchwald type ligands in the literature; however, dba does not fully dissociate even with increased equivalents of $[sSPhos]^-$ in MeOH or DMF.[227] It is possible that the apparent dba coordination is a result of the electrospray process (i.e. the dba ligand is uncoordinated, but persists as a component of an aggregate in the gas-phase); however, the strength of the association seems rather high for an aggregate species, as may be demonstrated by MSMS and cone voltage experiments performed at higher energies. This is only indirect evidence and could possibly be cleared up with a successfully grown crystal of the activated product for X-ray analysis.

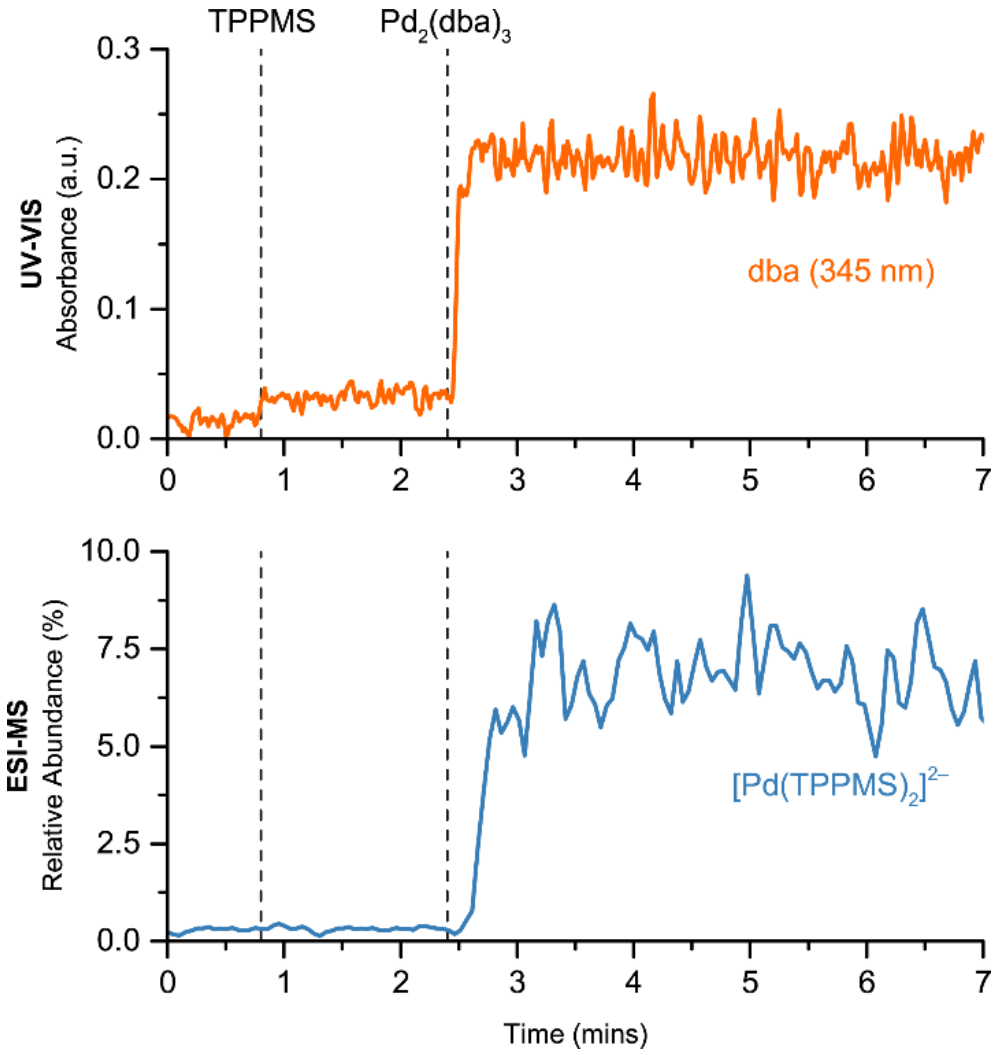

Figure 61. UV-Vis (top) and ESI-MS (bottom) chromatograms of activation of $Pd_2(dba)_3$ precatalyst with $[TPPMS]^-$ in DMF at room temperature

5.5.3 Activation of $Pd_2(dba)_3$ in fluorobenzene and toluene

Many catalytic reactions involving $Pd_2(dba)_3$ are carried out in toluene and it was therefore prudent to monitor the *in-situ* activation process under similar conditions. Activations performed in toluene were met with minor success, though only with relatively high concentrations of precatalyst and ligand. In order to perform ESI-MS experiments in non-polar solvents, at least one of two conditions must be met: high concentrations of

electrolyte which promotes the electrospray process,[97] or extreme source conditions (high gas flow rates and temperatures) which invariably forces evaporation of the solvent and expels gas-phase analytes. Since toluene is less amenable to electrospray ionization than other more polar solvents, we chose fluorobenzene as a toluene analogue thus pushing the limits of normally accessible ESI solvents. As in methanol, the primary species observed at low cone voltages is $[Pd(TPPMS)(dba)]^-$.

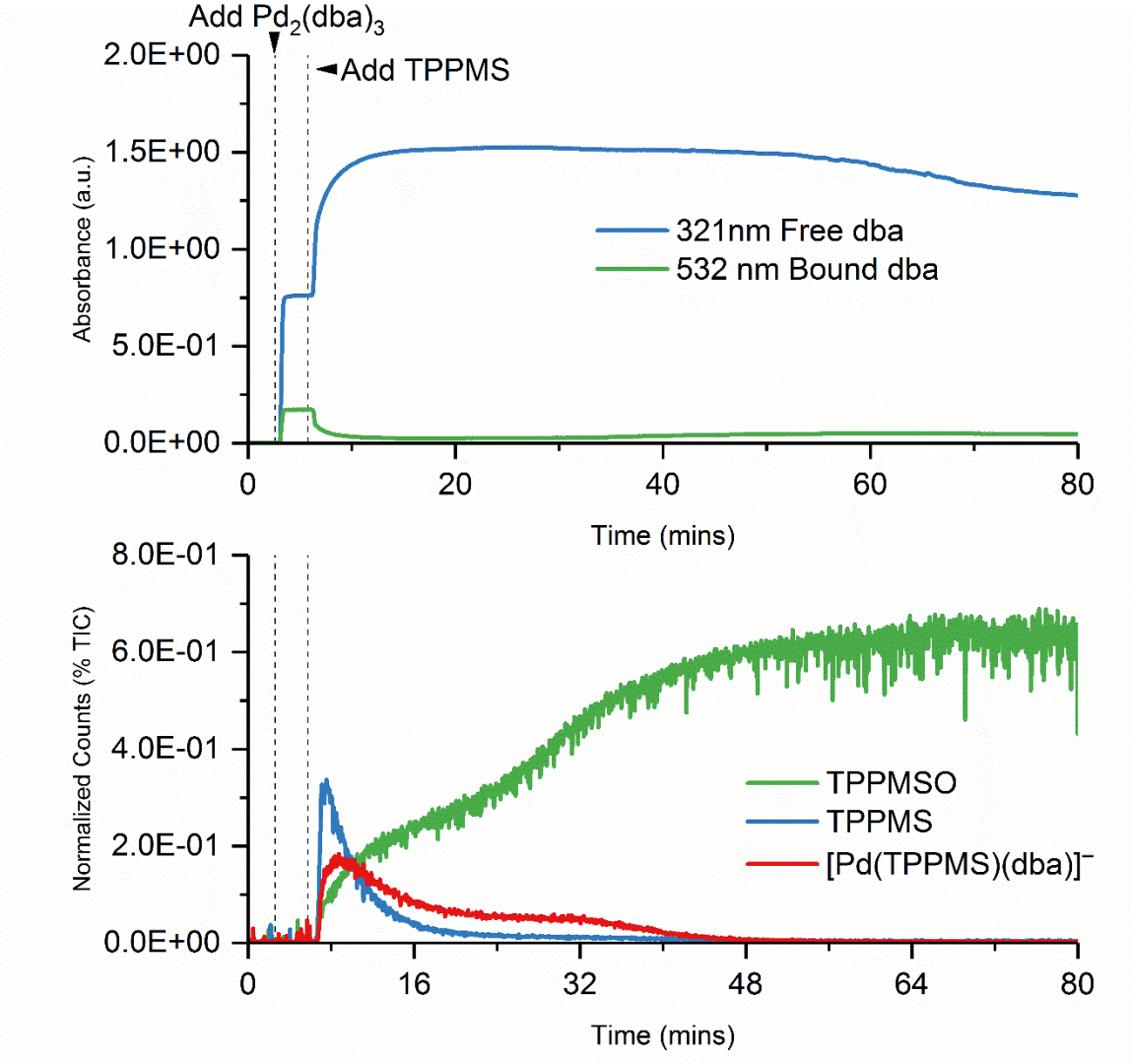

Figure 62. Activation of $Pd_2(dba)_3$ with 4 eq. TPPMS in fluorobenzene demonstrating the high risk of TPPMS oxidation over time

As already mentioned, toluene was not amenable to real-time monitoring of the activation by ESI-MS which adds some mystery to the duration of the reaction. However, given sufficiently aggressive desolvation conditions and an extended amount of time, the speciation of a reaction mixture in toluene can be characterized.[97] A mixture of $Pd_2(dba)_3$ and 4eq. TPPMS in toluene appears to yield $[Pd(TPPMS)(dba)]^-$ exclusively, though the signal-to-noise ratio is very poor and other species could be present (Figure 63). The matching results here (and in other projects from the McIndoe group) between toluene and fluorobenzene suggests that fluorobenzene is an acceptable substitute for toluene for ESI-MS experiments.

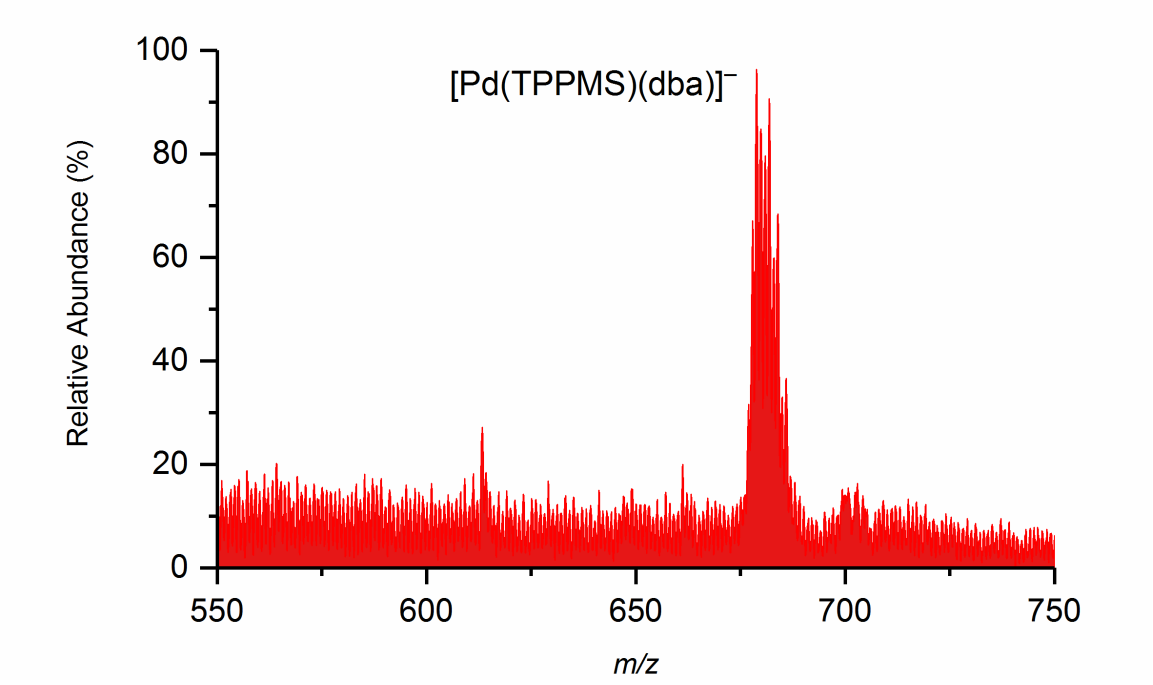

Figure 63. Mass spectrum of $Pd_2(dba)_3$ activation with 4 eq. TPPMS in room-temperature toluene

5.6 Experimental

The sulfonated phosphine ligand bis(triphenylphosphine)iminium (PPN) triphenylphosphine-meta-sulfonate ($[PPN]^+[TPPMS]^-$) (**1**), was synthesized according to literature procedures.[66,263] Both tris(dibenzylideneacetone)dipalladium ($Pd_2(dba)_3$), and Sodium 2′-dicyclohexylphosphino-2,6-dimethoxy-1,1′-biphenyl-3-sulfonate hydrate ($Na^+[sSPhos]^-$) (**2**), were purchased from Sigma-Aldrich and used as received. All solvents were purchased from Sigma-Aldrich and used as received. UHP200 Argon and HP300 4.8 Nitrogen were purchased from Airgas (Calgary, Canada) and used without further purification.

In a typical reaction, 10.0 mL HPLC grade methanol or ACS grade DMF is transferred to a custom PSI flask (vide infra) which is then sparged with nitrogen for 15 minutes before being connected to the instrumentation. Heating was effected with an IKA C-MAG HS 7 stirring hotplate equipped with an ETS-D5 thermocouple and oil bath. All reagent stock solutions were prepared under an inert nitrogen atmosphere in a glovebox. The stock solution was prepared using 0.0020 g $Pd_2(dba)_3$ dissolved in 4.0 mL anhydrous tetrahydrofuran (0.55 mM $Pd_2(dba)_3$, 1.1 mM Pd). $[PPN]^+[TPPMS]^-$, (**1**), stock solution was prepared by dissolving 0.0077 g of (**1**) into 4.0 mL of degassed HPLC grade methanol (2.2 mM $[TPPMS]^-$). $Na^+[sSPhos]^-$, (**2**), stock was prepared by dissolving 0.0045 g of the salt in 4.0 mL degassed HPLC grade methanol (2.2 mM $[sSPhos]^-$). 100 μL of each solution was injected via syringe into 10.0 mL degassed methanol yielding a Pd concentration of 11.0 μM and 2 equivalents of ligand. The PSI flask was charged a stir bar and reagent stock

solutions were injected using Hamilton GASTIGHT® syringes when required. The flask is pressurized with 4 psi of argon using a PRAXAIR ProStar Platinum regulator.

The UV-Vis instrument of choice for these experiments was an ASEQ Instruments LR-1 compact spectrometer (version 2.1, Configuration B) equipped with a reflection fiber optic Y-cable probe (F01_R03) fitted with a teflon transflectance dip probe (LQ_R01) and a D2-S1 deuterium/halogen light source. The spectral range of the LR-1 is 200 – 1200 nm with a resolution of < 2 nm. Exposure time was set to 100 ms with a 5 scan average and data was collected from 200 – 1200 nm at a rate of one spectrum per second. Raw spectral data was collected using the ASEQ 16 bits version 1.54 software and chromatographic data was extracted using a custom Python script. A reference scan is collected initially to remove solvent from the background of the UV-Vis spectrum.

The dip probe was fitted with a thermometer adaptor and coupled to the custom PSI flask featuring a built-in condenser,[41] Kontes HI-VAC® extended tip valve with PTFE plug, and two 14/20 size ground glass joints. A 30-cm length of Vici Blue PEEK tubing (inner diameter of .010") was inserted through a rubber septum fitted to the custom PSI flask and into the solution to be analyzed. The delay time for solution to reach the ESI source was calculated based on replicate trials to be 12.06 s and this is corrected for in all chromatograms. The opposite end of the tubing was connected to the ESI source of a Waters Acquity Triple Quadrupole Detector.

All electrospray ionization mass spectra were recorded using a Waters Acquity Triple Quadrupole Detector equipped with a Z-Spray electrospray ionization source. The capillary voltage was held at 3.1 kV, cone voltage at 10.0 V, and extraction cone at 3.0 V. Importantly, the MS cone voltage was optimized to eliminate in-source fragmentation and guarantee the speciation reported are not artifacts of the ESI process (see section titled "Effect of cone voltage on speciation in ESI-MS"). Source nitrogen gas flow rates and temperatures varied depending on solvent and were set to provide optimal desolvation conditions. For methanol, the desolvation gas flow rate was 200 L/hr, cone gas flow rate 100 L/hr, source temperature 80°C, desolvation temperature 180°C. For DMF, the desolvation gas flow rate was 500 L/hr, cone gas flow rate 100 L/hr, source temperature 130°C, desolvation temperature 230°C. The detector gain was set to an optimal voltage of 470 V. Scan time was set to 5 s, with an inter-scan time of 0.1 s. For all experiments, the ESI spray head was left in a position near-perpendicular to the sampling cone with a 7° incline toward the cone. MSMS experiments were performed with a collision energy between 2-20 V with an Argon collision gas flow rate of 0.1 mL/hr.

5.7 Conclusions

We wanted to extend our grasp on what was occurring in solution beyond ESI-MS and the pairing of UV-Vis to our traditional PSI methodology has enabled this. The combination of UV-Vis and ESI-MS allows for straightforward, real-time monitoring of $Pd_2(dba)_3$ activation. Using $[TPPMS]^-$ or $[sSPhos]^-$ the time needed to achieve equilibrium concentrations of the active catalyst, the influence of addition order, and effect of

preparation conditions on activated catalyst in both MeOH and DMF could be obtained. This shows that using orthogonal methods we can observe exactly what is happening in solution and obtain a clear understanding of the *in situ* activation process under a variety of conditions. In most conditions dba is not fully displaced from the active catalytic species by either the simple triarylphosphine ligand (**1**) or a Buchwald-type ligand (**2**); the exception being the activation in DMF with (**1**). The techniques used accurately inform us of what these species are and how they behave. Based on these results, useful instructions for optimal $Pd_2(dba)_3$ activation can be prepared. Future work will focus on the activation of different Pd catalyzed systems and the implication of activation protocol on the actual catalysis and catalytic activity.

Chapter 6. Future Work: Exploiting tandem mass spectrometry for real-time reaction monitoring

This work describes work currently underway with the goal of further developing methods for mechanistic investigation of organometallic reactions using combined techniques, including tandem mass spectrometry. Both reactions discussed in this chapter are palladium-catalyzed cross-coupling reactions: the Buchwald-Hartwig C-N coupling and the Sonogashira C-C coupling reaction. The instruments mentioned herein are electrospray ionization mass spectrometry (ESI-MS) and ultraviolet-visible (UV/Vis) spectroscopy both of which are commonly used analytical techniques. While ESI-MS and UV-Vis have been discussed and employed in other sections, an introduction to the unique advantages of triple-quadrupole mass spectrometers will be addressed in this chapter.

6.1 Introduction: Orthogonal Analytical Techniques

An ideal methodology for the study of complex systems should employ multiple analytical tools. This is especially true for monitoring homogeneous catalytic reactions since the chemical space (choice of ligands, metal, substrates, temperature, time, solvent, reagents etc) in these reactions is enormous. Unquestionably, some tools are more appropriate than others in particular scenarios. For example, Nuclear Magnetic Resonance is widely used in scrutinizing the behaviour of some organometallic species simply due to the fact that both structural and abundance information are obtainable; however, no single instrument is capable of providing a complete picture of all dynamic chemical species in a mixture for many reasons. The temporal existence of a reaction intermediate may range

from ephemeral to long-lived; consequently, time of analysis may be key. Further, the abundance of individual species in solution can vary by many orders of magnitude thus placing a requirement on enhanced dynamic range of the instrument used. Therefore, a comprehensive investigation is commonly performed in sections with a combination of *in situ* and *ex situ* techniques of mixed capabilities (*in situ* spectroscopic measurements of a mixture and *ex situ* analysis of product mixtures by GC-MS, for example).

There exist many examples of combined *in situ* techniques applied to the examination of heterogeneous and homogeneous catalytic systems.[27,264] These include, but are certainly not limited to, various combinations of spectroscopic techniques such as EXAFS/UV-Vis,[265,266] WAXS/XANES/UV-Vis,[267] NMR/UV-Vis,[268,269] or EPR/UV-Vis.[270,271] In order to answer deeper questions about a catalytic reaction, a rigorous analytical approach is required. We wanted to push the limits of what type of systems we could study with our usual techniques, while complementing these methods in a synergistic way. To best accomplish this, the analytical approach should involve examination using fundamentally distinct principles, that is, orthogonal techniques.

The McIndoe group primarily uses mass spectrometry in order to facilitate the collection of dynamic physical data about a system.[272] An obvious orthogonal analytical technique to mass spectrometry was one of the many forms of spectroscopy. Spectroscopy uses the interaction of electromagnetic radiation with matter in order to detect a particular analyte; on the other hand, spectrometric techniques employ electromagnetic radiation to facilitate the detection of an analyte. In other words, spectroscopy and spectrometry are truly

orthogonal methods of analysis. We had already developed a methodology for tandem UV-Vis and MS analysis of a single system (Chapter 5) and we decided to apply this to reaction monitoring of a more complex and catalytic system. Interestingly, a key opportunity was missing from our methods as well as the literature. A triple-quadrupole (QqQ) mass spectrometer is the go-to analytical instrument for quantification in many fields due to the unique modes available to the tandem mass analyzer. The most common QqQ mode used for quantitation is Multiple Reaction Monitoring (MRM) which is inherently both highly sensitive and selective; this facilitates the quantification of many analytes in a single experiment. With this in mind, we chose to include this mode, and others, to our toolbox for monitoring organometallic catalytic reactions. To the best of our knowledge, MRM has not been used to follow homogeneous palladium catalyzed cross-coupling reactions, nor has this reaction monitoring mode been paired with a simultaneous orthogonal technique for this application.

6.2 Theory and Application of Triple-Quadrupole (QqQ) Mass Spectrometry for Reaction Monitoring

Techniques employing more than one mass analyzer are referred to as "tandem mass spectrometry". These tandem instruments incorporate two to (theoretically) unlimited mass analyzers (termed MS^2 and MS^n, respectively). Triple-quadrupole (triple-quad or QqQ) mass analyzers feature a set of three linear quadrupoles that allow for more than one ion sorting step. The first and third quadrupoles facilitate mass separation (i.e. they are scanning quadrupoles) whereas the second quadrupole (which can also be a hexapole, octapole etc – it serves only to contain the ions rather than separate them) is used as an ion

guide during collisional fragmentation within an inert gas cell. Because of this unique layout, the triple-quad may be used for a variety of MS/MS experiments such as selected and multiple reaction monitoring (SRM, MRM), parent and daughter ion scan, as well as neutral loss scans.

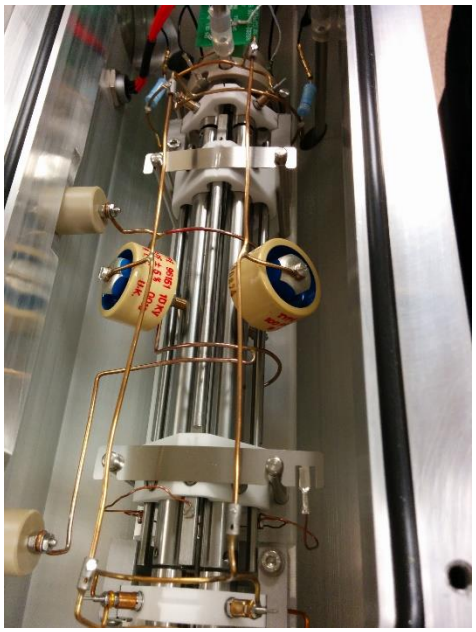

Figure 64. First quadrupole and gas cell of a Waters Ultima triple-quad mass spectrometer

The experiments enabled through use of a triple-quad uniquely facilitate the online monitoring of catalytic reactions. In order to study the mechanism of a catalytic reaction we must be able to characterize both low-concentration and transient intermediate species while also monitoring reactant and product concentrations for kinetic analysis.[39]

In a typical MS scan, only the first quadrupole is set to scan across a broad range of mass-to-charge ratios. A complete sweep from *m/z* 50 to 2000 requires that the instrument is given enough time to scan the entire range with good sensitivity. The most common tandem

mass spectrometric technique used for quantitation is **multiple reaction monitoring** (MRM) which is inherently both highly sensitive and selective for target analytes. MRM (or SRM when a single precursor-parent transition is being monitored) experiments are the principal competitive advantage of triple-quad instruments over competing instruments (single quads, ion traps, Q-TOFs) and make triple-quad mass spectrometers the key MS instrument for quantitation and sensitivity. As opposed to a typical scan across many values of *m/z*, these experiments involve selecting a single mass (the "precursor" ion) using Q1, fragmenting it in Q2, and setting Q3 to the mass of a particular fragment (the "product ion"). Ions are only detected if they meet *both* criteria, so the principal feature of this mode is an increase in sensitivity (due to the ability to dwell only on *m/z* values of interest) and a large increase in signal-to-noise (because of the filtering at Q3). The instrument can be tuned across a broad range of parameters to selectively detect the precursor ion, but because only one channel on the first and third quadrupole are being used, the experiment can be completed in milliseconds.

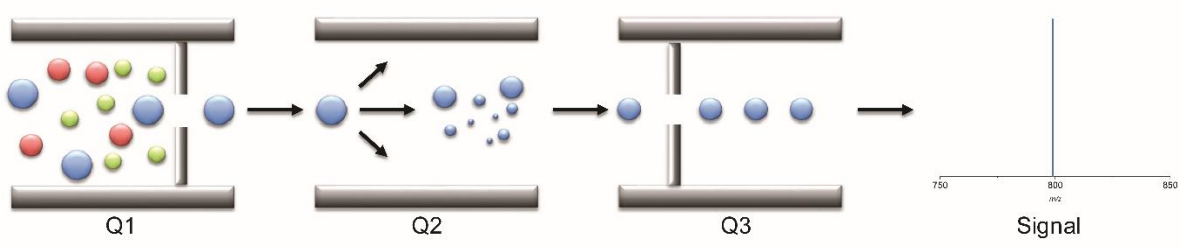

Figure 65. Representation of an MRM experiment. The precursor ion is isolated, fragmented, and results in a signal if the selected product ion is detected

Because of the MRM experiment, the linear dynamic range of a triple-quad mass spectrometer is around six to eight orders of magnitude in terms of analyte concentration.

For comparison, time-of-flight instruments span around 2-3 order of magnitude of linear dynamic range. This vast range allows very effectively monitoring of even very low abundances of (intermediate) species in a reaction. Furthermore, the MRM scanning mode overcomes the low resolution of the triple-quad by verifying the target analyte. In other words, overlapping species are no longer an issue with MRM.

The product and precursor ion scans are a form of MS/MS in which a single mass is selected in one quadrupole and fragmented in the gas cell. The **product ion scan** involves collisional fragmentation of a single mass (selected in the first quadrupole, Q_1) and analysis of the resulting spectrum comprised of fragment ions containing useful structural information.

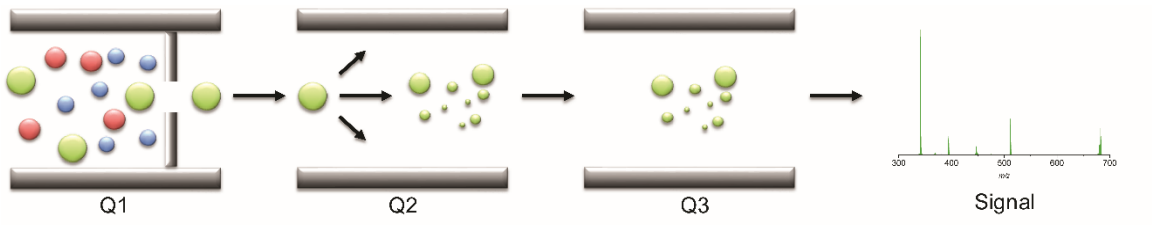

Figure 66. Representation of a product ion scan. The first quadrupole sits on a single channel while the third quadrupole scans for fragments

The **precursor ion scan** selects for a single mass in the third quadrupole while the first quadrupole scans the whole spectrum. This mode is useful when searching for similar compounds which fragment in a particular way to generate the same product ion. The **neutral loss scan** is used when an ion loses a particular diagnostic fragment (i.e. loss of a common ligand such as PPh_3, or elimination of a small molecule such as H_2O).

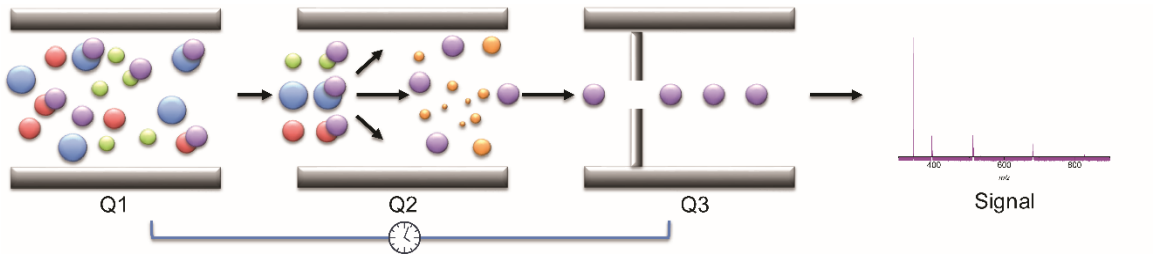

Figure 67. Representation of a precursor ion scan. The first quadrupole scans while the third quadrupole sits on a single channel

When using the neutral loss scan mode, the first quadrupole scans across a given mass range. Ions are then fragmented in the collision cell and pass on to the third quadrupole which scans across a similar mass range as the first, though with an offset equal to the mass of the diagnostic fragment. In doing so, only ions which lose a neutral molecule equal to the offset in Q_3 are detected. This mode can be very useful when studying organometallic systems in which loss of neutral ligand (such as a phosphine) from a catalyst is quite common. Furthermore, triple quad mass spectrometers are able to perform a great variety of scan modes near-simultaneously in differing polarities. This allows for the acquisition of tandem-MS and high sensitivity data to be collected in either positive or negative ion mode.

For an MRM or SRM experiment, the cone voltage and collision energy generally need to be optimized to provide the best signal possible. Cone voltage optimization (as discussed in Chapter 5) must be done carefully and should ideally improve signal (higher cone voltages increase ion transmission from source to mass analyzer) without fragmenting the target (higher cone voltages increase the internal energy of ions via collision). Collision energy (CE), the energy applied to analytes in the collision chamber for MS/MS

experiments, may be optimized using several methods. General methods are used when many analytes are involved and the process of optimizing the collision energy for every molecular weight is inefficient. For example, a general formula has been developed for a given precursor *m/z* for peptide analysis (Equation 3).[273]

$$CE = 0.034 \times (m/z_{precursor}) + 1.314$$

Equation 3. A general formula for collision energy (CE) optimization of peptides

Unfortunately, these types of general approaches are not necessarily reliable in all cases. There also exist automated survey scans with some instrument manufacturers (including the Waters TQD); however, performing these survey scans saves little time since a high amount of awareness is required to ensure proper CE optimization. The survey scan has also been found to provide low sensitivity to low-abundance species which may be optimized better manually.[274] In all cases, the best mode of MRM parameter optimization is to perform individual product ion scans of each parent *m/z* and maximize the product signal abundance.[275]

Few catalytic studies have exploited the unique advantage that a triple-quadrupole mass analyzer brings to the table. In fact, catalytic studies involving tandem techniques seem to be exclusively biochemical in nature (enzymatic catalysis).[276,277]

6.3 Palladium-catalysed cross-coupling reactions

Some of the most important reactions in organometallic and synthetic organic chemistry are the family of palladium-catalyzed cross-couplings. This class of reaction is generally associated with the formation of carbon-carbon bonds due to the popularity of reaction such as the Sonogashira, Suzuki and Heck coupling which have extensive applications in the production of pharmaceuticals, natural products, and polymers.[23–25]

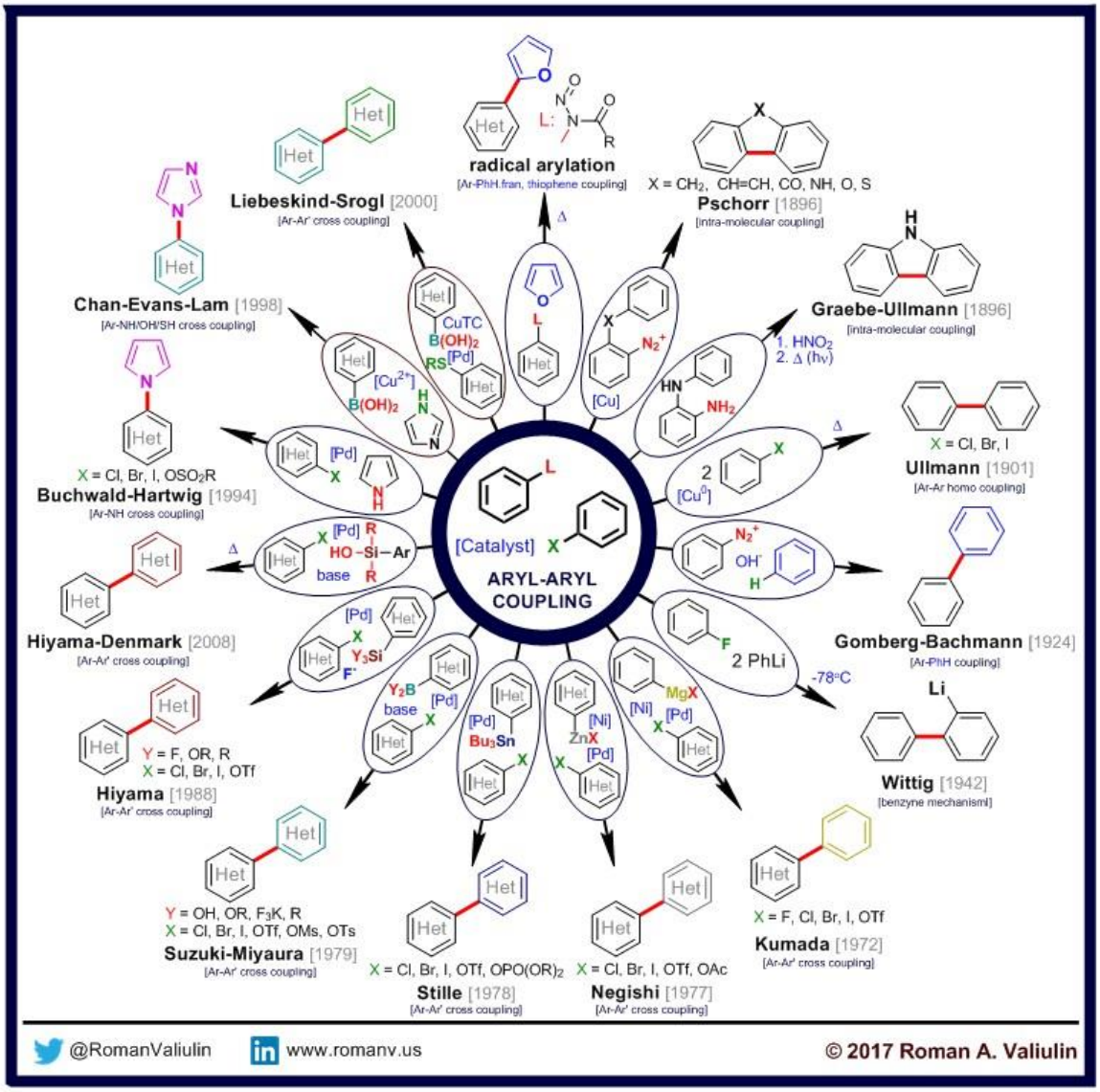

Figure 68. Infographic featuring the wide scope of palladium catalyzed aryl-aryl coupling reactions (used with permission from Dr. Roman A. Valiulin)

6.3.1 The Buchwald-Hartwig Amination

Included in this family of palladium-mediated transformations is the Buchwald-Hartwig amination, a method for the formation of carbon-nitrogen bonds, which has received a boost in popularity in recent years since triarylamines have become targets for OLEDs.[278] The Buchwald-Hartwig amination continues to be used extensively due in part to the weaknesses of previous methodologies for the formation of carbon-nitrogen bonds. For example, the Goldberg reaction generally involves high temperatures and high catalyst loading[279] and the Petasis reaction suffers from long reaction times.[280] More traditional reductive amination and nucleophilic substitution methods have largely been replaced by palladium-catalyzed processes because of the limited scope or functional group tolerance of these reactions.[281] The Buchwald-Hartwig amination remains a versatile reaction with a wide scope.

The name of the reaction is credited to those who developed the reaction, Stephen Buchwald and John F. Hartwig. In December of 1994 the two pioneering papers for this reaction were received seven days apart each describing palladium-catalyzed cross-coupling of aryl halides to secondary amines.[282,283] Since then, the development of this reaction has led to a small amount of mechanistic investigation;[250,284,285] however, the usefulness of the reaction has not been matched with similar levels of in-depth analysis.

In a general sense, the Buchwald-Hartwig amination facilitates the formation of C-N bonds between aryl halides (or triflates) and primary or secondary amines using catalytic quantities of palladium. The scope of the reaction has been expanded over the last two decades owing in large part to the development of new ligands which modulate the palladium catalyst. In the mid to late 90's, the so-called "first-generation" ligands used were fairly simple and relatively compact phosphines.[286] Early examples are tri(*o*-tolyl)phosphine palladium complexes, though this limited the reaction to secondary amine substrates.

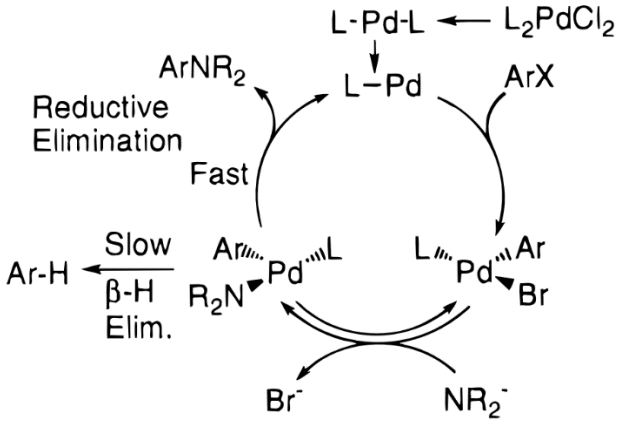

Figure 69. First proposed catalytic cycle for palladium-catalyzed coupling of aryl bromides to (tin-free) secondary amines.[287] Here, L = P(o-tolyl)3.

Newer ligands used in this coupling involve bulkier, more electron-rich bidentate phosphine ligands. Ligands such as 2,2'-bis(diphenylphosphino)-1,1'-binaphthyl (BINAP) proved to sufficiently widen the scope of the reaction to allow access to primary and secondary amines.[288] Other bisphosphines continue to prove to be useful as ligands. Sterically hindered phosphine and bisphosphine ligands were found to feature even better performance and tunability which has opened up the scope of the reaction to include electron deficient and heterocyclic amines to be coupled to a diverse range of aryl halides

because of the high activity of the catalyst.[227,286] These ligands are readily available for purchase from major chemical companies.

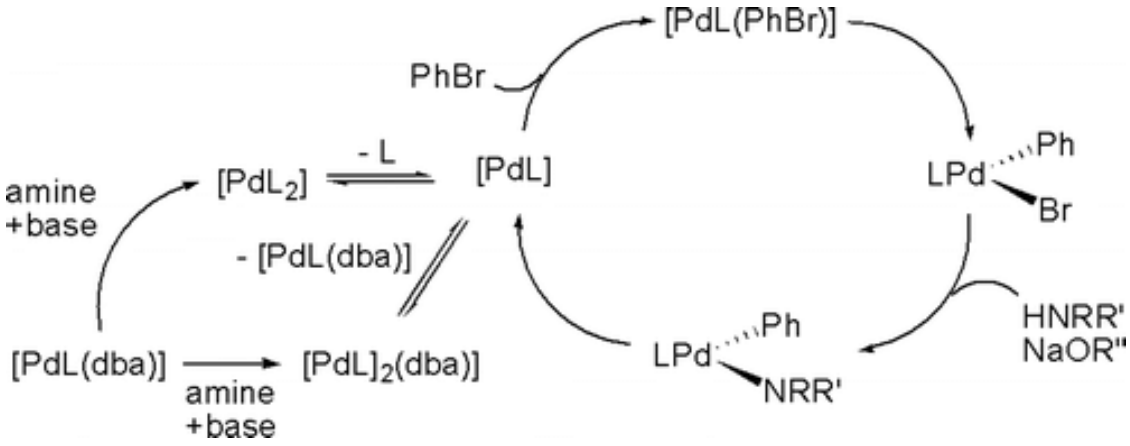

Figure 70. Proposed catalytic cycle for the Buchwald-Hartwig Amination with detail on the precatalyst activation[250]

As the ligand and substrate choices for the Buchwald-Hartwig amination continue to grow so too does mechanistic examination of the reaction. Several iterations of proposed cycles have appeared throughout the years[285,289,290] with the most thorough and recent investigation deciding on the mechanism shown in Figure 70 in which the oxidative addition of the aryl halide occurs before the amine, and PdL_2 lies off-cycle (two points which were previously ambiguous).[250] Despite this, there remains a large degree of ambiguity in exactly how precatalyst activation occurs, along with what happens following oxidative addition of the aryl halide, as demonstrated by the following "accepted" catalytic cycles.

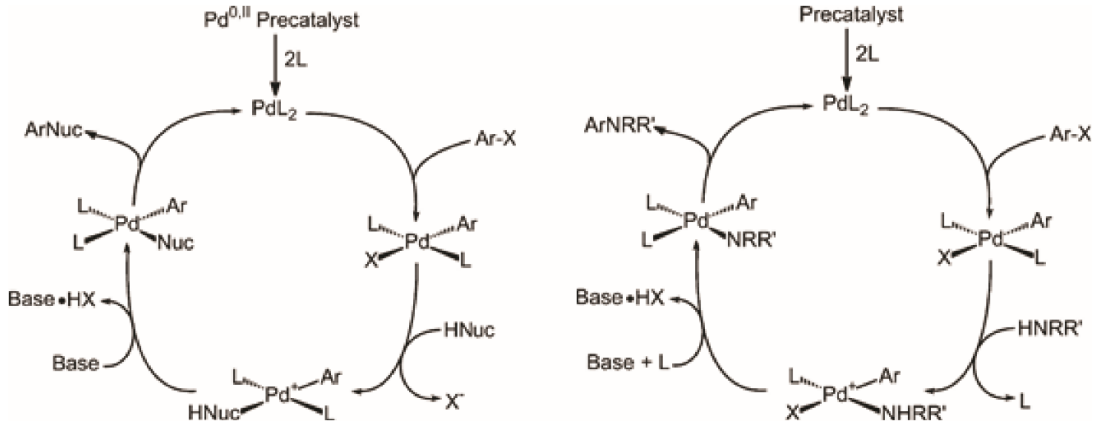

Figure 71. Modern proposed catalytic cycles for the Buchwald-Hartwig Amination. Note the disparity between the two schemes at the amine coordination and base-mediated Pd-N bond formation steps[291]

6.3.2 The Sonogashira Cross-Coupling

Following the discovery of the Heck alkynylation, a palladium-mediated C-C coupling between a terminal alkyne and an aryl or vinyl halide, in 1975 by Heck and Cassar, Sonogashira reported a similar cross coupling.[292–294] Sonogashira's reaction called for the addition of copper iodide, which acted as a co-catalyst and greatly enhanced the reaction since it allowed for milder conditions and higher yields. Today, it is one of the most powerful and heavily used palladium-catalyzed cross-coupling reactions used in the production of a variety of materials.[295,296] The general reaction scheme and initial proposed catalytic cycle may be seen in Figure 72.

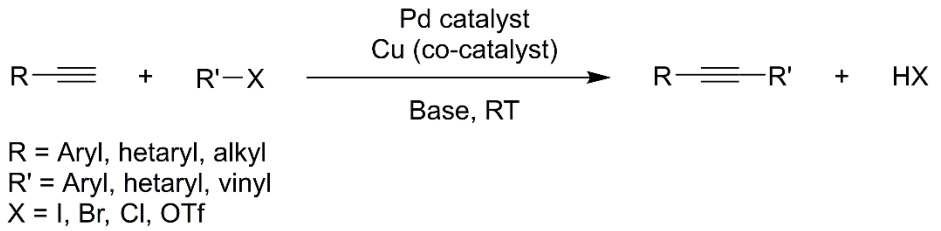

Figure 72. Generic Sonogashira Pd-catalyzed cross-coupling reaction conditions[296]

Most mechanisms describe the main steps as:

1. Oxidative addition of the aryl halide to palladium
2. Transmetallation of the alkyne
3. Reductive elimination yielding the final product

The second step in the list above brings the two carbon fragments together onto the palladium centre. It is important to note that this step is still referred to transmetallation in the copper-free variant of the Sonogashira reaction and is the most ambiguous step in the catalytic cycle. This copper-free variation of the reaction is heavily used, since it eliminates the propensity for homocoupling of the alkynes.[297]

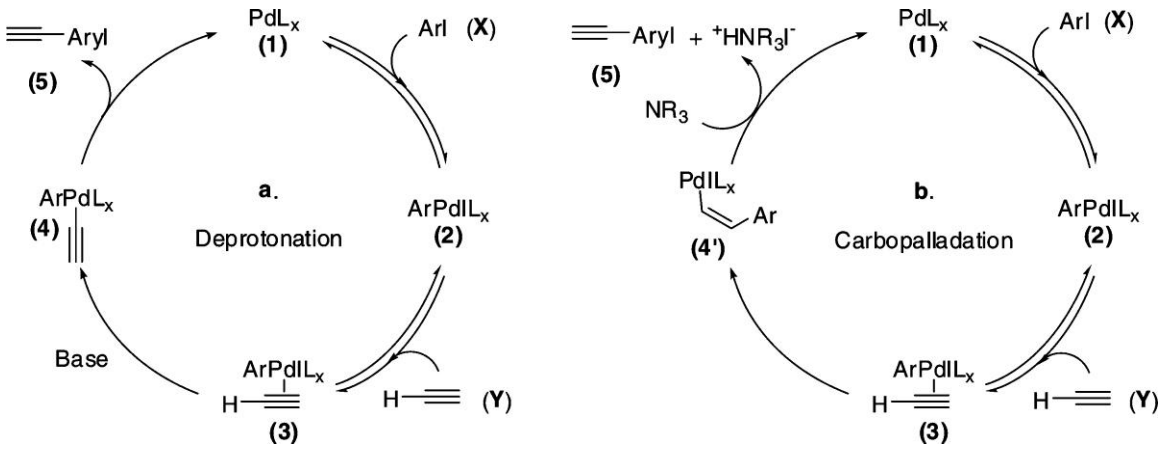

Figure 73. The proposed catalytic cycles, deprotonation and carbopalladation, of the copper-free Sonogashira coupling reaction

Proposed mechanisms for the copper-free Sonogashira reaction include carbopalladation and deprotonation.[292,298–301] The particulars of these two mechanisms are summed up in the original proposed cycles in Figure 73. The ambiguity between the two mechanisms is a function of the fact that amines in solution are not strong enough bases to effect deprotonation of the terminal alkyne, hence deprotonation is thought to occur following the formation of a η^2-coordinated alkyne to the palladium centre. In theory, this should serve to draw electron density away from the alkyne, thus weakening the C-H bond and enhancing acidity.[299,300] The carbopalladation mechanism suggests that following the formation of the η^2-coordinated alkyne-palladium complex, the base facilitates β-hydride elimination.[292,298]

The carbopalladation mechanism was supported by an NMR based study by Amatore and Jutand in 2004.[298] In this work, the reaction between a synthetically prepared *trans*-$Pd(PPh_3)_2PhI$ and $EtO_2C–C{\equiv}CH$ was investigated. It was found that carbopalladation was occurring following formation of a *cis*-adduct, $EtO_2C–C(PdIL_2)=CHPh$ (L = PPh_3), as the major product.

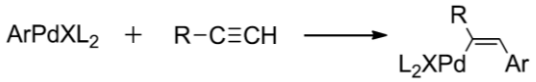

Figure 74. Carbopalladation of a terminal alkyne with the synthetically prepared Pd complex[298]

A subsequent study by Ljungdahl suggested that the carbopalladation mechanism was not catalytic in nature.[300] In this work, a carbopalladation product was synthetically prepared to

detect base-assisted *trans*-elimination or intramolecular β-hydride elimination. No product was observed in the presence of phenylacetylene, casting doubt on the carbopalladation mechanism. These doubts regarding the carbopalladation mechanism was further supported by DFT calculations by Garcia-Melchor and co-workers.[302]

Following the initial carbopalladation and deprotonation proposals, two separate deprotonation mechanisms have been proposed and it is possible that the nature of the substrates have an effect on whether the mechanism follows the anionic or cationic mechanism (see Figure 75).[300,302]

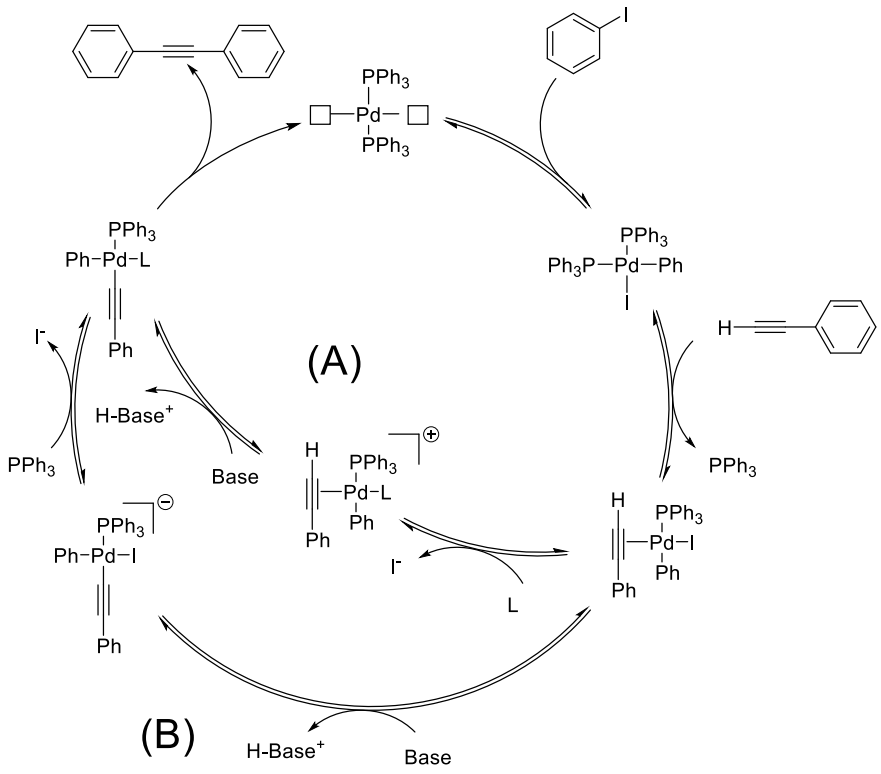

Figure 75. The competing deprotonation mechanisms of the copper-free Sonogashira reaction. The cationic pathway (A), and the anionic pathway (B) (where L = ligand)

In the cationic pathway, the halide is substituted by the phosphine ligand or amine which yields a cationic intermediate. The reductive elimination is then facilitated following deprotonation. This mechanism is considered to be favourable when electron withdrawing groups are present on the alkyne providing acidity to the alkyne. Conversely, deprotonation is key in the anionic pathway, as it initially serves to produce the anionic intermediate involving a C-Pd σ bond. This complex then goes through halide-ligand exchange and then proceeds to reductive elimination. In contrast, the anionic mechanism is favourable when electron donating groups are present on the alkyne and the *sp*-proton is less acidic. The reaction conditions (especially in cases where the amine used competes for coordination) produced studies which appear draw the correct conclusions, yet are in disagreement.[66,300,301,303–305] The McIndoe group has recently shed some light on the reaction using our techniques of pressurized sample infusion, charge-tagging using a sulfonated phosphine ligand, and ESI-MS resulting in a proposed catalytic cycle seen in Figure 76.

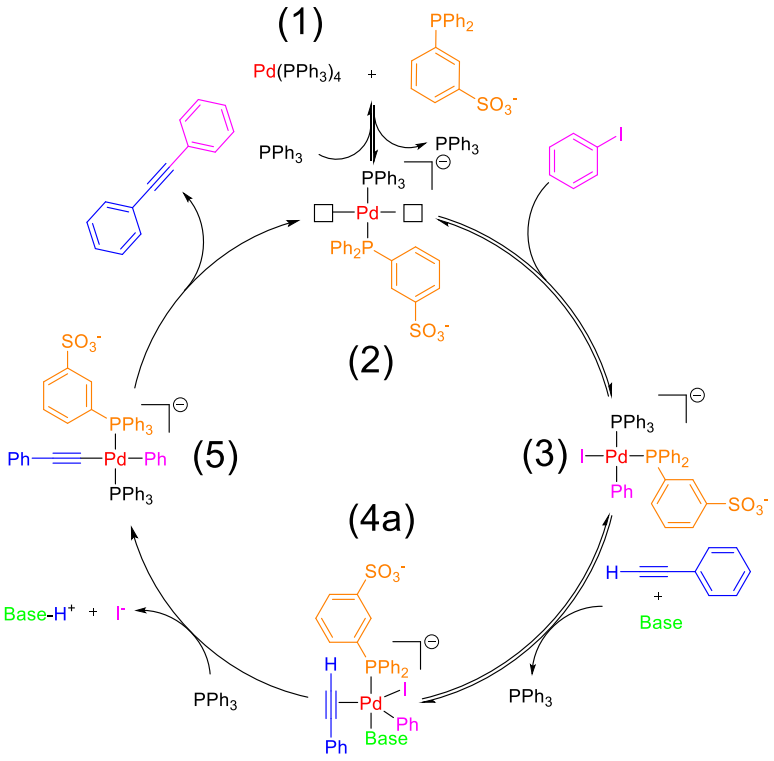

Figure 76. Proposed catalytic cycle for the copper-free Sonogashira reaction[66]

6.4 Experimental

Palladium acetate, $Pd(OAc)_2$, sodium 2′-dicyclohexylphosphino-2,6-dimethoxy-1,1′-biphenyl-3-sulfonate hydrate, $Na^+[sSPhos]^-$, aniline, iodobenzene, potassium phosphate (K_3PO_4), and all solvents were purchased from Sigma-Aldrich and used as received. UHP200 Argon and HP300 4.8 Nitrogen were purchased from Airgas (Calgary, Canada) and used without further purification.

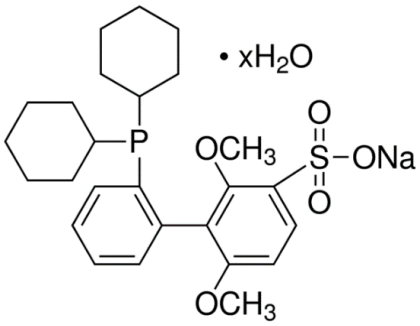

Figure 77. The sulfonated SPhos Buchwald-ligand, $Na^{+}[sSPhos]^{-}$

In a typical reaction, a 20.0 mL mixture of 66% HPLC grade methanol and 33% deionized water was transferred to a custom PSI flask (vide infra), sparged with nitrogen for 15 minutes, and connected to the mass spectrometer via capillary tubing passed through a rubber septum. Heating was effected with an IKA C-MAG HS 7 stirring hotplate equipped with an ETS-D5 thermocouple and oil bath. The thermocouple was set to heat the oil bath to 100°C. All reagent stock solutions were prepared under an inert nitrogen atmosphere in a glovebox. The palladium stock solution was prepared using 0.0010 g $Pd(OAc)_2$ dissolved in 4.0 mL anhydrous tetrahydrofuran (1.1 mM $Pd(OAc)_2$, 1.1 mM Pd). $Na^{+}[sSPhos]^{-}$, stock was prepared by dissolving 0.0045 g of the salt in 4.0 mL degassed HPLC grade methanol (2.2 mM $[sSPhos]^{-}$). Potassium phosphate stock was prepared in deionized water at a concentration of 5.0 mM.

Each stock solution was injected via syringe into the custom PSI flask in a specific order: 600 µL of $[sSPhos]^{-}$ stock, then 300 µL of $Pd(OAc)_2$ yielding a Pd concentration of 33.0 µM and 2 equivalents of ligand. 100 µL each of iodobenzene and 100 µL aniline was injected, then finally 100 µL of K_3PO_4 stock. The PSI flask was charged a stir bar and reagent stock solutions were injected using Hamilton GASTIGHT® syringes when

required. The flask was pressurized with 4 psi of argon using a PRAXAIR ProStar Platinum regulator.

All electrospray ionization mass spectra were recorded using a Waters Acquity Triple Quadrupole Detector equipped with a Z-Spray electrospray ionization source. The capillary voltage was held at 3.0 kV, cone voltage at 10.0 V, and extraction cone at 3.0 V. The MS cone voltage was optimized to eliminate in-source fragmentation of the catalyst. Source nitrogen gas flow rates and temperatures varied depending on solvent and were set to provide optimal desolvation conditions. The desolvation gas flow rate was 500 L/hr, cone gas flow rate 100 L/hr, source temperature 110°C, desolvation temperature 210°C. The detector gain was set to an optimal voltage of 470 V. For full scan experiments, scan time was set to 10 s, with an inter-scan time of 0.1 s and a range of *m/z* 400-1000. For all experiments, the ESI spray head was left in a position near-perpendicular to the sampling cone with a 7° incline toward the cone. MRM experiments were performed with a collision energy between 5-35 V with an argon collision gas flow rate of 0.1 mL/hr. The full MRM parameter list is below in Table 7. All species were optimized at a cone voltage of 10 V and the MRM scan was set to select the precursor and product with a span of 2. Each channel has a dwell time of 1 s. High-mass and low-mass resolutions were set to 15.00 for both Q_1 and Q_3.

Table 7. Optimized MRM parameters for Buchwald-Hartwig coupling reaction*

Compound Name	Precursor (*m/z*)	Product (*m/z*)	Collision (V)
[sSPhos]$^-$	489	375	35
[Pd(sSPhos)]$^-$	595	489	25

[Pd(sSPhos)(NHAr)(Ar)]$^-$	764	595	5
[Pd(sSPhos)(Ar)(I)]$^-$	799	525	20
[Pd(sSPhos)(NH$_2$Ar)(Ar)]$^-$	892	799	7

6.5 Multiple Reaction Monitoring of the Buchwald-Hartwig Reaction

The preliminary work presented here involves the investigation of the Buchwald-Hartwig amination (BHA) and serves as a proof of concept for the use of Multiple Reaction Monitoring to investigate a homogeneous catalytic reaction. Unfortunately, the system was found to be incredibly difficult to study using ESI-MS, as well as with our fibre optic UV-Vis spectrometer (*vide infra*). That being said, these experiments yielded some interesting results. The general conditions are summarized Figure 78.

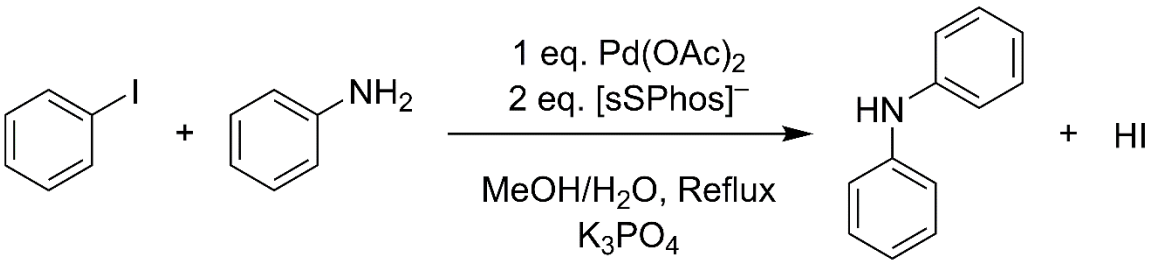

Figure 78. Optimized Buchwald-Hartwig amination conditions

6.5.1 Choice of reagents: Ligand and Palladium source

Two of the simplest possible substrates for the C-N coupling, aniline and iodobenzene, were used since reactions performed with more hindered substrates generally require

several hours of reaction time, even with an ideal catalyst and elevated temperatures.[286] It is worth noting at this point that it is theoretically possible to run an ESI-MS experiment for an extended period of time. This is particularly true with quadrupole mass spectrometers as they are extremely robust instruments and do not vary a great deal with changes to ambient conditions. [c] Practically, however, this becomes an issue, depending on the nature of the reaction involved. The McIndoe group frequently employs relatively concentrated mixtures, especially compared to routine mass spectrometric analyses. Oftentimes, metal complexes or insoluble constituents are present (or formed in the reaction) which can deposit within the PEEK tubing used to infuse the solution to the ESI source. Further, despite the use of filters or thick gauge PEEK tubing, ESI sources are inherently prone to deposition or clogging issues due to the required thin gauge of the source capillary. Because of this, it is prudent to reduce the run-time as much as possible (dependent on the reaction in question), while still preserving realistic "bench-top" conditions as close as possible.

[c] A particularly interesting example of the robustness of quadrupole trap instruments is the ability to mobilize these instruments for deployment in the field. In one particular example, the instrument was capable of continually monitoring analytes while mobile in the rear of a vehicle.[345]

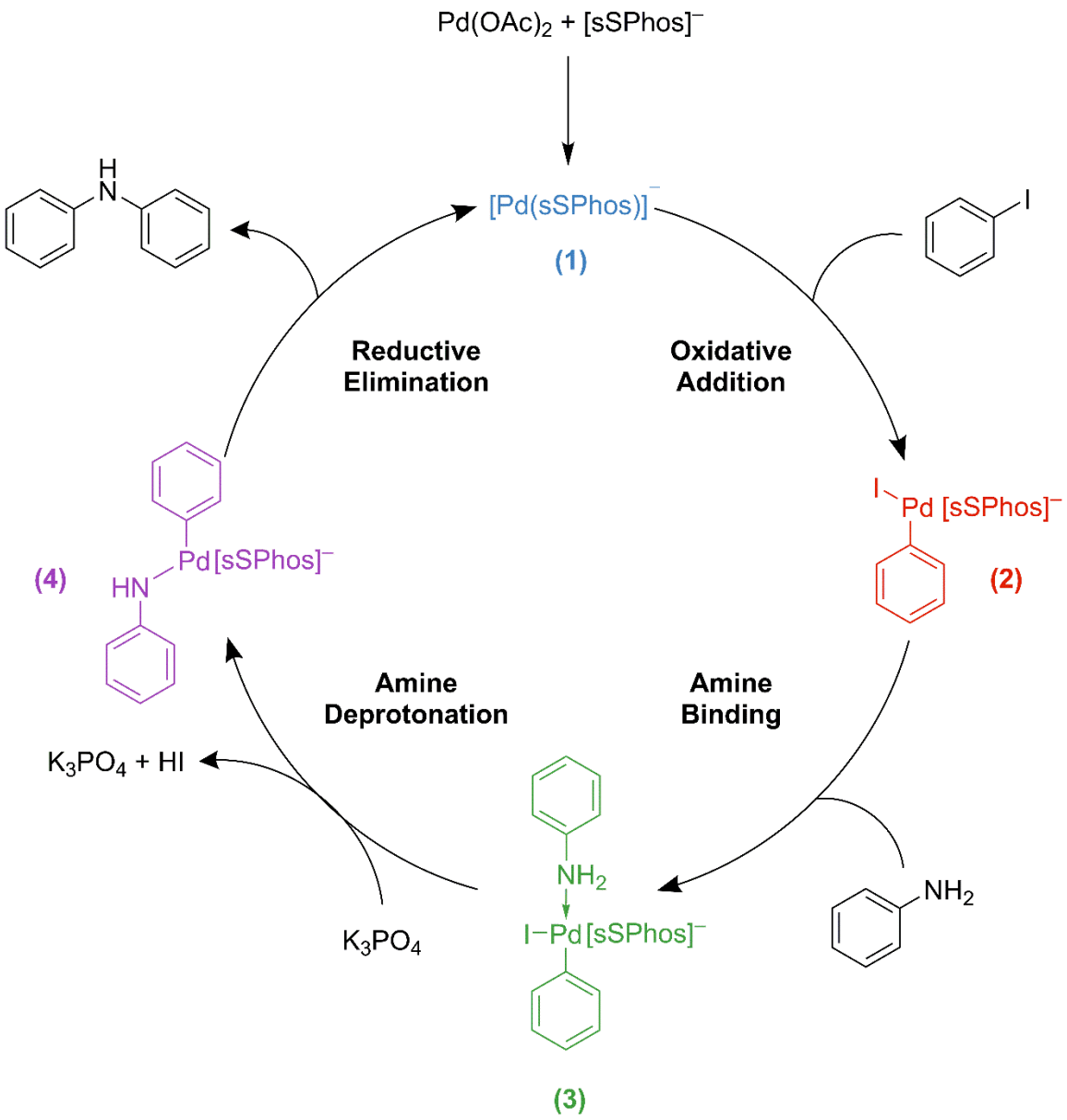

Figure 79. Proposed catalytic cycle for the Buchwald-Hartwig amination

Palladium acetate, $Pd(OAc)_2$ was used here instead of tris(dibenzylideneacetone)dipalladium, $Pd_2(dba)_3$, for several reasons. First, palladium acetate is generally used in these reactions more frequently than $Pd_2(dba)_3$. One speculative reason for this is price and aqueous solubility. Another reason is the fact that the free dibenzylideneacetone ligand appears to play a non-innocent role following activation in

many solvents.[47,218,223] For this reaction, $Pd_2(dba)_3$ was less attractive for reasons which become clear after reviewing evidence in Chapter 5 (namely, continued participation of the dba ligand after addition of phosphine). With solvents such as dimethylformamide (DMF), the activation is relatively quick, yielding the active species $[Pd(sSPhos)(dba)]^-$ after roughly 1 minute at room temperature; however, the reaction did not proceed to the subsequent catalytic steps in good abundance due to significant DMF and methylformamide coordination. Other contaminants in DMF, formic acid in particular, may have also contributed to this failure; however, there is insufficient information to conclude the exact cause of the lack of oxidative addition. Methanol appeared to be an attractive solvent since at 65°C the active species, $[Pd(sSPhos)(dba)]^-$, forms relatively quickly. Unfortunately, following several trials at elevated temperatures, it appeared that hydrodehalogenation was occurring (within three minutes of iodobenzene injection). Evidence for hydrodehalogenation is based on the accumulation of iodide and triiodide ($[I_3]^-$) in the mass spectrum, and is therefore conjecture only. Trials in which all reagents are mixed quickly and the catalyst is preformed resulted in the rapid formation of the deprotonated amine, (**4**), with no apparent reductive elimination over a three-hour period. As such, $Pd_2(dba)_3$ did not seem to be an ideal precatalyst for this reaction and consequently $Pd(OAc)_2$ was used instead.

Palladium (II) sources such as $Pd(OAc)_2$ must be reduced to Pd(0) to form the active catalytic species before entry into the catalytic cycle. This activation process is suspected to proceed through β-hydride elimination of a Pd(II)-amine complex, suggesting the amine requires hydrogen atoms α to the nitrogen atom.[286] There is also evidence of phosphine

oxidation facilitating this reduction, which is heavily supported by the immediate appearance of sSPhos oxide following injection of only $Pd(OAc)_2$ and sSPhos.

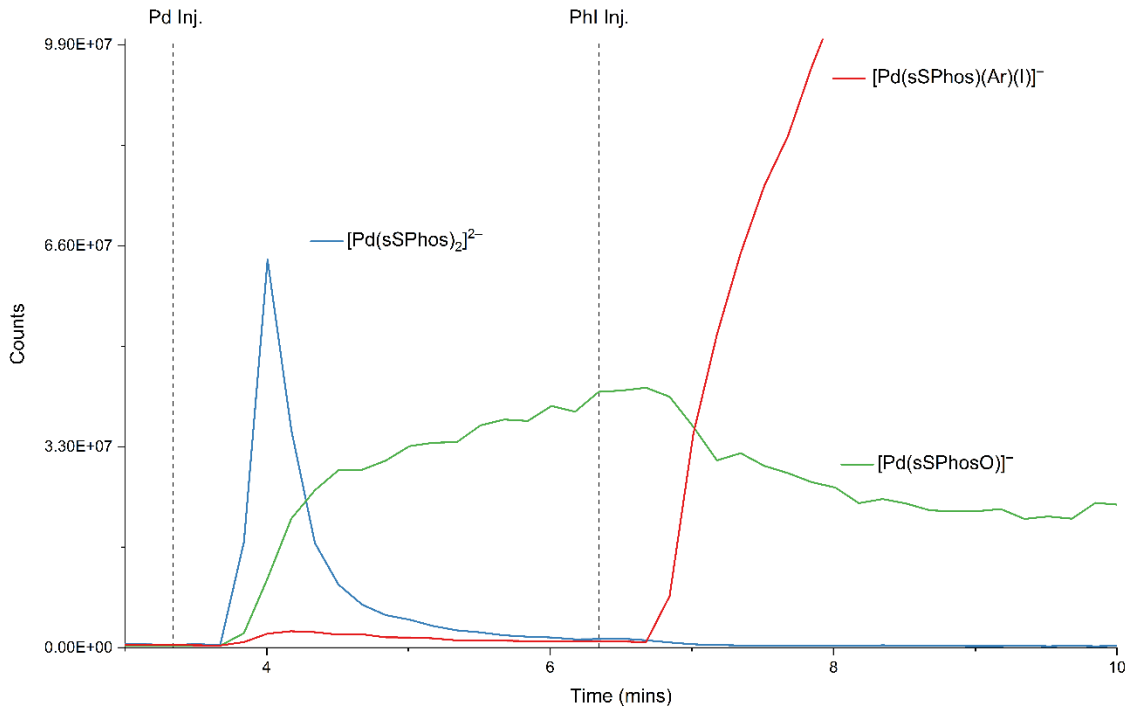

Figure 80. Close-up of precatalyst activation and iodobenzene injection during Buchwald-Hartwig reaction

Ligand oxidation is generally undesirable, since the ligand is no longer available for coordination once oxidized. Another issue is that poorly oxidizing phosphine ligands (such as the Buchwald-type ligands), or poor amine reducing agents, can result in long activation times.

The reaction was originally monitored in the negative ion mode using a traditional full scan. Following identification of species of interest, a product ion scan of each species was performed to find the optimal collision energy. This particular reaction was an excellent

candidate for an MRM scan due to the presence of an activation by-product (*m/z* 887) which overlapped with the important catalytic cycle species, (**3**), which appears following the addition of aniline. The MRM experiment was performed with the precursor and product combinations listed in Table 7. Optimized MRM parameters for Buchwald-Hartwig coupling reaction.

The activation of $Pd(OAc)_2$ in methanol, or a methanol/water mixture using the Buchwald-type sSPhos ligand was immediately interesting, especially in light of the results of activation of $Pd_2(dba)_3$ with the same ligand (see Chapter 5). The lack of the non-innocent dibenzylideneacetone ligand results in rapid formation of the bis-ligated complex, $[Pd(sSPhos)_2]^{2-}$. This ion should have excellent reactivity as the active species, $[Pd(sSPhos)]^-$, should form more favourably via loss of a single, weakly bound sSPhos ligand as compared to dibenzylideneacetone dissociation. Concurrent with the formation of the bis-ligated complex, sSPhos is slowly oxidized yielding $[Pd(sSPhosO)]^-$ and free $[sSPhosO]^-$.

Interestingly, $[Pd(sSPhos)_2]^{2-}$ achieved its maximum abundance shortly after ligand and palladium are mixed (less than one minute), then appears to decompose rapidly. Part of this loss may be explained by phosphine ligand oxidation required to reduce palladium. However, several other low-abundance palladium species appear in tandem with the disappearance of $[Pd(sSPhos)_2]^{2-}$. Based on the isotope pattern, at least one of these appears to be multiply charged (*m/z* 673.5). The structural details evaluated by product ion scans

(on some of the more abundant species) are unsurprising, but uninformative, since the only apparent product ion is sSPhos.

Following the addition of iodobenzene, the oxidative addition product (**2**) appears quickly and in large quantities. The disparity between observable post-activation palladium species' total abundance and (**2**) suggests that at least some of the following scenarios are occurring:

1. Part of the $[Pd(sSPhos)_2]^{2-}$ produced is deactivated due to ligand oxidation
2. Some post-activation palladium species are not deactivated, but produce multiple low-level aggregates, metal adducts, multi-nuclear palladium complexes, or metal clusters shortly after activation (see Figure 81)
3. Some of species available to form (**2**) are invisible to mass spectrometry and exist either as neutrals, zwitterionic compounds, or strong ion-pairs with sodium
4. There exists a large spray-quality difference between observable products and product (**2**)

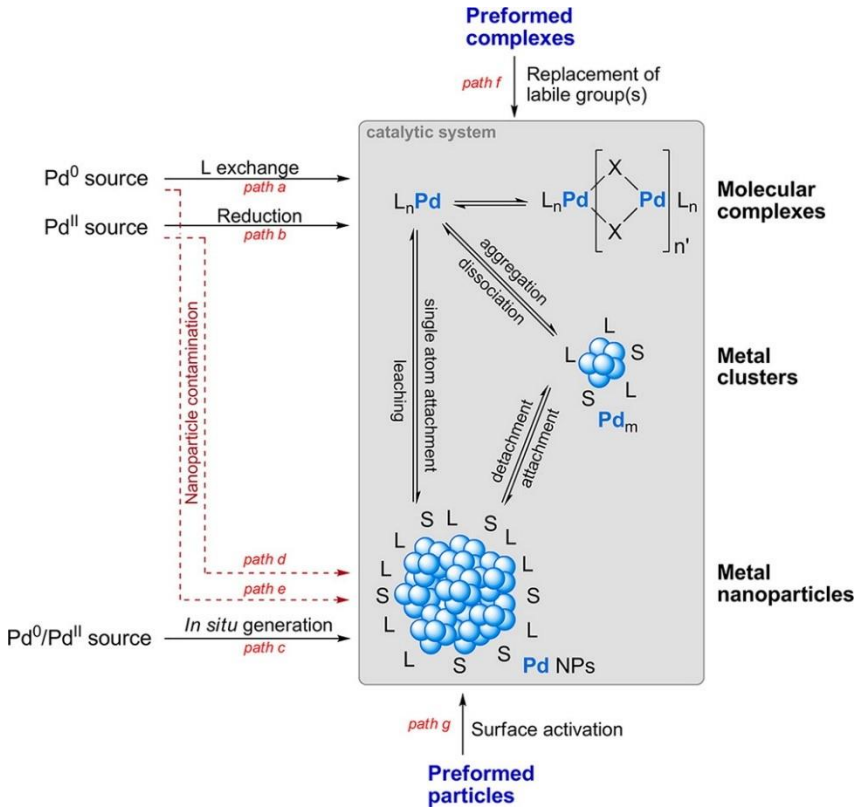

Figure 81. Example from Ananikov of the potential formation of palladium metal clusters and nanoparticles[214]

Point 4 is unlikely since most of the observable palladium species are likely similar in structure; however, it is a possible explanation for discrepancy in absolute counts observed for a species in ESI-MS. Spray quality effects between analytes is quantifiable, if all species in a mixture are isolable. This is obviously an issue for unknown mixtures, or catalytic reactions in which several species may be transient or not isolable. Changes to reaction mixture composition may also affect the spray quality and is apparent in this reaction following the addition of aniline which results in a large drop in the total ion current.

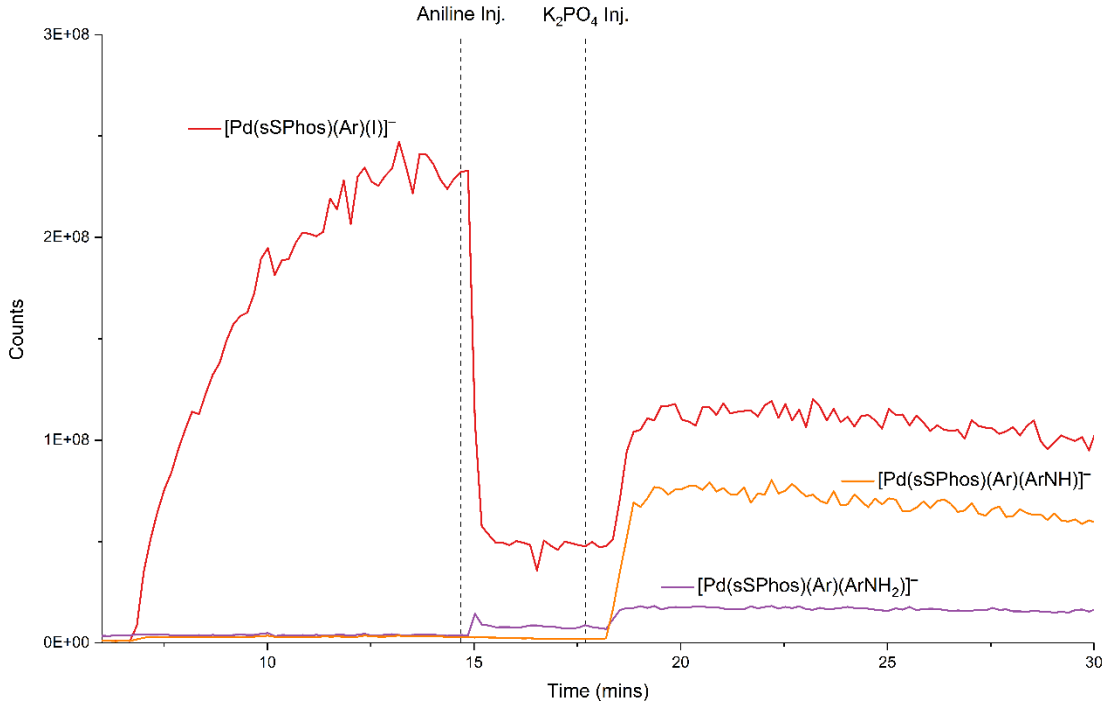

Figure 82. Initiation of Buchwald-Hartwig coupling following injection of base

The combination of the substrates without the addition of base produces a small amount of product (**3**) following amine coordination to the palladium metal centre. Once the inorganic base potassium phosphate is added in relatively large quantities, the spray quality improves. This change is expected since added electrolyte has been found to improve ESI spray quality.[34,97]

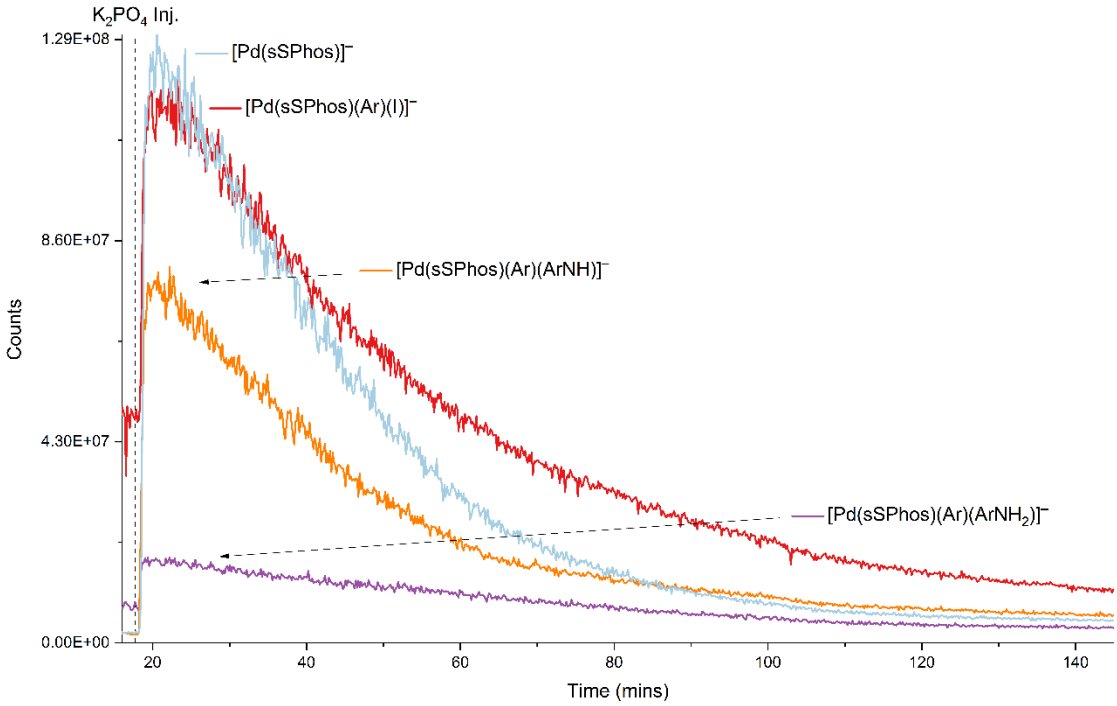

Figure 83. Decay of Buchwald-Hartwig reaction intermediate species following addition of base

Finally, the addition of base finally initiates the reaction by facilitating deprotonation of the amine and reductive elimination of the product. Overall, the reaction appears to conclude after a 133-minute decay of all intermediate species.

It should be noted that the results described above are preliminary and will not be the focus of a publication without additional experiments. The main goal should be to demonstrate the benefit of the MRM scanning mode to monitor low-level intermediate species, while also tracking reaction progress with *in situ* UV-Vis. In order to accomplish this, the MRM scan must be directly comparable with a typical ESI-MS full scan, run separately so as not to interfere with a nominal full scan in which the collision gas does not reduce the absolute abundance of all species. While further studies are required to complete

this goal, a second candidate reaction has shown great promise and will ultimately be slated for publication to demonstrate a combined reaction monitoring technique involving UV-Vis and tandem MS methods.

All intermediates contain a fixed charge from the sSPhos ligand and we are able to track them very effectively by ESI-MS; unfortunately, the substrates and products cannot be followed since they are neutral. This reaction seemed to be an ideal case for the use of combined orthogonal techniques as discussed in Chapter 5.

6.6 Current and future work: Real-time UV-Vis/ESI MS of the Sonogashira reaction

The Buchwald-Hartwig reaction described above calls for conditions at elevated temperatures, as do most similar couplings. Unfortunately, this presents a technical issue since our particular fiber optic probe is inoperable at temperatures above 60°C which limits the scope of reaction conditions. Attempts to run this particular Buchwald-Hartwig amination below 60°C resulted in extremely long reaction times inevitably resulting in PEEK tubing or capillary clogging effectively shutting down the analysis and limiting a complete picture of a reaction.

Alongside the work described above, we were also investigating the Sonogashira palladium-catalyzed cross coupling as a candidate reaction to demonstrate the use of combined tandem mass spectrometry and UV-Vis monitoring. Importantly, the temperatures and solvent involved are suitable for use with our fiber optic probe. The aim

of the present work is to produce a UV-Vis chromophore, diphenylacetylene using simple reagents and conditions.

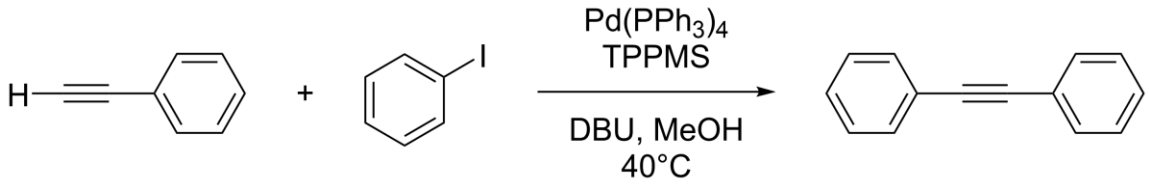

Figure 84. Sonogashira reaction with general reaction conditions used for simultaneous UV-Vis/ESI-MS monitoring

A Sonogashira coupling, between phenylacetylene and iodobenzene, was performed with tetrakis(triphenylphosphine)palladium(0) and an anionic triphenylphosphine analogue, TPPMS, as a supporting ligand to facilitate detection by ESI-MS (Figure 84). The combination of *in situ* fiber optic UV-Vis dip probe data, with simultaneous ESI-MS full scan data is seen in Figure 85 below. Here, the oxidative addition product $[Pd(PPh_3)(TPPMS)(Ph)(I)]^-$ (yellow trace) is rapidly produced and consumed. Another important intermediate, $[Pd(PPh_3)(TPPMS)(Ph)(PhC_2)]^-$ (red trace) was also observed by ESI-MS. The blue trace demonstrates the ability of UV-Vis to follow reaction progress by monitoring production of the diphenylacetylene product.

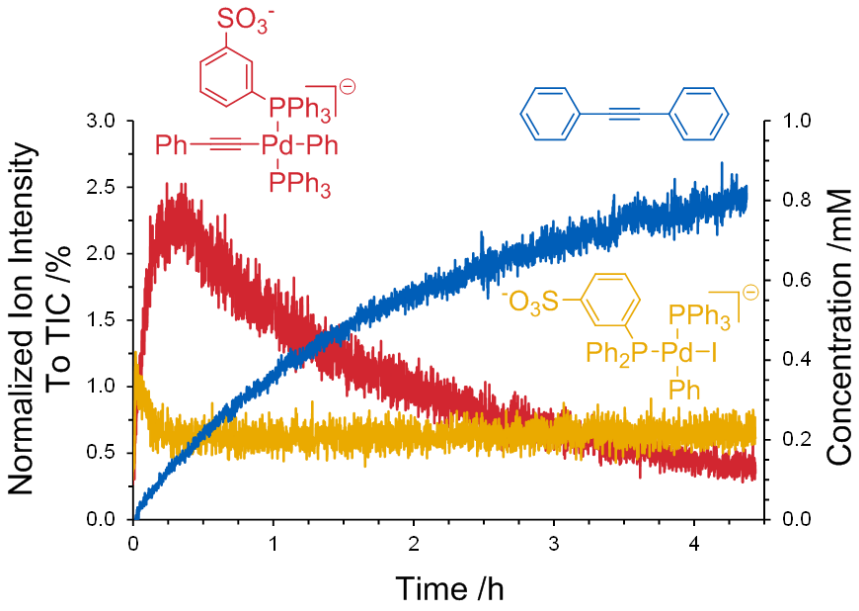

Figure 85. Simultaneous UV-Vis and ESI-MS analysis of a Sonogashira cross-coupling[306]

These results are a promising example of the ability for orthogonal techniques to shed light on the mechanism of a reaction. The mass spectrometer is used to do the "heavy lifting" and detect low level, transient intermediates where high specificity is required. At the same time, the overall reaction progress can be rapidly measured with high sensitivity, yielding high data density. Interestingly, several previously unseen anionic palladium-containing species, including amine-coordinated and diiodo palladium species, were observed in the reaction mixture. It is expected that with MRM and other tandem techniques (including the ion scan), in addition to high-resolution mass spectrometry analysis, that we will be able to accurately and selectively monitor and characterize these species.

6.7 Conclusions

Mass spectrometry in full scan or tandem modes provides excellent selectivity compared to other common analytical instrumentation. Through multiple reaction monitoring, a high level of sensitivity and accuracy is afforded which can yield incredible limits of detection. The lack of literature on the subject affords us an excellent opportunity to introduce valuable new tools to organometallic chemists. We will continue to develop our methodology for the real-time study of homogeneous catalytic reactions with a focus on tandem mass spectrometric methods and supporting spectroscopic techniques.

Chapter 7. Conclusion

Since its inception, electrospray ionization mass spectrometry (ESI-MS) has proven to be a useful analytical tool to study complicated chemical systems in detail. Our current techniques enable us to gather kinetic and mechanistic information of air- and moisture-sensitive organometallic reactions. However, the electrospray process itself is not perfectly explained in current literature despite a great deal of research effort. In particular cases, especially when delicate organometallic species are involved (see section 5.4 for a notable example), a lack of understanding may lead to erroneous conclusions. The work presented in this dissertation has developed the technique considerably and improves our ability to collect high-quality ESI-MS data. Importantly, we have also demonstrated the synergistic value of pairing mass spectrometry with simultaneous orthogonal instrumentation. Overall, we have improved the ability of scientists to monitor chemical transformations as they occur within the flask.

We approached common, yet previously unaddressed, issues with electrospray ionization in order to improve our own work. As was demonstrated in Chapter 2, the role of ESI solvent is dramatic and requires carefully designed experiments beforehand to improve results and rationally compare analyte responses. Source design is often overlooked in the literature; however, analyte signal could potentially be artificially enhanced or suppressed depending on spray head positioning (Chapter 3). These investigations improved our ability to monitor reactions with mass spectrometry in addition to other, ambient, electrospray techniques. Following a closer look at the ESI process, we applied our real-time monitoring methodology to new derivatization strategies for the notoriously

problematic petroleum matrix in Chapter 4. The chemoselective charge-tagging methodology used in this work serves to drastically raise signal-to-noise in ESI-MS for low-level detection of specific analytes. We anticipate that these new tools will improve mass spectrometry performance in examinations of petroleum samples and other troublesome matrices. Finally, Chapters 5 and 6 employed unique in-situ monitoring using an orthogonal analytical technique. The results in these chapters establish that we are able to supplement our interpretation of ESI-MS real-time monitoring results with additional analytical techniques without perturbing the system.

In the future, combined analytical techniques in real-time reaction monitoring will facilitate the observation of low concentration transient intermediate species via ESI-MS with high sensitivity; at the same time, in-depth structural analysis or overall reaction progress will be accomplished through the use of additional analytical equipment. Overall this work has improved the lens under which chemical reactions are inspected and will produce more precise and valuable information in catalytic chemistry and other fields.

Bibliography

(1) Ahmadi, Z.; McIndoe, J. S. A Mechanistic Investigation of Hydrodehalogenation Using ESI-MS. *Chem. Commun. (Camb).* **2013**, *49* (98), 11488–11490.

(2) Vikse, K. L.; Ahmadi, Z.; Manning, C. C.; Harrington, D. A.; McIndoe, J. S. Powerful Insight into Catalytic Mechanisms through Simultaneous Monitoring of Reactants, Products, and Intermediates. *Angew. Chemie - Int. Ed.* **2011**, *50* (36), 8304–8306.

(3) Stoddard, R. L.; Collins, S.; McIndoe, J. S. *Mass Spectrometry of Organoaluminum Derivatives*; Rappoport, Z., Ed.; John Wiley & Sons, Ltd: Chichester, UK, 2016.

(4) Henderson, M. A.; Luo, J.; Oliver, A.; McIndoe, J. S. The Pauson-Khand Reaction: A Gas-Phase and Solution-Phase Examination Using Electrospray Ionization Mass Spectrometry. *Organometallics* **2011**, *30* (20), 5471–5479.

(5) Dyson, P. J.; McIndoe, J. S. Analysis of Organometallic Compounds Using Ion Trap Mass Spectrometry. *Inorganica Chim. Acta* **2003**, *354*, 68–74.

(6) Borman, S. Chemistry Crystalizes into Modern Science. *Chem. Eng. News* **1998**, *76* (2), 39–75.

(7) Gross, J. H. *Mass Spectrometry: A Textbook: Second Edition*; Springer Science & Business Media, 2011.

(8) Hayen, H.; Karst, U. Strategies for the Liquid Chromatographic-Mass Spectrometric Analysis of Non-Polar Compounds. *J. Chromatogr. A* **2003**, *1000* (1–2), 549–565.

(9) Wiseman D. R., J. M. . I. Desorption Electrospray Ionization MassSpectrometry: Imaging Drugs and Metabolitesin Tissues. *PNAS* **2008**, *105* (47), 18120–18125.

(10) Cooks, R. G.; Mueller, T. Through a Glass Darkly: Glimpses into the Future of Mass Spectrometry. *Mass Spectrom. (Tokyo, Japan)* **2013**, *2* (Spec Iss), S0001.

(11) Kebarle, P.; Verkcerk, U. H. Electrospray: From Ions in Solution to Ions in the Gas Phase, What We Know Now. *Mass Spectrom. Rev.* **2009**, *28* (6), 898–917.

(12) Yamashita, M.; Fenn, J. B. Negative Ion Production with the Electrospray Ion Source. *J. Phys. Chem.* **1984**, *88* (20), 4671–4675.

(13) Whitehouse, C. M.; Dreyer, R. N.; Yamashita, M.; Fenn, J. B. Electrospray Interface for Liquid Chromatographs and Mass Spectrometers. *Anal. Chem.* **1985**, *57* (3), 675–679.

(14) Fenn, J. B.; Mann, M.; Meng, C. K.; Wong, S. F.; Whitehouse, C. M. Electrospray Ionization-Principles and Practice. *Mass Spectrom. Rev.* **1990**, *9* (1), 37–70.

(15) Henderson, W.; McIndoe, J. S. *Mass Spectrometry of Inorganic and Organometallic Compounds*; J. Wiley, 2005.

(16) Hinderling, C.; Adlhart, C.; Chen, P. Olefin Metathesis of a Ruthenium Carbene Complex by Electrospray Ionization in the Gas Phase. *Angew. Chemie Int. Ed.* **1998**, *37* (19), 2685–2689.

(17) Adlhart, C.; Chen, P. Comparing Intrinsic Reactivities of the First- and Second-Generation Ruthenium Metathesis Catalysts in the Gas Phase. *Helv. Chim. Acta* **2003**, *86* (4), 941–949.

(18) Wu, W.-Y.; Chen, S.-N.; Tsai, F.-Y. Recyclable and Highly Active Cationic 2,2′-Bipyridyl palladium(II) Catalyst for Suzuki Cross-Coupling Reaction in Water.

Tetrahedron Lett. **2006**, *47* (52), 9267–9270.

(19) Chen, P. Electrospray Ionization Tandem Mass Spectrometry in High-Throughput Screening of Homogeneous Catalysts. *Angew. Chemie Int. Ed.* **2003**, *42* (25), 2832–2847.

(20) Feichtinger, D.; Plattner, D. A.; Chen, P. Ziegler−Natta-like Olefin Oligomerization by Alkylzirconocene Cations in an Electrospray Ionization Tandem Mass Spectrometer. *J. Am. Chem. Soc.* **1998**, *120* (28), 7125–7126.

(21) Johnson, L. K.; Killian, C. M.; Brookhart, M. New Pd(II)- and Ni(II)-Based Catalysts for Polymerization of Ethylene and .alpha.-Olefins. *J. Am. Chem. Soc.* **1995**, *117* (23), 6414–6415.

(22) Blaser, H. U.; Spindler, F.; Studer, M. Enantioselective Catalysis in Fine Chemicals Production. *Appl. Catal. A Gen.* **2001**, *221* (1–2), 119–143.

(23) Heck, R. F.; Nolley, J. P. Palladium-Catalyzed Vinylic Hydrogen Substitution Reactions with Aryl, Benzyl, and Styryl Halides. *J. Org. Chem.* **1972**, *37* (14), 2320–2322.

(24) Sonogashira, K. Development of Pd–Cu Catalyzed Cross-Coupling of Terminal Acetylenes with sp2-Carbon Halides. *J. Organomet. Chem.* **2002**, *653* (1–2), 46–49.

(25) Miyaura, N.; Suzuki, A. Palladium-Catalyzed Cross-Coupling Reactions of Organoboron Compounds. *Chem. Rev.* **1995**, *95* (7), 2457–2483.

(26) Nijhuis, T. A.; Tinnemans, S. J.; Visser, T.; Weckhuysen, B. M. Operando Spectroscopic Investigation of Supported Metal Oxide Catalysts by Combined Time-Resolved UV-VIS/Raman/on-Line Mass Spectrometry. *Phys. Chem. Chem.*

Phys. **2003**, *5* (20), 4361.

(27) Tinnemans, S. J.; Mesu, J. G.; Kervinen, K.; Visser, T.; Nijhuis, T. A.; Beale, A. M.; Keller, D. E.; van der Eerden, A. M. J.; Weckhuysen, B. M. Combining Operando Techniques in One Spectroscopic-Reaction Cell: New Opportunities for Elucidating the Active Site and Related Reaction Mechanism in Catalysis. *Catal. Today* **2006**, *113* (1–2), 3–15.

(28) Weckhuysen, B. M. Determining the Active Site in a Catalytic Process: Operando Spectroscopy Is More than a Buzzword. *Phys. Chem. Chem. Phys.* **2003**, *5* (20), 4351.

(29) Siu, K. W. M.; Guevremont, R.; Le Blanc, J. C. Y.; Gardner, G. J.; Berman, S. S. Electrospray Interfacing for the Coupling of Ion-Exchange and Ion-Pairing Chromatography to Mass Spectrometry. *J. Chromatogr. A* **1991**, *554* (1–2), 27–38.

(30) Canty, A. J.; Traill, P. R.; Colton, R.; Thomas, I. M. Coordination Complexes and Organometallic Complexes of Palladium and Platinum with Polydentate Ligands Containing Pyrazole Groups and Related Ligands: An Electrospray Mass Spectrometric Study. *Inorganica Chim. Acta* **1993**, *210* (1), 91–97.

(31) Colton, R.; Traeger, J. C. The Application of Electrospray Mass Spectrometry to Ionic Inorganic and Organometallic Systems. *Inorganica Chim. Acta* **1992**, *201* (2), 153–155.

(32) Ahmadi, Z.; Oliver, A. G.; McIndoe, J. S. An Unexpected Pathway for Ligand Substitution in an Aryl Halide Complex of Palladium. *Chempluschem* **2013**, *78* (7), 632–635.

(33) Vikse, K.; Naka, T.; McIndoe, J. S.; Besora, M.; Maseras, F. Oxidative Additions

of Aryl Halides to Palladium Proceed through the Monoligated Complex. *ChemCatChem* **2013**, *5* (12), 3604–3609.

(34) Dyson, P. J.; McIndoe, J. S.; Zhao, D.; Gross, M. L.; Seddon, K. R. Direct Analysis of Catalysts Immobilised in Ionic Liquids Using Electrospray Ionisation Ion Trap Mass Spectrometry. *Chem. Commun.* **2003**, *41* (4), 508–509.

(35) Johnson, H. C.; Torry-Harris, R.; Ortega, L.; Theron, R.; McIndoe, J. S.; Weller, A. S. Exploring the Mechanism of the Hydroboration of Alkenes by Amine–boranes Catalysed by [Rh(xantphos)] +. *Catal. Sci. Technol.* **2014**, *4* (10), 3486–3494.

(36) Stoddard, R. L.; Luo, J.; van der Wal, N.; O'Rourke, N. F.; Wulff, J. E.; McIndoe, J. S. A Multi-Pronged Mechanistic Study of the Phosphine-Mediated Conjugate Addition of an Alcohol to an Acetylenic Ester. *New J. Chem.* **2014**, *38* (11), 5382–5390.

(37) Trefz, T. K.; Henderson, M. A.; Linnolahti, M.; Collins, S.; Scott McIndoe, J. Mass Spectrometric Characterization of Methylaluminoxane-Activated Metallocene Complexes. *Chem. - A Eur. J.* **2015**, *21* (7), 2980–2991.

(38) Vikse, K. L.; McIndoe, J. S. Mechanistic Insights from Mass Spectrometry: Examination of the Elementary Steps of Catalytic Reactions in the Gas Phase. *Pure Appl. Chem.* **2015**, *87* (4), 361–377.

(39) Vikse, K. L.; Ahmadi, Z.; Scott McIndoe, J. The Application of Electrospray Ionization Mass Spectrometry to Homogeneous Catalysis. *Coord. Chem. Rev.* **2014**, *279*, 96–114.

(40) Luo, J.; Oliver, A. G.; McIndoe, J. S. A Detailed Kinetic Analysis of Rhodium-

Catalyzed Alkyne Hydrogenation. *Dalton Trans.* **2013**, *42* (31), 11312–11318.

(41) Vikse, K. L.; Woods, M. P.; McIndoe, J. S. Pressurized Sample Infusion for the Continuous Analysis of Air- And Moisture-Sensitive Reactions Using Electrospray Ionization Mass Spectrometry. *Organometallics* **2010**, *29* (23), 6615–6618.

(42) Vikse, K. L.; Ahmadi, Z.; Luo, J.; Van Der Wal, N.; Daze, K.; Taylor, N.; McIndoe, J. S. Pressurized Sample Infusion: An Easily Calibrated, Low Volume Pumping System for ESI-MS Analysis of Reactions. *Int. J. Mass Spectrom.* **2012**, *323–324* (0), 8–13.

(43) Adlhart, C.; Chen, P. Fishing for Catalysts: Mechanism-Based Probes for Active Species in Solution. *Helv. Chim. Acta* **2000**, *83* (9), 2192–2196.

(44) Gut, I. G.; Jeffery, W. A.; Pappin, D. J. C.; Beck, S. Analysis of DNA by "Charge Tagging" and Matrix-Assisted Laser Desorption/Ionization Mass Spectrometry. *Rapid Commun. Mass Spectrom.* **1997**, *11* (1), 43–50.

(45) Janusson, E.; McGarvey, B.; Islam, F.; Rowan, C.; McIndoe, J. S. Selective Mass Spectrometric Analysis of Thiols Using Charge-Tagged Disulfides. *Analyst* **2016**.

(46) Sabino, A. A.; Machado, A. H. L.; Correia, C. R. D.; Eberlin, M. N. Probing the Mechanism of the Heck Reaction with Arene Diazonium Salts by Electrospray Mass and Tandem Mass Spectrometry. *Angew. Chemie Int. Ed.* **2004**, *43* (19), 2514–2518.

(47) Janusson, E.; Zijlstra, H. S.; Nguyen, P. P. T.; MacGillivray, L.; Martelino, J.; McIndoe, J. S. Real-Time Analysis of Pd2(dba)3 Activation by Phosphine Ligands. *Chem. Commun.* **2017**, *53* (5), 854–856.

(48) Daguenet, C.; Scopelliti, R.; Dyson, P. J. Mechanistic Investigations on the

Hydrogenation of Alkenes Using Ruthenium(II)-Arene Diphosphine Complexes. *Organometallics* **2004**, *23* (21), 4849–4857.

(49) Pelagatti, P.; Carcelli, M.; Calbiani, F.; Cassi, C.; Elviri, L.; Pelizzi, C.; Rizzotti, U.; Rogolino, D. Transfer Hydrogenation of Acetophenone Catalyzed by Half-Sandwich Ruthenium (II) Complexes Containing Amino Amide Ligands. Detection of the Catalytic Intermediates by Electrospray Ionization Mass Spectrometry. *Organometallics* **2005**, *24* (24), 5836–5844.

(50) Dyson, P. J.; Russell, K.; Welton, T. Electrospray Mass Spectrometry of [Ru4 (η6-C6H6)4 (OH)4]4+: First Direct Evidence for the Persistence of the Cubane Unit in Solution and Its Role as a Precatalyst in the Hydrogenation of Benzene. *Inorg. Chem. Commun.* **2001**, *4* (10), 571–573.

(51) Gilbert, B. C.; Lindsay Smith, J. R.; Mairata I Payeras, A.; Oakes, J.; Pons I Prats, R. A Mechanistic Study of the Epoxidation of Cinnamic Acid by Hydrogen Peroxide Catalysed by Manganese l,4,7-Trimethyl-l,4,7-Triazacyclononane Complexes. *J. Mol. Catal. A Chem.* **2004**, *219* (2), 265–272.

(52) Chevrin, C.; Le Bras, J.; Hénin, F.; Muzart, J.; Pla-Quintana, A.; Roglans, A.; Pleixats, R. Allylic Substitution Mediated by Water and Palladium: Unusual Role of a palladium(II) Catalyst and ESI-MS Analysis. *Organometallics* **2004**, *23* (20), 4796–4799.

(53) Raminelli, C.; Prechtl, M. H. G.; Santos, L. S.; Eberlin, M. N.; Comasseto, J. V. Coupling of Vinylic Tellurides with Alkynes Catalyzed by Palladium Dichloride: Evaluation of Synthetic and Mechanistic Details. *Organometallics* **2004**, *23* (16), 3990–3996.

(54) Wilson, S. R.; Wu, Y. A Study of Nickel-Catalyzed Coupling Reactions by Electrospray Ionization Mass Spectrometry. *Organometallics* **1993**, *12* (4), 1478–1480.

(55) Vicent, C.; Viciano, M.; Mas-Marzá, E.; Sanaú, M.; Peris, E. Electrospray Ionization Mass Spectrometry Studies on the Mechanism of Hydrosilylation of Terminal Alkynes Using an N-Heterocyclic Carbene Complex of Iridium, Allow Detection/Characterization of All Reaction Intermediates ⊥. *Organometallics* **2006**, *25* (15), 3713–3720.

(56) Chen, H.; Tagore, R.; Olack, G.; Vrettos, J. S.; Weng, T.-C.; Penner-Hahn, J.; Crabtree, R. H.; Brudvig, G. W. Speciation of the Catalytic Oxygen Evolution System: [MnIII/IV2(mu-O)2(terpy)2(H2O)2](NO3)3 + HSO5-. *Inorg. Chem.* **2007**, *46* (1), 34–43.

(57) Bonchio, M.; Licini, G.; Modena, G.; Bortolini, O.; Moro, S.; Nugent, W. A. Enantioselective Ti(IV) Sulfoxidation Catalysts Bearing C 3 -Symmetric Trialkanolamine Ligands: Solution Speciation by 1 H NMR and ESI-MS Analysis. *J. Am. Chem. Soc.* **1999**, *121* (26), 6258–6268.

(58) Ahmadi, Z.; Yunker, L. P. E.; Oliver, A. G.; McIndoe, J. S. Mechanistic Features of the Copper-Free Sonogashira Reaction from ESI-MS. *Dalt. Trans.* **2015**, *44* (47), 20367–20375.

(59) Guo, H.; Qian, R.; Liao, Y.; Ma, S.; Guo, Y. ESI-MS Studies on the Mechanism of Pd0-Catalyzed Three-Component Tandem Double Addition-Cyclization Reaction. *J. Am. Chem. Soc.* **2005**, *127* (37), 13060–13064.

(60) Wilson, S. R.; Wu, Y. A Study of Nickel-Catalyzed Coupling Reactions by

Electrospray Ionization Mass Spectrometry. *Organometallics* **1993**, *12* (4), 1478–1480.

(61) Bonchio, M.; Licini, G.; Modena, G.; Bortolini, O.; Moro, S.; Nugent, W. A. Enantioselective Ti(IV) Sulfoxidation Catalysts Bearing C3-Symmetric Trialkanolamine Ligands: Solution Speciation by 1H NMR and ESI-MS Analysis. *J. Am. Chem. Soc.* **1999**, *121* (26), 6258–6268.

(62) Aramendía, M. A.; Lafont, F.; Moreno-Manas, M.; Pleixats, R.; Roglans, A. Electrospray Ionization Mass Spectrometry Detection of Intermediates in the Palladium-Catalyzed Oxidative Self-Coupling of Areneboronic Acids. *J. Org. Chem.* **1999**, *64* (10), 3592–3594.

(63) Brown, J. M.; Hii, K. K. M. Characterization of Reactive Intermediates in Palladium-Catalyzed Arylation of Methyl Acrylate (Heck Reaction). *Angew. Chemie Int. Ed. English* **1996**, *35* (6), 657–659.

(64) Quirke, J. M. E.; Adams, C. L.; Van Berkel, G. J. Chemical Derivatization for Electrospray Ionization Mass Spectrometry. 1. Alkyl Halides, Alcohols, Phenols, Thiols, and Amines. *Anal. Chem.* **1994**, *66* (8), 1302–1315.

(65) Vikse, K.; Khairallah, G. N.; McIndoe, J. S.; O'Hair, R. a J. Fixed-Charge Phosphine Ligands to Explore Gas-Phase Coinage Metal-Mediated Decarboxylation Reactions. *Dalton Trans.* **2013**, *42* (18), 6440–6449.

(66) Vikse, K. L.; Henderson, M. a; Oliver, A. G.; McIndoe, J. S. Direct Observation of Key Intermediates by Negative-Ion Electrospray Ionisation Mass Spectrometry in Palladium-Catalysed Cross-Coupling. *Chem. Commun.* **2010**, *46* (39), 7412–7414.

(67) Schade, M. A.; Fleckenstein, J. E.; Knochel, P.; Koszinowski, K. Charged Tags as

Probes for Analyzing Organometallic Intermediates and Monitoring Cross-Coupling Reactions by Electrospray-Ionization Mass Spectrometry. *J. Org. Chem* **2010**, *75* (20), 6848–6857.

(68) Jackson, S. M.; Chisholm, D. M.; McIndoe, J. S.; Rosenberg, L. Using NMR and ESI-MS to Probe the Mechanism of Silane Dehydrocoupling Catalyzed by Wilkinson's Catalyst. *Eur. J. Inorg. Chem.* **2011**, *2011* (3), 327–330.

(69) Chisholm, D. M.; Oliver, A. G.; McIndoe, J. S. Mono-Alkylated Bisphosphines as Dopants for ESI-MS Analysis of Catalytic Reactions. *Dalt. Trans.* **2010**, *39* (2), 364–373.

(70) Farrer, N. J.; McDonald, R.; McIndoe, J. S. Proton Sponge Phosphines: Electrospray-Active Ligands. *Dalt. Trans.* **2006**, No. 38, 4570–4579.

(71) Kostas, I. D.; Coutsolelos, A. G.; Charalambidis, G.; Skondra, A. The First Use of Porphyrins as Catalysts in Cross-Coupling Reactions: A Water-Soluble Palladium Complex with a Porphyrin Ligand as an Efficient Catalyst Precursor for the Suzuki–Miyaura Reaction in Aqueous Media under Aerobic Conditions. *Tetrahedron Lett.* **2007**, *48* (38), 6688–6691.

(72) Li, Y.; Hong, X. M.; Collard, D. M.; El-Sayed, M. A. Suzuki Cross-Coupling Reactions Catalyzed by Palladium Nanoparticles in Aqueous Solution. *Org. Lett.* **2000**, *2* (15), 2385–2388.

(73) Sawoo, S.; Srimani, D.; Dutta, P.; Lahiri, R.; Sarkar, A. Size Controlled Synthesis of Pd Nanoparticles in Water and Their Catalytic Application in C-C Coupling Reactions. *Tetrahedron* **2009**, *65* (22), 4367–4374.

(74) Corma, A.; García, H.; Leyva, A. Comparison between Polyethylenglycol and

Imidazolium Ionic Liquids as Solvents for Developing a Homogeneous and Reusable Palladium Catalytic System for the Suzuki and Sonogashira Coupling. *Tetrahedron* **2005**, *61* (41), 9848–9854.

(75) Phan, N. T. S.; Van Der Sluys, M.; Jones, C. W. On the Nature of the Active Species in Palladium Catalyzed Mizoroki-Heck and Suzuki-Miyaura Couplings - Homogeneous or Heterogeneous Catalysis, a Critical Review. *Adv. Synth. Catal.* **2006**, *348* (6), 609–679.

(76) Roelfes, G.; Lubben, M.; Hage, R.; Que, L.; Feringa, B. Catalytic Oxidation with a Non-Heme Iron Complex That Generates a Low-Spin Fe(III)OOH Intermediate. *Chemistry* **2000**, *6* (12), 2152–2159.

(77) Owens, G. S.; Durazo, A.; Abu-Omar, M. M. Kinetics of MTO-Catalyzed Olefin Epoxidation in Ambient Temperature Ionic Liquids: UV/Vis and 2H NMR Study. *Chemistry* **2002**, *8* (13), 3053–3059.

(78) Bauer, M.; Kauf, T.; Christoffers, J.; Bertagnolli, H. Investigations into the Metal Species of the Homogeneous iron(III) Catalyzed Michael Addition Reactions. *Phys. Chem. Chem. Phys.* **2005**, *7* (13), 2664–2670.

(79) Liu, Y.; Khemtong, C.; Hu, J. Synthesis and Catalytic Activity of a poly(N,N-Dialkylcarbodiimide)/palladium Nanoparticle Composite: A Case in the Suzuki Coupling Reaction Using Microwave and Conventional Heating. *Chem. Commun. (Camb).* **2004**, No. 4, 398–399.

(80) Groothaert, M. H.; Lievens, K.; Leeman, H.; Weckhuysen, B. M.; Schoonheydt, R. A. An Operando Optical Fiber UV–vis Spectroscopic Study of the Catalytic Decomposition of NO and N2O over Cu-ZSM-5. *J. Catal.* **2003**, *220* (2), 500–512.

(81) Ohde, H.; Wai, C. M.; Kim, H.; Kim, J.; Ohde, M. Hydrogenation of Olefins in Supercritical CO2 Catalyzed by Palladium Nanoparticles in a Water-in-CO2 Microemulsion. *J. Am. Chem. Soc.* **2002**, *124* (17), 4540–4541.

(82) Fischer, C.; Beweries, T.; Preetz, A.; Drexler, H.-J.; Baumann, W.; Peitz, S.; Rosenthal, U.; Heller, D. Kinetic and Mechanistic Investigations in Homogeneous Catalysis Using Operando UV/vis Spectroscopy. *Catal. Today* **2010**, *155* (3–4), 282–288.

(83) Shi, H.; Lercher, J. A.; Yu, X.-Y. Sailing into Uncharted Waters: Recent Advances in the in Situ Monitoring of Catalytic Processes in Aqueous Environments. *Catal. Sci. Technol.* **2015**.

(84) Maxwell, E. J.; Chen, D. D. Y. Twenty Years of Interface Development for Capillary Electrophoresis-Electrospray Ionization-Mass Spectrometry. *Anal. Chim. Acta* **2008**, *627* (1), 25–33.

(85) Cech, N. B.; Enke, C. G. Practical Implications of Some Recent Studies in Electrospray Ionization Fundamentals. *Mass Spectrom. Rev.* **2002**, *20*, 362–387.

(86) Ho, C. S.; Lam, C. W. K.; Chan, M. H. M.; Cheung, R. C. K.; Law, L. K.; Lit, L. C. W.; Ng, K. F.; Suen, M. W. M.; Tai, H. L. Electrospray Ionisation Mass Spectrometry: Principles and Clinical Applications. *Clin. Biochem. Rev.* **2003**, *24* (1), 3–12.

(87) Huang, M.-Z.; Cheng, S.-C.; Cho, Y.-T.; Shiea, J. Ambient Ionization Mass Spectrometry: A Tutorial. *Anal. Chim. Acta* **2011**, *702* (1), 1–15.

(88) Li, J.; Taraszka, J. A.; Counterman, A. E.; Clemmer, D. E. Influence of Solvent Composition and Capillary Temperature on the Conformations of Electrosprayed

Ions: Unfolding of Compact Ubiquitin Conformers from Pseudonative and Denatured Solutions. *Int. J. Mass Spectrom.* **1999**, *185*, 37–47.

(89) Manisali, I.; Chen, D. D. Y.; Schneider, B. B. Electrospray Ionization Source Geometry for Mass Spectrometry: Past, Present, and Future. *TrAC Trends Anal. Chem.* **2006**, *25* (3), 243–256.

(90) Stahnke, H.; Kittlaus, S.; Kempe, G.; Hemmerling, C.; Alder, L. The Influence of Electrospray Ion Source Design on Matrix Effects. *J. Mass Spectrom.* **2012**, *47* (7), 875–884.

(91) Pape, J.; Vikse, K. L.; Janusson, E.; Taylor, N.; McIndoe, J. S. Solvent Effects on Surface Activity of Aggregate Ions in Electrospray Ionization. *Int. J. Mass Spectrom.* **2014**, *373*, 66–71.

(92) Konermann, L.; Ahadi, E.; Rodriguez, A. D.; Vahidi, S. Unraveling the Mechanism of Electrospray Ionization. *Anal. Chem.* **2013**, *85* (1), 2–9.

(93) Kebarle, P.; Verkerk, U. H. Electrospray: From Ions in Solution to Ions in the Gas Phase, What We Know Now. *Mass Spectrom. Rev.* **2009**, *28* (6), 898–917.

(94) Jorabchi, K.; Smith, L. M. Single Droplet Separations and Surface Partition Coefficient Measurements Using Laser Ablation Mass Spectrometry. *Anal. Chem.* **2009**, *81* (23), 9682–9688.

(95) Hallet, J. P.; Welton, T. Room-Temperature Ionic Liquids. Solvents for Synthesis and Catalysis. *Chem. Rev.* **2011**, *111* (5), 3508–3576.

(96) Ngo, H. L.; LeCompte, K.; Hargens, L.; McEwen, A. B. Thermal Properties of Imidazolium Ionic Liquids. *Thermochim. Acta* **2000**, *357–358*, 97–102.

(97) Henderson, M. a.; McIndoe, J. S. Ionic Liquids Enable Electrospray Ionisation

Mass Spectrometry in Hexane. *Chem. Commun.* **2006**, No. 27, 2872.

(98) Fei, Z.; Zhu, D.-R.; Yan, N.; Scopelliti, R.; Katsuba, S. A.; Laurenczy, G.; Chisholm, D. M.; McIndoe, J. S.; Seddon, K. R.; Dyson, P. J. Electrostatic and Non-Covalent Interactions in Dicationic Imidazolium-Sulfonium Salts with Mixed Anions. *Chemistry* **2014**, *20* (15), 4273–4283.

(99) Kim, I. D.; Rothschild, A.; Hyodo, T.; Tuller, H. L. Microsphere Templating as Means of Enhancing Surface Activity and Gas Sensitivity of CaCu 3Ti 4O 12 Thin Films. *Nano Lett.* **2006**, *6* (2), 193–198.

(100) McClements, D. J. Modulation of Globular Protein Functionality by Weakly Interacting Cosolvents. *Crit. Rev. Food Sci. Nutr.* **2002**, *42* (5), 417–471.

(101) Auzély, R.; Rinaudo, M. Controlled Chemical Modifications of Chitosan. Characterization and Investigation of Original Properties. In *Macromolecular Bioscience*; 2003; Vol. 3, pp 562–565.

(102) He, Q. T.; Li, X. P.; Chen, L. F.; Zhang, L.; Wang, W.; Su, C. Y. Nanosized Coordination Cages Incorporating Multiple Cu(I) Reactive Sites: Host-Guest Modulated Catalytic Activity. *ACS Catal.* **2013**, *3* (1), 1–9.

(103) Akiyoshi, K.; Deguchi, S.; Moriguchi, N.; Yamaguchi, S.; Sunamoto, J. Self-Aggregates of Hydrophobized Polysaccharides in Water. Formation and Characteristics of Nanoparticles. *Macromolecules* **1993**, *26* (12), 3062–3068.

(104) Capek, I. Preparation of Metal Nanoparticles in Water-in-Oil (W/o) Microemulsions. *Adv. Colloid Interface Sci.* **2004**, *110* (1–2), 49–74.

(105) Zhou, S.; Cook, K. D. A Mechanistic Study of Electrospray Mass Spectrometry: Charge Gradients within Electrospray Droplets and Their Influence on Ion

Response. *J. Am. Soc. Mass Spectrom.* **2001**, *12* (2), 206–214.

(106) Kebarle, P. A Brief Overview of the Present Status of the Mechanisms Involved in Electrospray Mass Spectrometry. *J. Mass Spectrom.* **2000**, *35*, 804–817.

(107) Kebarle, P.; Peschke, M. On the Mechanisms by Which the Charged Droplets Produced by Electrospray Lead to Gas Phase Ions. *Anal. Chim. Acta* **2000**, *406* (1), 11–35.

(108) Amad, M.H.; Cech, N.B.; Jackson, G. S. .; Enke, C. G. G.; Amad, M. H.; Cech, N. B.; Jackson, G. S.; Enke, C. G. G. Importance of Gas-Phase Proton Response, Affinities in Determining the ESI Mass, for Analytes and Solvents. *J. Spectrom.* **2000**, *35* (January), 784–789.

(109) Tang, S.; Babai, A.; Mudring, A. Europium-based Ionic Liquids as Luminescent Soft Materials. *Angew. Chemie Int. Ed.* **2008**, *47* (40), 7631–7634.

(110) Bruins, A. P. Mechanistic Aspects of Electrospray Ionization. *J. Chromatogr. A* **1998**, *794* (1–2), 345–357.

(111) Fyles, T. M.; Zeng, B. On the Assessment of Complex Cation-Crown Ether Equilibria by Electrospray Mass Spectrometry. *Supramol. Chem.* **1998**, *10* (1), 143–153.

(112) Greaves, T. L.; Drummond, C. J. Protic Ionic Liquids: Properties and Applications. *Chem. Rev.* **2008**, *108* (1), 206–237.

(113) Dyson, P. J.; Khalaila, I.; Luettgen, S.; McIndoe, J. S.; Zhao, D. Direct Probe Electrospray (and Nanospray) Ionization Mass Spectrometry of Neat Ionic Liquids. *Chem. Commun.* **2004**, No. 19, 2204–2205.

(114) Gozzo, F. C.; Santos, L. S.; Augusti, R.; Consorti, C. S.; Dupont, J.; Eberlin, M. N.

Gaseous Supramolecules of Imidazolium Ionic liquids:“Magic” Numbers and Intrinsic Strengths of Hydrogen Bonds. *Chem. Eur. J.* **2004**, *10* (23), 6187–6193.

(115) Bini, R.; Bortolini, O.; Chiappe, C.; Pieraccini, D.; Siciliano, T. Development of Cation/anion “interaction” Scales for Ionic Liquids through ESI-MS Measurements. *J. Phys. Chem. B* **2007**, *111* (3), 598–604.

(116) Fernandes, A. M.; Coutinho, J. A. P.; Marrucho, I. M. Gas-phase Dissociation of Ionic Liquid Aggregates Studied by Electrospray Ionisation Mass Spectrometry and Energy-variable Collision Induced Dissociation. *J. Mass Spectrom.* **2009**, *44* (1), 144–150.

(117) Chiappe, C.; Pieraccini, D. Ionic Liquids: Solvent Properties and Organic Reactivity. *J. Phys. Org. Chem.* **2005**, *18* (4), 275–297.

(118) Anderson, J. L.; Ding, J.; Welton, T.; Armstrong, D. W. Characterizing Ionic Liquids on the Basis of Multiple Solvation Interactions. *J. Am. Chem. Soc.* **2002**, *124* (47), 14247–14254.

(119) Greenwood, N. N.; Earnshaw, A. *Chemistry of the Elements (2nd Ed.)*; Butterworth-Heinemann: Oxford, 1997.

(120) Jenkins, H. D. B.; Thakur, K. P. Reappraisal of Thermochemical Radii for Complex Ions. *J. Chem. Educ.* **1979**, *56* (9), 576.

(121) Romero, C.; Baldelli, S. Sum Frequency Generation Study of the Room-Temperature Ionic Liquids/quartz Interface. *J. Phys. Chem. B* **2006**, *110* (12), 6213–6223.

(122) Tang, L.; Kebarle, P. Dependence of Ion Intensity in Electrospray Mass Spectrometry on the Concentration of the Analytes in the Electrosprayed Solution.

Anal. Chem. **1993**, *65* (24), 3654–3668.

(123) Marcus, Y. Gibbs Energies of Transfer of Anions from Water to Mixed Aqueous Organic Solvents. *Chem. Rev.* **2007**, *107* (9), 3880–3897.

(124) Frahm, J. L.; Muddiman, D. C.; Burke, M. J. Leveling Response Factors in the Electrospray Ionization Process Using a Heated Capillary Interface. *J. Am. Soc. Mass Spectrom.* **2005**, *16* (5), 772–778.

(125) Katritzky, A. R.; Fara, D. C.; Yang, H.; Tämm, K.; Tamm, T.; Karelson, M. Quantitative Measures of Solvent Polarity. *Chem. Rev.* **2004**, *104* (1), 175–198.

(126) Snyder, L. R. Classification off the Solvent Properties of Common Liquids. *J. Chromatogr. Sci.* **1978**, *16* (6), 223–234.

(127) Barton, A. F. M. *CRC Handbook of Polymer-Liquid Interaction Parameters and Solubility Parameters*; CRC press, 1990.

(128) Chandler, D. Interfaces and the Driving Force of Hydrophobic Assembly. *Nature* **2005**, *437* (7059), 640–647.

(129) Jacquemin, J.; Husson, P.; Padua, A. A. H.; Majer, V. Density and Viscosity of Several Pure and Water-Saturated Ionic Liquids. *Green Chem.* **2006**, *8* (2), 172–180.

(130) Micromass UK Limited. Q-Tof 2 User's Guide. Micromass UK Limited: Wythenshawe 2003, p 154.

(131) Parvin, L.; Galicia, M. C.; Gauntt, J. M.; Carney, L. M.; Nguyen, A. B.; Park, E.; Heffernan, L.; Vertes, A. Electrospray Diagnostics by Fourier Analysis of Current Oscillations and Fast Imaging. *Anal. Chem.* **2005**, *77* (13), 3908–3915.

(132) Jaworek, A.; Krupa, A. Studies of the Corona Discharge in Ehd Spraying. *J.*

Electrostat. **1997**, *40–41*, 173–178.

(133) Robb, D. B.; Covey, T. R.; Bruins, A. P. Atmospheric Pressure Photoionization: An Ionization Method for Liquid Chromatography− Mass Spectrometry. *Anal. Chem.* **2000**, *72* (15), 3653–3659.

(134) Zhu, H.; Janusson, E.; Luo, J.; Piers, J.; Islam, F.; McGarvey, G. B.; Oliver, A.; Granot, O.; McIndoe, J. S. Phenol-Selective Mass Spectrometric Analysis of Petroleum Fractions. *Analyst* **2017**.

(135) Hiraoka, K.; Murata, K.; Kudaka, I. Species-Selectivity Effects in the Production of Electrospray Ions. *Rapid Commun. Mass Spectrom.* **1993**, *7* (5), 363–373.

(136) Evans, D. J.; Hughes, D. L. Structure of Tetramethylammonium Bromide: A Redetermination. *Acta Crystallogr. Sect. C Cryst. Struct. Commun.* **1990**, *46* (8), 1452–1454.

(137) Cech, N. B.; Enke, C. G. Selectivity in Electrospray Ionization Mass Spectrometry. *Electrospray MALDI Mass Spectrom. Fundam. Instrumentation, Pract. Biol. Appl.* **2010**, 49–73.

(138) Quirke, J. M. E.; Hsu, Y.-L.; Van Berkel, G. J. Ferrocene-Based Electroactive Derivatizing Reagents for the Rapid Selective Screening of Alcohols and Phenols in Natural Product Mixtures Using Electrospray−Tandem Mass Spectrometry. *J. Nat. Prod.* **2000**, *63* (2), 230–237.

(139) Bruins, A. P.; Covey, T. R.; Henion, J. D. Ion Spray Interface for Combined Liquid Chromatography/atmospheric Pressure Ionization Mass Spectrometry. *Anal. Chem.* **1987**, *59* (22), 2642–2646.

(140) Page, J. S.; Kelly, R. T.; Tang, K.; Smith, R. D. Ionization and Transmission

Efficiency in an Electrospray Ionization-Mass Spectrometry Interface. *J. Am. Soc. Mass Spectrom.* **2007**, *18* (9), 1582–1590.

(141) Benkestock, K.; Sundqvist, G.; Edlund, P.-O.; Roeraade, J. Influence of Droplet Size, Capillary-Cone Distance and Selected Instrumental Parameters for the Analysis of Noncovalent Protein-Ligand Complexes by Nano-Electrospray Ionization Mass Spectrometry. *J. Mass Spectrom.* **2004**, *39* (9), 1059–1067.

(142) Tang, K.; Page, J. S.; Smith, R. D. Charge Competition and the Linear Dynamic Range of Detection in Electrospray Ionization Mass Spectrometry. *J. Am. Soc. Mass Spectrom.* **2004**, *15* (10), 1416–1423.

(143) Wang, R.; Zenobi, R. Evolution of the Solvent Polarity in an Electrospray Plume. *J. Am. Soc. Mass Spectrom.* **2010**, *21* (3), 378–385.

(144) Ikonomou, M.; Blades, A.; Kebarle, P. Investigations of the Electrospray Interface for Liquid Chromatography/mass Spectrometry. *Anal. Chem.* **1990**, 957–967.

(145) Cole, R. B.; Harrata, A. K. Solvent Effect on Analyte Charge State, Signal Intensity, and Stability in Negative Ion Electrospray Mass Spectrometry; Implications for the Mechanism of Negative Ion Formation. *J. Am. Soc. Mass Spectrom.* **1993**, *4* (7), 546–556.

(146) Enke, C. G. A Predictive Model for Matrix and Analyte Effects in Electrospray Ionization of Singly-Charged Ionic Analytes. *Anal. Chem.* **1997**, *69* (23), 4885–4893.

(147) Cech, N. B.; Enke, C. G. Relating Electrospray Ionization Response to Nonpolar Character of Small Peptides. *Anal. Chem.* **2000**, *72* (13), 2717–2723.

(148) Constantopoulos, T. L.; Jackson, G. S.; Enke, C. G. Effects of Salt Concentration

on Analyte Response Using Electrospray Ionization Mass Spectrometry. *J. Am. Soc. Mass Spectrom.* **1999**, *10* (7), 625–634.

(149) Loo, J. A. Electrospray Ionization Mass Spectrometry: A Technology for Studying Noncovalent Macromolecular Complexes. *Int. J. Mass Spectrom.* **2000**, *200* (1), 175–186.

(150) Murata, H.; Takao, T.; Shimonishi, Y.; Matsuo, T. Optimization of Skimmer Voltages of an Electrospray Ion Source Coupled with a Magnetic Sector Instrument. *Rapid Commun. Mass Spectrom.* **1994**, *8* (2), 205–210.

(151) Page, J. S.; Marginean, I.; Baker, E. S.; Kelly, R. T.; Tang, K.; Smith, R. D. Biases in Ion Transmission through an Electrospray Ionization-Mass Spectrometry Capillary Inlet. *J. Am. Soc. Mass Spectrom.* **2009**, *20* (12), 2265–2272.

(152) Chen, Y. H.; Hill Jr, H. H.; Wittmer, D. P. Thermal Effects on Electrospray Ionization Ion Mobility Spectrometry. *Int. J. Mass Spectrom. Ion Process.* **1996**, *154* (1), 1–13.

(153) Mirza, U. A.; Cohen, S. L.; Chait, B. T. Heat-Induced Conformational Changes in Proteins Studied by Electrospray Ionization Mass Spectrometry. *Anal. Chem.* **1993**, *65*, 1–6.

(154) Patiny, L.; Borel, A. ChemCalc: A Building Block for Tomorrow's Chemical Infrastructure. *J. Chem. Inf. Model.* **2013**, *53* (5), 1223–1228.

(155) Royal Dutch/Shell Group of Companies. *The Petroleum Handbook*, 6th ed.; Elsevier: Amsterdam, 1986.

(156) Ritter, S. K. Water For Oil. *Chem. Eng. News* **2011**, *89* (36), 56–59.

(157) El, M.; Arouri, H.; Rault, C. Oil Prices and Stock Markets in Gcc Countries :

Empirical Evidence From Panel Analysis. *Int. J. Financ. Econ.* **2012**, *253* (January 2011), 242–253.

(158) Birol, F. (IEA). *Medium-Term Oil Market Report 2016*; Paris, 2016.

(159) Muggeridge, A.; Cockin, A.; Webb, K.; Frampton, H.; Collins, I.; Moulds, T.; Salino, P. Recovery Rates, Enhanced Oil Recovery and Technological Limits. *Philos. Trans. A. Math. Phys. Eng. Sci.* **2014**, *372* (2006), 20120320.

(160) Pereira, J. F. B.; Gudiña, E. J.; Costa, R.; Vitorino, R.; Teixeira, J. A.; Coutinho, J. A. P.; Rodrigues, L. R. Optimization and Characterization of Biosurfactant Production by Bacillus Subtilis Isolates towards Microbial Enhanced Oil Recovery Applications. *Fuel* **2013**, *111*, 259–268.

(161) Lane, R. M.; Frampton, H.; Craddock, H. A.; Dunlop, J.; Reid, P.; Payne, G.; Balson, T. *Chemistry in the Oil Industry VII*; Special Publications; The Royal Society of Chemistry, 2002.

(162) Farouq Ali, S. M.; Thomas, S. A Realistic Look at Enhanced Oil Recovery. *Sci. Iran.* **1994**, *1* (3), 219–230.

(163) Oleen, D. C. Waterflood Process Using Organic Phosphate Esters. Google Patents November 25, 1969.

(164) Marshall, A. G.; Rodgers, R. P. Petroleomics: Chemistry of the Underworld. *Proc. Natl. Acad. Sci. U. S. A.* **2008**, *105* (47), 18090–18095.

(165) Müller, H.; Andersson, J. T.; Schrader, W. Characterization of High-Molecular-Weight Sulfur-Containing Aromatics in Vacuum Residues Using Fourier Transform Ion Cyclotron Resonance Mass Spectrometry. *Anal. Chem.* **2005**, *77* (8), 2536–2543.

(166) Nizio, K. D.; McGinitie, T. M.; Harynuk, J. J. Comprehensive Multidimensional Separations for the Analysis of Petroleum. *J. Chromatogr. A* **2012**, *1255*, 12–23.

(167) Harynuk, J. J.; Rossé, A. D.; McGarvey, G. B. Study of Alkyl Phosphates in Industrial Petroleum Mixtures by Comprehensive Two-Dimensional Gas Chromatography Time-of-Flight Mass Spectrometry. *Anal. Bioanal. Chem.* **2011**, *401* (8), 2415–2422.

(168) Oro, N. E.; Lucy, C. A. Analysis of the Nitrogen Content of Distillate Cut Gas Oils and Treated Heavy Gas Oils Using Normal Phase HPLC, Fraction Collection and Petroleomic FT-ICR MS Data. *Energy & Fuels* **2013**, *27* (1), 35–45.

(169) Frysinger, G. S.; Gaines, R. B. Comprehensive Two-Dimensional Gas Chromatography with Mass Spectrometric Detection (GC × GC/MS) Applied to the Analysis of Petroleum. *J. High Resolut. Chromatogr.* **1999**, *22* (5), 251–255.

(170) Liu, P.; Shi, Q.; Pan, N.; Zhang, Y.; Chung, K. H.; Zhao, S.; Xu, C. Distribution of Sulfides and Thiophenic Compounds in VGO Subfractions: Characterized by Positive-Ion Electrospray Fourier Transform Ion Cyclotron Resonance Mass Spectrometry. *Energy & Fuels* **2011**, *25* (7), 3014–3020.

(171) Focant, J.-F.; Sjödin, A.; Patterson, D. G. Improved Separation of the 209 Polychlorinated Biphenyl Congeners Using Comprehensive Two-Dimensional Gas Chromatography-Time-of-Flight Mass Spectrometry. *J. Chromatogr. A* **2004**, *1040* (2), 227–238.

(172) Marshall, A. G.; Rodgers, R. P. Petroleomics: The Next Grand Challenge for Chemical Analysis. *Acc. Chem. Res.* **2004**, *37* (1), 53–59.

(173) Ventura, G. T.; Raghuraman, B.; Nelson, R. K.; Mullins, O. C.; Reddy, C. M.

Compound Class Oil Fingerprinting Techniques Using Comprehensive Two-Dimensional Gas Chromatography (GC×GC). *Org. Geochem.* **2010**, *41* (9), 1026–1035.

(174) Korytár, P.; Haglund, P.; de Boer, J.; Brinkman, U. A. T. Comprehensive Two-Dimensional Gas Chromatography for the Analysis of Organohalogenated Micro-Contaminants. *TrAC Trends Anal. Chem.* **2006**, *25* (4), 373–396.

(175) Eckert, P. A.; Roach, P. J.; Laskin, A.; Laskin, J. Chemical Characterization of Crude Petroleum Using Nanospray Desorption Electrospray Ionization Coupled with High-Resolution Mass Spectrometry. *Anal. Chem.* **2012**, *84* (3), 1517–1525.

(176) Liu, P.; Shi, Q.; Chung, K. H.; Zhang, Y.; Pan, N.; Zhao, S.; Xu, C. Molecular Characterization of Sulfur Compounds in Venezuela Crude Oil and Its SARA Fractions by Electrospray Ionization Fourier Transform Ion Cyclotron Resonance Mass Spectrometry. *Energy & Fuels* **2010**, *24* (9), 5089–5096.

(177) Purcell, J. M.; Juyal, P.; Kim, D.-G.; Rodgers, R. P.; Hendrickson, C. L.; Marshall, A. G. Sulfur Speciation in Petroleum: Atmospheric Pressure Photoionization or Chemical Derivatization and Electrospray Ionization Fourier Transform Ion Cyclotron Resonance Mass Spectrometry. *Energy & Fuels* **2007**, *21* (5), 2869–2874.

(178) Purcell, J. M.; Hendrickson, C. L.; Rodgers, R. P.; Marshall, A. G. Atmospheric Pressure Photoionization Fourier Transform Ion Cyclotron Resonance Mass Spectrometry for Complex Mixture Analysis. *Anal. Chem.* **2006**, *78* (16), 5906–5912.

(179) Marotta, E.; Seraglia, R.; Fabris, F.; Traldi, P. Atmospheric Pressure

Photoionization Mechanisms: 1. The Case of Acetonitrile. *Int. J. Mass Spectrom.* **2003**, *228* (2–3), 841–849.

(180) Hesketh, A. V.; Nowicki, S.; Baxter, K.; Stoddard, R. L.; McIndoe, J. S. Simplified Real-Time Mass Spectrometric Analysis of Reactions. *Organometallics* **2015**, *34* (15), 3816–3819.

(181) Kleber, A. G.; Fast, V. Molecular and Cellular Aspects of Re-Entrant Arrhythmias. *Basic Res.Cardiol.* **1997**, *92 Suppl 1*, 111–119.

(182) Gilbert, H. F. *Advances in Enzymology and Related Areas of Molecular Biology, Volume 63*; John Wiley & Sons: Houston, 2009.

(183) Jeffries, T. *Organic Chemistry*; Cengage Learning, 1970; Vol. i.

(184) Taylor, P.; Bennett, B.; Jones, M.; Larter, S. The Effect of Biodegradation and Water Washing on the Occurrence of Alkylphenols in Crude Oils. *Org. Geochem.* **2001**, *32* (2), 341–358.

(185) Meredith, W.; Kelland, S.-J.; Jones, D. M. Influence of Biodegradation on Crude Oil Acidity and Carboxylic Acid Composition. *Org. Geochem.* **2000**, *31* (11), 1059–1073.

(186) Slavcheva, E.; Shone, B.; Turnbull, A. Review of Naphthenic Acid Corrosion in Oil Refining. *Br. Corros. J.* **1999**, *34* (2), 125–131.

(187) Clemente, J. S.; Fedorak, P. M. A Review of the Occurrence, Analyses, Toxicity, and Biodegradation of Naphthenic Acids. *Chemosphere* **2005**, *60* (5), 585–600.

(188) Kurti, L.; Czako, B. *Strategic Applications of Named Reactions in Organic Synthesis*, 1st ed.; Elsevier: Burlington, 2014.

(189) Liang, H. Diphenylphosphoryl Azide (DPPA) - A Reagent with Manifold

Applications. *Synlett* **2008**, *2008* (16), 2554–2555.

(190) Hamada, Y.; Shioiri, T. Recent Progress of the Synthetic Studies of Biologically Active Marine Cyclic Peptides and Depsipeptides. *Chem. Rev.* **2005**, *105* (12), 4441–4482.

(191) Shioiri, T.; Ninomiya, K.; Yamada, S. Diphenylphosphoryl Azide. New Convenient Reagent for a Modified Curtius Reaction and for Peptide Synthesis. *J. Amer. Chem. Soc.* **1972**, *94* (17), 6203–6205.

(192) Kiselev, V. D.; Malkov, V. B.; Murzin, D. G.; SHAKIROV, I. M.; KONOVALOV, A. I. THERMOCHEMICAL STUDY OF ISOCYANATE-AMINE REACTIONS. *Dokl. Akad. Nauk SSSR* **1989**, *308* (1), 111–113.

(193) Chen, X.; Shen, B.; Sun, J.; Wang, C.; Shan, H.; Yang, C.; Li, C. Characterization and Comparison of Nitrogen Compounds in Hydrotreated and Untreated Shale Oil by Electrospray Ionization (ESI) Fourier Transform Ion Cyclotron Resonance Mass Spectrometry (FT-ICR MS). *Energy & Fuels* **2012**, *26* (3), 1707–1714.

(194) Singh, D.; Chopra, A.; Patel, M. B.; Sarpal, A. S. A Comparative Evaluation of Nitrogen Compounds in Petroleum Distillates. *Chromatographia* **2011**, *74* (1–2), 121–126.

(195) Fahim, M. A.; Al-Sahhaf, T. A.; Elkilani, A. *Fundamentals of Petroleum Refining*, 1st ed.; Elsevier: Radarweg, 2010.

(196) Yamamoto, M.; Taguchi, K.; Sasaki, K. Basic Nitrogen Compounds in Bitumen and Crude Oils. *Chem. Geol.* **1991**, *93* (1–2), 193–206.

(197) Castejon, H.; Wiberg, K. B. Solvent Effects on Methyl Transfer Reactions. 1. The Menshutkin Reaction. *J. Am. Chem. Soc.* **1999**, *121* (10), 2139–2146.

(198) de Souza, R. M.; Saraceno, A. L.; da Silveira, C. L. P.; Aucélio, R. Q. Determination of Trace Elements in Crude Oil by ICP-OES Using Ultrasound-Assisted Acid Extraction. *J. Anal. At. Spectrom.* **2006**, *21* (11), 1345–1349.

(199) Duyck, C.; Miekeley, N.; Porto da Silveira, C. L.; Szatmari, P. Trace Element Determination in Crude Oil and Its Fractions by Inductively Coupled Plasma Mass Spectrometry Using Ultrasonic Nebulization of Toluene Solutions. *Spectrochim. Acta Part B At. Spectrosc.* **2002**, *57* (12), 1979–1990.

(200) Ricard, E.; Pécheyran, C.; Sanabria Ortega, G.; Prinzhofer, A.; Donard, O. F. X. Direct Analysis of Trace Elements in Crude Oils by High-Repetition-Rate Femtosecond Laser Ablation Coupled to ICPMS Detection. *Anal. Bioanal. Chem.* **2011**, *399* (6), 2153–2165.

(201) Wauquier, J.-P. *Petroleum Refining. Vol. 1 Crude Oil*; Editions OPHRYS, 1995.

(202) Alleman, T. L.; McCormick, R. L.; Yanowitz, J. Properties of Ethanol Fuel Blends Made with Natural Gasoline. *Energy & Fuels* **2015**, 150707142503002.

(203) Speight, J. G. *The Chemistry and Technology of Petroleum, Fifth Edition - CRC Press Book*; CRC Press, 2011.

(204) Rawson, P. M.; Stansfield, C.-A.; Webster, R. L.; Evans, D. Re-Addition of Antioxidant to Aged MEROX and Hydroprocessed Jet Fuels. *Fuel* **2015**, *139*, 652–658.

(205) Song, C. An Overview of New Approaches to Deep Desulfurization for Ultra-Clean Gasoline, Diesel Fuel and Jet Fuel. *Catal. Today* **2003**, *86* (1–4), 211–263.

(206) Gilbert, H. F. Molecular and Cellular Aspects of Thiol-Disulfide Exchange. *Adv. Enzymol. Relat. Areas Mol. Biol.* **1993**, *63*, 69.

(207) McMurry, J. Organic Chemistry 7th Ed. *Belmont, CA Thomson Brooks/Cole* **2008**.

(208) Black, S. P.; Sanders, J. K. M.; Stefankiewicz, A. R. Disulfide Exchange: Exposing Supramolecular Reactivity through Dynamic Covalent Chemistry. *Chem. Soc. Rev.* **2014**, *43* (6), 1861–1872.

(209) Otto, S. Dynamic Combinatorial Libraries of Macrocyclic Disulfides in Water. *J. Am. Chem. Soc.* **12AD**, *122* (48), 12063–12064.

(210) Javadli, R.; Klerk, A. Desulfurization of Heavy Oil. *Appl. Petrochemical Res.* **2012**, *1* (1), 3–19.

(211) Shaked, Z.; Szajewski, R. P.; Whitesides, G. M. Rates of Thiol-Disulfide Interchange Reactions Involving Proteins and Kinetic Measurements of Thiol pKa Values. *Biochemistry* **1980**, *19* (18), 4156–4166.

(212) Singh, R.; Whitesides, G. M. Thiol-Disulfide Interchange. *Chem. sulphur-containing Funct. groups. Chichester, Engl. John Wiley Sons* **1993**, 633–658.

(213) Johansson Seechurn, C. C. C.; Kitching, M. O.; Colacot, T. J.; Snieckus, V. Palladium-Catalyzed Cross-Coupling: A Historical Contextual Perspective to the 2010 Nobel Prize. *Angew. Chemie - Int. Ed.* **2012**, *51* (21), 5062–5085.

(214) Zalesskiy, S. S.; Ananikov, V. P. Pd2(dba)3 as a Precursor of Soluble Metal Complexes and Nanoparticles: Determination of Palladium Active Species for Catalysis and Synthesis. *Organometallics* **2012**, *31* (6), 2302–2309.

(215) Sawadjoon, S.; Orthaber, A.; Sjöberg, P. J. R.; Eriksson, L.; Samec, J. S. M. Equilibrium Study of Pd(dba)2 and P(OPh)3 in the Pd-Catalyzed Allylation of Aniline by Allyl Alcohol. *Organometallics* **2014**, *33* (1), 249–253.

(216) Carole, W. A.; Colacot, T. J. Understanding Palladium Acetate from a User

Perspective. *Chem. - A Eur. J.* **2016**, *22* (23), 7686–7695.

(217) Amatore, C.; Jutand, A. Role of Dba in the Reactivity of palladium(0) Complexes Generated in Situ from Mixtures of Pd(dba)2 and Phosphines. *Coord. Chem. Rev.* **1998**, *178–180*, 511–528.

(218) Amatore, C.; Jutand, A.; Thuilliez, A. Mechanism of the Oxidative Addition of Pd0 Complexes Generated from Pd0(dba)2 and a Phosphole Ligand DBP: A Special Case Where Dba Does Not Play Any Inhibiting Role. *J. Organomet. Chem.* **2002**, *643–644*, 416–423.

(219) Amatore, C.; Jutand, A.; Khalil, F.; M'Barki, M. A.; Mottier, L.; Mbarki, M. A.; Mottier, L. Rates and Mechanisms of Oxidative Addition to Zerovalent Palladium Complexes Generated in-Situ from Mixtures of Pd0(dba)2 and Triphenylphosphine. *Organometallics* **1993**, *12* (8), 3168–3178.

(220) Fairlamb, I. J. S.; Kapdi, A. R.; Lee, A. F.; Ian J. S. Fairlamb, *; Anant R. Kapdi, and; Lee, A. F.; Fairlamb, I. J. S.; Kapdi, A. R.; Lee, A. F. η2-Dba Complexes of Pd(0): The Substituent Effect in Suzuki−Miyaura Coupling. *Org. Lett.* **2004**, *6* (24), 4435–4438.

(221) Fairlamb, I. J. S. π-Acidic Alkene Ligand Effects in Pd-Catalysed Cross-Coupling Processes: Exploiting the Interaction of Dibenzylidene Acetone (Dba) and Related Ligands with Pd(0) and Pd(ii). *Org. Biomol. Chem.* **2008**, *6* (20), 3645–3656.

(222) Macé, Y.; Kapdi, A. R.; Fairlamb, I. J. S.; Jutand, A. Influence of the Dba Substitution on the Reactivity of palladium(0) Complexes Generated from Pd02(dba-N,n′ -Z) 3 or Pd0(dba-N,n′-Z)2 and PPha 3 in Oxidative Addition with Iodobenzene. *Organometallics* **2006**, *25* (7), 1795–1800.

(223) Fairlamb, I. J. S.; Kapdi, A. R.; Lee, A. F.; McGlacken, G. P.; Weissburger, F.; De Vries, A. H. M.; Schmieder-Van De Vondervoort, L. Exploiting Noninnocent (E,E)-Dibenzylideneacetone (Dba) Effects in palladium(0)-Mediated Cross-Coupling Reactions: Modulation of the Electronic Properties of Dba Affects Catalyst Activity and Stability in Ligand and Ligand-Free Reaction Systems. *Chem. - A Eur. J.* **2006**, *12* (34), 8750–8761.

(224) Fairlamb, I. J. S.; Lee, A. F. In-Silico Prediction of Pd-Catalyzed Cross-Coupling Processes: Dibenzylidene Acetone (Dba) Ligand Control. *Organometallics* **2007**, *26* (17), 4087–4089.

(225) de Meijere, A.; Meyer, F. E. Fine Feathers Make Fine Birds: The Heck Reaction in Modern Garb. *Angew. Chemie Int. Ed. English* **1995**, *33* (2324), 2379–2411.

(226) Littke, A. F.; Fu, G. C. Heck Reactions in the Presence of P(t-Bu)3: Expanded Scope and Milder Reaction Conditions for the Coupling of Aryl Chlorides. *J. Org. Chem.* **1999**, *64* (1), 10–11.

(227) Surry, D. S.; Buchwald, S. L. Dialkylbiaryl Phosphines in Pd-Catalyzed Amination : A User's Guide. *Chem. Sci.* **2011**, *2* (age 10), 27–50.

(228) Urgaonkar, S.; Verkade, J. G. Scope and Limitations of Pd2(dba)3/P(i-BuNCH2CH2)3N-Catalyzed Buchwald-Hartwig Amination Reactions of Aryl Chlorides. *J. Org. Chem.* **2004**, *69* (26), 9135–9142.

(229) Hartwig, J. F.; Kawatsura, M.; Hauck, S. I.; Shaughnessy, K. H.; Alcazar-Roman, L. M. Room-Temperature Palladium-Catalyzed Amination of Aryl Bromides and Chlorides and Extended Scope of Aromatic C-N Bond Formation with a Commercial Ligand. *J. Org. Chem.* **1999**, *64* (15), 5575–5580.

(230) Kirchhoff, J. H.; Dai, C.; Fu, G. C. A Method for Palladium-Catalyzed Cross-Couplings of Simple Alkyl Chlorides: Suzuki Reactions Catalyzed by [Pd2 (Dba) 3]/PCy3. *Angew. Chemie* **2002**, *114* (11), 2025–2027.

(231) Kawatsura, M.; Hartwig, J. F. Simple, Highly Active Palladium Catalysts for Ketone and Malonate Arylation: Dissecting the Importance of Chelation and Steric Hindrance. *J. Am. Chem. Soc.* **1999**, *121* (7), 1473–1478.

(232) Kapdi, A. R.; Whitwood, A. C.; Williamson, D. C.; Lynam, J. M.; Burns, M. J.; Williams, T. J.; Reay, A. J.; Holmes, J.; Fairlamb, I. J. S. The Elusive Structure of Pd2(dba)3. Examination by Isotopic Labeling, NMR Spectroscopy, and X-Ray Diffraction Analysis: Synthesis and Characterization of Pd2(dba-Z)3 Complexes. *J. Am. Chem. Soc.* **2013**, *135* (22), 8388–8399.

(233) Huang, D.; Poon, S. F.; Chapman, D. F.; Chung, J.; Cramer, M.; Reger, T. S.; Roppe, J. R.; Tehrani, L.; Cosford, N. D. P.; Smith, N. D. 2-(2-[3-(Pyridin-3-Yloxy)phenyl]-2H-Tetrazol-5-Yl) Pyridine: A Highly Potent, Orally Active, Metabotropic Glutamate Subtype 5 (mGlu5) Receptor Antagonist. *Bioorg. Med. Chem. Lett.* **2004**, *14* (22), 5473–5476.

(234) Isabel, E.; Aspiotis, R.; Black, W. C.; Colucci, J.; Fortin, R.; Giroux, A.; Grimm, E. L.; Han, Y.; Mellon, C.; Nicholson, D. W.; Rasper, D. M.; Renaud, J.; Roy, S.; Tam, J.; Tawa, P.; Vaillancourt, J. P.; Xanthoudakis, S.; Zamboni, R. J. Solid-Phase Analogue Synthesis of Caspase-3 Inhibitors via Palladium-Catalyzed Amination of 3-Bromopyrazinones. *Bioorg. Med. Chem. Lett.* **2007**, *17* (6), 1671–1674.

(235) Movassaghi, M.; Ondrus, A. E. Enantioselective Total Synthesis of Tricyclic

Myrmicarin Alkaloids. *Org. Lett.* **2005**, *7* (20), 4423–4426.

(236) Ganton, M. D.; Kerr, M. A. Aryl Amidation Routes to dihydropyrrolo[3,2-E]indoles and pyrrolo[3,2-F]tetrahydroquinolines: Total Synthesis of the (+/-)-CC-1065 CPI Subunit. *J. Org. Chem.* **2007**, *72* (2), 574–582.

(237) Yu, M.; Wang, M.; Chen, X.; Hong, B.; Zhang, X. Synthesis of OLED Materials of Several Triarylamines by Palladium Catalysts and Their Light Emitting Property. *J. Chem. Res.* **2005**, *2005* (9), 558–560.

(238) You, J.; Dou, L.; Yoshimura, K.; Kato, T.; Ohya, K.; Moriarty, T.; Emery, K.; Chen, C.-C.; Gao, J.; Li, G.; Yang, Y. A Polymer Tandem Solar Cell with 10.6% Power Conversion Efficiency. *Nat. Commun.* **2013**, *4*, 1446.

(239) Nguyen, T. L.; Choi, H.; Ko, S.-J.; Uddin, M. A.; Walker, B.; Yum, S.; Jeong, J.-E.; Yun, M. H.; Shin, T. J.; Hwang, S.; Kim, J. Y.; Woo, H. Y. Semi-Crystalline Photovoltaic Polymers with Efficiency Exceeding 9% in a ∼300 Nm Thick Conventional Single-Cell Device. *Energy Environ. Sci.* **2014**, *7* (9), 3040–3051.

(240) Amatore, C.; Broeker, G.; Jutand, A.; Khalil, F. Identification of the Effective palladium(0) Catalytic Species Generated in Situ from Mixtures of pd(dba)2 and Bidentate Phosphine Ligands. Determination of Their Rates and Mechanism in Oxidative Addition. *J. Am. Chem. Soc.* **1997**, *119* (22), 5176–5185.

(241) Melvin, P. R.; Balcells, D.; Hazari, N.; Nova, A. Understanding Precatalyst Activation in Cross-Coupling Reactions: Alcohol Facilitated Reduction from Pd(II) to Pd(0) in Precatalysts of the Type (??3-allyl)Pd(L)(Cl) and (??3-indenyl)Pd(L)(Cl). *ACS Catal.* **2015**, *5* (9), 5596–5606.

(242) Christensen, H.; Kiil, S.; Dam-Johansen, K.; Nielsen, O.; Sommer, M. B. Effect of

Solvents on the Product Distribution and Reaction Rate of a Buchwald-Hartwig Amination Reaction. *Org. Process Res. Dev.* **2006**, *10* (4), 762–769.

(243) Proutiere, F.; Schoenebeck, F. Solvent Effect on Palladium-Catalyzed Cross-Coupling Reactions and Implications on the Active Catalytic Species. *Angew. Chemie Int. Ed.* **2011**, *50* (35), 8192–8195.

(244) Sun, K.; Xiao, Z.; Lu, S.; Zajaczkowski, W.; Pisula, W.; Hanssen, E.; White, J. M.; Williamson, R. M.; Subbiah, J.; Ouyang, J.; Holmes, A. B.; Wong, W. W. H.; Jones, D. J. A Molecular Nematic Liquid Crystalline Material for High-Performance Organic Photovoltaics. *Nat. Commun.* **2015**, *6*, 6013.

(245) Kotecki, B. J.; Fernando, D. P.; Haight, A. R.; Lukin, K. A. A General Method for the Synthesis of Unsymmetrically Substituted Ureas via Palladium-Catalyzed Amidation. *Org. Lett.* **2009**, *11* (4), 947–950.

(246) Cropper, E. L.; Yuen, A. P.; Ford, A.; White, A. J. P.; (Mimi) Hii, K. K. Delineating Ligand Effects in Intramolecular Aryl Amidation Reactions: Formation of a Novel Spiro-Heterocycle by a Tandem Cyclisation Process. *Tetrahedron* **2009**, *65* (2), 525–530.

(247) Kuethe, J. T.; Childers, K. G.; Humphrey, G. R.; Journet, M.; Peng, Z. A Rapid, Large-Scale Synthesis of a Potent Cholecystokinin (CCK) 1R Receptor Agonist. *Org. Process Res. Dev.* **2008**, *12* (6), 1201–1208.

(248) Harding, B. A.; Melvin, P. R.; Dougherty, W.; Kassel, S.; Goodson, F. E. Capturing a Ghost. Synthesis and Structural Characterization of Pd(dba)[P(O - Tol) 3] 2. *Organometallics* **2013**, *32* (12), 3570–3573.

(249) Jana, R.; Pathak, T. P.; Sigman, M. S. Advances in Transition Metal (Pd,Ni,Fe)-

Catalyzed Cross-Coupling Reactions Using Alkyl-Organometallics as Reaction Partners. *Chem. Rev.* **2011**, *111* (3), 1417–1492.

(250) Shekhar, S.; Ryberg, P.; Hartwig, J. F.; Mathew, J. S.; Blackmond, D. G.; Strieter, E. R.; Buchwald, S. L. Reevaluation of the Mechanism of the Amination of Aryl Halides Catalyzed by BINAP-Ligated Palladium Complexes. *J. Am. Chem. Soc.* **2006**, *128* (11), 3584–3591.

(251) Kashin, A. S.; Ananikov, V. P. Catalytic C-C and C-Heteroatom Bond Formation Reactions: In Situ Generated or Preformed Catalysts? Complicated Mechanistic Picture behind Well-Known Experimental Procedures. *J. Org. Chem.* **2013**, *78* (22), 11117–11125.

(252) Milford, M. S. Waters 996 PDA Detector http://www.ecs.umass.edu/eve/facilities/equipment/Alliance/PDA 996 manual.pdf (accessed Mar 31, 2015).

(253) Pashynska, V. A.; Kosevich, M. V.; Van Den Heuvel, H.; Claeys, M. The Effect of Cone Voltage on Electrospray Mass Spectra of the Bisquaternary Ammonium Salt Decamethoxinum. *Rapid Commun. Mass Spectrom.* **2006**, *20* (5), 755–763.

(254) Barder, T. E.; Walker, S. D.; Martinelli, J. R.; Buchwald, S. L. Catalysts for Suzuki-Miyaura Coupling Processes: Scope and Studies of the Effect of Ligand Structure. *J. Am. Chem. Soc.* **2005**, *127* (13), 4685–4696.

(255) Barder, T. E.; Biscoe, M. R.; Buchwald, S. L. Structural Insights into Active Catalyst Structures and Oxidative Addition to (Biaryl)phosphine−Palladium Complexes via Density Functional Theory and Experimental Studies. *Organometallics* **2007**, *26* (9), 2183–2192.

(256) Barder, T. E.; Buchwald, S. L. Rationale behind the Resistance of Dialkylbiaryl Phosphines toward Oxidation by Molecular Oxygen. *J. Am. Chem. Soc.* **2007**, *129* (16), 5096–5101.

(257) Bruno, N. C.; Tudge, M. T.; Buchwald, S. L. Design and Preparation of New Palladium Precatalysts for C–C and C–N Cross-Coupling Reactions. *Chem. Sci.* **2013**, *4* (3), 916.

(258) Crabtree, R. H. Deactivation in Homogeneous Transition Metal Catalysis: Causes, Avoidance, and Cure. *Chem. Rev.* **2015**, *115* (1), 127–150.

(259) Buncel, E.; Symons, E. A. The Inherent Instability of Dimethylformamide–water Systems Containing Hydroxide Ion. *Chem. Commun.* **1970**, No. 3, 164–165.

(260) Szabó, P. T.; Kele, Z. Electrospray Mass Spectrometry of Hydrophobic Compounds Using Dimethyl Sulfoxide and Dimethylformamide as Solvents. *Rapid Commun. Mass Spectrom.* **2001**, *15* (24), 2415–2419.

(261) Striegel, A. M.; Piotrowiak, P.; Bou??, S. M.; Cole, R. B. Polarizability and Inductive Effect Contributions to Solvent-Cation Binding Observed in Electrospray Ionization Mass Spectrometry. *J. Am. Soc. Mass Spectrom.* **1999**, *10* (3), 254–260.

(262) Hu, G. Z.; Nitze, F.; Jia, X.; Sharifi, T.; Barzegar, H. R.; Gracia-Espino, E.; Wågberg, T. Reduction Free Room Temperature Synthesis of a Durable and Efficient Pd/ordered Mesoporous Carbon Composite Electrocatalyst for Alkaline Direct Alcohols Fuel Cell. *RSC Adv.* **2014**, *4* (2), 676–682.

(263) Barton, M. R.; Zhang, Y.; Atwood, J. D. Mono-Sulfonated Derivatives of Triphenylphosphine, [NH4]TPPMS and M(TPPMS)2 (TPPMS = P(Ph)2(m-

C6H4SO− 3); M = Mn2+, Fe2+, Co2+ and Ni2+). Crystal Structure Determinations for [NH4][TPPMS]·½H2O, [Fe(H2O)5(TPPMS)]TPPMS, [Co(H2O)5TPPMS]TPPMS and [Ni(H2O)6](T. *J. Coord. Chem.* **2002**, *55* (8), 969–983.

(264) Bentrup, U. Combining in Situ Characterization Methods in One Set-up: Looking with More Eyes into the Intricate Chemistry of the Synthesis and Working of Heterogeneous Catalysts. *Chem. Soc. Rev.* **2010**, *39* (12), 4718–4730.

(265) Tromp, M.; Sietsma, J. R. A.; van Bokhoven, J. A.; van Strijdonck, G. P. F.; van Haaren, R. J.; van der Eerden, A. M. J.; van Leeuwen, P. W. N. M.; Koningsberger, D. C. Deactivation Processes of Homogeneous Pd Catalysts Using in Situ Time Resolved Spectroscopic Techniques. *Chem. Commun.* **2003**, No. 1, 128–129.

(266) Bauer, M.; Heusel, G.; Mangold, S.; Bertagnolli, H. Spectroscopic Set-up for Simultaneous UV-Vis/(Q) EXAFS in Situ and in Operando Studies of Homogeneous Reactions under Laboratory Conditions. *J. Synchrotron Radiat.* **2010**, *17* (2), 273–279.

(267) O'Brien, M. G.; Beale, A. M.; Jacques, S. D. M.; Weckhuysen, B. M. A Combined Multi-Technique in Situ Approach Used to Probe the Stability of Iron Molybdate Catalysts during Redox Cycling. *Top. Catal.* **2009**, *52* (10), 1400–1409.

(268) Hunger, M. In Situ Flow MAS NMR Spectroscopy: State of the Art and Applications in Heterogeneous Catalysis. *Prog. Nucl. Magn. Reson. Spectrosc.* **2008**, *53* (3), 105–127.

(269) Hunger, M.; Wang, W. Formation of Cyclic Compounds and Carbenium Ions by

Conversion of Methanol on Weakly Dealuminated Zeolite H-ZSM-5 Investigated via a Novel in Situ CF MAS NMR/UV-Vis Technique. *Chem. Commun. (Camb).* **2004**, *5* (5), 584–585.

(270) Bruckner, A. Simultaneous Combination of in Situ-EPR/UV-VIS/on Line GC: A Novel Setup for Investigating Transition Metal Oxide Catalysts under Working Conditions. *Chem. Commun.* **2001**, No. 20, 2122–2123.

(271) Nijhuis, T. A.; Tinnemans, S. J.; Visser, T.; Weckhuysen, B. M. Towards Real-Time Spectroscopic Process Control for the Dehydrogenation of Propane over Supported Chromium Oxide Catalysts. *Chem. Eng. Sci.* **2004**, *59* (22–23), 5487–5492.

(272) McNaught, A. D.; Wilkinson, A. *IUPAC Compendium of Chemical Terminology: Gold Book*; 2014.

(273) Sherwood, C. A.; Eastham, A.; Lee, L. W.; Risler, J.; Mirzaei, H.; Falkner, J. A.; Martin, D. B. Rapid Optimization of MRM-MS Instrument Parameters by Subtle Alteration of Precursor and Product M/z Targets. *J. Proteome Res.* **2009**, *8* (7), 3746–3751.

(274) Anderson, L.; Hunter, C. L. Quantitative Mass Spectrometric Multiple Reaction Monitoring Assays for Major Plasma Proteins. *Mol. Cell. Proteomics* **2006**, *5* (4), 573–588.

(275) MacLean, B.; Tomazela, D. M.; Abbatiello, S. E.; Zhang, S.; Whiteaker, J. R.; Paulovich, A. G.; Carr, S. A.; MacCoss, M. J. Effect of Collision Energy Optimization on the Measurement of Peptides by Selected Reaction Monitoring (SRM) Mass Spectrometry. *Anal. Chem.* **2010**, *82* (24), 10116–10124.

(276) Liesener, A.; Karst, U. Monitoring Enzymatic Conversions by Mass Spectrometry: A Critical Review. *Anal. Bioanal. Chem.* **2005**, *382* (7), 1451–1464.

(277) Norris, A. J.; Whitelegge, J. P.; Faull, K. F.; Toyokuni, T. Analysis of Enzyme Kinetics Using Electrospray Ionization Mass Spectrometry and Multiple Reaction Monitoring: Fucosyltransferase V. *Biochemistry* **2001**, *40* (13), 3774–3779.

(278) Yamamoto, A.; Nishimura, Y.; Nishihara, Y. *Applied Cross-Coupling Reactions*; Lecture Notes in Chemistry; Springer Berlin Heidelberg: Berlin, Heidelberg, 2013; Vol. 80.

(279) Klapars, A.; Antilla, J. C.; Huang, X.; Buchwald, S. L. A General and Efficient Copper Catalyst for the Amidation of Aryl Halides and the N -Arylation of Nitrogen Heterocycles. *J. Am. Chem. Soc.* **2001**, *123* (31), 7727–7729.

(280) Frauenlob, R.; García, C.; Bradshaw, G. A.; Burke, H. M.; Bergin, E. A Copper-Catalyzed Petasis Reaction for the Synthesis of Tertiary Amines and Amino Esters. *J. Org. Chem.* **2012**, *77* (9), 4445–4449.

(281) Hartwig, J. F. Evolution of a Fourth Generation Catalyst for the Amination and Thioetherification of Aryl Halides. *Acc. Chem. Res.* **2008**, *41* (11), 1534–1544.

(282) Guram, A. S.; Rennels, R. A.; Buchwald, S. L. A Simple Catalytic Method for the Conversion of Aryl Bromides to Arylamines. *Angew. Chemie - Int. Ed.* **1995**, *34* (12), 1348–1350.

(283) Louie, J.; Hartwig, J. F. Palladium-Catalyzed Synthesis of Arylamines from Aryl Halides. Mechanistic Studies Lead to Coupling in the Absence of Tin Reagents. *Tetrahedron Lett.* **1995**, *36* (21), 3609–3612.

(284) Paul, F.; Patt, J.; Hartwig, J. F. Palladium-Catalyzed Formation of Carbon-

Nitrogen Bonds. Reaction Intermediates and Catalyst Improvements in the Hetero Cross-Coupling of Aryl Halides and Tin Amides. *J. Am. Chem. Soc.* **1994**, *116* (14), 5969–5970.

(285) Ikawa, T.; Barder, T. E.; Biscoe, M. R.; Buchwald, S. L. Pd-Catalyzed Amidations of Aryl Chlorides Using Monodentate Biaryl Phosphine Ligands: A Kinetic, Computational, and Synthetic Investigation. *J. Am. Chem. Soc.* **2007**, *129* (43), 13001–13007.

(286) Surry, D. S.; Buchwald, S. L. Biaryl Phosphane Ligands in Palladium-Catalyzed Amination. *Angew. Chemie - Int. Ed.* **2008**, *47* (34), 6338–6361.

(287) Hartwig, J. F.; Richards, S.; Baranano, D.; Paul, F. Influences on the Relative Rates for C-N Bond-Forming Reductive Elimination and ??-Hydrogen Elimination of Amides. A Case Study on the Origins of Competing Reduction in the Palladium-Catalyzed Amination of Aryl Halides. *J. Am. Chem. Soc.* **1996**, *118* (15), 3626–3633.

(288) Harrowven, D. C. Handbook of Organopalladium Chemistry for Organic Synthesis. In *Synthesis*; John Wiley & Sons, Inc., 2003; Vol. 2003, pp 632–632.

(289) Singh, U. K.; Strieter, E. R.; Blackmond, D. G.; Buchwald, S. L. Mechanistic Insights into the Pd(BINAP)-Catalyzed Amination of Aryl Bromides: Kinetic Studies under Synthetically Relevant Conditions. *J. Am. Chem. Soc.* **2002**, *124* (47), 14104–14114.

(290) Alcazar-Roman, L. M.; Hartwig, J. F. Mechanistic Studies on Oxidative Addition of Aryl Halides and Triflates to Pd(BINAP)2 and Structural Characterization of the Product from Aryl Triflate Addition in the Presence of Amine.

Organometallics **2002**, *21* (3), 491–502.

(291) Borjian, S.; Tom, D. M. E.; Baird, M. C. Pd(η3-1-PhC3H4)(η5- C5H5) as a Catalyst Precursor for Buchwald-Hartwig Amination Reactions. *Organometallics* **2014**, *33* (15), 3928–3935.

(292) Dieck, H. A.; Heck, F. R. Palladium Catalyzed Synthesis of Aryl, Heterocyclic and Vinylic Acetylene Derivatives. *J. Organomet. Chem.* **1975**, *93* (2), 259–263.

(293) Cassar, L. Synthesis of Aryl- and Vinyl-Substituted Acetylene Derivatives by the Use of Nickel and Palladium Complexes. *J. Organomet. Chem.* **1975**, *93* (2), 253–257.

(294) Sonogashira, K.; Tohda, Y.; Hagihara, N. A Convenient Synthesis of Acetylenes: Catalytic Substitutions of Acetylenic Hydrogen with Bromoalkenes, Iodoarenes and Bromopyridines. *Tetrahedron Lett.* **1975**, *16* (50), 4467–4470.

(295) Chinchilla, R.; Naera, C. Chemicals from Alkynes with Palladium Catalysts. *Chem. Rev.* **2014**, *114* (3), 1783−1826.

(296) Chinchilla, R.; Najera, C. Recent Advances in Sonogashira Reactions. *Chem. Soc. Rev.* **2011**, *40* (10), 5084–5121.

(297) Karak, M.; Barbosa, L. C. A.; Hargaden, G. C. Recent Mechanistic Developments and next Generation Catalysts for the Sonogashira Coupling Reaction. *RSC Adv.* **2014**, *4* (96), 53442–53466.

(298) Amatore, C.; Bensalem, S.; Ghalem, S.; Jutand, A. Mechanism of the Carbopalladation of Alkynes by Aryl-Palladium Complexes. *J. Organomet. Chem.* **2004**, *689* (24), 4642–4646.

(299) Soheili, A.; Albaneze-Walker, J.; Murry, J. A.; Dormer, P. G.; Hughes, D. L.

Efficient and General Protocol for the Copper-Free Sonogashira Coupling of Aryl Bromides at Room Temperature. *Org. Lett.* **2003**, *5* (22), 4191–4194.

(300) Ljungdahl, T.; Bennur, T.; Dallas, A.; Emtenäs, H.; Mårtensson, J. Two Competing Mechanisms for the Copper-Free Sonogashira Cross-Coupling Reaction. *Organometallics* **2008**, *27* (11), 2490–2498.

(301) Ljungdahl, T.; Pettersson, K.; Albinsson, B.; Mårtensson, J. Solvent and Base Dependence of Copper-Free Palladium-Catalyzed Cross-Couplings between Terminal Alkynes and Arylic Iodides: Development of Efficient Conditions for the Construction of Gold(III)/Free-Base Porphyrin Dimers. *J. Org. Chem.* **2006**, *71* (4), 1677–1687.

(302) García-Melchor, M.; Pacheco, M. C.; Naera, C.; Lledo, A.; Ujaque, G. Mechanistic Exploration of the Pd-Catalyzed Copper-Free Sonogashira Reaction. *ACS Catal.* **2012**, *2* (1), 135–144.

(303) Plenio, H.; Immel, S.; Burello, E.; Rothenberg, G.; Hoefsloot, H. C. J. Insights into Sonogashira Cross-Coupling by High-Throughput Kinetics and Descriptor Modeling. *Chem. Eur. J.* **2008**, *14* (9), 2857–2866.

(304) Jutand, A.; Négri, S.; Principaud, A. Formation of ArPdXL(amine) Complexes by Substitution of One Phosphane Ligand by an Amine in Trans-ArPdX(PPh3)2 Complexes. *Eur. J. Inorg. Chem.* **2005**, *2005* (4), 631–635.

(305) Tougerti, A.; Negri, S.; Jutand, A. Mechanism of the Copper-Free Palladium-Catalyzed Sonagashira Reactions: Multiple Role of Amines. *Chem. – A Eur. J.* **2007**, *13* (2), 666–676.

(306) Nguyen, P. Real-Time Analysis of Catalytic Reactions Using UV/Vis + ESI-MS,

University of Victoria, 2017.

(307) Strelnikova, E. B.; Serebrennikova, O. V. Ketones of Western Siberian Jurassic Oils. *Pet. Chem.* **2011**, *51* (4), 264–269.

(308) Wilkes, H.; Disko, U.; Willsch, H. *Characterization of Polycyclic Aromatic Hydrocarbons in Geological Samples by Charge-Transfer Liquid Chromatography Atmospheric Pressure Chemical Ionization Mass Spectrometry.*; AMER CHEMICAL SOC 1155 16TH ST, NW, WASHINGTON, DC 20036 USA, 1998; Vol. 215.

(309) Silva, S. L.; Silva, A. M. S.; Ribeiro, J. C.; Martins, F. G.; Da Silva, F. A.; Silva, C. M. Chromatographic and Spectroscopic Analysis of Heavy Crude Oil Mixtures with Emphasis in Nuclear Magnetic Resonance Spectroscopy: A Review. *Anal. Chim. Acta* **2011**, *707* (1–2), 18–37.

(310) Fahim, M. A.; Al-Sahhaf, T. A.; Elkilani, A. *Fundamentals of Petroleum Refining*; Elsevier: Amsterdam, 2009.

(311) Lazny, R.; Nodzewska, A. N, N-Dialkylhydrazones in Organic Synthesis. From Simple N, N-Dimethylhydrazones to Supported Chiral Auxiliaries. *Chem. Rev.* **2010**, *110* (3), 1386–1434.

(312) Peters, R.; Enders, D.; Job, A.; Janeck, C. F.; Bettray, W. The SAMP- / RAMP-Hydrazone Methodology in Asymmetric Synthesis. *Tetrahedron* **2002**, *58* (601), 2253–2329.

(313) Clayden, J.; Greeves, N.; Warren, S.; Wothers, P.; ed., 1st. *Organic Chemistry*; Oxford University Press: United Kingdom, 2001.

(314) Davis, M. Guitar Strings as Standing Waves: A Demonstration. *J. Chem. Educ.*

2007, *84* (8), 1287.

(315) Yamana, S. Observation of Stationary Waves. *J. Chem. Educ.* **1967**, *44* (5), A465.

(316) Chakraborty, M.; Mukhopadhyay, S.; Das, R. S. A Simple Demonstration of Atomic and Molecular Orbitals Using Circular Magnets. *J. Chem. Educ.* **2014**, *91* (9), 1505–1507.

(317) Lambert, F. L. Atomic and Molecular Orbital Models. *J. Chem. Educ.* **1957**, *34* (5), 217.

(318) Ogryzlo, E. A.; Porter, G. B. Contour Surfaces for Atomic and Molecular Orbitals. *J. Chem. Educ.* **1963**, *40* (5), 256.

(319) Emerson, D. W. A Colorful Demonstration To Simulate Orbital Hybridization. **1988**.

(320) Winter, M. The Orbitron: a gallery of atomic orbitals and molecular orbitals https://winter.group.shef.ac.uk/orbitron/AOs/2s/index.html (accessed Jun 23, 2016).

(321) Hoogenboom, B. E. Three-Dimensional Models of Atomic Orbitals. *J. Chem. Educ.* **1962**, *39* (1), 40.

(322) Kiefer, E. F. An Attention-Getting Model for Atomic Orbitals. *J. Chem. Educ.* **1995**, *72* (6), 500.

(323) Aristov, N.; Habekost, A. Chemische Untersuchungen Mit Mitteln Der Akustik - Einsatz Im Chemieunterricht. *CHEMKON* **2012**, *19* (3), 123–130.

(324) Wiener, O. *Stehende Lichtwellen Und Die Schwingungsrichtung Polarisierten Lichtes*; 1890.

(325) Myoungsik, C. Demonstration of Standing Light Wave with a Laser Pointer. *J.*

Korean Phys. Soc. **2010**, *56* (5), 1542.

(326) Tully, S. P.; Stitt, T. M.; Caldwell, R. D.; Hardock, B. J.; Hanson, R. M.; Maslak, P. Interactive Web-Based Pointillist Visualization of Hydrogenic Orbitals Using Jmol. *J. Chem. Educ.* **2013**, *90* (1), 129–131.

(327) Liebl, M. Orbital Plots of the Hydrogen Atom. *J. Chem. Educ.* **1988**, *65* (1), 23.

(328) Kijewski, L. Graphing Orbitals in Three Dimensions with Rotatable Density Plots. *J. Chem. Educ.* **2007**, *84* (11), 1887.

(329) Esselman, B. J.; Hill, N. J. Integration of Computational Chemistry into the Undergraduate Organic Chemistry Laboratory Curriculum. *J. Chem. Educ.* **2016**, *75* (2), 241.

(330) Douglas, J. E. Visualization of Electron Clouds in Atoms and Molecules. *J. Chem. Educ.* **1990**, *67* (1), 42.

(331) Ramachandran, B.; Kong, P. C. Three-Dimensional Graphical Visualization of One-Electron Atomic Orbitals. *J. Chem. Educ.* **1995**, *72* (5), 406.

(332) Johnson, J. L. Visualization of Wavefunctions of the Ionized Hydrogen Molecule. *J. Chem. Educ.* **2004**, *81* (10), 1535.

(333) Rhile, I. J. Comment On "visualizing Three-Dimensional Hybrid Atomic Orbitals Using Winplot: An Application for Student Self Instruction." *J. Chem. Educ.* **2015**, *92* (12), 1973–1974.

(334) Preece, D.; Williams, S. B.; Lam, R.; Weller, R. "Let's Get Physical": Advantages of a Physical Model over 3D Computer Models and Textbooks in Learning Imaging Anatomy. *Anat. Sci. Educ.* **2013**, *6* (4), 216–224.

(335) Dori, Y. J.; Barak, M. Virtual and Physical Molecular Modeling: Fostering Model

Perception and Spatial Understanding. *Educ. Technol. Soc.* **2001**, *4* (1), 61–74.

(336) McQuarrie, D. A. *Quantum Chemistry*; University Science Bks; University Science Books, 1983.

(337) Jayatilaka, D. Atomic Orbitals and Chladni Figures http://dylan-jayatilaka.net/articles/atomic-orbitals-and-chladni-figures/.

(338) Berry, R. S. *Understanding Energy: Energy, Entropy and Thermodynamics for Everyman*; World Scientific: Singapore, 1991.

(339) de Silva, C. W. *Vibration: Fundamentals and Practice, Second Edition*; Taylor & Francis, 2006.

(340) Stanford, N. J. CYMATICS: Science Vs. Music - Nigel Stanford https://www.youtube.com/watch?v=Q3oItpVa9fs (accessed Jun 28, 2016).

(341) Heller, E. J. *Why You Hear What You Hear: An Experiential Approach to Sound, Music, and Psychoacoustics*; Princeton University Press, 2013.

(342) Mason, F. P.; Richardson, R. W. Why Doesn't the Electron Fall into the Nucleus? *J. Chem. Educ.* **1983**, *60* (1), 40.

(343) Engel, T.; Hehre, W. J. *Quantum Chemistry and Spectroscopy*, 2nd ed.; Prentice Hall, 2010.

(344) Dzhamay, A. Partial Differential Equations Higher-dimensional PDE: Vibrating rectangular membranes and nodes http://www.maplesoft.com/applications/view.aspx?SID=4518&view=html&L=F (accessed Jun 28, 2016).

(345) Etzkorn, J. M.; Davey, N. G.; Thompson, A. J.; Creba, A. S.; Leblanc, C. W.; Simpson, C. D.; Krogh, E. T.; Gill, C. G. The Use of MIMS-MS-MS in Field

Locations as an on-Line Quantitative Environmental Monitoring Technique for Trace Contaminants in Air and Water. *J. Chromatogr. Sci.* **2009**, *47* (1), 57–66.

Appendix A
Solvent Effects on Surface Activity of Aggregate Ions in Electrospray Ionization

Section A1. BMIM Aggregate Response Ratio in the Positive Ion Mode

Table 8. Response Ratio of $[(BMIM)_2 + anion]^+$ aggregates in various solvents.

a)

Cl^- vs:	**1:1 H_2O: MeCN**	**MeOH**	**MeCN**	**CH_2Cl_2**
I^-	0.14	3.5	1.8	5.4
$[BF_4]^-$	1.5	0.17	0.75	1.5
$[PF_6]^-$	0.049	0.026	0.74	3.9
$[NTf_2]^-$	0.021	0.0069	0.15	19

b)

I^- vs:	**1:1 H_2O: MeCN**	**MeOH**	**MeCN**	**CH_2Cl_2**
Cl^-	7.2	0.28	0.55	0.19
$[BF_4]^-$	0.41	0.69	0.88	0.92
$[PF_6]^-$	0.061	0.023	1.6	1.4
$[NTf_2]^-$	0.025	0.018	1.2	2.6

c)

$[BF_4]^-$ vs:	**1:1 H_2O: MeCN**	**MeOH**	**MeCN**	**CH_2Cl_2**
Cl^-	0.66	6.0	1.3	0.66
I^-	2.4	1.5	1.1	1.1
$[PF_6]^-$	0.040	0.14	0.34	1.1
$[NTf_2]^-$	0.051	0.040	0.88	3.0

d)

$[PF_6]^-$ vs:	**1:1 H_2O: MeCN**	**MeOH**	**MeCN**	**CH_2Cl_2**
Cl^-	21	39	1.4	0.25
I^-	16	44	0.62	0.70
$[BF_4]^-$	25	7.1	3.0	0.89
$[NTf_2]^-$	0.41	0.37	1.3	0.96

e)

$[NTf_2]^-$ vs:	**1:1 H_2O:MeCN**	**MeOH**	**MeCN**	**CH_2Cl_2**
Cl^-	47	150	0.52	0.16
I^-	40	56	0.81	0.39

$[BF_4]^-$	20	25	1.1	0.34
$[PF_6]^-$	2.4	2.7	0.80	1.0

Section A2. [BMIM]I and [BMIM][NTf_2] Pairs in the Negative Ion Mode

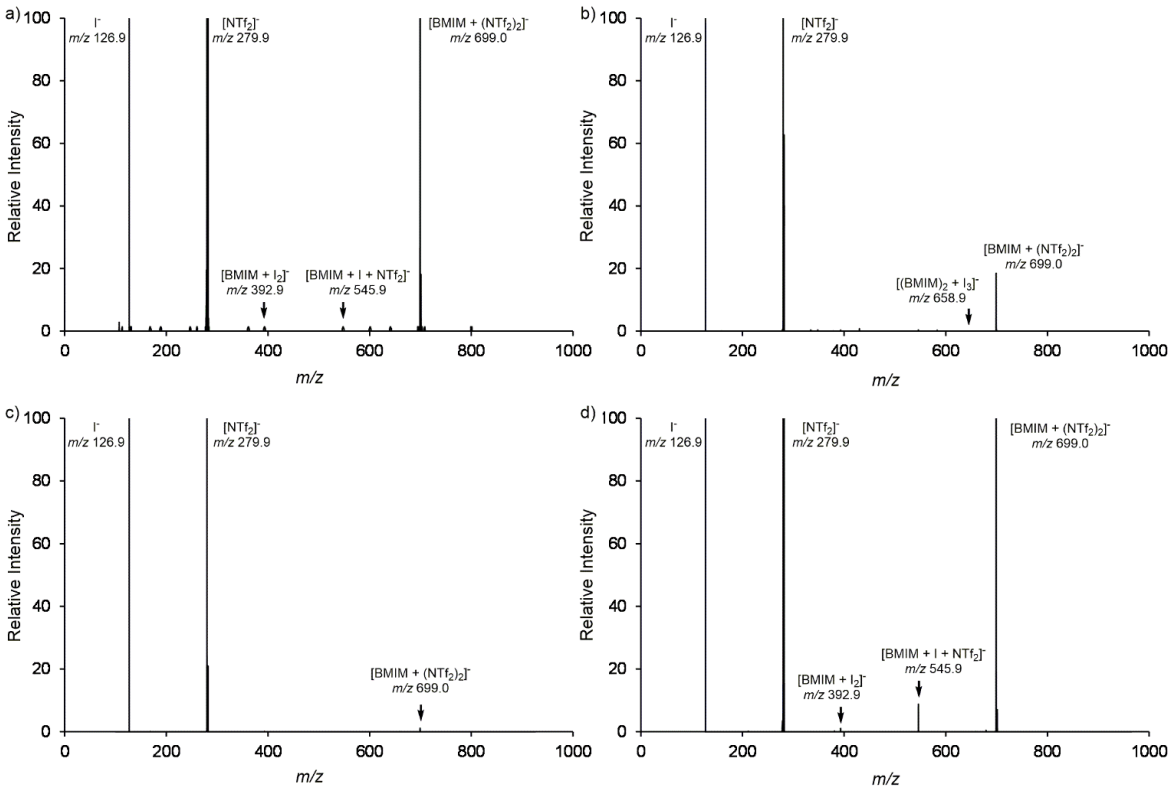

Figure 86. Negative Ion Mode ESI mass spectrum of equimolar [BMIM]I and [BMIM][NTf_2], showing the iodide-normalized intensities of free iodide (*m/z* 126.9), NTf_2^- (*m/z* 279.9), $[(BMIM) + I_2]^-$ (*m/z 392.9*), $[(BMIM) + I + NTf_2]^-$ (*m/z 545.9*), $[(BMIM)_2 + I_3)]^-$ (*m/z* 658.9), and $[BMIM + (NTf_2)_2]^-$ (*m/z* 699.0) in a) 1:1 H_2O:MeCN, b) MeOH, c) MeCN, d) CH_2Cl_2.

Table 9. Relative Ion Pair Intensities.

I^- vs:	**1:1 H_2O:MeCN**	**MeOH**	**MeCN**	**CH_2Cl_2**
I-	72	18178	88384	3225
NTf_2^-	0.0005	0.02	0.2	0.005
$[(BMIM) + I_2]^-$	-	350	775	-
$[(BMIM) + I + NTf_2]^-$	-	280	-	-

[BMIM + $(NTf_2)_2$]$^-$	0.07	5	90	0.07
[$(BMIM)_2$ + I_3)]$^-$	-	3640	2000	1600

Appendix B
Spatial Effects on Electrospray Ionization Response

Table 10. Experiment Parameters

Experiment #	Cone Gas / $L \cdot hr^{-1}$	Desolvation Gas / $L \cdot hr^{-1}$	Source Temperature /°C	Desolvation Temperature /°C	PPN and TMA Concentration / mM	Solvent
1	0	100	89	189	0.260	MeCN
2	100	100	89	189	0.260	MeCN
3	50	100	89	189	0.260	MeCN
4	100	100	89	189	0.0260	MeCN
5	100	100	68	168	0.0260	MeOH
6	100	50	89	189	0.0260	MeCN
7	100	200	89	189	0.0260	MeCN
8	100	25	89	189	0.0260	MeCN
9	100	0	89	189	0.0260	MeCN
10	100	100	39	189	0.0260	MeCN
11	100	100	100	200	0.0260	H_2O
12	100	100	89	89	0.0260	MeCN
13	100	100	150	189	0.0260	MeCN

Experiment Figures by Number (Combined)

Figure 87. Experiment 1

PPN	TMA
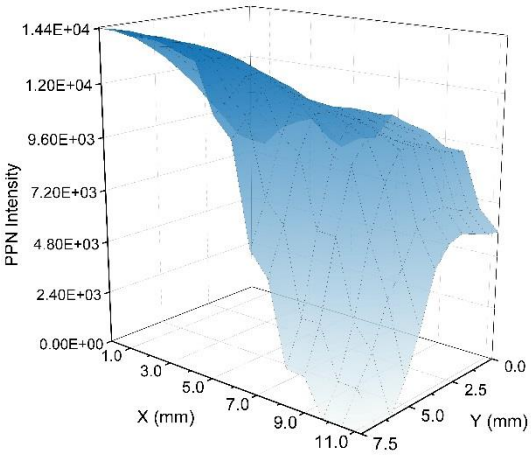	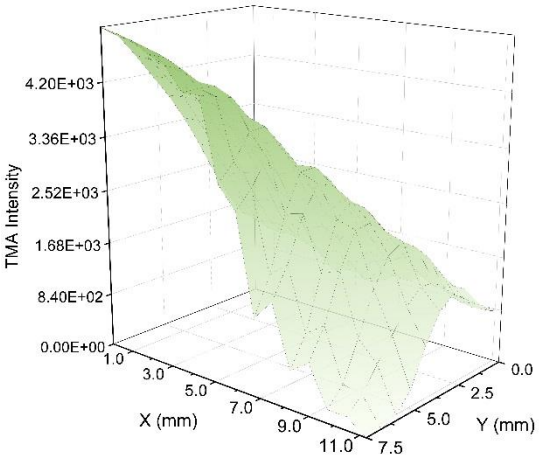

Figure 88. Experiment 2

PPN	TMA
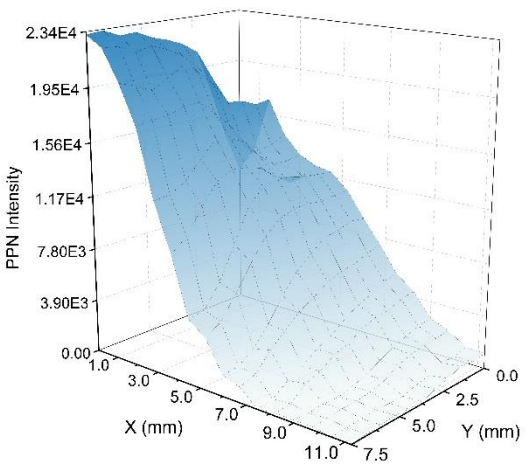	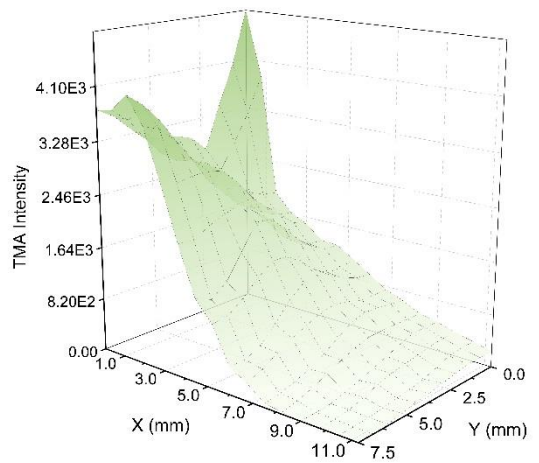

Figure 89. Experiment 3

PPN	TMA
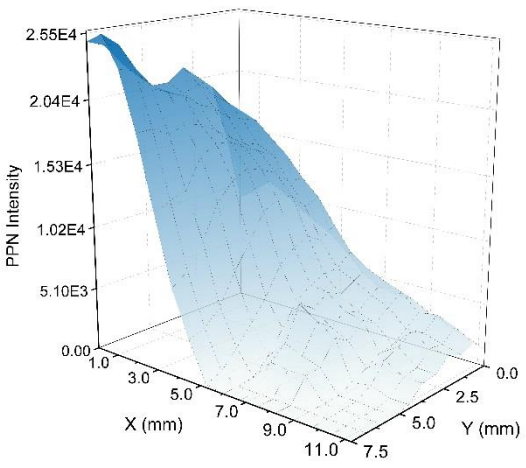	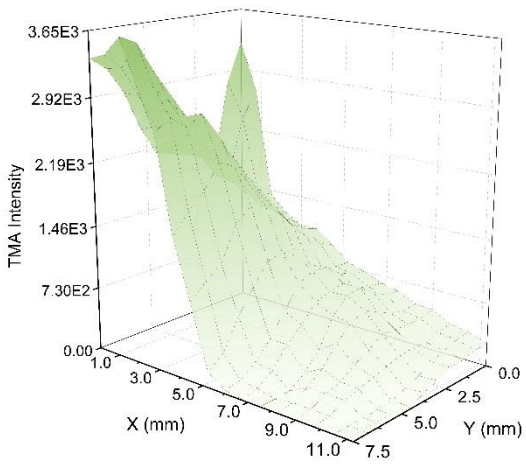

Figure 90. Experiment 4

PPN	TMA
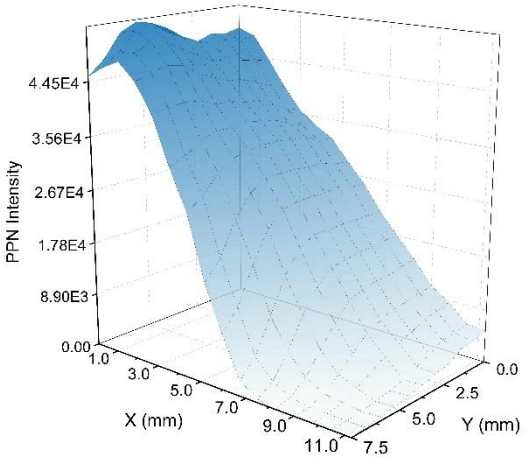	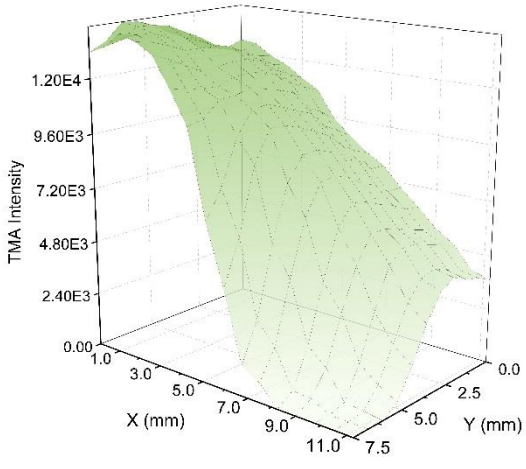

Figure 91. Experiment 5

PPN	TMA
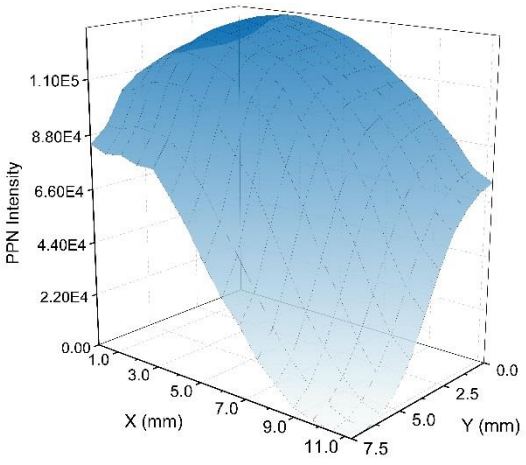	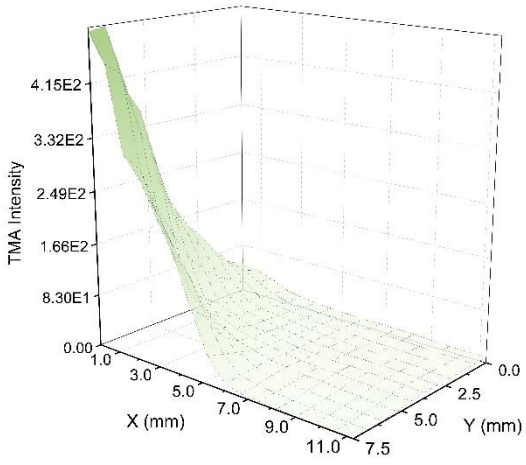

Figure 92. Experiment 6

PPN	TMA
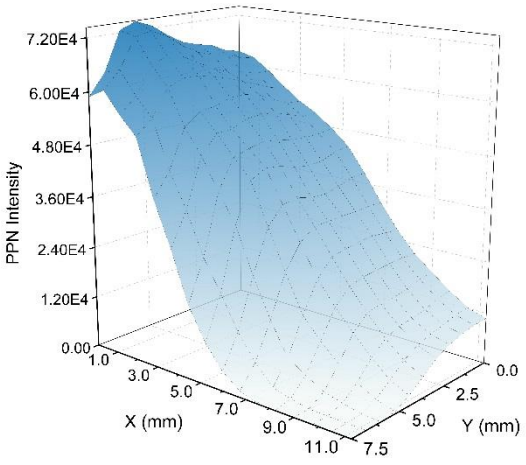	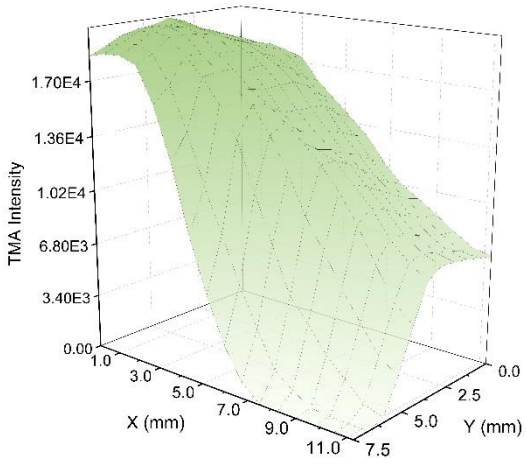

Figure 93. Experiment 7

PPN	TMA
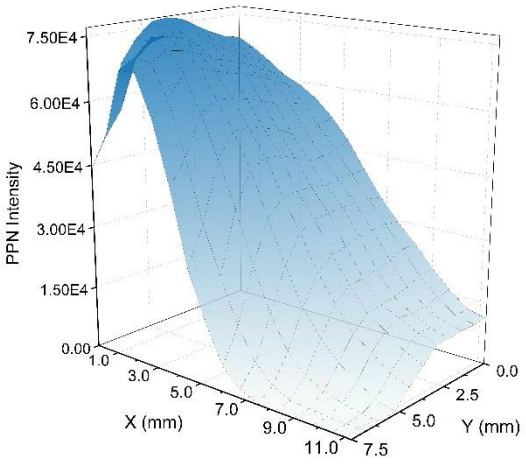	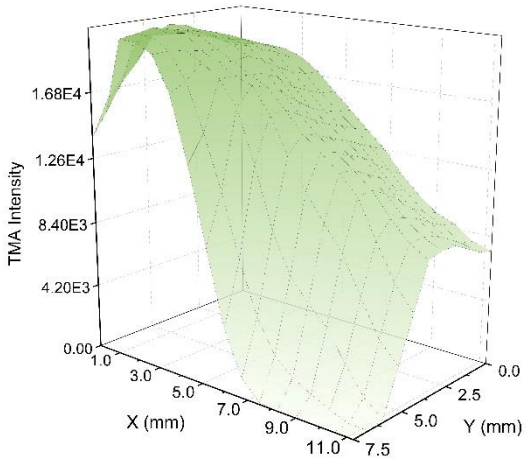

Figure 94. Experiment 8

PPN	TMA
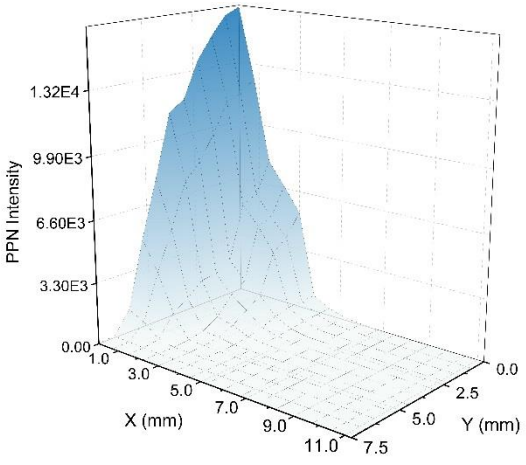	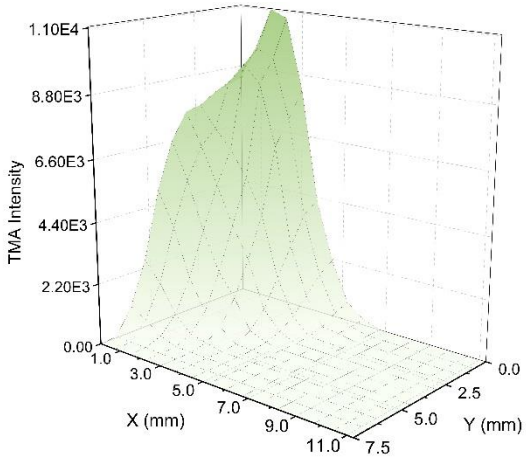

Figure 95. Experiment 9

PPN	TMA
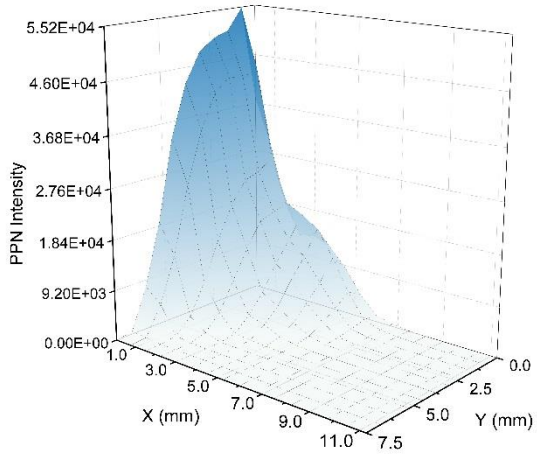	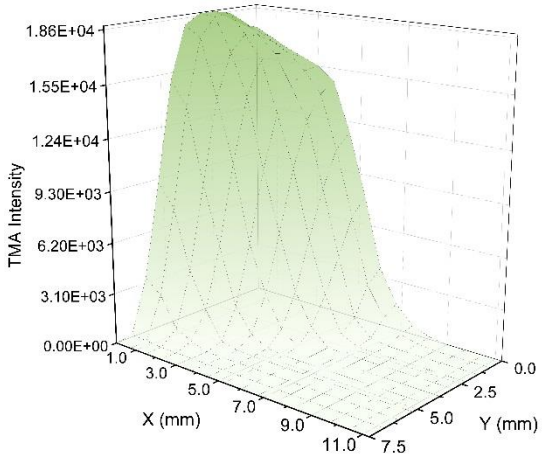

Figure 96. Experiment 10

PPN	TMA
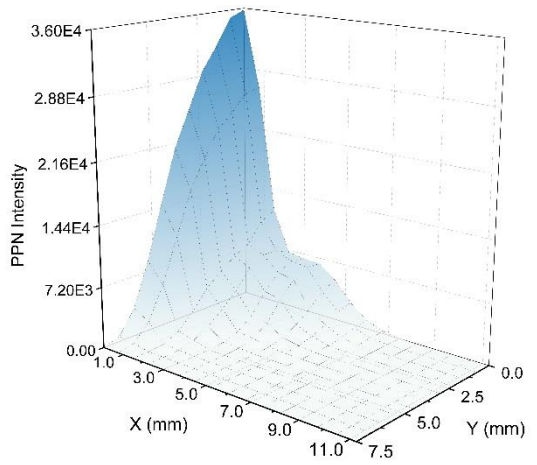	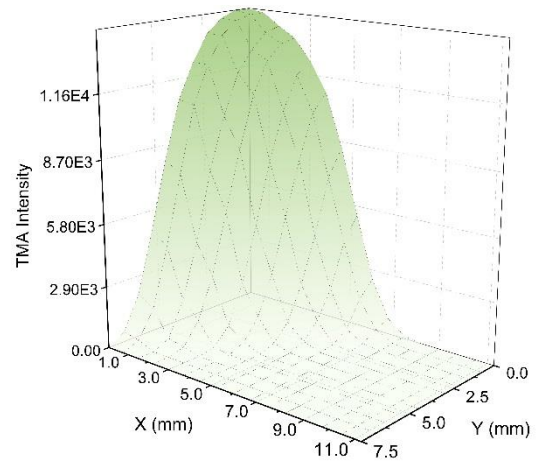

Figure 97. Experiment 11

PPN	TMA
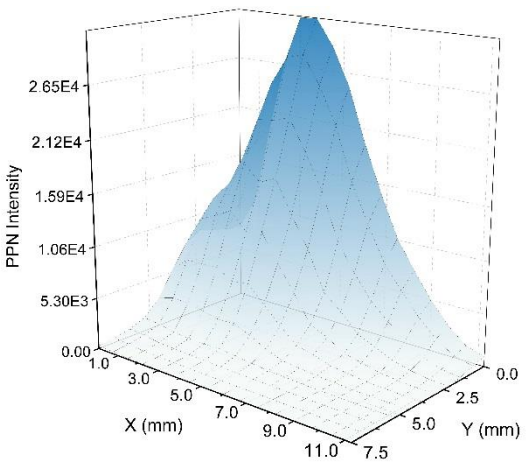	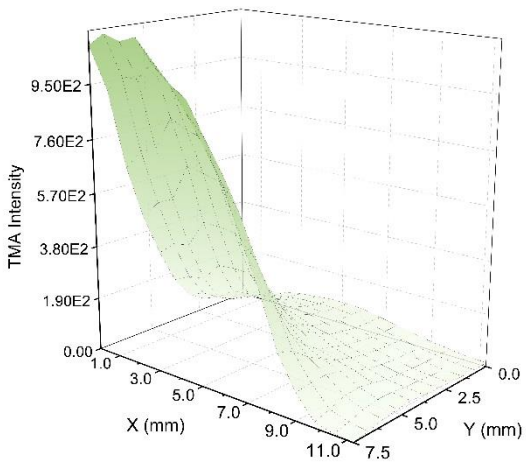

Figure 98. Experiment 12

PPN	TMA
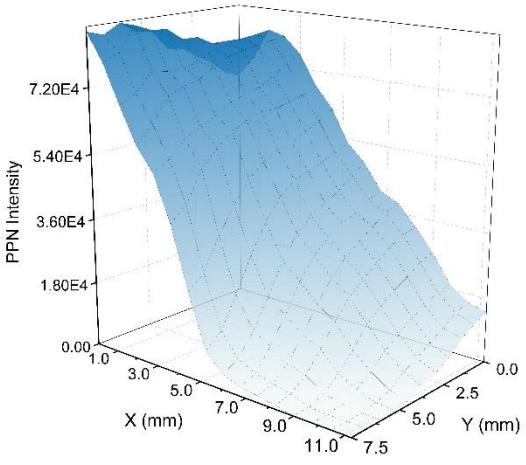	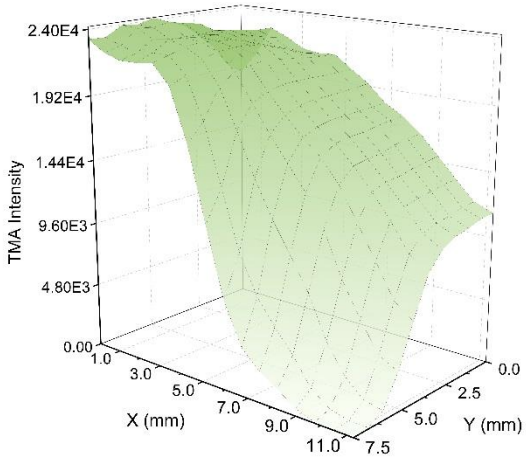

Figure 99. Experiment 13

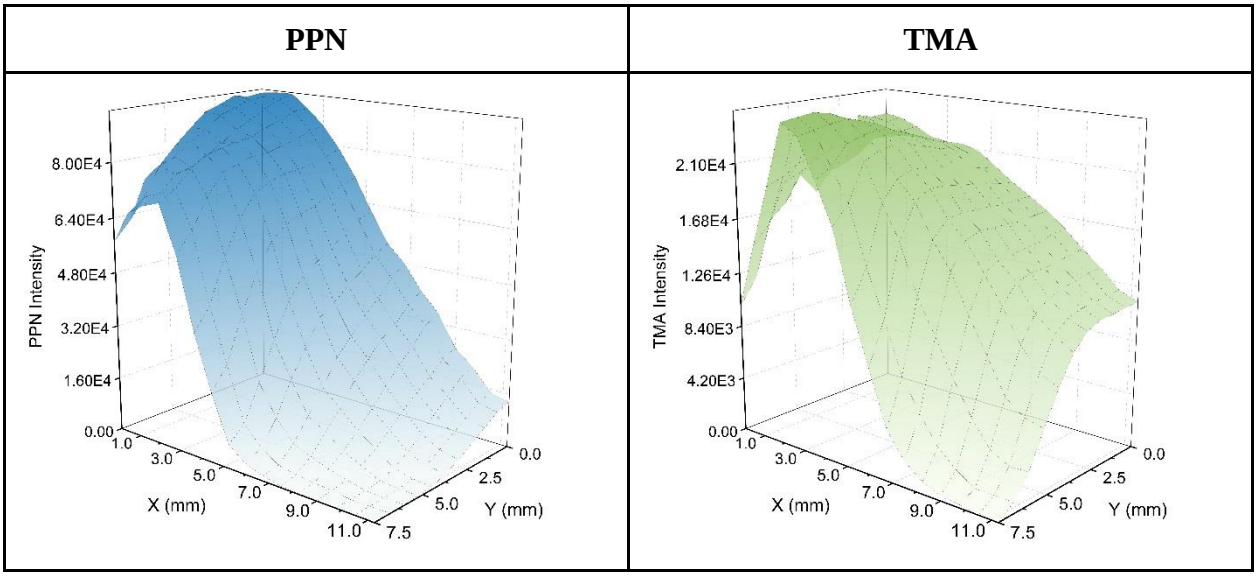

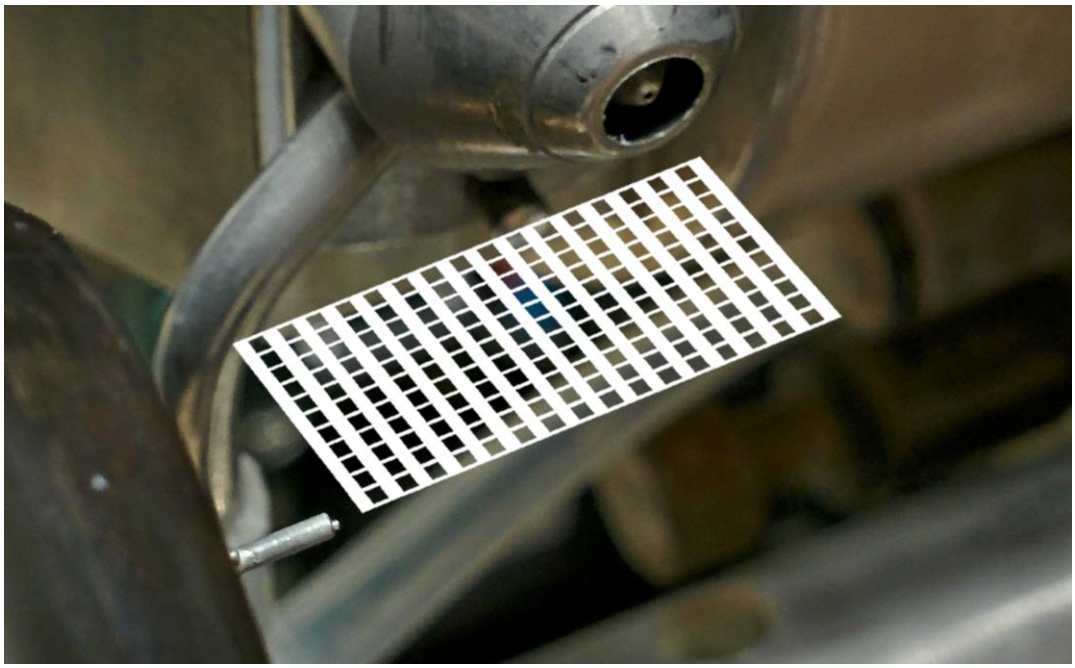

Figure 100. Photo of the ESI Source and Capillary with sampling grid overlay.

Appendix C
Selective Mass Spectrometric Analysis using Charge-Tagged Reagents

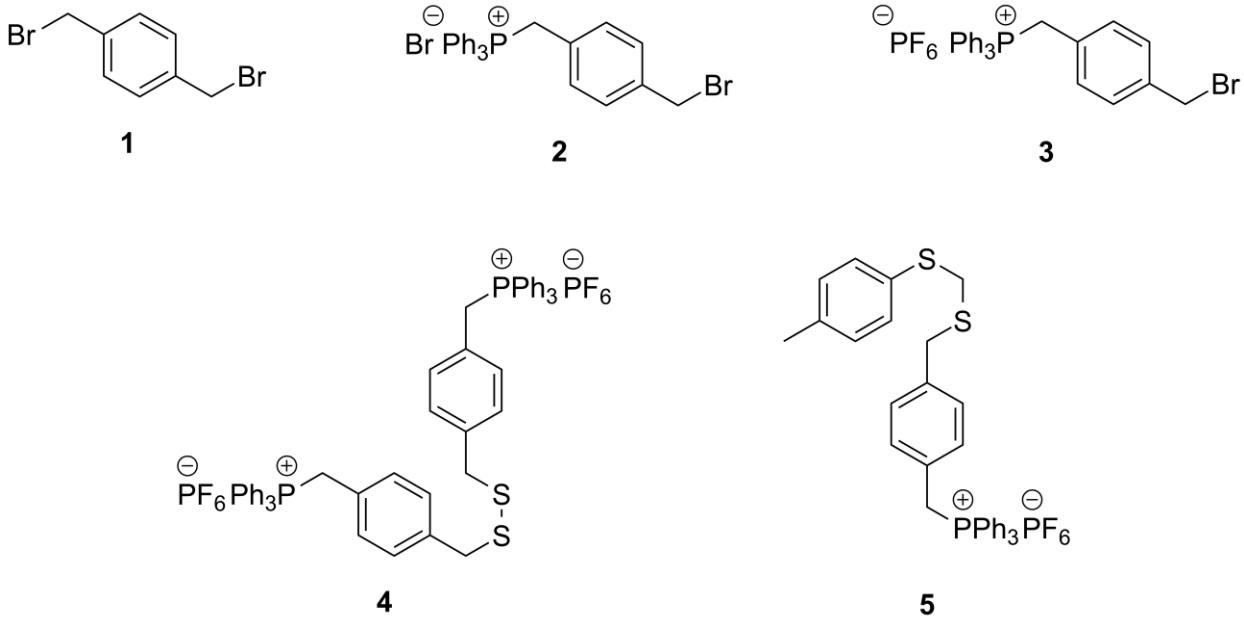

Figure 101. Collection of relevant species by number (as they appear in the main body of the chapter)

Instrumental Parameters

Table 11. Complete list of QTOF Micro Quadrupole parameters

Ion Energy (V)	**2.0**
Collison Energy	**2.0**
Low mass resolution	**4.1**
High mass resolution	**4.2**
RF Lens 1	**0.4**
Pre/Post Filter	**4.8**
RF Lens 2	**5.5**
Aperture (V)	**6.1**
Set mass	**0.0**
Plate one	**1.1**
Entrance	**110.0**
Gas cell RF	**600.0**

Can	**0.0**
Plate two	**-3.2**
Pusher cycle time	**Auto (47.0)**
Pusher frequency	**21276.60**

Table 12. Complete list of QTOF Micro TOF parameters

Acceleration (V)	**200.0**
Focus (V)	**0.0**
Steering (V)	**1.5**
Tube Lens (V)	**76.0**
Grid 2 (V)	**0.0**
TOF Flight Tube (V)	**5630.0**
Reflectron (V)	**1780.0**
Pusher offset	**0.0**
Pusher	**818.0**
Puller	**634.7**

Table 13. Complete list of QTOF Micro TDC parameters

Inhibit Push	**13.0**
Np Multiplier	**0.70**
Resolution	**5000.0**
Lteff	**1080.00**
Veff	**5630.00**

NMR Data

This report was created by ACD/NMR Processor Academic Edition. For more information go to www.acdlabs.com/nmrproc/

Acquisition Time (sec)	3.4166	Comment	EJ - 100915 - Pure Br-Phosphonium Salt			Date	10 Sep 2015 15:21:52
Date Stamp	10 Sep 2015 15:21:52						
Frequency (MHz)	300.27	Nucleus	1H	Number of Transients	16	Origin	spect
Original Points Count	16384	Owner	av300user	Points Count	16384	Pulse Sequence	zg30
Receiver Gain	203.00	SW(cyclical) (Hz)	4795.40	Solvent	CHLOROFORM-d		
Spectrum Offset (Hz)	1800.8390	Spectrum Type	STANDARD	Sweep Width (Hz)	4795.10	Temperature (degree C)	27.000

^{1}H NMR (300 MHz, CHLOROFORM- d) δ ppm4.39 (s, 2 H) 4.57 (d, J=14.05 Hz, 2 H) 6.89 (dd, J=8.20, 2.34 Hz, 2 H) 7.18 (d, J=7.90 Hz, 2 H) 7.44 - 7.85 (m, 16 H)

First Product - HNMR - -100915-Br-498PPh3.001.001.1r.esp

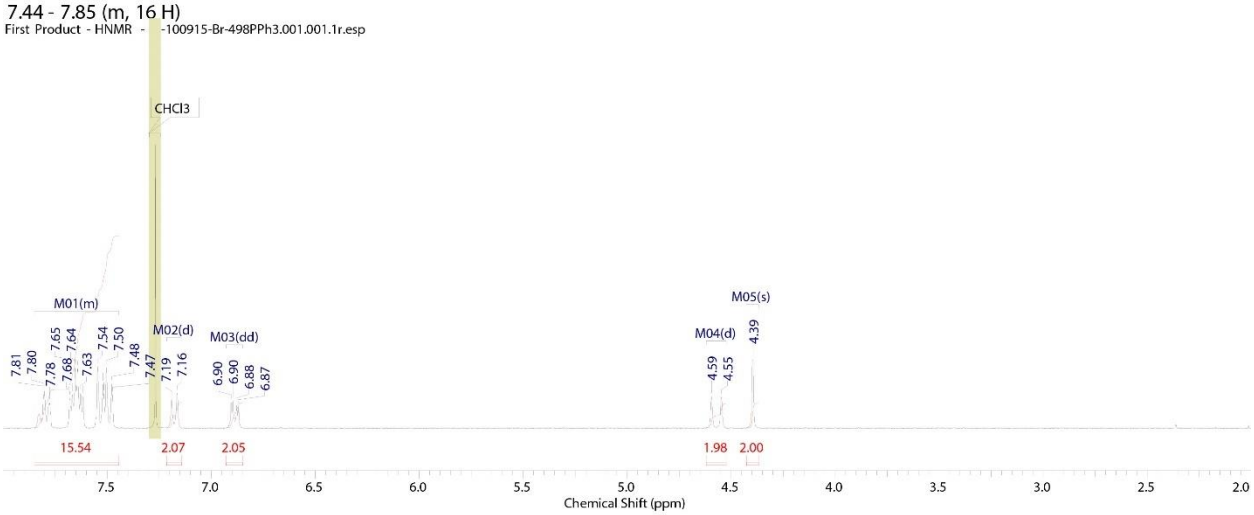

No.	(ppm)	Annotation	Layer No.	Created By	Created At	Modified By	Modified At
1	[1.47 .. 1.63]	Water	1	Eric	Mon 14/09/2015 2:18:36 PM	Eric	Tue 15/09/2015 10:50:49 AM
2	[7.24 .. 7.30]	CHCl3	1	Eric	Mon 14/09/2015 2:18:48 PM	Eric	Tue 15/09/2015 10:57:27 AM

No.	Shift1 (ppm)	H's	Type	J (Hz)	Multiplet1	(ppm)
1	4.39	2	s	-	M05	[4.37 .. 4.43]
2	4.57	2	d	14.05	M04	[4.52 .. 4.62]
3	6.89	2	dd	8.20, 2.34	M03	[6.85 .. 6.93]
4	7.18	2	d	7.90	M02	[7.14 .. 7.21]
5	7.62	16	m	-	M01	[7.44 .. 7.85]

No.	(ppm)	Value	Absolute Value	Non-Negative Value
1	[4.3678 .. 4.422	2.00000000	5.78073800e+6	2.00000000
2	[4.5238 .. 4.615	1.97551250	5.70996000e+6	1.97551250
3	[6.8483 .. 6.922	2.04578424	5.91307150e+6	2.04578424
4	[7.1421 .. 7.212	2.07188320	5.98850700e+6	2.07188320
5	[7.4431 .. 7.841	15.53992558	4.49161200e+7	15.53992558

Figure 102. 300 MHz Proton NMR report of (3); 4-(bromomethyl)benzyl)triphenylphosphonium hexafluorophosphate

Acquisition Time (sec)	1.3369	Comment	EJ - 100915 - Pure Br-Phosphonium Salt			Date	10 Sep 2015 15:30:24
Date Stamp	10 Sep 2015 15:30:24						
Frequency (MHz)	121.55	Nucleus	31P	Number of Transients	128	Origin	spect
Original Points Count	65536	Owner	av300user	Points Count	32768	Pulse Sequence	zgpg30
Receiver Gain	203.00	SW(cyclical) (Hz)	49019.61	Solvent	CHLOROFORM-d		
Spectrum Offset (Hz)	1950.9169	Spectrum Type	STANDARD	Sweep Width (Hz)	49018.11	Temperature (degree C)	27.000

^{31}P NMR (122 MHz, CHLOROFORM- d) δ ppm-144.24 (spt, J=712.10 Hz, 1 P) 22.65 (s, 119 P)

First Product 31P NMR - EJ-100915-Br-498PPh3.002.001.1r.esp

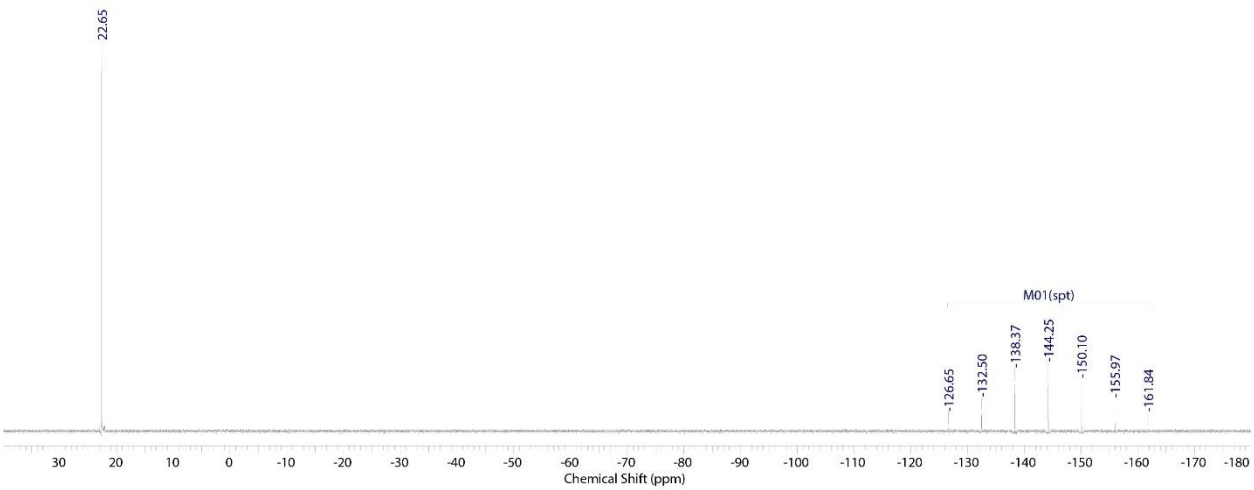

No.	Shift1 (ppm)	P's	Type	J (Hz)	Multiplet1	(ppm)
1	-144.24	1	spt	712.10	M01	[-162.38 .. -126.47]
2	22.65	119	s	-	M02	[22.39 .. 22.83]

No.	(ppm)	(Hz)	Height
1	-161.84	-19672.4	0.0071
2	-155.97	-18958.9	0.0445
3	-150.10	-18245.3	0.0971
4	-144.25	-17533.2	0.1406
5	-138.37	-16819.6	0.1244
6	-132.50	-16106.1	0.0464
7	-126.65	-15394.0	0.0083
8	22.65	2753.5	1.0000

Figure 103. 300 MHz ^{31}P NMR of (3) (4-(bromomethyl)benzyl)triphenylphosphonium hexafluorophosphate

Acquisition Time (sec)	3.4166	Comment	EJ - 251114 - 498DS (Large Batch)			Date	25 Nov 2014 17:36:00
Date Stamp	25 Nov 2014 17:36:00						
Frequency (MHz)	300.27	Nucleus	1H	Number of Transients	16	Origin	spect
Original Points Count	16384	Owner	av300user	Points Count	16384	Pulse Sequence	zg30
Receiver Gain	203.00	SW(cyclical) (Hz)	4795.40	Solvent	CHLOROFORM-d		
Spectrum Offset (Hz)	1800.8390	Spectrum Type	STANDARD	Sweep Width (Hz)	4795.10	Temperature (degree C)	27.000

^{1}H NMR (300 MHz, CHLOROFORM- d) δ ppm4.59 (d, J=14.34 Hz, 2 H) 7.42 - 7.85 (m, 20 H)

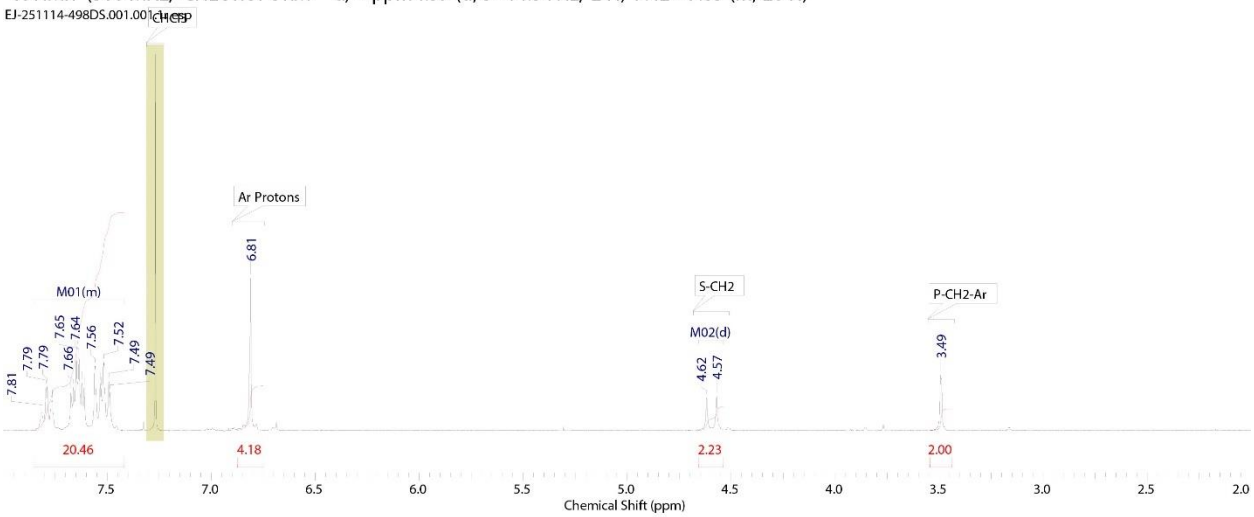

No.	(ppm)	Annotation	Layer No.	Created By	Created At	Modified By	Modified At
1	[3.43 .. 3.55]	P-CH2-Ar	1	Eric	Thu 27/11/2014 11:59:21 AM		
2	[4.51 .. 4.68]	S-CH2	1	Eric	Thu 27/11/2014 12:00:18 PM		
3	[6.74 .. 6.90]	Ar Protons	1	Eric	Thu 27/11/2014 12:08:03 PM		
4	[7.23 .. 7.31]	CHCl3	1	Eric	Thu 27/11/2014 9:49:50 AM		

No.	Shift1 (ppm)	H's	Type	J (Hz)	Multiplet1	(ppm)
1	4.59	2	d	14.34	M02	[4.54 .. 4.66]
2	7.65	20	m	-	M01	[7.42 .. 7.85]

No.	(ppm)	Value	Absolute Value	Non-Negative Value
1	[3.4397 .. 3.54	2.00000000	5.22331350e+6	2.00000000
2	[4.5381 .. 4.65	2.22606540	5.81371900e+6	2.22606540
3	[6.7497 .. 6.87	4.18111277	1.09196310e+7	4.18111277
4	[7.4182 .. 7.84	20.45514679	5.34218200e+7	20.45514679

Figure 104. 300 MHz Proton NMR of compound (4)

Acquisition Time (sec)	1.3369	Comment	EJ - 251114 - 498DS (Large Batch)			Date	25 Nov 2014 17:42:24
Date Stamp	25 Nov 2014 17:42:24						
						Frequency (MHz)	121.55
Nucleus	31P	Number of Transients	128	Origin	spect	Original Points Count	65536
Owner	av300user	Points Count	32768	Pulse Sequence	zgpg30	Receiver Gain	203.00
SW(cyclical) (Hz)	49019.61	Solvent	CHLOROFORM-d	Spectrum Offset (Hz)	1950.9169	Spectrum Type	STANDARD
Sweep Width (Hz)	49018.11	Temperature (degree C)	27.000				

31P NMR (122 MHz, CHLOROFORM- d) δ ppm-145.64 (m, J=713.60, 713.60, 713.60, 713.60, 713.60, 713.60 Hz, 15 P)

EJ-251114-498DS - 31P NMR.esp

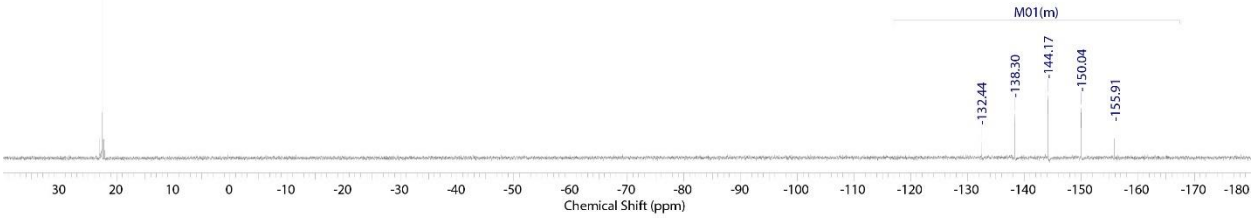

No.	Shift1 (ppm)	P's	Type	J (Hz)	Multiplet1	(ppm)
1	-145.64	15	m	713.60	M01	[-167.35 .. -117.02]

No.	(ppm)	(Hz)	Height
1	-155.91	-18951.4	0.0521
2	-150.04	-18237.8	0.1279
3	-144.17	-17524.2	0.1612
4	-138.30	-16810.7	0.1135
5	-132.44	-16098.6	0.0430
6	22.48	2732.6	1.0000

Figure 105. 300 MHz ^{31}P NMR of compound (4)

ESI-QToF MS Data

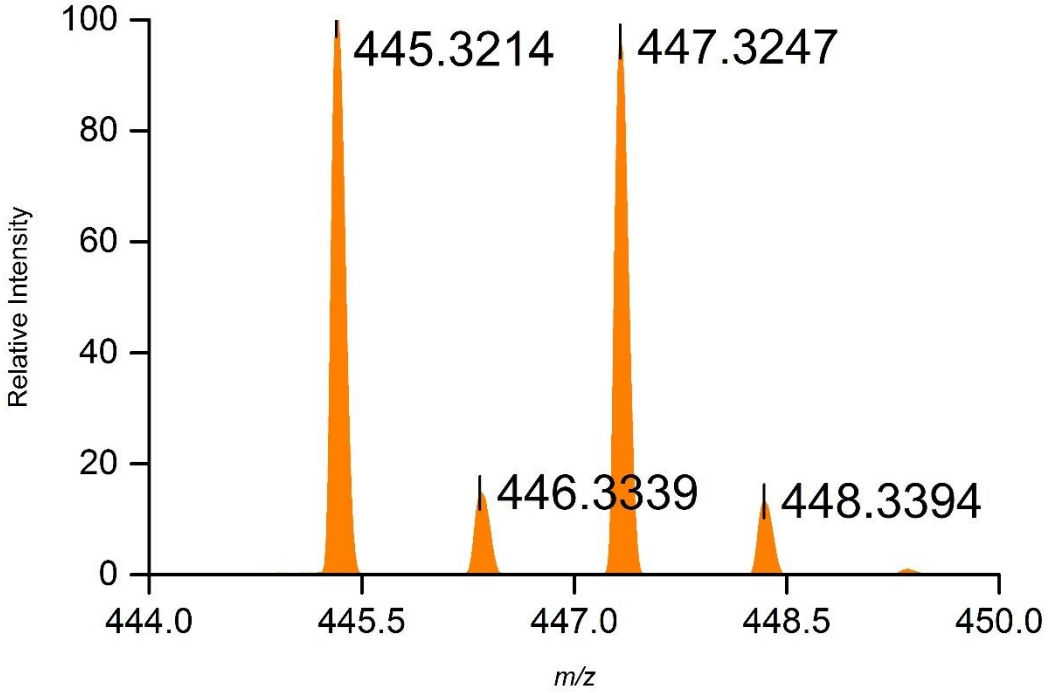

Figure 106. sitive-ion ESI-MS of (4-(bromomethyl)benzyl)triphenylphosphonium hexafluorophosphate

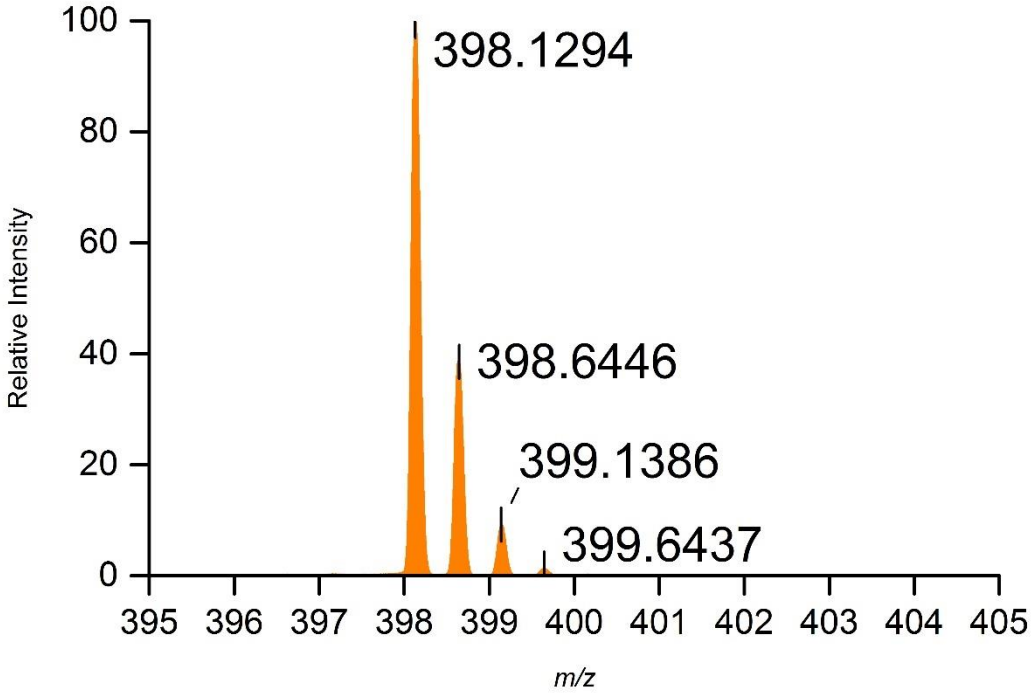

Figure 107. Positive-ion ESI-MS of the charge-tagged disulfide

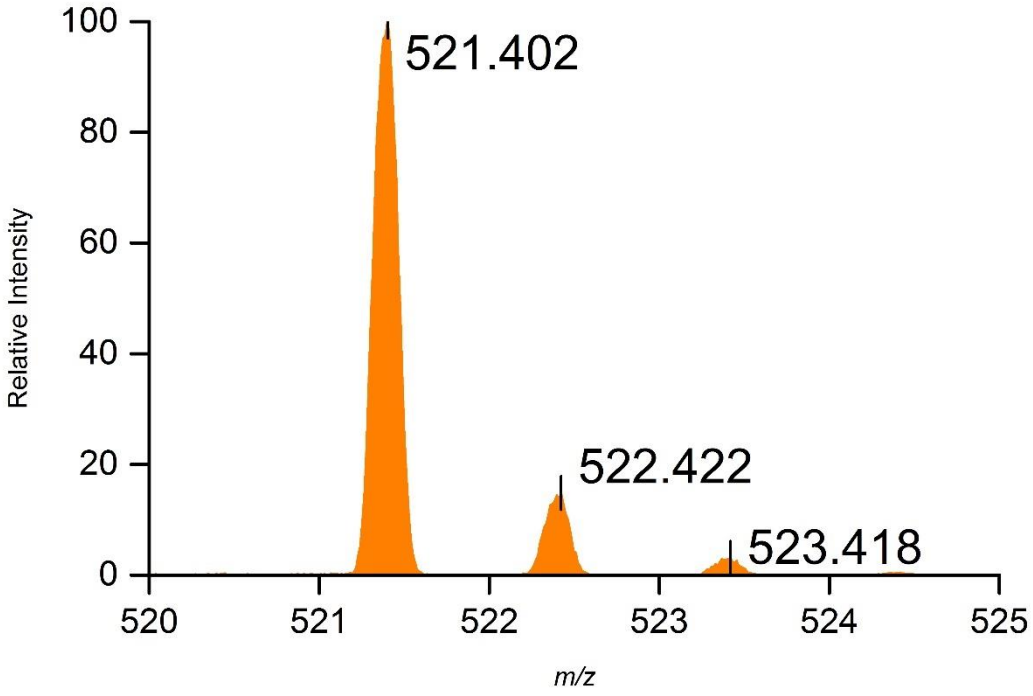

Figure 108. Positive-ion ESI-MS of the mixture of charge-tag and 4-methylbenzenethiol

Imperial Oil Clay Treater Fraction Sample Mass Spectra

Table 14. Sample Acidification Data

Note: Acidified samples are composed of 1.0 mL of sample, 0.1% formic acid, and are diluted to 10 mL total volume with ethanol.

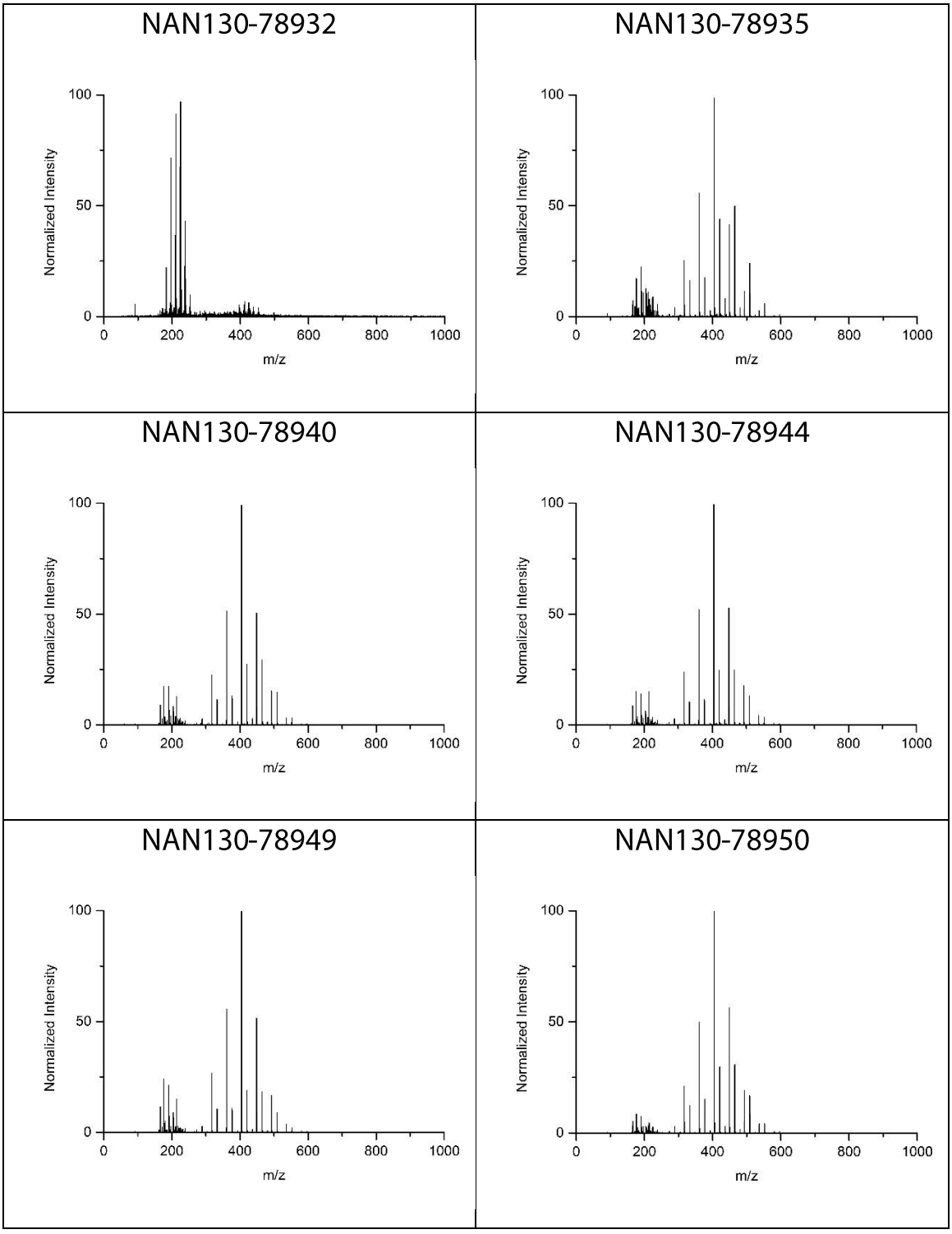

Table 15. Sample Deprotonation (KOH treated) Data

Note: Caustic treated samples are composed of 1.0 mL of sample, 0.02% potassium hydroxide, and are diluted to 10 mL total volume with ethanol.

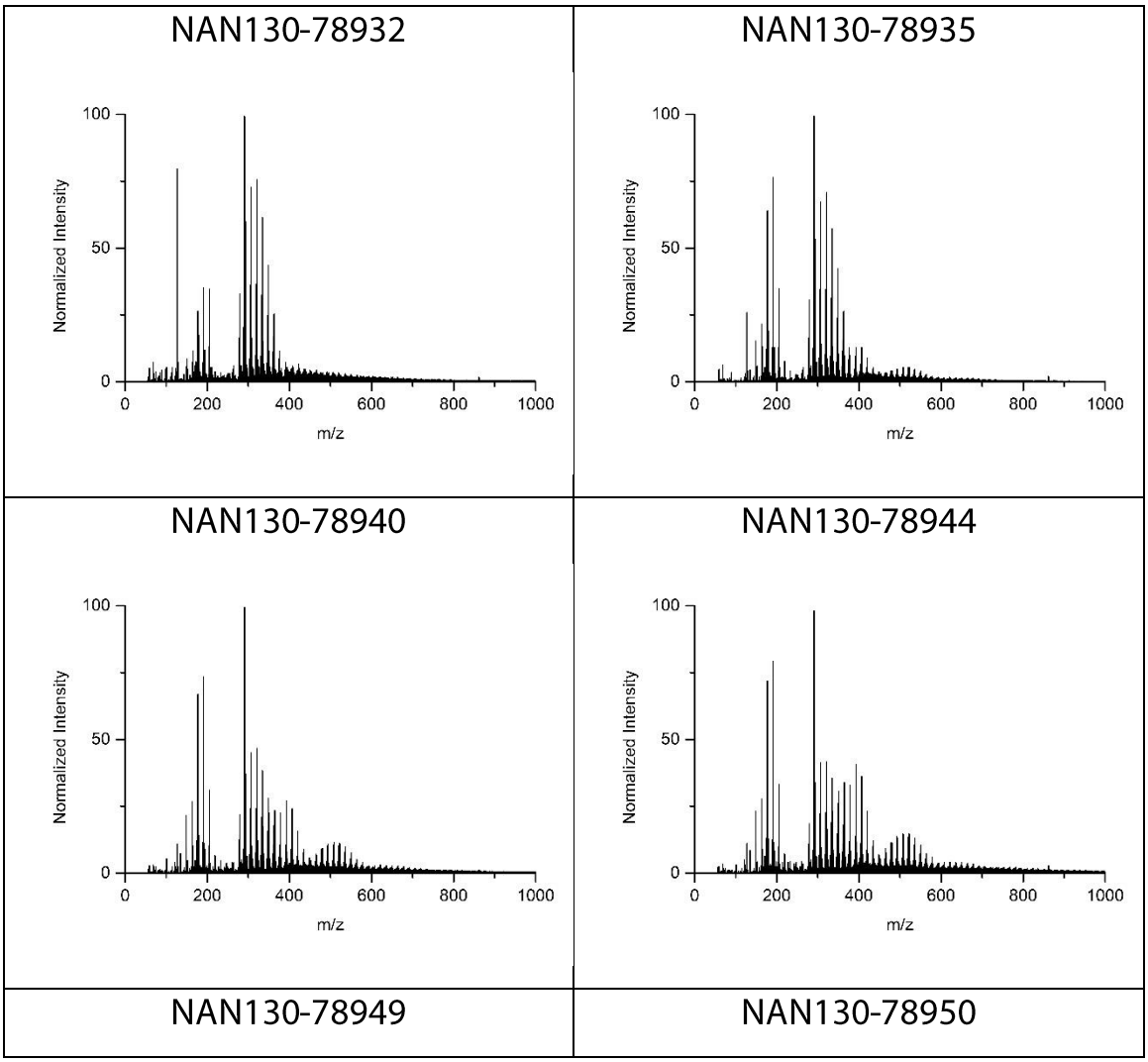

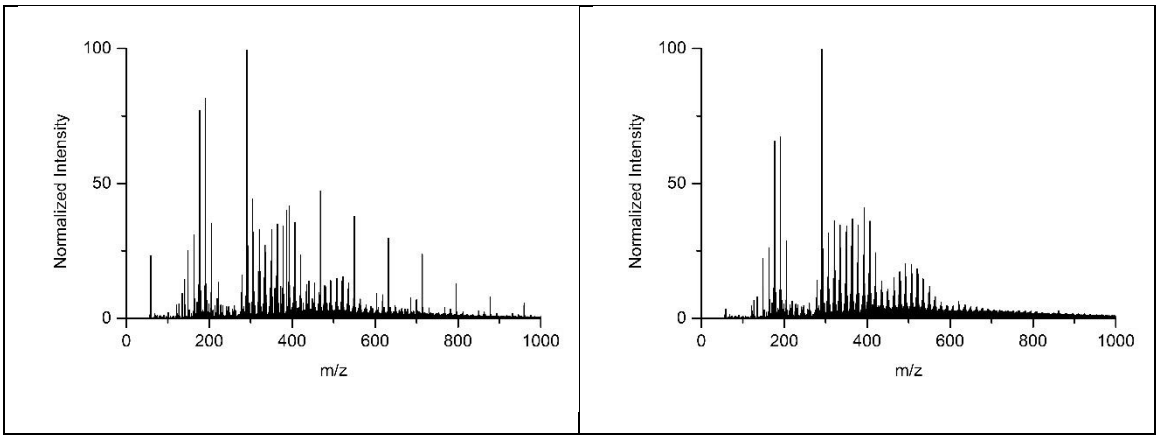

Table 16. Sample Methylation Data

Note: Methylated samples are composed of 1.0 mL of sample, 0.01% iodomethane, and are diluted to 10 mL total volume with ethanol.

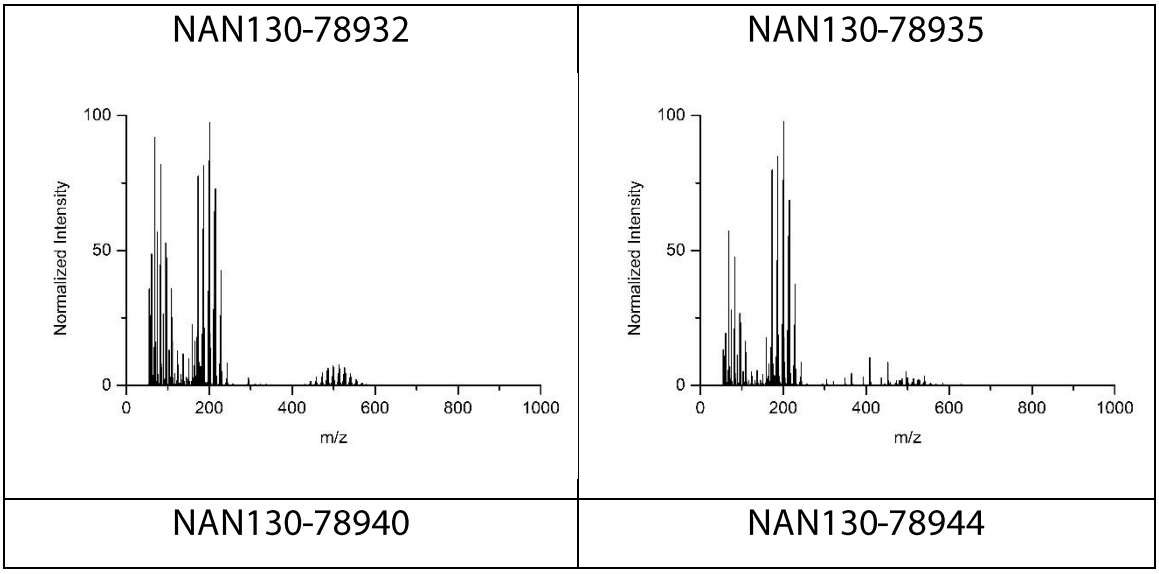

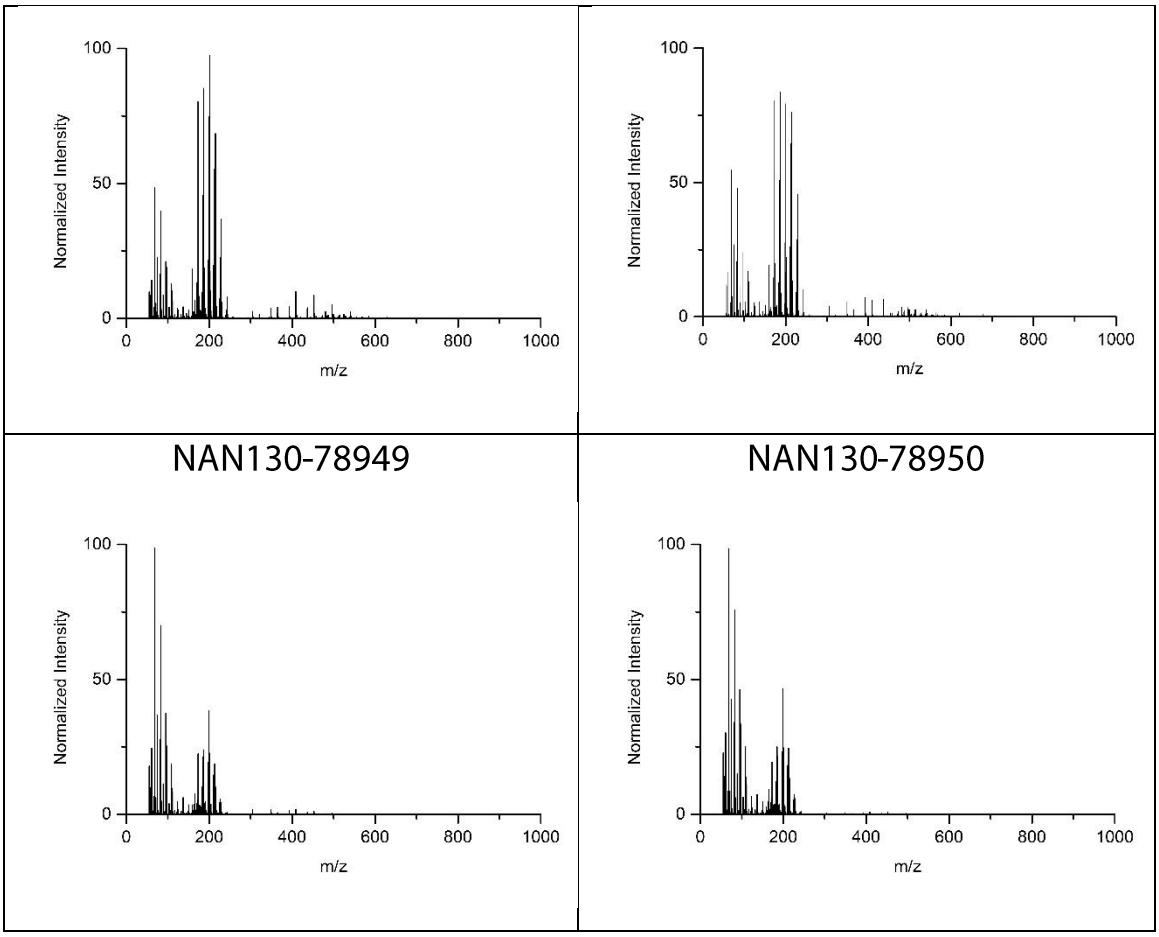
Normalized Intensity
m/z
NAN130-78949
NAN130-78950

Future Work: Additional Derivatization Strategies

Ketones and aldehydes to charged hydrazones

Several forms of naturally occurring oxygen-containing compounds are present within crude oil. Ketones and aldehydes (aliphatic ketones) are one class of oxygen-containing compound, having been discovered in oil shales and sediments.[307] In previous studies, it has been shown that aromatic ketones such as fluorenones, benzo, dibenzo and naphthofluorenones and make up the majority of ketones in some oil samples.[28] The concentration of oxidized compounds such as these has been shown to correlate to the increased thermal maturity of the oil.[308]

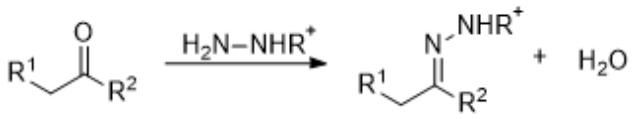

Scheme 12. General scheme of hydrazone formation using a charge-tagged hydrazine compound

These ketones and aldehydes may be partially responsible for the acidity of some crude oils.[309] The enhanced acidity afforded by these compounds is especially problematic in refining due to corrosion in equipment and pipelines. Much of the readily available information on oxidized compounds deals with the more polar compounds which are recoverable from crude oil through alkali extraction. Far less information is available on ketone and aldehyde content in crude oils due to the difficulty in their isolation.[308] For this reason, the identification of ketones and aldehydes in crude oil through the method

proposed below is highly significant. The identification of such compounds could lead to a means of reducing the acidity in crude oil, ultimately reducing costly processing issues.[310]

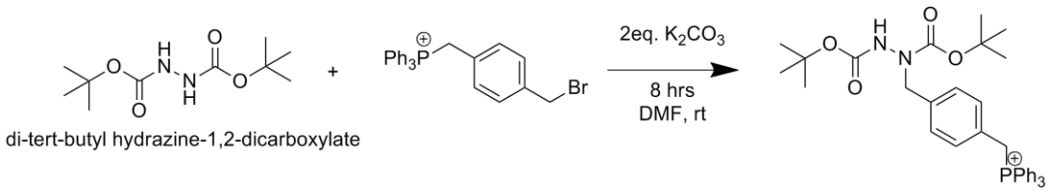

Scheme 13. Prototypical charge-tagged hydrazone synthesis

Addition of a charge-tagged hydrazine, $H_2N\text{-}NHR^+$, will result in aldehydes and ketones (RCOR) in the mixture reacting to form a charged hydrazone, $R_2C{=}NNHR^+$.[311] The traditional method for the synthesis of hydrazones involves the combination of a hydrazine with an aldehyde or ketone. This is done either in a neat mixture or in an organic solvent such as benzene, dichloromethane or hexane. The reaction often occurs readily and spontaneously with simple carbonyl compounds and the separation of the produced water from the immiscible organic mixture occurs quickly and readily; however, hindered or less reactive carbonyl species (especially ketones) may require acidic catalysts, heating and aided removal of water to achieve practical reaction times and high conversions.[170] The synthesized hydrazone is quite stable and may be purified by distillation or chromatography, should that be necessary.[312,313]

Esterification of Carboxylic acids

A simple and well-known reaction of carboxylic acids is the esterification of carboxylic acids upon reaction with an alcohol. The use of a charge-tagged alcohol could

be used in this regard to charge-tag carboxylic acids, allowing the MS characterization of the ester derivative. The esterification of carboxylic acids is slow and reversible; therefore, the reaction typically involves heating and the use of an acid catalyst, such as concentrated sulfuric acid, to speed up the reaction.

The acid catalyst must be strong in order to protonate the carbonyl group of the carboxylic acid. Protonation of the carboxylic acid carbonyl promotes electrophilicity of the moiety, thus facilitating attack on the primary carbon by the oxygen of a hydroxyl group. One issue surrounding this reaction is the reversibility.[313] Water is formed during the reaction and this may attack the protonated ester derivative, effectively reversing the reaction. Some residual water may exist in crude oil samples, further hampering progress of the reaction. In this case, an excess of charge tagged alcohol should push the reaction forward. Furthermore, sulfuric acid or other dehydrating agents (such as silica gel) may be used to extract water from the mixture subsequently driving the reaction forward.

Another complication to this reaction involves unwanted transesterification. The ester formed from a carboxylic acid in a sample of crude oil may be subject to attack by other alcohols in the mixture forming a different ester, minus the charge-tag. This transesterification side reaction is also acid catalyzed which could lead to problems if an acid catalyst needs to be employed in the esterification of carboxylic acids. However, the charge-tagged analytes should be of sufficient intensity in the mass spectra that esterified carboxylic acids are easily identifiable since ionization efficiency issues are negligible.

Appendix D
Activation of Palladium Catalyst Precursors

ESI-MS Chromatograms

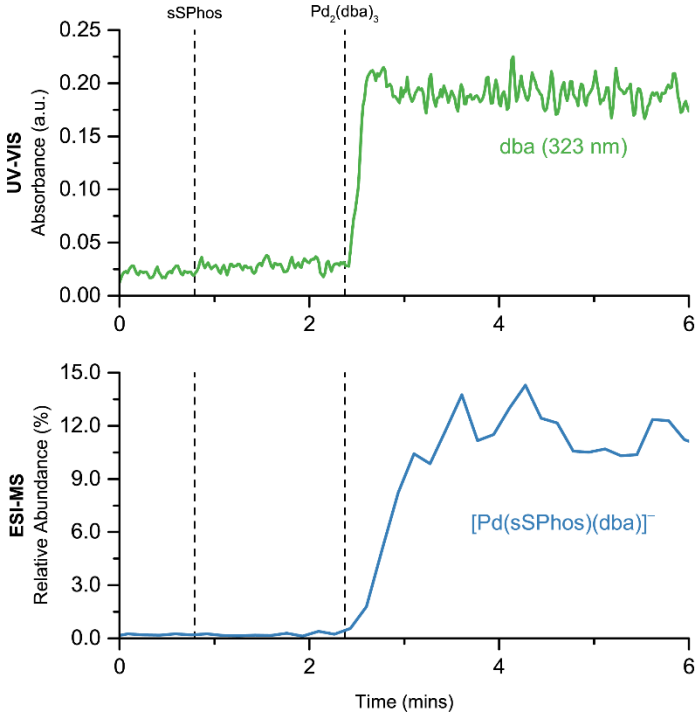

Figure 109. Reaction of $[sSPhos]^-$ with $Pd_2(dba)_3$ in DMF at room temperature (21°C)

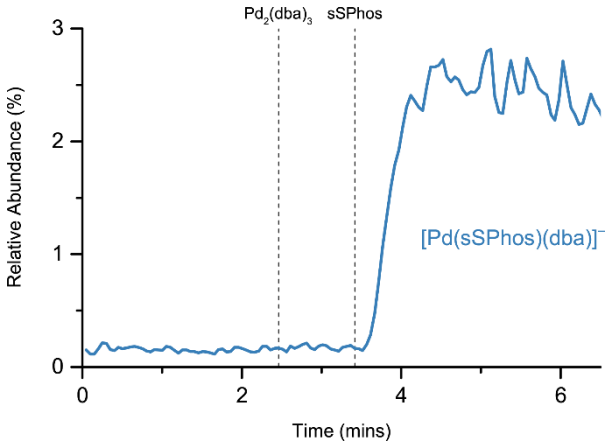

Figure 110. Reaction of $[sSPhos]^-$ with $Pd_2(dba)_3$ in MeOH at reflux (65°C)

ESI-MS Mass Spectra

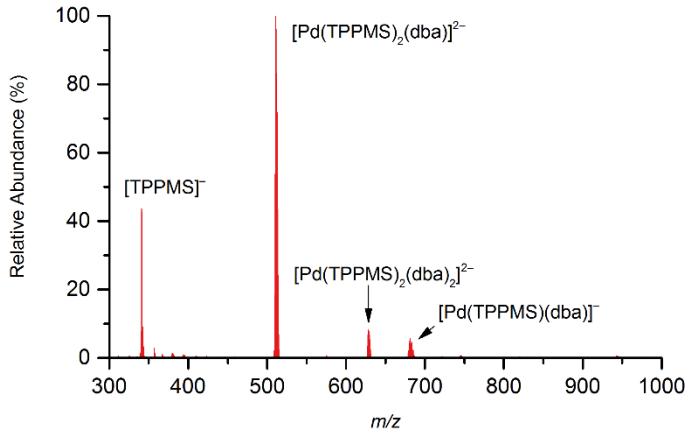

Figure 111. Mass spectrum of the mixture of 4 eq. [TPPMS]– with 1 eq. $Pd_2(dba)_3$ in MeOH

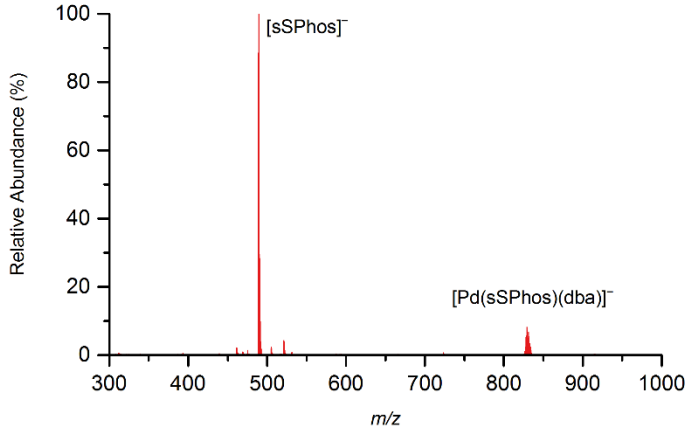

Figure 112. Mass spectrum of the mixture of 4 eq. $[sSPhos]^-$ with 1 eq. Pd2(dba)3 in MeOH

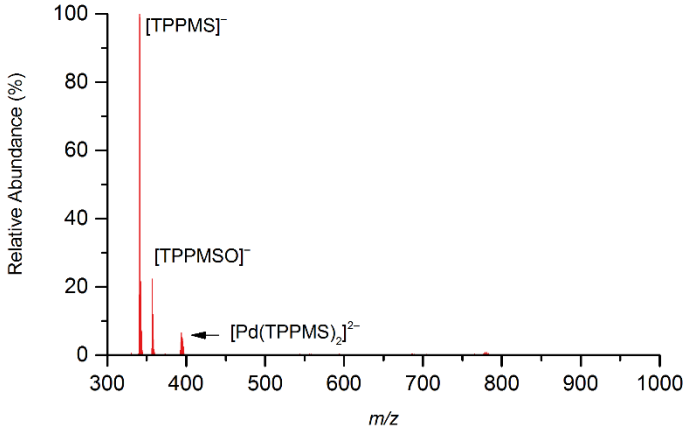

Figure 113. Mass spectrum of the mixture of 4 eq. $[TPPMS]^-$ with 1 eq. $Pd_2(dba)_3$ in DMF

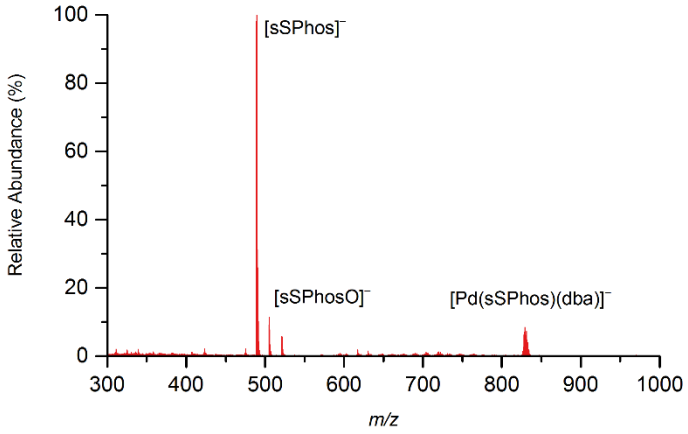

Figure 114. Mass spectrum of the mixture of 4 eq. $[sSPhos]^-$ with 1 eq. $Pd_2(dba)_3$ in DMF

ESI-MSMS product ion scan spectra

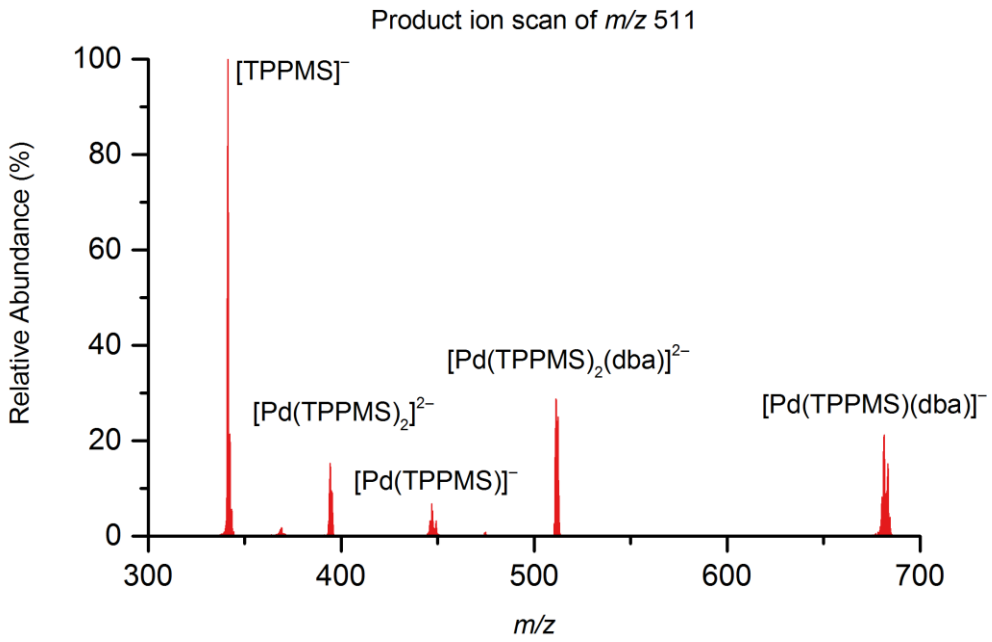

Figure 115. Product ion scan of $[Pd(TPPMS)_2(dba)]^{2-}$ (m/z 511)

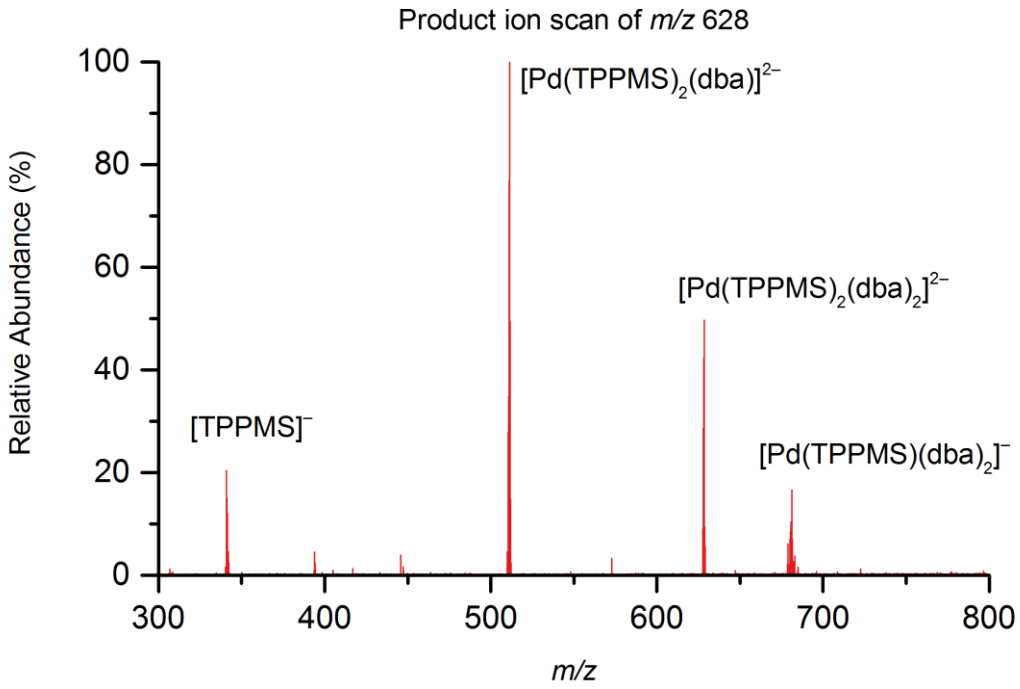

Figure 116. Product ion scan of $[Pd(TPPMS)_2(dba)_2]^{2-}$ (m/z 628)

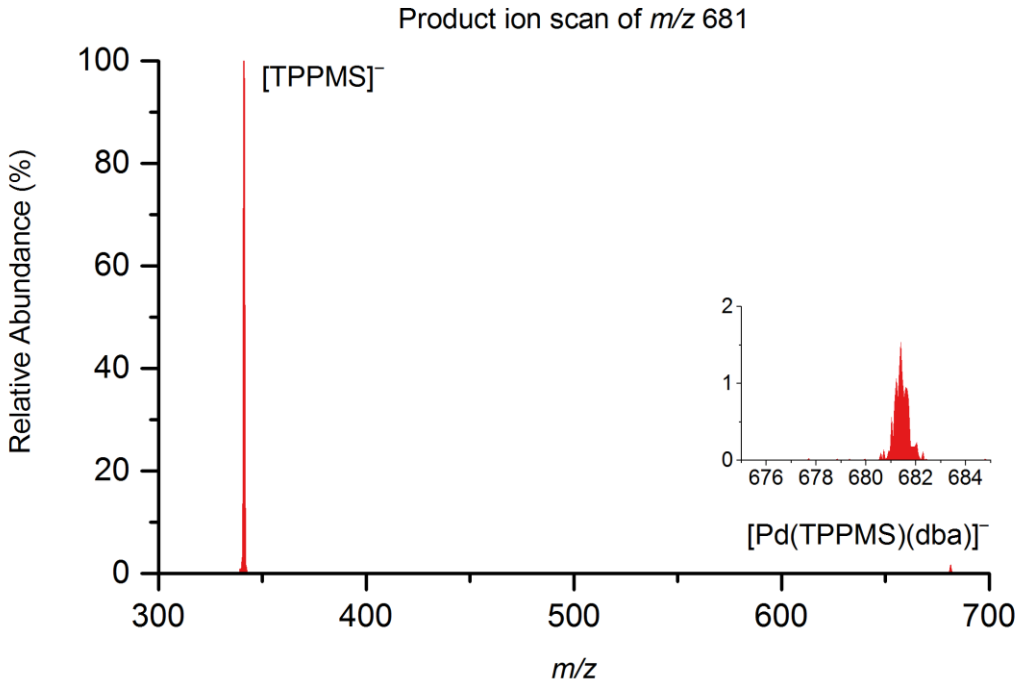

Figure 117. Product ion scan of $[Pd(TPPMS)(dba)]^-$ (m/z 681)

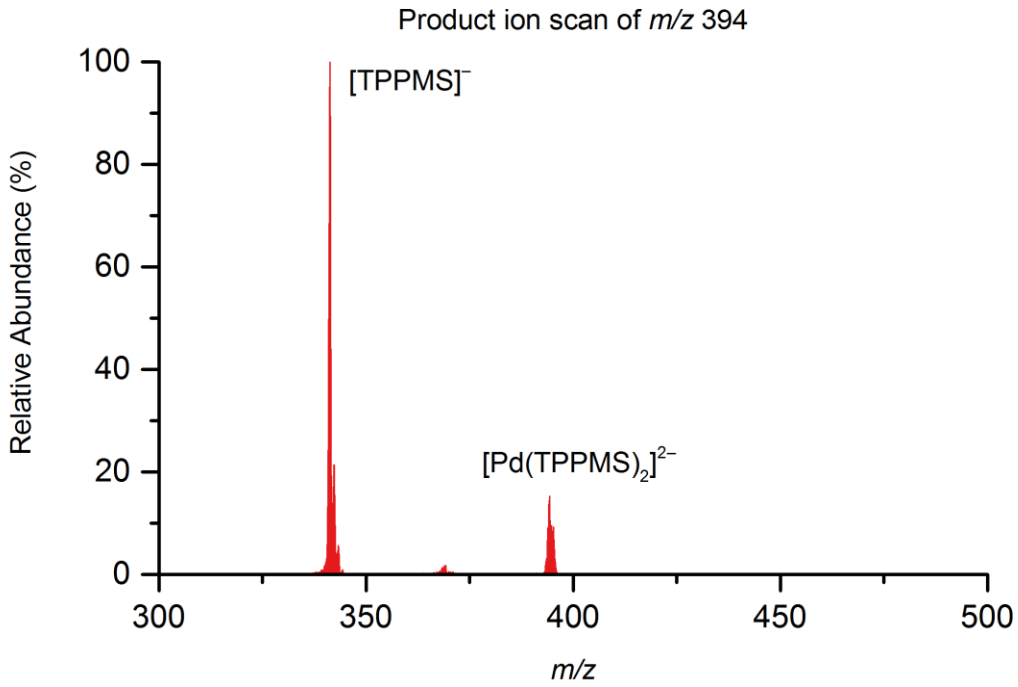

Figure 118. Product ion scan of $[Pd(TPPMS)_2]^{2-}$ (m/z 394)

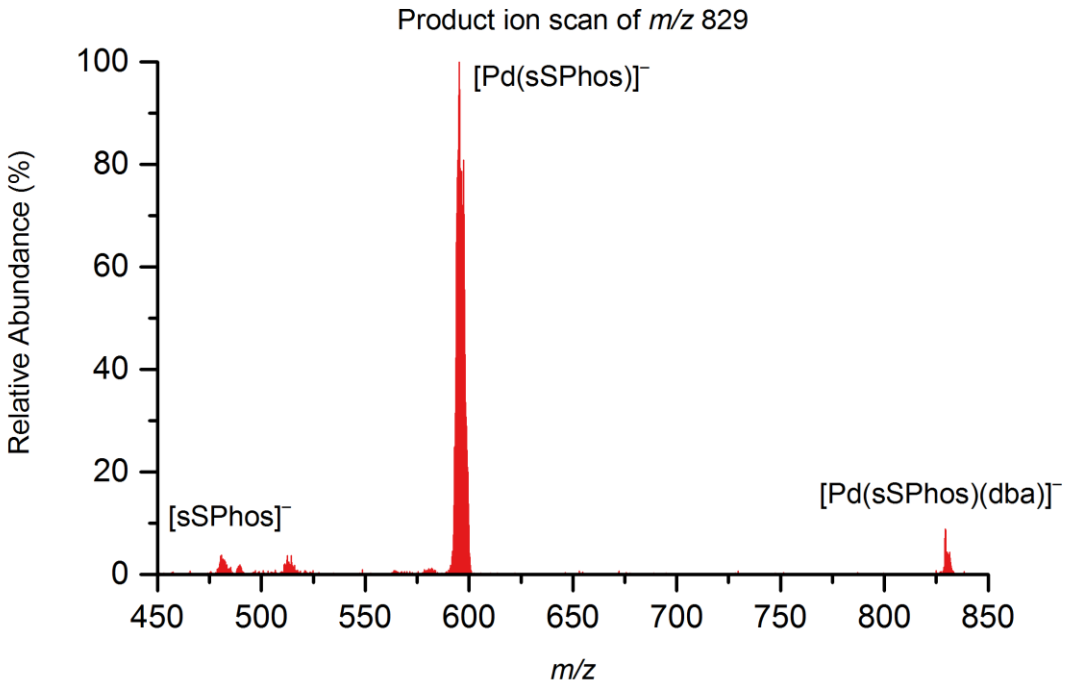

Figure 119. Product ion scan of $[Pd(sSPhos)(dba)]^-$ (m/z 829)

Waters 996 PDA Experimental

Several experiments performed with the Waters 996 Photodiode Array Detector were not featured in this chapter; however, these experiments served as the basis of much of the work described. Therefore, this section deals with the experimental parameters and setup of these initial experiments. The 996 PDA detector was a flow cell-equipped photodiode array (PDA) detector, commonly utilized as a detector for HPLC instruments. The flow cell design allows for continuous infusion of solution from a pressurized vessel directly to the UV-Vis then to the ESI-MS probe. A spectrum from 190-800 nm is obtained each second with a resolution of 1.2 nm. Initial experiments were aimed at identifying signals of interest for the activation process.

For a given experiment, 10.0 mL of HPLC methanol, HPLC acetonitrile, DMF, or distilled fluorobenzene is transferred to a Schlenk tube (or PSI flask) which is then placed under vacuum with agitation and backfilled with nitrogen (except with Fluorobenzene, which was distilled under argon). This is process is repeated a minimum of three times to degas. The solvent is subsequently sparged for 20 minutes with argon before being connected to the instrumentation.

All reagent stock solutions were prepared under an inert nitrogen atmosphere in a glovebox. Tris(dibenzylideneacetone)dipalladium(0) was purchased and used as-is from Sigma-Aldrich. The stock solution was prepared using 0.0020 g Pd2(dba)3 dissolved in 4.0 mL SPS purified tetrahydrofuran (0.55 mM Pd2(dba)3, 1.1 mM Pd). PPN TPPMS stock was prepared by dissolving 0.0077 g PPN TPPMS (Bis(triphenylphosphine)iminium triphenylphosphine-meta-sulfonate) into 4.0 mL of degassed HPLC grade methanol (2.2

mM TPPMS). sSPhos (Sodium 2-dicyclohexylphosphino-2',6'-dimethoxybiphenyl-3'-sulfonate stock was prepared by dissolving 0.0045g of the salt in 4.0 mL degassed HPLC grade methanol (2.2 mM sSPhos). 100 uL of each solution was injected via syringe into 10.0 mL degassed methanol yielding a Pd concentration of 11.0 μM and 2 equivalents of ligand.

In a typical experiment, a 30 cm length of Vici Blue PEEK tubing was connected to the inlet of the Waters photodiode array detector. The opposite end of this piece was inserted through the septum of a Schlenk tube (or custom PSI flask [41]) and into the solution to be analyzed. A second length of Vici Blue PEEK tubing (~10 cm) was connected to the outlet of the UV-Vis PDA and to the probe of a Waters Acquity Triple Quadrupole Detector. The length of the PEEK tubing is kept to a minimum, especially between the UV-Vis outlet and ESI-MS probe. Once the Schlenk tube (or PSI flask) was charged with degassed solvent and a stir bar, reagents were injected to initiate the reaction. The flask is pressurized with 4 psi of argon using a PRAXAIR ProStar Platinum regulator. An IKA stirring hot plate was used to provide mechanical stirring. Additionally, an oil bath, and IKA thermocouple were used to regulate solution temperature when necessary. Acquisition was triggered via contact closure between the instruments such that the UV-Vis PDA and MS begin acquisition simultaneously. The Waters 996 PDA exposure time was set to 15 ms, resolution to 1.2 nm, with a filter response of 1 nm. UV-Vis spectra were recorded between 200-800 nm wavelength at a rate of one scan per second. A reference scan is collected automatically at the beginning of an experiment to remove solvent from the background of the UV-Vis spectrum.

Appendix E
Orbital Shaped Standing Waves Using Chladni Plates

Portions of this appendix have been submitted for publication, and are reproduced in part with permission from "Orbital shaped standing waves using Chladni plates" E. Janusson, S. MacLean, A. MacDonald, I. Paci, and J. S. McIndoe, Canadian Journal of Science, Mathematics and Technology Education, *article submitted* 2017.

Chemistry students are often introduced to the concept of atomic orbitals with a representation of a one-dimensional standing wave. The classic example is the harmonic frequencies which produce standing waves on a guitar string; a concept which is easily replicated in class with a length of rope. From here, students are typically exposed to a more realistic three-dimensional model, which can often be difficult to visualize. Extrapolation from a two-dimensional model, such as the vibrational modes of a drumhead, can be used to convey the standing wave concept to students more easily. We wanted to use Chladni plates, which may be tuned to give a two-dimensional standing wave, to serve as a cross-sectional representation of atomic orbitals. The demonstration we developed, intended for first year chemistry students, facilitated the examination of nodal and anti-nodal regions of a Chladni figure. Further, the demonstration was used in a first year course to help students connect the two-dimensional figure to the concept of quantum mechanical parameters and their relationship to atomic orbital shape.

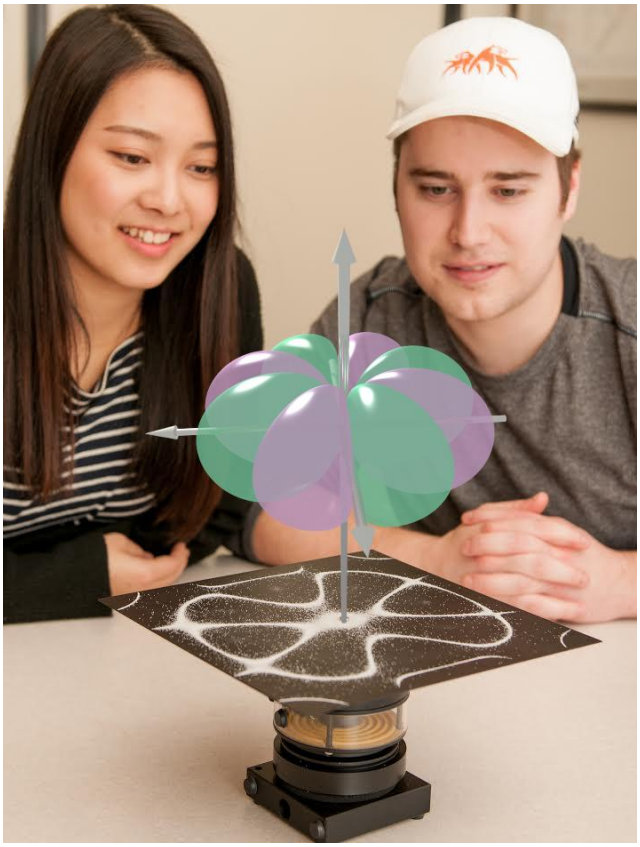

Figure 120. Chladni Plate demonstration setup featuring the characteristic nodal lines of a Chladni pattern

Introduction

Understanding that an electron in an orbital can be thought of as a three-dimensional standing wave is a tough concept to wrap one's head around. A one-dimensional standing wave is easy to visualize and indeed demonstrate in a lecture environment - a length of rope held at each end by volunteers can be induced into a standing wave, which if energetic enough, will readily display nodes.[314,315] However, making the jump to a three-dimensional wave is much tougher, perhaps because our minds run out of dimensions to consider. Length, breadth, and depth are conceivable; but where does the amplitude go?

The meanings of the different regions of the wave can be even more confusing given the multi-dimensionality of the problem. If we back off one dimension, and consider a two-dimensional standing wave, it becomes easier - we can use the third dimension to convey the amplitude, and the standing waves, if chosen carefully, can illustrate the cross-sectional shape of the orbital. A physical demonstration of wave behaviour in two dimensions, prior to three-dimensional illustration through computer-based models, allows for direct student involvement and easier conceptualization of a complex problem in first-year chemistry classes.

The shape of orbitals has been taught to students using media as diverse as circular magnets,[316] Styrofoam models,[317,318] beakers of coloured water,[319] websites,[320] and balloons.[321] Various simple models have been used to introduce the concept of standing waves to students in the context of atomic (and/or molecular) orbitals. Instructors have tapped the rim of a coffee cup to relate nodes to the energies of aromatic molecular orbitals,[322] have used Kundt's tubes (devices that set up acoustic standing waves in different gaseous media as a characterization tool),[323] and have reproduced Wiener's historic experiment on a standing light wave using a laser pointer.[324,325] Computer-based orbital illustrations are an extremely valuable advance, allowing direct visualization of the quantum mechanical solutions for atomic orbitals. There exist excellent examples in the literature of two- and three-dimensional visualizations of atomic orbitals. These make use of custom or proprietary software in order to produce plots of atomic and molecular orbitals and examine the orbital's shape based on a given change in parameters.[326–333]

Understanding and correctly interpreting these illustrations has become a fundamental learning goal in introductory quantum atomic structure. However, orbital shapes can be conceptually disconnected from the ideas of wave behavior in quantum chemistry, in the same way Styrofoam models are. Demonstrations of wave mechanics, preferably with direct student involvement, are an effective way to illustrate and promote the correct conceptualization of wavefunction shapes, their properties and the quantum mechanical wave equation.[334–336] An appealing and effective way to perform this illustration is by using the Chladni experiment discussed in the following pages. It should be noted here that the two-dimensional acoustic waves that produce Chladni patterns have been used previously to illustrate theoretically wave behaviour: The two-dimensional wave equation is discussed at some length in Donald McQuarrie's standard textbook "Quantum Chemistry" and pictures of a drum with low-frequency Chladni patterns are given on page 63.[336] A series of analogies including Chladni patterns, jellyfish and viscous glop are used in a fascinating account of quantum chemical equivalencies by Dylan Jayatilaka.[d][337] The purpose of this chapter is to illustrate how Chladni patterns can be used to physically, interactively demonstrate wave behaviour in a first-year chemistry lecture.

[d] Original post is now archived on Github at https://github.com/dylan-jayatilaka/dylan-jayatilaka.github.io/commit/802183c4f6d4da12fbcad4c63ecefbd7610a6852

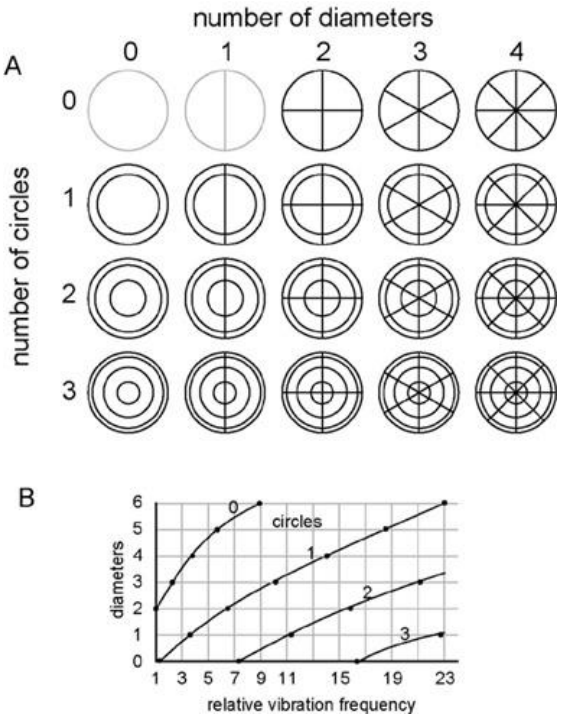

Figure 121. Simple theoretical schematic of achievable Chladni figures[337]

A two-dimensional standing wave can be generated using common percussion instruments. When the appropriate harmonic frequency is applied to a drumhead the wave pattern remains in one position as the amplitude of the wave fluctuates. Above the fundamental harmonic frequency (first harmonic), the drumhead becomes segmented by nodal lines in which there is no change in amplitude; conversely, in between these nodal lines are antinodes where the change in amplitude is at a maximum.[338,339] The standing wave formed on a drumhead is a useful analogy; however, these waves are not detectable to the unassisted naked eye, and we can more easily control and visualize two-dimensional standing waves using devices known as Chladni plates. Ernst Chladni (1756-1827) was a German physicist and musician most well known for his study of vibrational modes produced on metal plates. In Chladni's experiment, excitation was achieved by drawing the bow of a violin across the edge of the plate. Sprinkling sand across the surface of the

plate while doing so caused the sand to settle in specific patterns shaped by the nodal regions of the vibrational mode, now referred to as Chladni figures. These patterns appear as the sand is tossed away from regions of the plate where a strong vibration is occurring (primarily the antinodal regions) and settles into regions where nodal lines are present. There is a particularly striking music video involving a variety of visualized standing waves by N. J. Stanford in which a Chladni plate plays a prominent role.[340] The modern method of generating Chladni figures is achieved through the use of a frequency generator, a voice coil and metal plate. This in-class demonstration enables students to participate in active learning by producing a tangible representation of an atomic orbital, which they can control. The process of creating these beautiful cymatic figures is a unique way to intrigue and educate students.

Materials

The source of the excitation signal used was a Keysight (Agilent) 33522A function-generator. A custom power-amplifier, consisting of a Canakit (cat. # CK003) 10-Watt single-channel audio amplifier circuit, volume (amplitude) control and associated power-supply, was used to boost the signal to the levels required to drive the voice-coil that vibrates the plate. The voice-coil used was a PASCO SF-9324 mechanical wave driver.

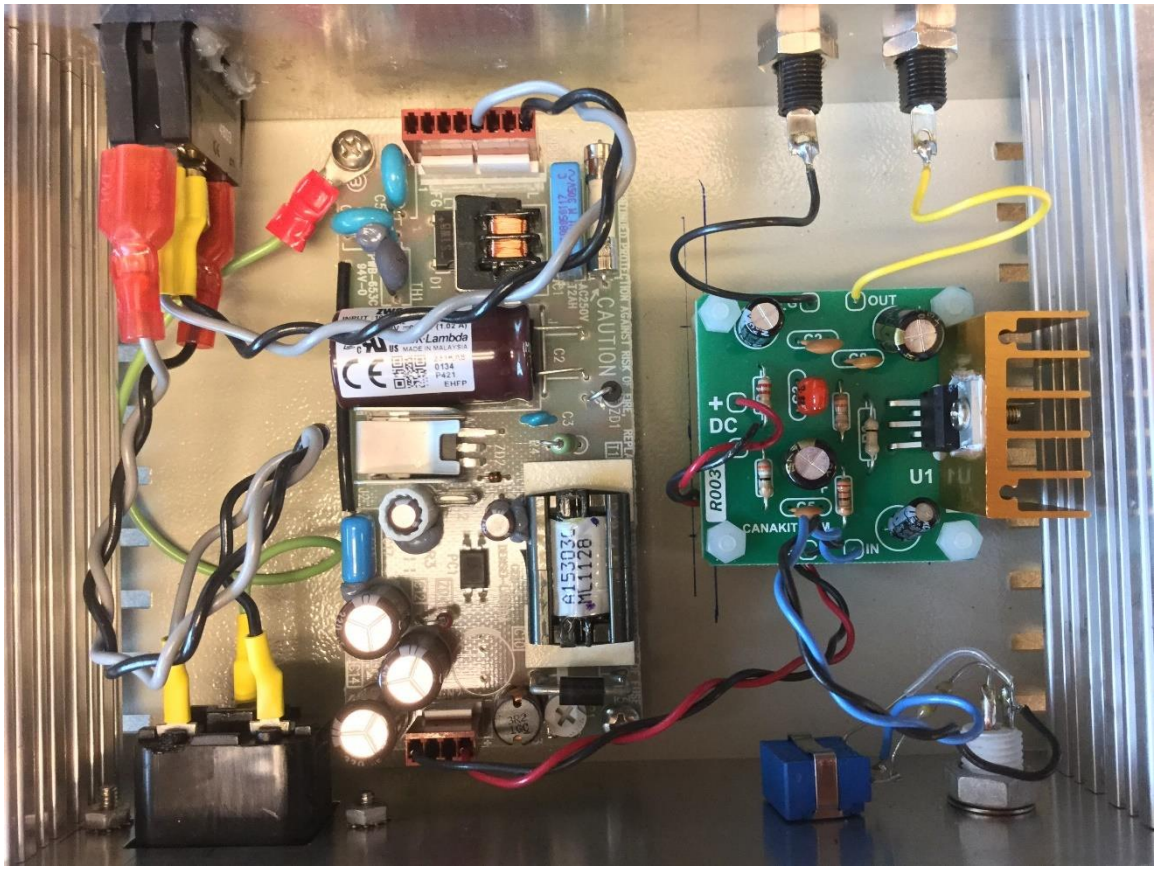

Figure 122. Photograph of power amplifier wiring

The function-generator was connected to the power-amplifier by a BNC cable. The power-amplifier positive and negative outputs were connected to the voice-coil by banana-connector cables. The plates used were round and square aluminium metal plates were used with measurements of 24 cm in diameter, and 24×24 cm, respectively. Each plate was 0.1 cm in thickness. The plates were anchored to the voice-coil at their centre. ACS reagent grade sodium bicarbonate powder was purchased from EMD Chemicals and was used as the visualization medium.

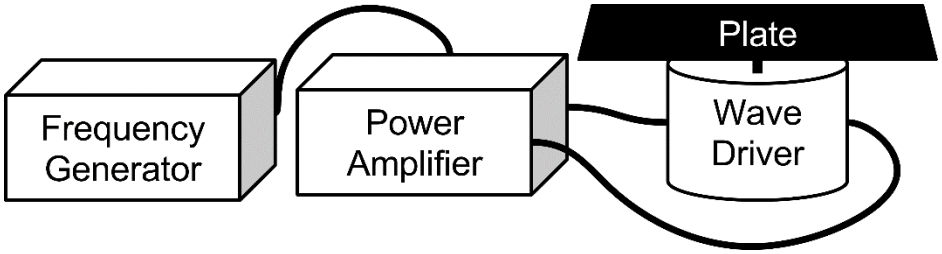

Figure 123. Schematic diagram of the demonstration setup

Procedure

A thin layer of sodium bicarbonate is poured over the surface of the metal plate prior to applying a frequency. The frequency generator was set to deliver a continuous 100 mVpp sine wave (without a sound-dampening cover, less than 70 mVpp may be more suitable for higher frequency patterns and will often yield similar results), and the frequency was swept through a range of approximately 50 to 4000 Hz during a test of the apparatus. Different sized plates may produce different vibrational modes of interest at any given frequency, so a sweep from approximately 50 Hz to as high as 5 kHz (see Safety section) at a slow rate is recommended in order to observe the progression of standing wave patterns in order to find the frequencies that produce patterns of interest. For demonstration purposes, custom software was employed to quickly recall and apply the frequency and amplitude settings that produce desired standing wave patterns.

Hazards and Safety

At higher frequencies, Chladni plates can become extremely loud and high-pitched.[341] Therefore, during a demonstration it is recommended to have the plates placed within a

transparent, sound-dampening box to prevent aural discomfort. When initially testing a Chladni setup, ear protection is recommended since the operator will spend considerably more time working with the setup than during the demonstration itself (which takes only a few minutes).

Sodium bicarbonate (aka baking soda) is generally safe to handle; however, some care must be taken to avoid inhalation or eye contact. There is an increased risk of aerosolizing fine sodium bicarbonate due to the nature of this experiment. Inhalation and exposure is not considered hazardous, as baking soda is generally harmless.

Discussion

Many students struggle to imagine the wave-like properties of an electron in three dimensions; a concept which becomes crucial later in the first-year semester and beyond for topics including periodic trends, chemical bonding, and reactivity. The shapes of atomic orbitals are also critical for students to fully understand as the concept is used to expound on molecular shapes, hybridization and molecular orbitals, which necessitate a spatial understanding of atomic orbitals. The association of electronic behaviour with the concept of a standing wave can also help explain questions like “Why doesn’t the electron fall into the nucleus?”,[342] and “How does the 2p electron go from one side of the wavefunction through the node to the other side?”.[343] The goal of this experiment is to introduce first year chemistry students to fundamental quantum theory essential in understanding atomic orbitals by facilitating a means for students to visualize simple atomic orbitals in three-

dimensions through the extrapolation of the analogous two-dimensional standing-wave system generated by means of Chladni plates.

Physical underpinnings of the experiment

Standing waves are produced by the interference of outgoing and incoming waves in a material, at resonance frequencies, which are device-specific. Guitar strings, for example, are anchored at both ends. Plucking the string creates a set of outgoing waves. Each of these reflects at the ends of the string into returning waves. The interference between an outgoing and a reflected wave produces a standing wave with nodes at the anchoring points, which presumably cannot vibrate.[314] All the harmonics have these two nodes, as well as an increasing number of nodes along the string length, for higher harmonics (see SI). The fundamental frequency of the vibration depends on the length of the string, the tension in the string, and its mass, so each of these factors can in turn be used to change the tune that is played. All the harmonics are solutions of the wave equation for the guitar string, with boundary conditions given by the requirement for nodes at the anchoring points.

A drum or stretched membrane functions in a similar way, with boundary conditions (nodes at the edge because of the attachment of the membrane) imposing the periodicity of the vibrational wave. The two-dimensional standing waves are solutions of a two-dimensional wave equation in cylindrical coordinates (for circular membranes) or Cartesian coordinates (for square membranes), and are shaped such that the width of the membrane fits multiples of half a wavelength (for pictures and animations of the square

membrane vibrational modes, see the Partial Differential Equations app for Mathematica, by Dzamay, A.).[344] Nodes on a circular membrane are diametric or circular, whereas nodes on square membranes can become significantly more complex. The free-edge Chladni apparatus used in this experiment has a distinct set of non-zero boundary conditions, based on the confinement of the wave to the size and rigidity of the plate, and the elastic behavior of the material. However, because of the principles of wave reflection and the symmetry of the problem, nodal curvatures in free-edge Chladni plates and attached-edge membranes are similar. The Chladni plate nodal planes discussed in the present work are also similar to the two-dimensional projections (which is a usual representation) of the nodal surfaces of hydrogen atomic orbitals. Parallels between the two systems can help drive home the wave nature of quantum mechanical particles in general and of the electron in particular.

From the point of view of mathematical formalism, several distinctions arise. One is that the physical problem of the electron in a hydrogen atom is a three-dimensional problem, where only the kinetic part of the quantum mechanical wave equation resembles vibrational wave mechanics. The potential, an important and often troublesome part of the Schrödinger equation, is not involved in the vibrational wave equation. For the hydrogen atom, the attractive interaction between the electron and nucleus confines the electron within the atom, leading to quantization. The separable solutions of the Schrödinger equation are stationary states, with angular and radial nodes arising from imposing radial and angular boundary conditions on the different components of the wave function.[343]

A second point that should be made clear is that the shapes obtained are nodes of a wavefunction (vibrational or electronic), not contour plots of the atomic orbital itself. For circular symmetry, the shapes are similar to contour plots (non-zero value cutouts) of the three-dimensional wavefunction, and could be used as such, although that may cause some confusion at the end of the day. For the s-orbitals, both nodes and non-zero contours are spherical (circular in 2D projection), whereas orbitals with angular dependence (p, d, f and g) have spherical radial nodes and planar and conical angular nodes. Simple diagonal Chladni shapes equivalent to the nodes of a $2p_z$ or the $3d_{xy}$ and $3d_{x^2-y^2}$ orbitals are obtainable, as are the (4 planes, 1 sphere) nodes of the $6g_z^4$ orbital (see supporting information).[320] However, diagonal nodes appear sporadically on centrally-driven circular plates, requiring the usage of higher amplitudes.

Learning objectives

After viewing this demonstration, students should be able to:

1. Explain the idea of a standing wave and how it relates to atomic orbitals
2. Understand the wave-like properties of electrons.
3. Understand the nodal and anti-nodal regions (regions of non-zero amplitude) of an atomic orbital and how these affect the three-dimensional shape of an atomic orbital.

Rather than verbally presenting the atomic orbital as the probability of an electron's position, the aim of this demonstration is to help students qualitatively observe the behaviour of two-dimensional waves, and the meaning of nodal structures in two

dimensions. However, the demonstration should open with a presentation introducing the idea of a standing wave, preferably with the use of an example such as the aforementioned guitar string, or a telephone wire fixed at two ends. The especially important point to cover is that standing waves demonstrate low-energy nodes at each higher harmonic equal to the overtone number (first overtone yields one node, the second yields two, and so on). These nodes give the guitar string a particular shape when plucked appropriately because of the nodal and anti-nodal regions.

The wave-like properties of an electron, as explained by Schrödinger's wave equation, should be connected to these standing waves. Take the opportunity to have the students consider the shape of such a wave in three-dimensions, vis-à-vis the nodal (see Figure 124 for an example of this on the Chladni plates) and anti-nodal behaviour of a standing wave. This abstract concept is likely to have some students perplexed at which point the Chladni plates demonstration, in which they will observe a two-dimensional example of a standing wave representative of an atomic orbital, can be exhibited.

The accessible atomic orbital representations available to the round plate are the 2s, 3s, 4s and 5s orbitals (Figure 124a, b, c), and the planar nodes of the $3d_{xy}$ orbital can be generated on the square plate (Figure 124d). The required frequencies and amplitudes required to generate the desired figures, as well as additional Chladni figure photographs and experimental settings are in the appendix for this chapter.

The two-dimensional example may then be explored by producing the node of the 2s orbital (or the 2p orbital) upon the circular Chladni plate. By slowly adjusting the frequency to the harmonic using the frequency generator, an illustration of the standing wave is obtained in real time, as the baking powder is tossed around. Ask students to point out how many nodes are present and relate this to which s orbital is currently being viewed as higher order s orbitals are accessed and to imagine the three-dimensional structure of each Chladni figure.

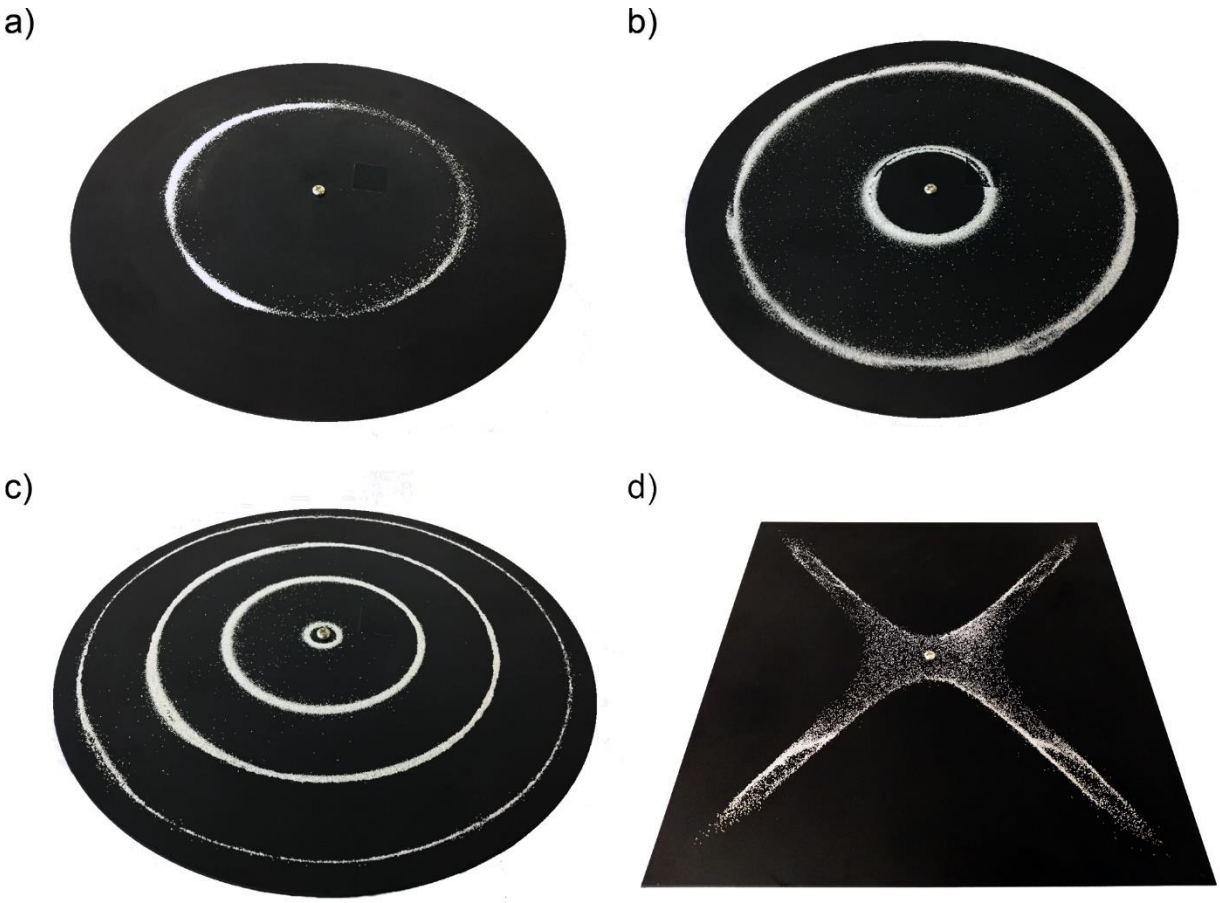

Figure 124. Exemplary standing waves produced on Chladni plates. a) 109 Hz, 300 mVpp (2s orbital), b) 354 Hz, 200 mVpp (3s), c) 1690 Hz, 100 mVpp (5s), d) 84 Hz, 100 mVpp (3dxy)

Post-demonstration Discussion

The concept of nodal and anti-nodal regions may then be elaborated on using the figure presently generated on the plate as a reference. Explain that this two-dimensional example illustrates the nodes of an atomic orbital. Following the demonstration, students may be introduced to increasingly complex ideas involving atomic orbitals. Using the 2s Chladni figure as an example, ask the students to point out the most likely position of an electron in a hydrogen atom. Is it inside the circular white line, outside the line or on the line? Discuss the implications of wave-particle duality of an electron and how this relates to the shape of an atomic orbital, that is, the shape of an atomic orbital is actually a containing surface around a cloud of electron density.

Conclusions

The aim of this demonstration is to help professors introduce atomic orbitals to students. The typical matter of course is to present standing waves and subsequently the properties of atomic orbitals. This is conceivably tricky for students to fully understand due to the nebulous idea of an atomic orbital. It is expected that this exciting demonstration will pique the interest of any student and help them visualize the structure of atomic orbitals as well as fully participate in the discussion which follows.

Materials and Equipment

The wave driver used in these experiments is a PASCO Mechanical Wave Driver model number SF-9324. The Chladni plates were purchased from PASCO scientific. The wave driver was purchased directly from PASCO Scientific. The amplifier was custom made by Andrew Macdonald of the UVic Chemistry instrument shop and used a 12 V / 0.85 A power supply, model number UK003, purchased from CanaKit as well as a TDK-Lambda Americas Inc. ZWS10-12 AC/DC 12 V 10 W converter purchased from Digi-Key Electronics. The function generator used was a 30 MHz Agilent 33522A Function/Arbitrary Waveform Generator purchased from Agilent Technologies.

List of Chladni plate standing waves and parameters

Table 17. Summary of experimental settings required for representative Chladni figures

Frequency (Hz)	Amplitude (mVpp)	Plate Shape	Orbital
109	300	Round	2s
354	200	Round	3s
1690	100	Round	5s
954	100	Square	3dxy
84	100	Square	3dxy (anti-nodal)

Table 18. Photos of standing waves using square Chladni plate

Frequency (Hz)	Amplitude (mVpp)	Photo of Standing Wave Pattern
84	100	
192	110	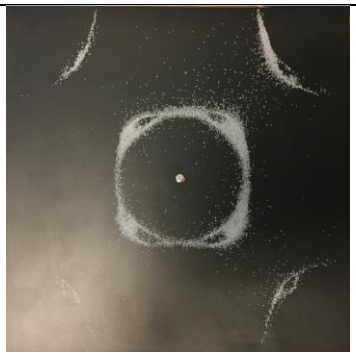
336	70	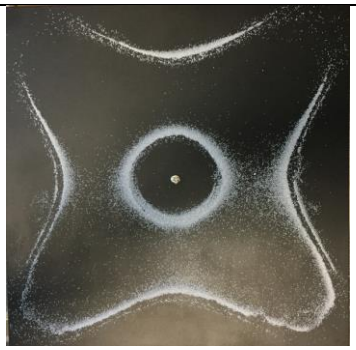
392	110	

485	50	
800	60	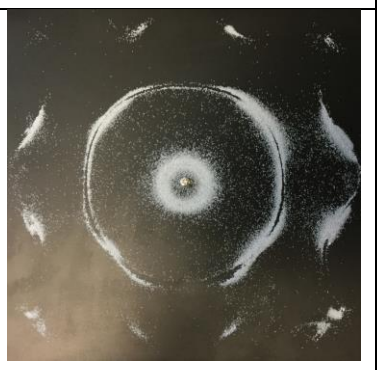
954	70	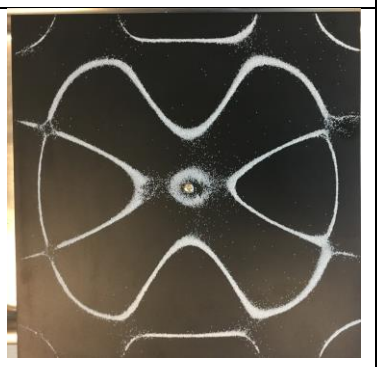 $3d_{xy}$
1058	60	

1710	50	
1876	50	
2112	100	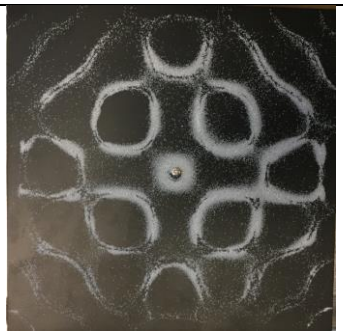
2270	90	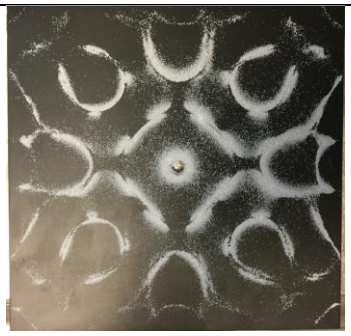

Table 19. Photos of standing waves using circular Chladni plate

Frequency (Hz)	Amplitude (mVpp)	Pattern/Orbital representation
43	200	
64	300	
91	300	
109	300	

		2s
115	300	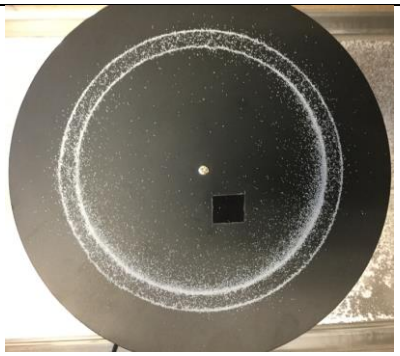
263	300	
354	200	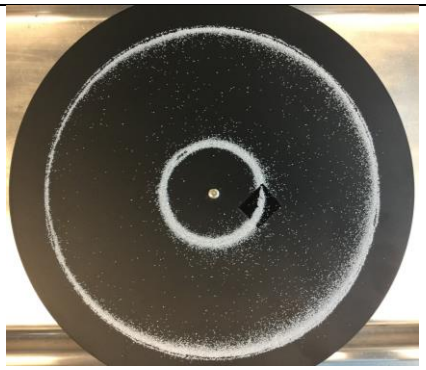 3s
896	300	 4s

1690	100	 5s